



MONASH University

Carnitine Acetyltransferase regulates metabolic sensing in AgRP neurons

Alexander Reichenbach

Master (Biochemistry)

A thesis submitted for the degree of

Doctor of Philosophy

at

Monash University

in

2018

Department of Physiology

Biomedicine Discovery Institute

Faculty of Medicine, Nursing and Health Sciences

Copyright notice

© *Alexander Reichenbach* 2018.

I certify that I have made all reasonable efforts to secure copyright permissions for third-party content included in this thesis and have not knowingly added copyright content to my work without the owner's permission.

Abstract

Energy homeostasis is controlled in the brain by various nuclei. The hypothalamus has long been implicated in the regulation of feeding and in particular AgRP neurons have the fundamental role sensing negative energy balance and mounting a counteractive response to energy deficit. This is in part achieved by integrating metabolic information in the form of circulating metabolites, nutrients and hormones.

Intriguingly, glucose, fatty acids, and amino acids are all metabolised to produce the common metabolic intermediate, acetyl-CoA, within the mitochondria. Recent studies describe the mitochondrial enzyme carnitine acetyltransferase (Crat) as a regulator of the mitochondrial acetyl-CoA pool and identify it as a molecular substrate switch between cellular glucose and fatty acid metabolism in skeletal muscle tissue. Building on that, we questioned whether or not Crat in AgRP neurons regulates physiological adaptation associated with changing metabolic conditions.

After confirmed selective deletion of Crat within AgRP neurons using AgRP cre mice crossed to Crat floxed mice, we provide compelling evidence that Crat in AgRP neurons controls substrate utilisation and influences feeding behaviour. In Chapter 2 we demonstrate the importance of Crat in AgRP neurons during the transition from fast to fed state and examine consequences of the metabolic shift towards lipid utilisation in liver, muscle, and adipose tissue. We present the first proteomic screen of cell sorted AgRP neurons and investigate alterations in feeding behaviour. In Chapter 3 we extend our observations to prolonged energy deficit during calorie restriction and describe the consequences of increased lipid utilisation on body fat loss. Moreover, we reveal a lack of adaptation to low caloric environments of feeding behaviour and thermogenesis in AgRP Crat KO mice. Finally, Chapter 4 describes the adaptation to restricted day time feeding. Here we show that AgRP Crat KO mice initiate feeding without delay but subsequently eat less and regain less body weight compared to WT mice. Paradoxically, AgRP Crat KO mice develop increased food anticipatory activity and reduced energy expenditure towards the end of the restricted feeding window, representing greater compensatory responses to reduced weight regain. Collectively our data suggest Crat in AgRP neurons functions as a component of an energy calculator computing responses to changes in metabolic state. In particular, the data herein emphasize the role of Crat in AgRP neurons to regulate substrate utilisation and nutrient partitioning. We discuss these findings and suggest future research.

Research output during enrolment

Publications

- WU, Q., LEMUS, M.B., STARK, R., BAYLISS, J., **REICHENBACH, A.**, LOCKIE, S.K.H., ANDREWS, Z.B., 2014, The temporal pattern of cfos activation in hypothalamic, cortical, and brainstem nuclei in response to fasting and refeeding in male mice, *Endocrinology [P]*, vol 155, issue 3, Endocrine Society, USA, pp. 840-853.
- BORG, M.L., LEMUS, M.B., **REICHENBACH, A.**, SELATHURAI, A., OLDFIELD, B.J., ANDREWS, Z.B., WATT, M.J., 2014, Hypothalamic neurogenesis is not required for the improved insulin sensitivity following exercise training, *Diabetes [P]*, vol 63, issue 11, American Diabetes Association, United States, pp. 3647-3658.
- BRIGGS, D.I., LOCKIE, S.K.H., BENZLER, J., WU, Q., STARK, R., **REICHENBACH, A.**, HOY, A.J., LEMUS, M.B., COLEMAN, H.A., PARKINGTON, H.C., TUPS, A., ANDREWS, Z.B., 2014, Evidence that diet-induced hyperleptinemia, but not hypothalamic gliosis, causes ghrelin resistance in NPY/AgRP neurons of male mice, *Endocrinology [P]*, vol 155, issue 7, Endocrine Society, USA, pp. 2411-2422.
- STARK, R., **REICHENBACH, A.**, ANDREWS, Z.B., 2015, Hypothalamic carnitine metabolism integrates nutrient and hormonal feedback to regulate energy homeostasis, *Molecular and Cellular Endocrinology [P]*, vol 418, Elsevier Ireland Ltd, Ireland, pp. 9-16.
- KU, J., ANDREWS, Z.B., BARSBY, T., **REICHENBACH, A.**, LEMUS, M.B., DRUMMOND, G.R., SLEEMAN, M., SPENCER, S.J., SOBEY, C.G., MILLER, A.A., 2015, Ghrelin-related peptides exert protective effects in the cerebral circulation of male mice through a nonclassical ghrelin receptor(s), *Endocrinology [P]*, vol 156, issue 1, The Endocrine Society, USA, pp. 280-290.
- STARK, R., **REICHENBACH, A.**, LOCKIE, S.K.H., PRACHT, C., WU, Q., TUPS, A., ANDREWS, Z.B., 2015, Acyl ghrelin acts in the brain to control liver function and peripheral glucose homeostasis in male mice, *Endocrinology [P]*, vol 156, issue 3, The Endocrine Society, USA, pp. 858-868.
- LEMUS, M.B., BAYLISS, J.A., LOCKIE, S.K.H., SANTOS, V.V., **REICHENBACH, A.**, STARK, R., ANDREWS, Z.B., 2015, A stereological analysis of NPY, POMC, Orexin, GFAP astrocyte, and Iba1 microglia cell number and volume in diet-induced obese male mice, *Endocrinology [P]*, vol 156, issue 5, The Endocrine Society, USA, pp. 1701-1713.
- HORNSBY, A.K.E., REDHEAD, Y.T., REES, D.J., RATCLIFF, M.S.G., **REICHENBACH, A.**, WELLS, T., FRANCIS, L., AMSTALDEN, K., ANDREWS, Z.B., DAVIES, J.S., 2016, Short-term calorie restriction enhances adult hippocampal neurogenesis and remote fear memory in a Ghrelin-dependent manner, *Psychoneuroendocrinology [P]*, vol 63, Pergamon Press, UK, pp. 198-207.
- BORG, M.L., **REICHENBACH, A.**, LEMUS, M.B., OLDFIELD, B.J., ANDREWS, Z.B., WATT, M.J., 2016, Central Administration of the CNTF Analogue, Axokine, does not Play a Role in Long-Term Energy Homeostasis in Adult Mice, *Neuroendocrinology [P]*, vol E-pub, S Karger AG, Switzerland, pp. 1-7.
- STARK R, SANTOS VV, GEENEN B, CABRAL A, DINAN T, BAYLISS JA, LOCKIE SH, **REICHENBACH A**, LEMUS MB, PERELLO M, SPENCER SJ, KOZICZ T, ANDREWS ZB., 2016, Des-Acyl Ghrelin and Ghrelin O-Acyltransferase Regulate Hypothalamic-Pituitary-Adrenal Axis Activation and Anxiety in Response to Acute Stress, *Endocrinology [P]*, vol 157, issue 10, The Endocrine Society, USA, pp. 3946-3957.
- REICHENBACH, A.**, STARK R., MEQUINION, M., DENIS, R.R.G., GOULARTE, J.F., CLARKE, R.E., LOCKIE, S.K.H., LEMUS, M., KOWALSKI, G.M., BRUCE, C.R., HUANG, C., SCHITTENHELM, R.B., MYNATT, R., OLDFIELD, B.J., WATT, M.J., LUQUET, S., ANDREWS, Z.B., 2018, AgRP neurons require carnitine acetyltransferase (Crat) to regulate metabolic flexibility and peripheral nutrient partitioning, *Cell Reports*, Accepted 22.1.2018
- REICHENBACH, A.**, STARK R., MEQUINION, M., LOCKIE, S.K.H., LEMUS, M.B., MYNATT, R., LUQUET, S., ANDREWS, Z.B., 2018, Carnitine acetyltransferase in AgRP neurons permits adaptation to calorie restriction by regulating nutrient partitioning. submitted
- REICHENBACH, A.**, MEQUINION, M., BAYLISS, J.A., LOCKIE, S.K.H., LEMUS, M.B., MYNATT, R., STARK R., ANDREWS, Z.B., 2018, Carnitine acetyltransferase in AgRP neurons is required for the adaptation to restricted feeding. submitted

Oral Presentations

- Reichenbach A**, Stark R, Lockie S, Watt M, Bruce C, Luquet S, Andrews, ZB (2016) Carnitine acetyltransferase in AgRP neurons enables metabolic sensing of negative energy balance., New Investigator Travel Award winner symposium at 26th Annual Meeting of the Society for the Study of Ingestive Behavior, **Porto, Portugal**
- Reichenbach A**, Stark R, Lockie S, Watt M, Bruce C, Luquet S, Andrews, ZB (2016) Carnitine acetyltransferase in AgRP neurons enables metabolic sensing of negative energy balance., *Postgraduate Biochemistry Research Symposium*, **Melbourne, Australia**
- Reichenbach A**, Stark R, Lockie S, Watt M, Bruce C, Luquet S, Andrews, ZB (2017) Metabolic processing of energy status by Carnitine acetyltransferase is required for physiological AgRP function, *ANZOS-OSSANZ-AOCO conference*, **Adelaide, Australia**
- Reichenbach A**, Stark R, Lockie S, Mequinion M, Watt M, Andrews, ZB (2017) The Yo-Yo Effect: The fat you want to lose, is the fat your body wants to keep, *ANZOS-OSSANZ-AOCO conference*, **Adelaide, Australia**
- Reichenbach A**, Stark R, Lockie S, Watt M, Bruce C, Luquet S, Andrews, ZB (2017) AgRP neurons require carnitine acetyltransferase (Crat) to regulate nutrient partitioning and metabolic flexibility, invited speaker at *HNNA symposia*, **Sydney, Australia**

Posters

- Reichenbach A**, Andrews, ZB (2014) Metabolic sensing by Carnitine acetyltransferase in AgRP neurons regulates feeding behaviour and liver function during negative energy balance., *International Congress of Neuroendocrinology*, **Sydney, Australia**
- Reichenbach A**, Stark R, Andrews, ZB (2015) Carnitine acetyltransferase in AgRP neurons regulates food intake and peripheral nutrient partitioning during negative energy balance., *Metabolic Disease and Obesity Program Inaugural Research Workshop*, **Melbourne, Australia**
- Reichenbach A**, Stark R, Lockie S, Watt M, Bruce C, Luquet S, Andrews, ZB (2016) Carnitine acetyltransferase in AgRP neurons enables metabolic sensing of negative energy balance., *Cell Symposia Metabolism and Aging*, **Sitges, Spain**
- Reichenbach A**, Stark R, Lockie S, Watt M, Bruce C, Luquet S, Andrews, ZB (2016) Carnitine acetyltransferase in AgRP neurons enables metabolic sensing of negative energy balance., Poster prize winner *Students of brain research 2016 symposium*, **Melbourne, Australia**
- Reichenbach A**, Stark R, Lockie S, Watt M, Bruce C, Luquet S, Andrews, ZB (2016) Carnitine acetyltransferase in AgRP neurons enables metabolic sensing of negative energy balance., *Metabolic Diseases; Breakthrough Discoveries in Diabetes & Obesity*, **Melbourne, Australia**
- Reichenbach A**, Stark R, Lockie S, Watt M, Bruce C, Luquet S, Andrews, ZB (2017) Metabolic processing of energy status by carnitine acetyltransferase (Crat) is required for physiological AgRP function, *Keystone Symposia Neuronal Control of Appetite, Metabolism and Weight*, **Copenhagen, Denmark**
- Reichenbach A**, Stark R, Lockie S, Watt M, Bruce C, Luquet S, Andrews, ZB (2017) Metabolic processing of energy status by carnitine acetyltransferase (Crat) is required for physiological AgRP function, *2017 MNHS Faculty ECR Symposium*, **Melbourne, Australia**
- Reichenbach A**, Stark R, Lockie S, Watt M, Bruce C, Luquet S, Andrews, ZB (2017) Metabolic processing of energy status by carnitine acetyltransferase (Crat) is required for physiological AgRP function, *2017 BDI workshop*, **Melbourne, Australia**

Thesis including published works declaration

I hereby declare that this thesis contains no material which has been accepted for the award of any other degree or diploma at any university or equivalent institution and that, to the best of my knowledge and belief, this thesis contains no material previously published or written by another person, except where due reference is made in the text of the thesis.

This thesis includes one original papers published in peer reviewed journals and two submitted publications. The core theme of the thesis is metabolic neuroscience. The ideas, development and writing up of all the papers in the thesis were the principal responsibility of myself, the student, working within the Department of Physiology under the supervision of Associate Professor Zane Andrews.

(The inclusion of co-authors reflects the fact that the work came from active collaboration between researchers and acknowledges input into team-based research.)

In the case of Chapter 2-4 my contribution to the work involved the following:

Thesis Chapter	Publication Title	Status (<i>published, in press, accepted or returned for revision, submitted</i>)	Nature and % of student contribution	Co-author name(s) and % of Co-author's contribution*	Nature of Co-author's contribution	Co-author(s), Monash student Y/N*
2	<i>AgRP neurons require carnitine acetyltransferase (Crat) to regulate metabolic flexibility and peripheral nutrient partitioning</i>	<i>accepted</i>	conceived the idea, designed and performed the experiments, analysed data, and wrote the manuscript Overall contribution: 70 %	Romana Stark, assisted with tissue collection for glucose stimulated glucose uptake and ex vivo lipid oxidation experiments 2%; Mathieu Mequinion, Jeferson F Goularte, Rachel E Clarke, Sarah H Lockie, Moyra B Lemus assisted with laboratory experiments 2% together; Moyra B Lemus assisted with immunohistochemistry and stereology, 2%; Greg M Kowalski and Clinton R Bruce, helped design and performed analysis of plasma samples from labelled oGTT and endogenous glucose production experiments 3% together; Raphael R.G. Denis, performed HPLC analysis of NETO experiments 2%; Cheng Huang, helped run Mass spec and processed raw data in MaxQuant and Perseus 2%;		<i>REC and CH are Monash HDR students</i>

3

Carnitine acetyltransferase in AgRP neurons permits adaption to calorie restriction by regulating nutrient partitioning

submitted

conceived the idea, designed and performed the experiments, analysed data, and wrote the manuscript
Overall contribution: 89%

Ralf B Schittenhelm, helped design proteomic screen experiments 1%; Randall Mynatt, provided Crat floxed mouse model 1%;
Brian J Oldfield, helped design experiments 1%
Mathew J Watt, provided radio labelled chemicals and helped design glucose stimulated glucose uptake and ex vivo lipid oxidation experiments and edited manuscript 2%;
Serge Luquet, helped design and perform NETO experiments and edited manuscript 2%;
Zane B Andrews, supervised and coordinated the project, conceived the idea, and assisted with designing the experiments and writing the manuscript 10%

Mathieu Mequinion, Romana Stark, Sarah H Lockie, Moyra B Lemus assisted with laboratory experiments 3% together;
Randall Mynatt, provided Crat floxed mouse model 1%;
Serge Luquet, helped design experiments and edited manuscript 2%;
Zane B Andrews, supervised and coordinated the project, conceived the idea, and assisted with designing the experiments and writing the manuscript 5%

4

Carnitine acetyltransferase in AgRP neurons is required for the adaptation to restricted feeding.

submitted

conceived the idea, designed and performed the experiments, analysed data, and wrote the manuscript

Mathieu Mequinion, Romana Stark, Sarah H Lockie, Jacqueline A Bayliss, Moyra B Lemus assisted with laboratory experiments 3% together;
Randall Mynatt, provided Crat floxed mouse model 1%;
Zane B Andrews, supervised and

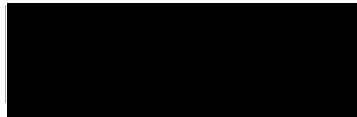
JAB was a Monash HDR student

Overall contribution: 91% coordinated the project, conceived the idea, and assisted with designing the experiments and writing the manuscript 5%

**If no co-authors, leave fields blank*

I have renumbered sections of submitted or published papers in order to generate a consistent presentation within the thesis.

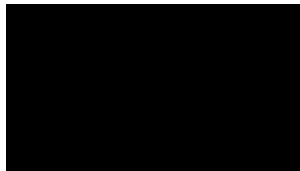
Student signature:



Date: 31. January 2018

The undersigned hereby certify that the above declaration correctly reflects the nature and extent of the student's and co-authors' contributions to this work. In instances where I am not the responsible author I have consulted with the responsible author to agree on the respective contributions of the authors.

Main Supervisor signature:



Date: 31. January 2018

Acknowledgements

Thank you to my supervisor Zane Andrews for trusting me with the best project that I could have asked for and guiding me through the last years. Even in the years before starting my PhD, you showed patience, faith, and taught me to focus on the important aspects of my project.

Thank you to my co-supervisors Matt Watt and Sarah Lockie for your help and advice.

Thank you to all my lab fellows for the great help, support and entertainment throughout the years. Special thanks to Moyra Lemus for being a friend over the last seven years. This thesis would not be the same without your help.

Thank you to Romana Stark for chatting in our mother language in the lab. This was a real joy for my soul.

Thank you to all my fellow PhD students providing a stimulating and fun environment to work in.

Thank you to all co-authors of my first publication during my PhD. You did a great job and this would have not been possible without you.

Thank you to Michael Reitsma for giving all the helpful advice to optimise the neuron dissociation protocol and cell-sorting my samples. You made the long days worthwhile.

Thank you to Enzo Huang for helping, and teaching me analysing mass spec data. Your skills made this exercise seem so simple.

Thank you to Helena Parkington for all the support around my PhD.

Thank you to all the MARP/ARL staff for looking after the wellbeing of my mice. Especially to Samantha O'Dea and Terry Lane for providing my mice with everything they needed.

Thank you to my parents and siblings for always supporting me.

Thank you to Mathilde and Michael for their support.

Thank you to my partner, Susie for all your love, support and encouragement, and for keeping me on my toes.

Thank you to my sons, Leander and Pascal, for all the love and always reminding me that work is only a part of life. You sure prevented a burnout.

Thank you to Doug Compton and the team from Research Diets for all the support with the BioDAQ feeding cages and awarding me with "The Research Diets, Inc. Goldschmidt Travel Award"

Thank you to the Australian taxpayer and the Australian government for funding me during my PhD. This research was supported by an Australian Government Research Training Program (RTP) Scholarship.

Abbreviations

2DG	=	2-deoxyglucose
ACC	=	Acetyl coenzyme A carboxylase
ADP	=	Adenosine diphosphate
AgRP	=	Agouti related peptide
AMP	=	Adenosine monophosphate
AMPK	=	AMP- activated protein kinase
ARC	=	Arcuate nucleus of the hypothalamus
ATP	=	Adenosine triphosphate
AUC	=	Area under the curve
BAT	=	Brown adipose tissue
BNST	=	Bed nucleus of the stria terminalis
CACT	=	Carnitine acylcarnitine translocase
CCK	=	Cholecystokinin
CD36	=	Cluster of differentiation 36, fatty acid translocase
CGRP	=	Calcitonin gene related peptide
CLAMS	=	Comprehensive lab animal monitoring system
CNS	=	Central nervous system
CoA	=	Coenzyme A
CPT	=	Carnitine palmitoyltransferase
CR	=	Calorie restriction
Crat	=	Carnitine acetyltransferase
cre	=	Cre recombinase
Crot	=	Carnitine octanoyltransferase
D ₂ O	=	Deuterium oxide, heavy water
DEXA	=	Dual-energy X-ray absorptiometry
DMH	=	Dorsomedial hypothalamic nucleus
EE	=	Energy expenditure
EGP	=	Endogenous glucose production
ETC	=	Electron transfer chain
FAA	=	Food anticipatory activity
FACS	=	Fluorescence Activated Cell Sorting
FAD/FADH ₂	=	Flavin adenine dinucleotide (reduced /oxidized)
FEO	=	Food entrainable oscillator
FFA	=	Free fatty acids
GABA	=	Gamma-aminobutyric acid
GC-MS	=	Gas chromatography–mass spectrometry
GE	=	Glucose excited
GFAP	=	Glial fibrillary acidic protein
GFP	=	Green fluorescent protein
GI	=	Glucose inhibited
Glut2	=	Glucose transporter 2
GO	=	Gene ontology
HFD	=	High fat diet
HPLC	=	High performance liquid chromatography
ICV	=	Intracerebroventricular
iWAT	=	Inguinal white adipose tissue
KATP channel	=	ATP sensitive potassium channel
KEGG	=	Kyoto Encyclopedia of Genes and Genomes
KO	=	Knock out
LC acyl CoA	=	Long chain fatty acyl-coenzyme A
LFQ	=	Label-free quantification
LH	=	Lateral hypothalamus
MC4R	=	Melanocortin receptor 4
mTORC	=	Mammalian target of rapamycin complex

NAD/NADH	=	Nicotinamide adenine dinucleotide (reduced /oxidized)
NADP/NADPH	=	Nicotinamide adenine dinucleotide phosphate (reduced /oxidized)
NAFLD	=	Non-alcoholic fatty liver disease
NE	=	Norepinephrine
NEFA	=	Non-esterified fatty acid
NMDA receptor	=	N-methyl-D-aspartate receptor
NPY	=	Neuropeptide Y
OCTN2	=	Sodium-dependent organic cation transporter 2
PAK	=	p21-activated kinase
pAKT	=	phosphorylated AKT
PBN	=	Parabrachial nucleus
PCR	=	Polymerase chain reaction
PDH	=	Pyruvate dehydrogenase
PGC1 α	=	Peroxisome proliferator-activated receptor gamma, coactivator 1 alpha
POMC	=	Proopiomelanocortin
PVN	=	Paraventricular nucleus of the hypothalamus
PVT	=	Paraventricular thalamus
RER	=	Respiratory exchange ratio
RF	=	Restricted feeding
RNA	=	Ribonucleic acid
ROS	=	Reactive oxygen species
SCN	=	Suprachiasmatic nucleus
SIRT	=	Sirtuin
SNS	=	Sympathetic nervous system
TCA	=	Tricarboxylic acid
TG	=	triglyceride
TRPC3	=	Transient receptor potential channel 3
UCP2	=	Uncoupling protein 2
WAT	=	White adipose tissue
WT	=	Wild type
α MPT	=	α -methyl-DL-p-tyrosine
α MSH	=	Alpha-melanocyte-stimulating hormone

Table of Content

Copyright notice	I
Abstract.....	II
Research output during enrolment	III
Thesis including published works declaration	V
Acknowledgements	VIII
Abbreviations	IX
<u>List of figures</u>	XII
<u>List of tables</u>	XII
Chapter 1: Introduction.....	1
1.1 Neuronal control of energy homeostasis.....	1
1.2 AgRP neurons	1
1.3 Nutrient sensing	4
1.4 Carnitine metabolism.....	7
1.5 Carnitine acetyltransferase	10
1.6 Project goals	11
Chapter 2: AgRP neurons require carnitine acetyltransferase (Crat) to regulate metabolic flexibility and peripheral nutrient partitioning.....	13
2.1 Abstract	14
2.2 Introduction.....	15
2.3 Experimental Procedures	17
2.4 Results	27
2.5 Discussion	44
2.6 Summary Chapter 2	48
Chapter 3: Carnitine acetyltransferase (Crat) in AgRP neurons permits adaptation to calorie restriction by regulating nutrient partitioning	49
3.1 Abstract	50
3.2 Introduction.....	51
3.3 Experimental Procedures	53
3.4 Results	56
3.5 Discussion	64
3.6 Summary Chapter 3	69
Chapter 4: Carnitine acetyltransferase in AgRP neurons is required for the adaptation to restricted feeding	70
4.1 Abstract	71
4.2 Introduction.....	72
4.3 Experimental Procedures	74
4.4 Results	77
4.5 Discussion	84
4.6 Summary Chapter 4	88
Chapter 5: Conclusion and future directions.....	89
5.1 Motivation for food	91
5.2 Reactive Oxygen Species as signalling molecule	93
5.3 Fine tuning ROS for glucose tolerance	95
5.4 Proposed role of Crat in AgRP neurons.....	96
5.5 Summary	98

References.....	99
Appendix	115

List of figures

Figure 1.1 Nutrient sensing pathways in neurons	6
Figure 1.2 Carnitine cycle regulates both fatty acid and glucose metabolism.....	9
Figure 2.1 Validation of cre-mediated recombination and Crat deletion in AgRP neurons.	27
Figure 2.2 AgRP Crat deletion does not affect adrenal morphology and function	28
Figure 2.3 AgRP Crat deletion does not affect gastric emptying.....	29
Figure 2.4 Deletion of Crat in AgRP neurons affects feeding behaviour and food intake in response to fasting.....	30
Figure 2.5 Crat in AgRP neurons is not required for sensing positive energy balance	32
Figure 2.6 Sensitivity to insulin and CCK	34
Figure 2.7 Deletion of Crat in AgRP neurons affects peripheral metabolism.	36
Figure 2.8 Deletion of Crat in AgRP neurons affects glucose homeostasis.....	38
Figure 2.9 AgRP Crat deletion impairs peripheral nutrient partitioning	39
Figure 2.10 Crat deletion affects protein regulation in AgRP neurons.	42
Figure 2.11 Summary of results from Chapter 2.	48
Figure 3.1: Crat in AgRP neurons is required for adaption of feeding behaviour in response to calorie restriction	57
Figure 3.2. Crat in AgRP neurons is needed to regulate nutrient partitioning and energy expenditure in response to calorie restriction.....	59
Figure 3.3. Crat in AgRP neurons affects hepatic function in response to calorie restriction.....	60
Figure 3.4. Crat in AgRP neurons influences rebound weight gain, food intake and adiposity after cessation of calorie restriction.	61
Figure 3.5 Influence of calorie restriction and refeeding on body composition and energy expenditure.	62
Figure 3.6. Crat in AgRP neurons regulates substrate selection during ad libitum refeeding	63
Figure 3.7 Summary of results from Chapter 3	69
Figure 4.1. AgRP Crat KO mice adjust to feeding entrainment, but show altered feeding behaviour.	78
Figure 4.2. AgRP Crat KO mice exhibit slower body weight regain on restricted feeding schedule.	79
Figure 4.3 Changes in BAT temperature.....	81
Figure 4.4. AgRP Crat KO mice exhibit greater food anticipatory activity	82
Figure 4.5 Summary of results from Chapter 4	88
Figure 5.1. Two-bottle-choice test	93
Figure 5.2. Oral Glucose Tolerance Test after ICV insulin administration	96
Figure 5.3. Proposed mechanism of Crat mediated AgRP function.....	97

List of tables

Table 1 BioDAQ Data Viewer settings for analysis of feeding behaviour.....	18
Table 2 Primer Sequences.....	115
Table 3 MSprotein_enrichment_KOvsWT_fed.....	117
Table 4 MSprotein_enrichment_KOvsWT_fast.....	119
Table 5 MSprotein_enrichment_KOvsWT_refed.....	126

Chapter 1: Introduction

1.1 Neuronal control of energy homeostasis

Energy conservation and expenditure is regulated through an interplay of neuronal populations throughout the brain. Arguably, the orexigenic agouti related peptide (AgRP) containing neurons, co-expressing neuropeptide Y (NPY) and gamma-aminobutyric acid (GABA), in the hypothalamic arcuate nucleus (ARC) are the most important. The proximity of the ARC to the compromised blood brain barrier allows these neurons to readily receive feedback and detect signals predicting changes in metabolic state, which therefore helps to maintain energy homeostasis. The accurate metabolic sensing in AgRP neurons is crucial to engage appropriate mechanisms to conserve energy in times of food scarcity and ensure survival (Luquet et al., 2005). It is well described that ghrelin, leptin, insulin but also glucose and fatty acids influence AgRP neuronal activity to regulate energy intake and energy conservation. While hormones are a proxy for the metabolic state of stored energy, circulating glucose and fatty acids represent a picture of acute nutrient availability and have the power to elicit rapid changes. This detection of sudden changes in nutrient availability functions on a molecular level through catabolism of glucose/fatty acids within neurons. Ghrelin facilitates fatty acid metabolism in AgRP neurons during energy deficit (Andrews et al., 2008) when available glucose reserves are limited, and when glucose concentrations rise, AgRP neurons are generally inhibited (van den Top et al., 2007) in order to promote normal physiological responses and maintain energy homeostasis.

1.2 AgRP neurons

AgRP neurons contain at least 3 currently identified important peptides relevant to the control of energy intake and energy conservation, AgRP, NPY, and GABA. Each of these peptides is sufficient to drive food intake independently, but elicit feeding at different time scales; NPY and GABA drive food intake rapidly, and AgRP elicits a slower feeding response due to the antagonism of the melanocortin-4-receptor (MC4R) (Krashes et al., 2013), which blocks the anorectic actions of α -melanocyte-stimulating hormone (α -MSH) at the MC4R. AgRP neurons communicate with multiple brain regions including paraventricular

nucleus of the hypothalamus (PVN), dorsomedial hypothalamus (DMH), parabrachial nucleus (PBN), bed nucleus of the stria terminalis (BNST), amygdala, preoptic area and the paraventricular thalamus (PVT) (Broberger et al., 1998). Although not all of these pathways promote food intake, they stimulate behavioural changes to prioritize the effective acquisition of food (Burnett et al., 2016). Some pathways directly drive food intake including circuits from AgRP to PVN, BNST, lateral hypothalamus (LH) and to a lesser extent PVT (Betley et al., 2013), while others prevent meal termination through GABA signalling via AgRP neurons in the PBN (Campos et al., 2016; Wu et al., 2009). AgRP signalling to PBN inhibits calcitonin gene related peptide (CGRP) neurons and overrides the effect of anorexigenic hormones and lithium chloride, a malaise provoking salt (Essner et al., 2017). Connections to the amygdala reduce fear (Verma et al., 2016) to facilitate food-seeking behaviour in a risky environment (Jikomes et al., 2016; Lockie et al., 2017) and limit competing behaviours such as territorial aggression (Padilla et al., 2016). This clearly highlights that AgRP neurons engage multiple strategies to ensure feeding.

AgRP neurons are classically described to increase food intake and reduce energy expenditure and are activated by a metabolic signature of energy deficit (such as that during fasting), including low leptin, insulin and glucose and high ghrelin and corticosterone levels (Lockie and Andrews, 2013). Furthermore, the circadian gene expression of AgRP and NPY is dependent on the metabolic state (Hahn et al., 1998) rising with diurnal corticosterone plasma levels (Lu et al., 2002) and mediated by mammalian target of rapamycin complex (mTORC) 1 signalling (Albert et al., 2015).

Fasting increases glutamatergic NMDA receptor expression at AgRP neurons (Qi and Yang, 2015) via corticosterone dependent mechanisms (Gyengesi et al., 2010) and induces spinogenesis (Liu et al., 2012). Moreover, AgRP neurons receive excitatory inputs from the PVN (Krashes et al., 2014) and activation requires NMDA receptors (Liu et al., 2012; Uner et al., 2015) and causes changes in physiology and behaviour to ensure survival by driving food intake (Luquet et al., 2005) and food seeking behaviour (Krashes et al., 2011), conserving energy by reducing thermogenesis (Ruan et al., 2014; Shi et al., 2013) and promoting carbohydrate oxidation (Cavalcanti-de-Albuquerque et al., 2016).

Ablation or inactivation of AgRP neurons shifts metabolism to increased lipid utilisation (Joly-Amado et al., 2012; Liu et al., 2012), and NPY KO mice have increased fat loss caused by lipolysis during calorie restriction (Park et al., 2017). Intriguingly, AgRP-like antagonism of MC4R increased the respiratory quotient (Nogueiras et al., 2007), whereas stimulating MC4R signalling increased lipolysis (Brito et al., 2007). These studies highlight that AgRP neurons, either via AgRP or NPY peptide release contribute to peripheral substrate

selection. This is in particular important when the predominant energy sources dynamically change during the transition from fasting to feeding in order to switch energy flux derived from adipose tissue (fatty acids) to that from newly available nutrients (glucose).

The sensory detection of food immediately reduces AgRP neuronal activity (Chen et al., 2015). Notably, this inhibition through sensory cues is dependent on the metabolic state as it is only seen in fasted and not in fed mice, whereas inhibition after nutrient ingestion is independent of nutritional state (Beutler et al., 2017). Moreover, removal of food after a short presentation increases AgRP neuronal activity again (Chen et al., 2015) and sustained suppression of activity is only achieved after ingestion of food and is proportional to the number of calories consumed (Betley et al., 2015; Beutler et al., 2017; Su et al., 2017). This demonstrates that AgRP neurons integrate feedforward and feedback signals to orchestrate dynamic changes in feeding behaviour (Andermann and Lowell, 2017).

Additionally, AgRP neurons integrate hormonal feedback (insulin, ghrelin) to control hepatic glucose production (Konner et al., 2007) and regulate blood glucose levels (Wang et al., 2014). Ghrelin requires GABAergic signalling to elicit feeding (Tong et al., 2008) and drives AgRP neuronal activation via SIRT1 and UCP2-dependent mechanisms that enhance mitochondrial bioenergetics and buffers reactive oxygen species (ROS) (Andrews et al., 2008; Dietrich et al., 2010). Besides buffering ROS, UCP2 also regulates mitochondrial dynamics (Toda et al., 2016), which have been shown to be important for proper electric activity in AgRP neurons (Dietrich et al., 2013). Moreover, mitochondrial uncoupling increases the ADP/ATP ratio, a cellular signal for reduced energy availability, which activates AMPK to alter synaptic plasticity in AgRP neurons via AMPK-PAK signalling (Claret et al., 2007; Kong et al., 2016; Yang et al., 2011). Also, chemogenetic activation of G-protein coupled receptors in AgRP neurons increases AgRP gene expression, induces sustained food intake and weight gain without electrical activation of AgRP neurons (Nakajima et al., 2016), underlining that AgRP neurons orchestrate numerous signalling cascades to promote energy intake and maintain homeostasis.

Finally, these neurons decrease energy expenditure. AgRP neuronal activation suppresses browning of white adipose tissue (WAT) (Ruan et al., 2014) and reduces brown adipose tissue (BAT) thermogenesis mediated by the sympathetic nervous system via ghrelin receptor signalling and NPY release (Brito et al., 2007; Shi et al., 2013; Wu et al., 2017). These signalling cascades depend on metabolic state and food availability, as activation of AgRP neurons does not reduce BAT temperature and energy expenditure in the presence of food (Burke et al., 2017). Moreover, under conditions of energy abundance (high-fat diet

feeding) increased mTORC signalling in a subpopulation of AgRP neurons increases BAT thermogenesis (Burke et al., 2017).

Collectively, AgRP/NPY/GABA neurons have evolved multiple, redundant and complementary strategies to re-establish energy balance during times of energy deficit. In order to effectively and efficiently promote energy intake during periods of food availability and promote energy conservation during energy deficit, such as fasting, these neurons need to integrate and respond accurately to acute changes in energetic state. Their location close to the compromised blood-brain barrier near the median eminence allows integration of information about acute peripheral metabolic state via circulating metabolites.

1.3 Nutrient sensing

Over 50 years ago, Anand described how neurons in feeding and satiety centres of the brain change their activity after intravenous glucose administration (Anand et al., 1962) and demonstrated the existence of glucose inhibited (GI) and glucose excited (GE) neurons in the hypothalamus (Anand et al., 1964). A decade later, studies revealed that these neurons can also be excited by free fatty acids (Oomura et al., 1975). Since then, several studies showed that neuronal glucose and fatty acid metabolism are dependent on metabolic state (Kasser et al., 1986; Kasser et al., 1985; Poplawski et al., 2010) and that central energy substrate utilisation controls peripheral metabolism (Moreno et al., 2013), as well as feeding and glucose homeostasis (He et al., 2006; Lam et al., 2005b; Obici et al., 2002). Both metabolic pathways are in competition with each other (Kasser et al., 1986; Randle et al., 1963) as fasting shifts neuronal substrate selection from glucose to fatty acid oxidation (Poplawski et al., 2010), the latter being a signal of energy deficit (Moreno et al., 2013). Increasing neuronal glucose oxidation or preventing beta-oxidation reduces food intake and hepatic glucose production (Kurata et al., 1986; Obici et al., 2003; Pociu et al., 2006; Pociu et al., 2005; Wortman et al., 2003). Conversely, disturbing glucose metabolism or increasing fatty acid oxidation rates within neurons drives food intake and causes obesity (He et al., 2006; Miselis and Epstein, 1975; Smith and Epstein, 1969; Zhou et al., 2011). Although these studies do not target specific neuronal populations, but always simultaneously act on glucose inhibited and glucose excited neurons, they highlight the importance of metabolic flexibility within neurons for whole body energy homeostasis.

Numerous mouse models demonstrate that interrupting central glucose or fatty acid metabolism at various steps affects nutrient sensing, beginning with detection of glucose or fatty acids by its respective receptors (Le Foll et al., 2009; Miyamoto et al., 2016; Moulle et al., 2013; Stolarczyk et al., 2010).

Glucose sensing pathways

The glucose transporter Glut2 can signal glucose availability independently of glucose metabolism through a cytoplasmic loop domain (Stolarczyk et al., 2010) and mutating this domain without affecting glucose transport causes an increase in meal size (Stolarczyk et al., 2010). Metabolic processing of glucose via glycolysis is also important for hypothalamic glucose sensing (Cheng et al., 2008) since preventing phosphorylation of glucose via glucokinase prevents elevation of calcium oscillation in GE neurons (Dunn-Meynell et al., 2002). Conversely, GI neurons maintain high Ca^{2+} oscillation after glucokinase inhibition which elicits a *cfos* response in AgRP neurons and induces feeding (Dunn-Meynell et al., 2002; Kang et al., 2006; Zhou et al., 2011).

Numerous studies suggest also a role for astrocytes in glucose sensing (Ainscow et al., 2002; Guillod-Maximin et al., 2004; Marty et al., 2007; Meng et al., 2016) communicating glucose availability to neurons. Glucose is taken up by astrocytes and metabolised to lactate, which is then shuttled to neighbouring neurons via lactate-monocarboxylate transporter. Indeed, an increase in central lactate has similar anorectic effects to increased central glucose, reducing food intake and body weight (Lam et al., 2008). In neurons, lactate is metabolised to pyruvate, joins then the glucose metabolism pathway feeding into the tricarboxylic acid (TCA) cycle and hypothalamic pyruvate metabolism also regulates blood glucose levels (Lam et al., 2005a). Although glucose and fatty acid metabolism cannot be simultaneously active within a cell at the same time, due to the Randle cycle, the ability to sense glucose via astrocytes may offer some degree of coupling glucose and fat metabolism within the same cell. This assumption, however, requires future experimental proof.

Glycolysis generates NADH (Cheng et al., 2008), which provides redox equivalents for oxidative phosphorylation and increases ATP to ADP ratio within neurons. Since the cellular energy sensor AMPK is sensitive to adenosine nucleotides and is inhibited by a greater ATP:ADP or AMP ratio, this provides another modulatory pathway to mediate neuronal responses to changing glucose levels (Beall et al., 2012; Claret et al., 2007). AMPK controls *Ucp2* gene expression in response to glucose (Beall et al., 2012; Xie et al., 2008) and UCP2 controls mitochondrial fission and reduces ROS (Toda et al., 2016) while ROS signalling is

required for hypothalamic glucose sensing (Leloup et al., 2006) by activating TRPC3 channels (Chretien et al., 2017). Moreover, the glucose metabolism increased ATP to ADP ratio causes the closure of ATP sensitive potassium (KATP) channels, depolarizes the cell membrane and regulates action potential frequency (Kong et al., 2010; Miki et al., 2001; van den Top et al., 2007).

These studies highlight the overarching importance of glycolysis for glucose sensing. Moreover, they emphasise that glucose metabolism within neurons initiates a signalling cascade that is not only involving catabolism of glucose but also elicits changes on a transcriptional and electrical level that convey information about glucose availability and is shared with fatty acid sensing (Figure 1.1).

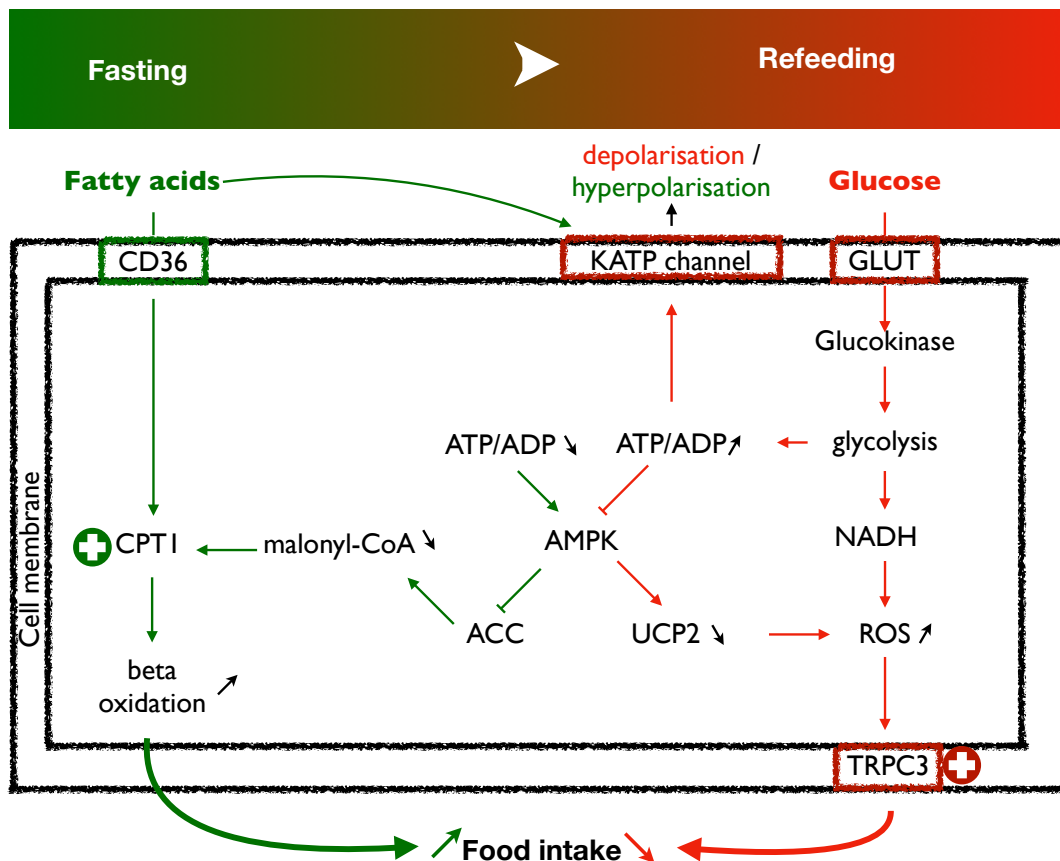


Figure 1.1 Nutrient sensing pathways in neurons

Metabolic sensing neurons take up fatty acids and glucose through their specific receptors. The catabolism of glucose elicits a signalling cascade (red arrows) leading to cell membrane depolarisation and reduced food intake, whereas fatty acid metabolism increases food intake (green arrows). AMPK functions as an energy sensor, activated by high energy states (high ATP/ADP ratio) and inhibited by low energy (ATP) availability, connecting both pathways and allows the sensing of changes in nutritional state.

Fatty acid sensing pathways

Fatty acid sensing is also mediated by AMPK and KATP channels. AMPK activity inhibits acetyl CoA carboxylase (ACC) which facilitates the conversion of acetyl CoA to malonyl CoA, a CPT1 inhibitor, thus promotes hypothalamic fatty acid metabolism (Andrews et al., 2008; Taib et al., 2013) and food intake (Yavari et al., 2016). Moreover, free fatty acids (FFA) induce autophagy in AgRP neurons and promote AgRP peptide expression to drive food intake (Kaushik et al., 2011)

But fatty acids, specifically oleic acid, can also interact directly with KATP channels to regulate food intake and glucose homeostasis (Branstrom et al., 1997; Dadak et al., 2017; Lam et al., 2005b; Obici et al., 2002) and modulate the excitability of neurons in a glucose concentration-dependent manner (Wang et al., 2006), highlighting the interdependence and integration of glucose and fatty acid sensing.

This shows, together with hormonal influence on metabolic-sensing neurons that they are a relay station for various streams of information from the periphery about the metabolic state, that computes and integrates metabolic feedback signals to maintain energy homeostasis.

In summary, competition between glucose and fatty acid metabolism within specific neurons affects whole body metabolism, regulates feeding and glucose production. The efficient switching between both metabolic pathways depending on substrate availability requires a convergence point controlling a common intermediate, enabling the proficient inhibition of one pathway by a product of the other as described for the glucose-fatty acid cycle (Randle et al., 1963). We found that the carnitine cycle and specifically carnitine acetyltransferase (Crat) to be such a convergence point regulating mitochondrial acetyl CoA levels (Stark et al., 2015a) and will demonstrate the importance of Crat in AgRP neurons for regulating peripheral substrate utilisation in Chapter 2.

1.4 Carnitine metabolism

Carnitine is mostly derived from dietary intake (up to 75%, mainly red meat) through intestinal absorption, but also renal recycling and endogenous biosynthesis from lysine and methionine provide carnitine (Rebouche, 2004; Steiber et al., 2004). Once available, the carnitine specific sodium-dependent organic cation transporter 2 (OCTN2) regulates

transport and uptake into tissues including heart, muscle, and brain from the circulation (Tamai et al., 1998).

The primary role of carnitine is the transport of acyl moieties across membranes. Long-chain fatty acids entering neurons get rapidly esterified to long chain fatty acyl-coenzyme A (LC acyl CoA), but in this form, they cannot pass the mitochondrial membrane for beta oxidation. To get into the mitochondrial matrix they use the carnitine shuttle, a cascade of enzymes that, in the periphery, play an important role in metabolism by maintaining appropriate substrate utilisation and mitochondrial function.

Dysfunctional carnitine metabolism can lead to severe insulin resistance, type-2 diabetes, obesity, early ageing and cardiovascular disease and is also seen in mouse models of RETT syndrome (Mucerino et al., 2017; Muoio et al., 2012; Noland et al., 2009; Power et al., 2007; Sharma and Black, 2009; Sharma et al., 2012). Carnitine metabolism is used to reversibly transfer acyl groups between carnitine and coenzyme A and a class of enzymes known as carnitine acyltransferases perform these reactions. The homology between nuclear encoded acyltransferases is high with differences in one or two amino acids in the acyl binding pocket defining the substrate chain length specificity (Cordente et al., 2006). Carnitine palmitoyltransferase (CPT) binds specifically long chain acyl CoA, carnitine octanoyltransferase (Crot) binds medium-chain acyl CoA, and carnitine acetyltransferase (Crat) binds short-chain acyl CoAs.

The most common carnitine acyltransferase is CPT and exists in three isoforms in the body. CPT1a is predominantly expressed in liver and brain. CPT1b is a specific muscle isoform, with little or no expression in the brain. CPT1c is only found in the brain but without acyl CoA transferase activity. CPT1a and CPT1c are both involved in the central regulation of energy homeostasis (Dai et al., 2007; Lee and Wolfgang, 2012; Obici et al., 2003). A recent study demonstrated that CPT1c regulates peripheral nutrient partitioning (Pozo et al., 2017). Specifically, they show that mice lacking CPT1c have impaired metabolic flexibility and are unable to switch from carbohydrate to fat metabolism with fasting due to impaired fasting-induced fatty acid oxidation in liver and muscle (Pozo et al., 2017).

The CPT system facilitates the transport of long chain fatty acyl CoA from cytosol into the mitochondrial matrix, the site of beta oxidation. This transport system consists of carnitine palmitoyltransferase 1 (CPT1), carnitine acylcarnitine translocase (CACT) and palmitoyltransferase 2 (CPT2). Indeed, CPT1-mediated fatty acid transport in mitochondria is critical to metabolism and human CPT1 deficiencies cause a host of severe metabolic

symptoms including muscle weakness, metabolic acidosis, hypoketotic hypoglycemia and central nervous system abnormalities (Longo et al., 2006; Sharma et al., 2009). However, carnitine metabolism also plays a key and often underappreciated role in glucose metabolism by regulating mitochondrial efflux of acetyl CoA. Beta-oxidation of acyl CoA generates acetyl CoA, which is the primary precursor entering the mitochondrial tricarboxylic acid (TCA) cycle for energy production and an allosteric inhibitor of glucose metabolism by inhibiting the key glycolytic enzyme pyruvate dehydrogenase (PDH). Crat regulates the pool of acetyl CoA in the mitochondrial matrix by catalysing a reaction that uses carnitine and acetyl CoA to produce acetylcarnitine. Carnitine supplementation studies in obese and diabetic rats demonstrated an improvement in whole body glucose tolerance (Noland et al., 2009), linking carnitine availability and glucose metabolism and indicating that perturbations in carnitine metabolism may contribute to glucose intolerance and impaired metabolic flexibility (Muio et al., 2012; Noland et al., 2009; Power et al., 2007). This places Crat as a key enzyme regulating mitochondrial substrate selection.

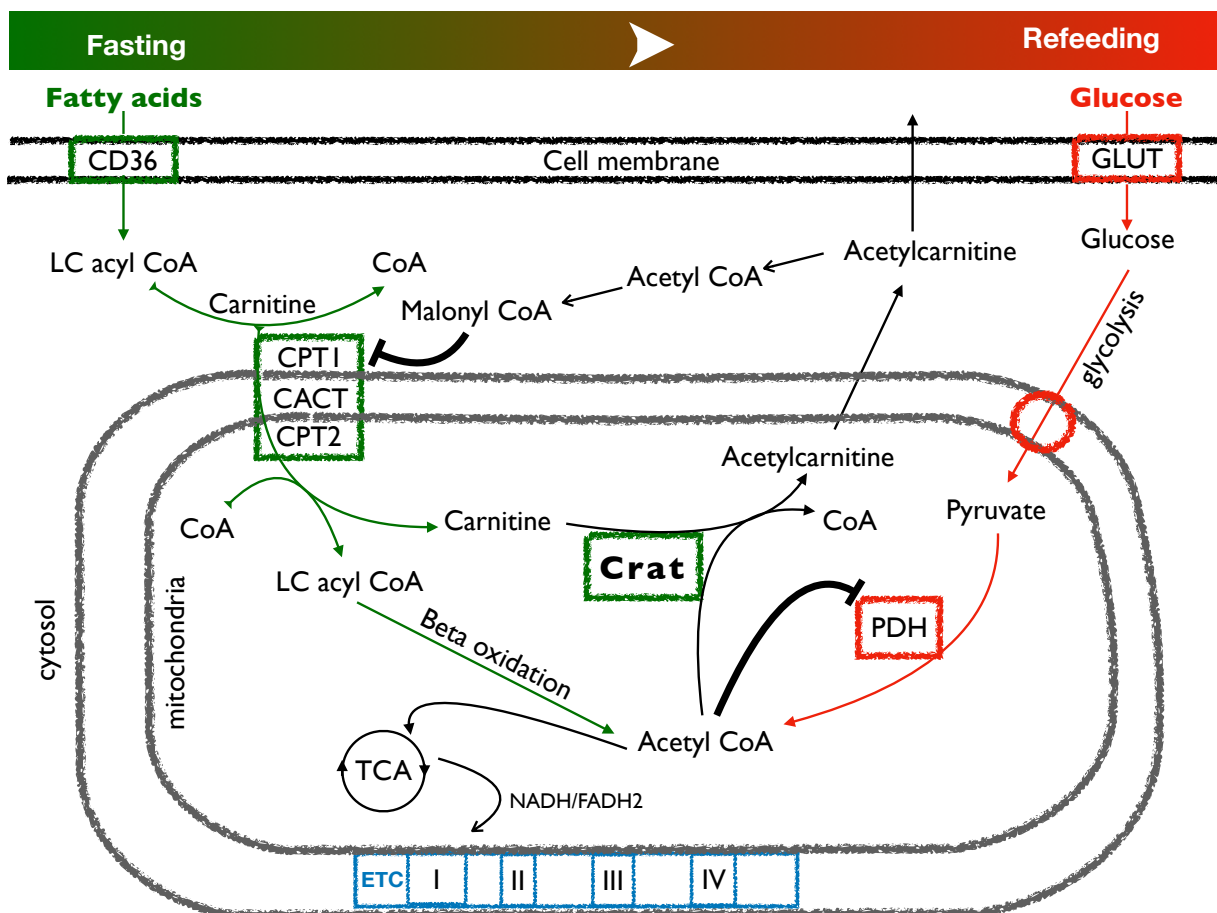


Figure 1.2 Carnitine cycle regulates both fatty acid and glucose metabolism.

The carnitine shuttle allows the transport of long chain acyl CoA (LC acyl CoA) across membranes. CPT1 conjugates cytosolic acyl CoA to carnitine and is sensitive to inhibition from malonyl-CoA generated by cytosolic acetyl CoA. CACT (carnitine acylcarnitine translocase) is the mitochondrial exchange carrier of carnitine and its esters. CPT2 is localised on the inner mitochondrial membrane with the catalytic domain facing the matrix where it conjugates acyl-carnitine back to its acyl-CoA

ester in order to undergo beta-oxidation. Acetyl CoA, product of beta-oxidation or pyruvate decarboxylation can enter the tricarboxylic acid (TCA) cycle only when redox equivalents (NAD⁺, FAD) are available to receive electrons for the electron transfer chain (ETC). High intra-mitochondrial acetyl CoA levels inhibit pyruvate dehydrogenase (PDH) and thus reduce the rate of glycolysis. The short chain carnitine acyltransferase Crat (Carnitine acetyltransferase) is localised within the mitochondrial matrix and converts acetyl CoA into acetylcarnitine, which can translocate into the cytosol. Thus, Crat regulates intra-mitochondrial acetyl CoA levels and therefore pyruvate dehydrogenase (PDH) activity and glucose metabolism. Hence, Crat is juxtaposed perfectly between beta-oxidation and glycolysis to control substrate switching between fat and glucose metabolism during the transition from fasting to refeeding.

In aggregate, acyl CoA trafficking through carnitine metabolism not only permits beta oxidation but also allows the control of glucose metabolism and therefore provides the means necessary to regulate substrate selection. A key enzyme of the carnitine cycle is carnitine acetyltransferase as it buffers the mitochondrial acetyl CoA pool and therefore influences PDH activity.

1.5 Carnitine acetyltransferase

Although Crat is subject to studies extensively investigating the physiological function of the enzyme in heart, muscle, and liver, little is known about its role in the brain.

Human Crat deficiency causes severe degeneration of Purkinje cells in the cerebellum and fatal ataxic encephalopathy linked to a functional defect of acetyl CoA utilisation (DiDonato et al., 1979; Melegh et al., 1999; Przyrembel, 1987). Moreover, exogenously administered acetyl-carnitine is rapidly taken up by the brain (Rebouche, 2004), increases cerebral metabolic rates (Freo et al., 2009), provides acetyl groups for neurotransmitter synthesis (Dolezal and Tucek, 1981; Scafidi et al., 2010; Smeland et al., 2012) and has neuroprotective and antidepressant effects (Ferreira and McKenna, 2017; Smeland et al., 2012; Tang et al., 2016).

As mentioned above, Crat catalyses the reversible reaction of acetyl CoA onto carnitine to generate acetylcarnitine, thus buffering the mitochondrial acetyl CoA pool, and permitting the export of acetyl groups out of the mitochondria into the cytosol. Protein acetylation disrupts or regulates protein function, and generally, enzymes of the deacetylase family of sirtuins are described to control acetylation status and thus protein function (Anderson and Hirschey, 2012; Osborne et al., 2016). Recent studies have demonstrated that also Crat controls protein acetylation within mitochondria through regulating acetyl CoA export into the cytosol (Davies et al., 2016). This spatial regulation of acetyl CoA controls concentration-dependent non-enzymatic acetylation of proteins in mitochondria and cytosol (James et al.,

2017) and may attribute to SIRT3 function in the adaptive responses of neurons to metabolic and excitatory challenges (Cheng et al., 2016).

As mentioned above, the regulation of acetyl CoA is important for glucose metabolism and metabolic flexibility (Noland et al., 2009) as acetyl CoA allosterically inhibits PDH. Additionally, acetyl CoA export into the cytosol provides substrate for acetyl CoA carboxylase to generate malonyl CoA, an inhibitor of CPT1, thus regulating beta oxidation. Moreover, Crat itself is reversibly inhibited by long chain acyl CoA (Chase, 1967) so that oversupply of fatty acyl CoA can inhibit glucose metabolism and cause mitochondrial stress (Seiler et al., 2014).

Studies on Crat deficient myocytes demonstrate the importance of Crat for the transition from fatty acid to glucose oxidation (Muio et al., 2012). In muscle, this switch in substrate utilisation is crucial during the transition from fast to a fed state, however, whether or not this is important in AgRP neurons has not been examined.

Considering that metabolic flexibility in neurons is important for the regulation of peripheral metabolism (Moreno et al., 2013) and that AgRP neurons contribute to peripheral substrate selection, we hypothesised that Crat in AgRP neurons regulates peripheral substrate selection and metabolic flexibility. To test this hypothesis, we created a mouse model with specific deletion of Crat in AgRP neurons to investigate the role of Crat in AgRP neurons.

1.6 Project goals

In muscle, Crat provides the metabolic flexibility necessary to respond to changing substrate availability (Muio et al., 2012). This is achieved by controlling the mitochondrial pool of acetyl CoA and subsequently glucose and fatty acid metabolic flux for energy production. The studies presented herein were designed to address the function of Crat in AgRP neurons. These data demonstrate the importance of Crat in AgRP neurons during fasting and the transition from fasting to refeeding and suggest that Crat is part of the molecular mechanism in AgRP neurons that facilitates the efficient peripheral switch from fatty acid oxidation to glucose metabolism during the transition fast/refeeding.

In Chapter 2 we aim to define the role of Crat in AgRP neurons as a molecular substrate switch allowing the efficient transition from predominantly peripheral fatty acid oxidation during fasting to peripheral glucose oxidation upon refeeding. Hypothalamic CPT1c, another enzyme of the carnitine cycle, regulates substrate selection from glucose to fatty acid metabolism during the converse transition from fed state to fasting (Pozo et al., 2017). This

underlines the importance of neuronal carnitine metabolism for whole body metabolism regulation.

We explore the effects of Crat deletion in AgRP neurons and report on the consequences of AgRP neuronal Crat deficiency for feeding behaviour and peripheral metabolism during fasting and refeeding. AgRP Crat KO mice have increased lipolysis and are unable to effectively inhibit lipid utilisation upon refeeding. Although this had no consequences for body weight and body composition after an overnight fast, there is the potential that this is affected during prolonged calorie restriction as seen in NPY KO mice (Park et al., 2017).

Consequently, the aim in Chapter 3 is to examine the magnitude of this defect for body fat loss during calorie restriction. We highlight also the consequences of impaired nutrient partitioning for rebound weight gain and adiposity. Furthermore, we show the inability of AgRP Crat KO mice to adapt feeding behaviour and thermogenesis to reduced food availability with consequences for energy expenditure.

Because of this lack of adaptation of feeding behaviour, and because it is shown that AgRP neurons are required for adaptation to restricted feeding (Tan et al., 2014), the aim of Chapter 4 is to investigate the possibility that Crat regulates adaptation to restricted feeding. We suggest that Crat is a critical component of an energy calculator in AgRP neurons assessing acute changes in metabolic state and that Crat deficiency results in paradoxical reduced food intake despite increased food anticipatory activity developed during time restricted feeding.

In summary, our data suggest Crat in AgRP neurons plays a fundamental role regulating substrate utilisation and feeding behaviour. We demonstrate that the lack of Crat exclusively in AgRP neurons impairs metabolic flexibility and discuss herein implications and conceivable future research.

Chapter 2: AgRP neurons require carnitine acetyltransferase (Crat) to regulate metabolic flexibility and peripheral nutrient partitioning

The results presented in this Chapter were accepted for publication in Cell Reports on 22.01.2018.

AgRP neurons require carnitine acetyltransferase (Crat) to regulate metabolic flexibility and peripheral nutrient partitioning

Alex Reichenbach^{1,2}, Romana Stark^{1,2}, Mathieu Mequinion^{1,2}, Raphael R.G. Denis³, Jeferson F Goularte¹, Rachel E Clarke^{1,2}, Sarah H Lockie^{1,2}, Moyra B Lemus^{1,2}, Greg M Kowalski⁴, Clinton R Bruce⁴, Cheng Huang^{1,5}, Ralf B Schittenhelm^{1,5}, Randall L Mynatt^{6,7}, Brian J Oldfield^{1,2}, Mathew J Watt^{1,2}, Serge Luquet³, Zane B Andrews^{1,8}

1. Monash Biomedicine Discovery Institute, Monash University, Clayton 3800, Victoria, Australia

2 Department of Physiology, Monash University, Clayton 3800, Victoria, Australia

3 Université of Paris Diderot, Sorbonne Paris Cité, Unité de Biologie Fonctionnelle et Adaptative, CNRS UMR 8251, F-75205 Paris, France.

4 Institute for Physical Activity and Nutrition, School of Exercise and Nutrition Sciences, Deakin University, Burwood 3125, Victoria, Australia.

5 Monash Biomedical Proteomics Facility & Department of Biochemistry, Monash Biomedicine Discovery Institute, Monash University, Clayton 3800, Victoria, Australia

6 Gene Nutrient Interactions Laboratory, Pennington Biomedical Research Center, Louisiana State University System, Baton Rouge, Louisiana, USA.

7 Transgenic Core Facility, Pennington Biomedical Research Center, Louisiana State University System, Baton Rouge, Louisiana, USA

8 Corresponding author and Lead Contact:

A/Prof Z. B. Andrews: Email: [REDACTED] Tel: [REDACTED]

Keywords: Fatty acid utilisation, Energy availability, Substrate switch, Glucose, Fasting, Refeeding, Liver, Acetylation, SNS, Metabolism

2.1 Abstract

AgRP neurons control peripheral substrate utilisation and nutrient partitioning during conditions of energy deficit and nutrient replenishment, although the molecular mechanism is unknown. We examined whether carnitine acetyltransferase (Crat), in AgRP neurons affects peripheral nutrient partitioning. Crat deletion in AgRP neurons reduced food intake, feeding behaviour and increased glycerol supply to the liver, as a gluconeogenic substrate, during fasting, which was mediated by changes to sympathetic output and peripheral fatty acid metabolism in the liver. Crat deletion in AgRP neurons increased peripheral fatty acid substrate utilisation and attenuated the switch to glucose utilisation after refeeding indicating altered nutrient partitioning. Proteomic analysis in AgRP neurons shows that Crat regulates protein acetylation and metabolic processing particularly during fasting and refeeding. Collectively, our studies highlight that AgRP neurons require Crat to provide the metabolic flexibility to optimise nutrient partitioning and regulate periphery substrate utilisation, particularly during fasting and refeeding.

2.2 Introduction

The maintenance of energy and glucose homeostasis requires the ability of the brain to detect and respond to acute changes in energy state. Under conditions of energy deficit, sensing low peripheral energy availability and hypoglycaemia primes the brain to initiate food intake and increase hepatic glucose production (Kleinridders et al., 2009). Agouti-related peptide (AgRP) neurons in the arcuate nucleus of the hypothalamus are a population of starvation-sensitive neurons that primarily function to increase appetite and promote energy conservation (Aponte et al., 2011; Gropp et al., 2005; Krashes et al., 2011; Luquet et al., 2005; Ruan et al., 2014). For example, the adult ablation of AgRP neurons in mice causes a rapid cessation of food intake and profound body weight loss, to the point of starvation (Luquet et al., 2005).

AgRP neurons primarily respond to signals of energy deficit and increase firing rates, mRNA expression and peptide secretion (Andrews et al., 2008; Baskin et al., 1999; Briggs and Andrews, 2011; Schwartz et al., 1998) in order to maintain energy homeostasis. Although AgRP neurons can respond to metabolic information in the form of hormonal feedback from ghrelin, leptin and insulin (Andrews, 2011; Andrews et al., 2008; Enriori et al., 2007; Konner et al., 2007; van de Wall et al., 2008; Wang et al., 2014) the mechanisms underlying nutrient sensing are less clear. This is not only important during fasting, but also during the transition from fasting to refeeding when there is a dynamic change in metabolic feedback information to the brain. An appropriate level of metabolic flexibility ensures that as glucose comes available for oxidation, such as during refeeding, high fasting fatty acid utilisation and oxidation is immediately suppressed to conserve energy reserves. Indeed, the ablation of AgRP neurons increases fatty acid utilisation, affects nutrient partitioning and attenuates body weight gain in mice fed a high fat diet (Joly-Amado et al., 2012). Thus, the ability of AgRP neurons to rapidly adjust substrate utilisation promotes maximal energy conservation and is a core component of nutrient partitioning. However, the molecular mechanism responsible for this action in AgRP neurons remains unknown.

Carnitine acetyltransferase (Crat) is an important enzyme regulating metabolic flexibility in muscle and increases exercise capacity (Muoio et al., 2012; Seiler et al., 2015). Crat is a fundamental enzyme in carnitine metabolism and is one of a number of enzymes, including carnitine palmitoyltransferase 1 (CPT1) and carnitine octanoyltransferase, involved in regulating intracellular pools of acyl-CoA esters (Ramsay and Zammit, 2004; Stark et al., 2015a). In mice with muscle-specific deletion of Crat, excessive build-up of acetyl-CoA allosterically inhibits glucose oxidation by suppressing pyruvate dehydrogenase activity and impairs the substrate switch from fatty acid to glucose oxidation during the fast/refeeding transition (Muoio et al., 2012). Consequently, we hypothesised that Crat plays an important role in AgRP neurons by providing the metabolic flexibility to respond to metabolic information particularly during fasting and the transition to refeeding, when

the need to detect and respond to energy availability is most important. Our results show that Crat in AgRP neurons influences feeding behaviour, hepatic substrates for gluconeogenesis and fatty acid metabolism, peripheral substrate utilisation and nutrient partitioning, and the AgRP proteome during fasting and the transition to refeeding.

2.3 Experimental Procedures

Animals

All experiments were conducted in compliance with the Monash University Animal Ethics Committee guidelines. Male mice were kept at standard laboratory conditions with free access to food (chow diet, cat no. 8720610 Barastoc stockfeeds, Victoria Australia), and water at 23 ° C in a 12-hour light/dark cycle and were group-housed to prevent isolation stress, unless otherwise stated. All male mice were aged 8 weeks or older for experiments unless otherwise stated. All male mice were aged 8 weeks or older for experiments unless otherwise stated. AgRP-ires-cre mice were obtained from Jackson Laboratory AgRP^{tm1(cre)Low/J} (stock no. 012899) and bred with NPY GFP mice (B6.FVB-Tg(Npy-hrGFP)1Lowl/J; stock number 006417; The Jackson Laboratory, Maine, USA). AgRP-ires-cre::NPY GFP mice were then crossed with *Crat*^{fl/fl} mice donated by Randall Mynatt (Pennington Biomedical Research Center, LA, USA) in order to delete *Crat* from AgRP neurons (AgRP *Crat* KO). These mice were also crossed to B6.Cg-Gt(Rosa)26Sor^{tm14(CAG-td-Tomato)Hze/J} to visualise cre-mediated recombination in AgRP neurons.

Food intake Experiments

To assess the impact of *Crat* deletion on food intake and feeding behaviour, mice were singled housed in specialised feeding cages (BioDAQ; Research Diets, NJ, USA), recordings were analysed after a three-day acclimation period. These cages were fitted with computer controlled automatic gates to prevent access to feeding hoppers during fasting experiments to allow stress free intervention without human interaction. Feeding behaviour after fasting, and short term fasting (3 hours) combined with i.p. CCK (0.25 µg/kg) or ICV insulin (0.025µU in 1.5 µl) administered at the onset of the active period were analysed. The ICV route was chosen to avoid potential indirect feedback effects caused by peripheral insulin.

For ICV surgery, mice were anaesthetised with isoflurane, and anaesthesia was maintained by constant nasal delivery of 2.5% isoflurane. Each animal received 50µL Metacam (0.25mg/mL Meloxicam; Boehringer Ingelheim) before the surgery to minimise post-surgery pain. The cannula was inserted into the third ventricle (1.0 mm lateral and 0.3 mm rostral to bregma to a depth of 2 mm).

BioDAQ feeding cage recordings were analysed using BioDAQ Data Viewer (v.2.3.09) and exported as excel files. We used following Data Viewer settings for analysing feeding behaviour:

Table 1 BioDAQ Data Viewer settings for analysis of feeding behaviour

Experiment /feeding behaviour	Reset on	Periods	Bout filter [include]	Inter meal interval	Meal minimum	comments
Ad lib food intake	Time of day [start light phase]	96 (15 min per period)	0-3g			
Ad lib meals	None		0-3g	300 sec	0.02g	6 consecutive days separately extracted, started just before dark phase
Refeeding food intake	Time of day [start refeeding]	96 (15 min per period)	0-3g			
Refeeding meals	None		0-3g	300 sec	0.02g	24hour recording after start refeeding
CCK IP food intake	Time of day [start at time of injection]	24 (1hour per period)	-0.01-9g			
CCK IP meals	Time of day [start at time of injection]	1 period (24hour per period)	-0.01-9g	300 sec	0.02g	
Insulin ICV food intake	Time of day [start at time of injection]	24 (1hour per period)	-0.01-9g			
Insulin ICV meals	Time of day [start at time of injection]	1 period (24hour per period)	-0.01-9g	300 sec	0.02g	

High fat diet feeding

Eight-week-old mice were placed on either chow (no. 8720610; Barastoc Stockfeeds) or high fat diet (Diet SF04-00; Specialty Feeds, Glen Forrest, Australia) for 20 weeks and bodyweight was measured weekly. Body composition (DEXA) was measured before and after 4, 8, 12, 16 and 20 weeks on HFD. To assess metabolic profiling during HFD feeding, mice were placed after 9 weeks on HFD in CLAMS for 4 days.

Gastric emptying

Acetaminophen enters the bloodstream only after it passes the stomach, so that the appearance of it in blood samples can be used as an estimate for gastric emptying. Mice were fasted for 6 hours, before receiving an oral gavage with a glucose solution (1.5g/kg BW) containing acetaminophen (0.1g/kg BW, Sigma-Aldrich). Plasma samples were taken before and 15, 30, 45, 60 and 120 minutes after the gavage. Acetaminophen in plasma samples were determined using a colorimetric assay (Acetaminophen LiquiColor Test, Stanbio Laboratory). Briefly, 10µl standards/samples were incubated with 200µl working reagent at 37C for 15 min and absorbance measured at 615nm.

Leptin treatment

Mice were singly housed for 3 days before injecting them with either saline or leptin twice daily (9am and 5pm). Blood glucose (ACCU-CHEK® Active, Roche Diagnostics GmbH, Tokyo, Japan), body weight and food intake were measured in the morning before injections.

Metabolic studies

For the triglyceride tolerance test mice had no access to food, starting the fast 3 hours before onset of the light phase. At this time baseline blood glucose measurement and plasma sample (10µl) for TG were taken, before mice received an oral gavage (15µl/g bodyweight) of olive oil. Additional samples for blood glucose measurements and plasma TG were taken at 2, 4, 6, 8 hours after gavage. For the lipoprotein lipase inhibition assay, animals were fasted for five hours and baseline blood glucose and plasma sample (10µl) were taken before receiving tyloxapol (300mg/kg bodyweight, i.p.). Additional blood glucose measurements and plasma samples were taken at 30, 60, 90, 120, 180, 240 minutes after injection.

For oral glucose tolerance tests (oGTT; 1.5g/kg) and glycerol tolerance test (GlyTT; 1g/kg i.p.), mice were fasted from 8am in the morning and tests were performed five hours later at 1pm. Blood glucose measurements were collected before and 15, 30, 60 and 120 min after injection. To distinguish between exogenous glucose and endogenous glucose concentrations during an oGTT, mice received a gavage of stable isotope labelled glucose (6,6²H glucose, Sigma Aldrich, USA, 1.5g/kg).

Labelled oGTT

This approach allows for the simultaneous estimate of endogenous glucose production and glucose disposal under conditions that mimic a postprandial change in glucose handling. Plasma was collected and used to perform mass isotopomer analysis of glucose via gas chromatography-mass spectrometry. This process allows for the identification of blood glucose from the labelled glucose load (M1 and M2 isotopomers representing glucose disposal) or from the unlabelled M0 glucose isotopomer, representing glucose from endogenous sources. Samples were deproteinized by adding 50 μ l of ice cold methanol to 2 μ l of plasma and centrifuged (4 °C, 16,000 rpm, 10 min). The supernatant was dried and methoximated at 90 °C for 1 h (20 μ l methoxyamine HCl in pyridine 20 mg/ml; Supelco, Sigma-Aldrich, St. Louis, USA). 20 μ l of N,O-bis(trimethylsilyl) trifluoroacetamide (BSTFA) + 1% trimethylchlorosilane (TMCS) (Thermo Fisher Scientific, Waltham, USA) was used to convert methoximated glucose to the TMS derivative. Samples were analysed using a 7890A gas chromatography (GC) system and a 5975C mass selective detector (MSD) (Agilent Technologies, Santa Clara, USA) in positive chemical ionisation (PCI) mode using methane as a reagent gas and helium as a carrier. The GC was equipped with a DB5 capillary column with a 10 m inert duraguard (J&W Scientific, 30 m, 250 μ m inner diameter, 0.25 μ m film thickness). The injector insert and GC-MS transfer line temperatures were 270 and 250 °C, respectively. The oven temperature gradient was set to: 70°C(1min);70°C to 295°C at 12.5°C/min; 295°C to 320°C at 25 °C/min; 320 °C for 2 min. Sample (1 μ l) was injected with the inlet set to split mode (split ratio 10 ml/min). The isotopomers of glucose TMS derivatives were identified and quantitated by selected ion monitoring (SIM) for ions m/z 554 to 562 corresponding to M0 to M8 of the fragment $[M + 1-16]^+$ of methyloxime penta-TMS glucose (m/z 569). The mass isotopomer abundances were determined using Mass Hunter Workstation (Agilent Technologies, Santa Clara, USA). M0 (endogenous glucose), M1 (2-²H glucose) and M2 (6,6-²H glucose) isotopomers were multiplied by the blood glucose concentration at each corresponding time point of the OGTT to calculate the absolute concentrations of load (labelled) and endogenous (unlabelled) glucose.

Endogenous glucose production

To measure the source of endogenous glucose production in a dynamic physiological setting, mice were injected with D₂O (0.9%NaCl in D₂O, 25ml/kg bodyweight, i.p.) and 10% D₂O mixed into drinking water. Five hours after injection, mice were subjected to a fast and plasma samples (20 μ l) were taken after 3 and 18 hours of fasting. The enrichment in plasma samples was measured via GC-MS as previously published (Kowalski et al., 2015)

Deuterium is an isotope of hydrogen with twice the mass due to the addition of a neutron to the deuterium atom. Deuterium is incorporated into metabolic intermediates of gluconeogenesis, so that circulating glucose receives a unique deuterium label depending on the gluconeogenic substrates it is derived from. Determination of deuterium enrichment on the 6 carbon atoms in glucose allows for

calculation of substrate contribution for endogenous glucose production. By measuring the ratio of ^2H enrichment in plasma glucose at carbon 5 and 2 (C5/C2) the proportion of glucose from gluconeogenesis (all substrate source) was calculated. The proportion of glucose glycogenolysis is calculated by subtracting the C5/C2 ratio from 1 (1-C5/C2). Sources of gluconeogenesis can be further separated by measuring the enrichment of ^2H at carbon 6 vs 2 (C6/C2) in plasma glucose while that from glycerol gluconeogenesis is estimated by calculating the difference between all source gluconeogenesis and PEP gluconeogenesis (C5/C2-C6/C2). 20 μl plasma was used to the ^2H enrichment in individual positions of glucose by measuring the enrichment (M0–M4) in six ions from three different glucose derivatives: glucose aldonitrile pentapropionate (5 μl plasma; m/z 173, m/z 259, m/z 284, m/z 370), glucose 1,2,5,6-di-isopropylidene propionate (10 μl plasma; m/z 301) and glucose methyloxime pentapropionate (5 μl plasma; m/z 145). The derivatives were analysed using an Agilent HP 6890 GC system coupled to an Agilent HP 5973 MSD (Agilent Technologies, Santa Clara, USA) in electron ionisation (EI) mode with helium as a carrier gas. The GC column and temperature settings were as described above for the analysis of penta-TMS glucose in the stable isotope labelled oGTT. Following the measurement of the mass isotopomer abundances of the six glucose fragments using Mass Hunter Workstation, the enrichment in individual glucose positions was determined using Matlab software (MathWorks, Natick, MA, USA)

Glucose stimulated glucose uptake

To localise glucose uptake in tissue we performed oGTT (1.5g/kg) combined with intraperitoneal injection of 2- ^3H -DG tracer (10 μCi in 200 μl saline). Blood samples were collected before (0) and after 2, 5, 10, 15, 20 and 30 minutes after gavage. Tissues were harvested 15 min or 30 min post gavage and snap frozen in liquid N_2 . Radioactivity in blood and tissue were measured using a Beckman Coulter scintillation counter.

To measure radioactivity from blood samples, 10 μl blood were added to 100 μl ZnSO_4 (0.3N, Sigma Aldrich), topped with 100 μl BaOH (0.3N, Sigma Aldrich) and vortexed immediately. After centrifuging (2 min, 13000g) 100 μl supernatant were taken to measure radioactivity.

Tissues were weight and homogenised in 1.4 ml ZnSO_4 (2.75%), and 400 μl of this homogenate were mixed with 140 μl saturated BaOH . Both homogenates were centrifuged (10min, 13000g) and 400 μl of the supernatant were taken to measure radioactivity using a scintillation counter (Beckman Coulter Scintillation counter).

CLAMS

To assess energy expenditure of AgRP Crat mice during *ad libitum* Chow, fasting and refeeding, and HFD conditions, singled housed mice were placed in comprehensive lab animal monitoring system (Oxymax-CLAMS) and recordings were analysed after one day acclimation period.

Analysis of blood chemistry

Plasma Insulin (in-house ELISA assay), acylated and des-acylated ghrelin (Mitsubishi Chemical Medience Corp), glucagon (Yanaihara Institute, Inc), corticosterone (Abnova, Heidelberg, Germany), non-esterified fatty acid concentration (NEFA C Assay Kit, Wako Pure Chemical Industries, Japan), triglycerides (triglyceride Assay kit, Roche/Hitachi, Roche Diagnostics GmbH) and ketone bodies β -hydroxybutyrate colorimetric assay kit, Cayman chemical company, Ann Arbor, Mi, USA) were all measured according to manufacturers instructions. Liver glycogen concentrations were determined with glucose oxidase assay kit (Sigma Aldrich, Saint Louis, Missouri 63103 USA) after glucose extraction. Triglycerides were determined with Triglyceride assay kit (Roche/Hitachi, Roche Diagnostics GmbH).

PCR

Total RNA was extracted from tissue with Qiazol (Qiazol Sciences) per instruction manual and cDNA synthesis and real-time quantitative PCR was performed as described previously (Stark et al., 2015b). Briefly, frozen, crushed tissue was dispersed in Qiazol and incubated for 5 minutes, before adding chloroform and 15 seconds mixing using a Vortexer. After centrifuging the samples, the upper aqueous phase was transferred to a new tube and incubated with isopropanol for 10 minutes to form a precipitate. The samples were centrifuged and the pellet washed with 75% ethanol and then air dried. The dry RNA pellets were dissolved in Tris-EDTA buffer, and the concentration was measured with a Nano Drop 1000 (Thermo Scientific). cDNA was synthesised using iScript cDNA synthesis kit (170-8890; Bio-Rad Laboratories). Real-time quantitative PCR was performed using SYBR Green Mastermix using a Real Plex4 Mastercycler (Eppendorf). All reactions confirmed a single product of the expected size by melting curve and agarose gel electrophoresis. Reaction efficiencies for primers were greater than 1.90. mRNA levels were expressed as the $\Delta\Delta C(t)$ normalised to the house keeping gene, where $C(t)$ is the cycle threshold. Primers were synthesised by IDT technologies (former: geneworks). For details refer to Appendix, Table 2

Glucose extraction

The crushed and weight frozen tissue was digested in KOH at 70°C for 20 minutes. Saturated NaSO_4 and 95% ethanol were added, mixed and centrifuged for 10 minutes. The pellet was resuspended in deionised water and digested at 70°C for 10 minutes, before adding 95% ethanol, mixing and centrifuging. The precipitate was resuspended in amyloglucosidase buffer (0.3mg/ml amyloglucosidase in 0.25M acetate) and incubated at 37°C overnight.

Liver Triglycerides

The crushed and weight frozen tissue was incubated with a chloroform:methanol (2:1) solution overnight. Then, pure chloroform and 0.9% NaCl were added and 10 minutes incubated on a shaker, followed by a 10 minute centrifugation step at 2000 rpm. The chloroform phase was transferred to a

fresh glass tube and evaporated to complete dryness under N₂ at 40°C. The dried extract was dissolved in absolute ethanol for the triglyceride assay.

Ex vivo fat oxidation assay

To measure beta oxidation rates in liver and soleus muscle, animals were deeply anaesthetised with isoflurane and tissues were collected and incubated in Krebs buffer (4.5% NaCl, 5.75% KCl, 6.1% CaCl₂, 10.55% KH₂PO₄, 19.1% MgSO₄·7H₂O, 2% fatty acid free BSA, 5mM glucose, 0.5mM oleate) containing ¹⁴C-oleate (1μCi/ml) and ¹⁴CO₂ was captured in 1M NaOH for a period of 2 hours. Tissues were removed, washed and frozen, weight before homogenised in PBS and incubated in CHCl₃:CH₃OH (2:1 v:v) and centrifuged. ¹⁴C radioactivity was measured in NaOH and aqueous phase. Triacylglycerides, Diacylglycerides and monoacylglycerides of the organic phase were separated using thin layer chromatography and radioactivity measured, as described previously (Meex et al., 2015).

Norepinephrine turnover

Catecholamine turnover was measured on the basis of the decline in tissue NE content after the inhibition of catecholamine biosynthesis with alpha-methyl-DL-tyrosine methyl ester hydrochloride as described previously (Brodie et al., 1966). Mice (n=24 and n=31 WT and KO mice respectively) were fasted overnight and injected with Saline (n=11 and n=15 WT and KO mice respectively) or α-methyl-DL-p-tyrosine (n=13 and n=16 WT and KO mice respectively) (tyrosine hydroxylase inhibitor, 200 mg/kg i.p, Sigma-Aldrich, USA) one hour after onset of light phase. Three hours after injections, fasted or re-fed animals were culled and blood and tissues were collected and snap frozen in liquid N₂. The weighed tissues were suspended in 200μl of ice-cold solution 0.1M perchloric acid containing 0.4% EDTA, and homogenised for 2 min using a tissue lyser II (Qiagen), then the homogenates were centrifuged at 3000 × *t/min* for 30 min at 4 °C, the supernatant was centrifuged at 16,000 g for 2 min and analysis for monoamine content on the same day. Monoamine content were analysed by reversed phase-HPLC using a Shimadzu system connected to a Waters 2465 electrochemical detector (Waters 2465, Shimadzu USA) with a glassy carbon working electrode (0.7V, 10nA). Samples were injected onto a Kromasil® AIT column (length 250mm; internal diameter 4.6mm; particle size 5μm) at 30°C. The mobile phase consisted of an acetate buffer containing 100μM EDTA, 1mM octanesulfonic acid, and 15% v/v methanol (pH 3.1) and which was delivered at a constant flow rate of 1ml/min. This system allowed detection of monoaminergic compounds: serotonin (5-HT), 5-hydroxyindolacetic acid (5-HIAA), dopamine (DA), dihydroxyphenylacetic acid (DOPAC), homovanillic (HVA), epinephrine (AD) and norepinephrine (NE) with a limit detectability of 0.5pg/injected volume. Compounds were separated by an isocratic flow (88% A/12% B) and quantified with LabSolution software (Shimadzu) by integration of the peak absorbance area, employing a calibration curve established with known concentrations. Norepinephrine turnover rates

were calculated after log transformation by $\log(\text{saline}) - \log(\alpha\text{MPT}) / 0.434$, where 0.434 is an estimate for the kinetic rate (Brodie et al., 1966)

AgRP neuron isolation

Hypothalamus was quickly dissected on ice and dissociated using papain dissociation system (Worthington Biochemical Corporation, Lakewood, NJ, USA) per kit instructions. Suspensions were sorted for GFP positive cells using an Influx cell sorter (Becton Dickinson (BD), Franklin Lakes, NJ, USA). We pooled sorted NPY GFP cells from 3 mice and thus each sample represents pooled protein from 3 mice treated in the same manner.

Proteomics of AgRP neurons

Approximately 70,000 GFP FAC sorted counts (range 60,000-110,000) were lysed in 50 μ l of 1% (w/v) sodium deoxycholate (SDC), 100mM Tris pH 8.0 for 5 min at 95°C. Samples were then sonicated for three cycles on a MSE Soniprep 150 Plus (15s on / 15s off at amplitude 10) and the protein concentration was determined using a Nano Drop 1000 (Thermo Scientific). Approx. 10 μ g of protein per replicate were then reduced for 30 min at 50°C using 10mM TCEP (tris(2-carboxyethyl)phosphine) followed by alkylation at room temperature in the dark for 20 min with 20mM chloroacetamide. Then, the samples were digested overnight with trypsin (Trypsin Gold, Promega) at 37°C. The digestion was stopped by adding formic acid to a final concentration of 5%, SDC was removed using 100% water-saturated ethyl acetate. Then, samples were cleaned with SDB-XC Stage-Tip (Rappsilber et al., 2007). After elution, peptides were dried in the SpeedVac and resuspended in 10 μ l of 2% ACN, 0.1% FA. Each sample has been repeated 3 times independently. A top12 method was applied with ms1 scan.

Using a Dionex UltiMate 3000 RSLCnano system equipped with a Dionex UltiMate 3000 RS autosampler, the samples were loaded via an Acclaim PepMap 100 trap column (100 μ m x 2 cm, nanoViper, C18, 5 μ m, 100 \AA ; Thermo Scientific) onto an Acclaim PepMap RSLC analytical column (75 μ m x 50 cm, nanoViper, C18, 2 μ m, 100 \AA ; Thermo Scientific). The peptides were separated by increasing concentrations of 80% ACN / 0.1% FA at a flow of 250 nl/min for 120 min and analysed with a Q Exactive Plus mass spectrometer (Thermo Scientific).

The eluent was nebulised and ionised using Thermo nano Flex electrospray source with a distal coated fused silica emitter (New Objective). Capillary voltage was set at 1.7 kV. The Q Exactive Plus instrument was operated in the data dependent mode to automatically switch between full scan MS and MS/MS acquisition. Survey full scan MS spectra (m/z 375–1600) were acquired in the Orbitrap with 70,000 resolution (at m/z 200) after accumulation of ions to a 3 e6 target value with maximum injection time of 50 ms. Dynamic exclusion was set to 20 seconds. The 12 most intense multiply charged ions ($z \geq 2$) were sequentially isolated and fragmented in the collision cell by higher-energy collisional dissociation (HCD) with a fixed injection time of 100 ms, 17,500 resolution, HCD collision energy at 27 and AGC target of 1e5.

Acquired .raw files were analysed with MaxQuant (v1.5.5.1, Cox and Mann, 2008) to globally identify and quantify proteins across the different conditions. Database searching was performed the following parameters: cysteine carbamidomethylation as a fixed modification; methionine oxidation and N-terminal acetylation as variable modifications; up to 2 missed cleavages; mass tolerance of 20 ppm; 1% protein false discovery rate (FDR) for protein and peptide identification; and minimum 2 peptides for pair-wise comparison in each protein for label-free quantitation. The mouse protein sequence database was downloaded from Uniprot on May 2016.

Data visualisation and statistical analyses were performed in Perseus (v1.5.5.3, Tyanova et al., 2016). After removing the reversed and known contaminating proteins, the LFQ values were log₂ transformed and the reproducibility across the biological replicates was evaluated by Pearson's correlation analysis. The replicates were grouped into WT fed vs KO fed, WT fasted vs KO fasted, and WT refed vs KO refed with categorical annotation rows. At least 2 valid values out of 3 repeat from in at least 1 treatment was set to filter out the proteins without LFQ intensity. The missed value after filtering was replaced by imputation. A two-sample T-tests was performed to obtain the significantly expressed proteins, with p value <0.05. Significantly changed proteins were further analysed to investigate association with KEGG pathways and GO terms using String database (Szklarczyk et al., 2015). Enrichment analysis for compartmentalisation of acetylated proteins was performed against Uniprot database (Rodents, Taxon ID: 9989) with FunRich 3.0.

Immunohistochemistry

Immunohistochemistry was performed as previously reported (Wu et al., 2014), using following primary antibodies: c-Fos rabbit polyclonal IgG (sc-52; Santa Cruz Biotechnology, Inc) and phospho-AKT (Ser473) Rabbit monoclonal IgG (9271s; Cell Signaling Technology Inc). The secondary antibody for both was Alexa Fluor goat anti-rabbit 594 antibody (A-11037; Invitrogen).

Cfos: Sections were washed in 0.1 M phosphate buffer (PB), incubated with 1% hydrogen peroxide (H₂O₂) for 15 minutes to prevent endogenous peroxidase, activity, and blocked for 1 hour with 5% normal horse serum (NHS) in 0.3% Triton in 0.1 M PB. Sections were incubated with c-Fos rabbit polyclonal IgG (sc-52; Santa Cruz Biotechnology, Inc) at 1:5000 in diluent of 5% NHS in 0.3% Triton in 0.1 M PB. After incubation, the sections were washed and incubated with Alexa Fluor goat anti-rabbit 594 antibody (A-11037; Invitrogen) at 1:500 in 0.3% Triton in 0.1 M PB. Sections were then washed, mounted, and coverslipped. We quantified Fos-positive NPY neurons in the arcuate nucleus (bregma -1.22 to -2.54).

pAKT: Sections were washed in 0.1 M PB and incubated with 1% sodium borohydride for 15 minutes and 1% NaOH and 1% H₂O₂ for 20 minutes to prevent endogenous peroxidase activity. Sections were then washed with 0.3% glycine for 10 minutes and 0.03% SDS for 10 minutes before being blocked (10% NHS in 0.3% Triton in 0.1 M PB) for 1 hour. Sections were incubated with phospho-AKT (Ser473) Rabbit monoclonal IgG (9271s; Cell Signaling Technology Inc) at 1:1000 in a diluent of 10% NHS in 0.3% Triton in 0.1 M PB. After incubation, the sections were washed and

incubated with Alexa Fluor goat anti-rabbit 594 antibody (A-11012; Invitrogen) at 1:400 in 0.3% Triton in 0.1 M PB. Sections were then washed, mounted, and coverslipped. We quantified pAKT-positive NPY neurons in the arcuate nucleus (bregma -1.22 to -2.54).

NPY neurons were analysed based on endogenous hrGFP fluorescence. Cells were visualised by a Zeiss ApoTome microscope, and immunoreactive cells were counted using a grid eyepiece from serial sections through the arcuate nucleus (every fourth section); the first section was chosen randomly. Fibre density was analysed as previously described and cell number and volume was measured a design-based unbiased stereology method (Stereoinvestigator, MicroBrightField, VT, USA), as previously described (Lemus et al., 2015).

Statistical Analysis

Statistical analyses were performed using GraphPad Prism for MacOS X (version 7.0b) All data are represented as mean \pm standard error of the mean (SEM). Two-Way ANOVAs with *post hoc* tests were used to determine statistical significance between treatment and genotype. A two-tailed Student's unpaired *t*-test was used when comparing genotype only. $p < 0.05$ was considered statistically significant.

2.4 Results

Validation of Crat deletion in AgRP neurons

We used a cre-lox approach to delete Crat from AgRP neurons. Crat floxed mice (Muio et al., 2012) were crossed to AgRP-ires-cre::NPY GFP mice to generate AgRP Crat WT and KO mice that expressed GFP in NPY neurons.

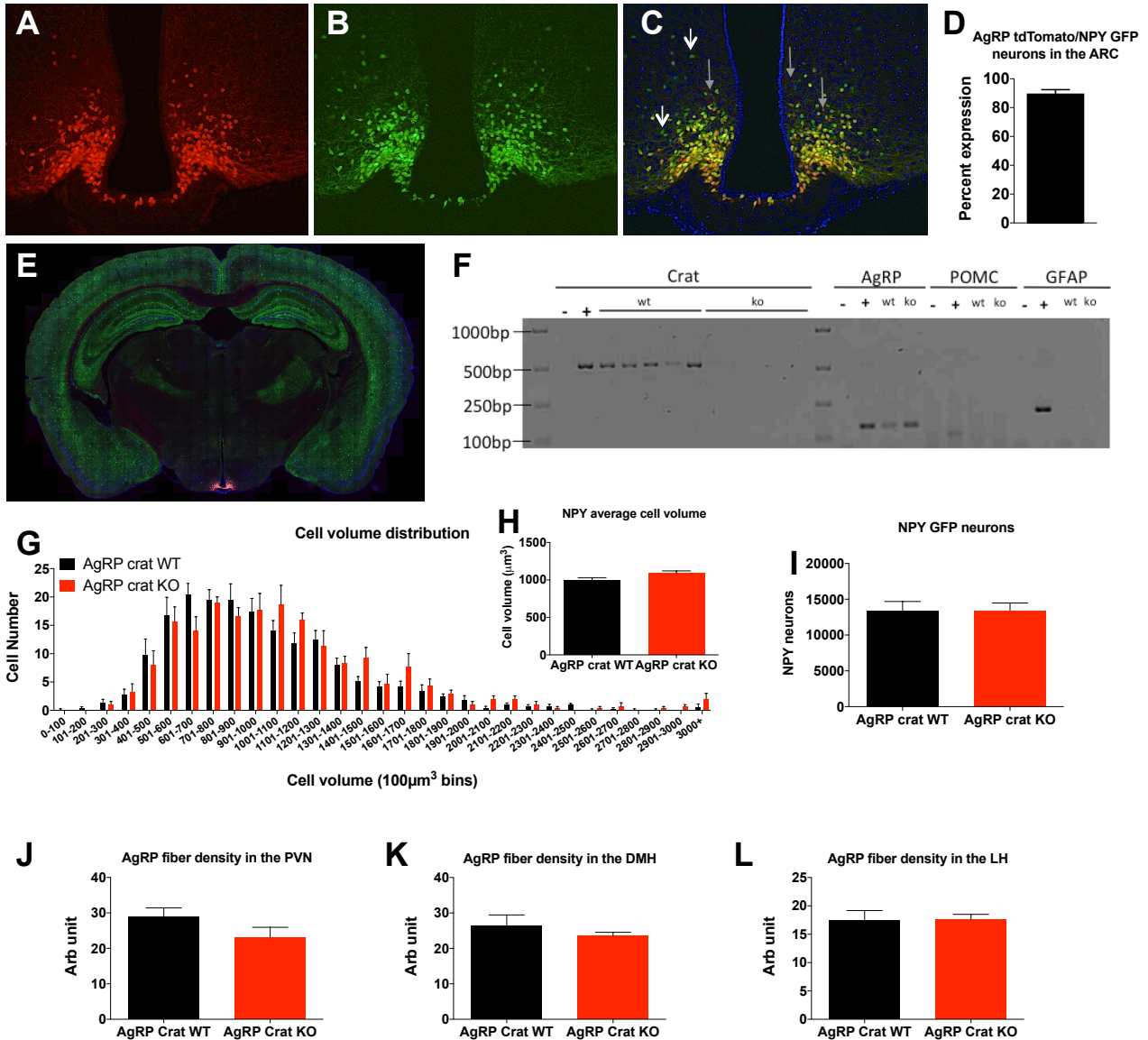


Figure 2.1 Validation of cre-mediated recombination and Crat deletion in AgRP neurons.

Crossing AgRP-ires-cre::NPY GFP with *rosa26-td-Tomato* mice reveals that >90% of NPY neurons in the ARC express tdTomato, as a marker of cre-dependent recombination in AgRP expressing neurons; scale bar 200 μm (A-D). Cre-dependent tdTomato expression only in the ARC, tiled montage; scale bar 1mm (E). FACS isolation of NPY-GFP neurons coupled with PCR analysis confirms no Crat mRNA transcripts in KO mice. AgRP mRNA transcript were observed, whereas neither POMC mRNA nor GFAP mRNA was observed from WT and KO mice (F). Stereological quantification of NPY GFP neurons confirms neither cell number nor cell volume distribution was affected by Crat deletion during development (G-I). No differences in AgRP fibre density in the PVN (J), LH (K) and DMH (L). All data are expressed as mean \pm sem; n=6-8.

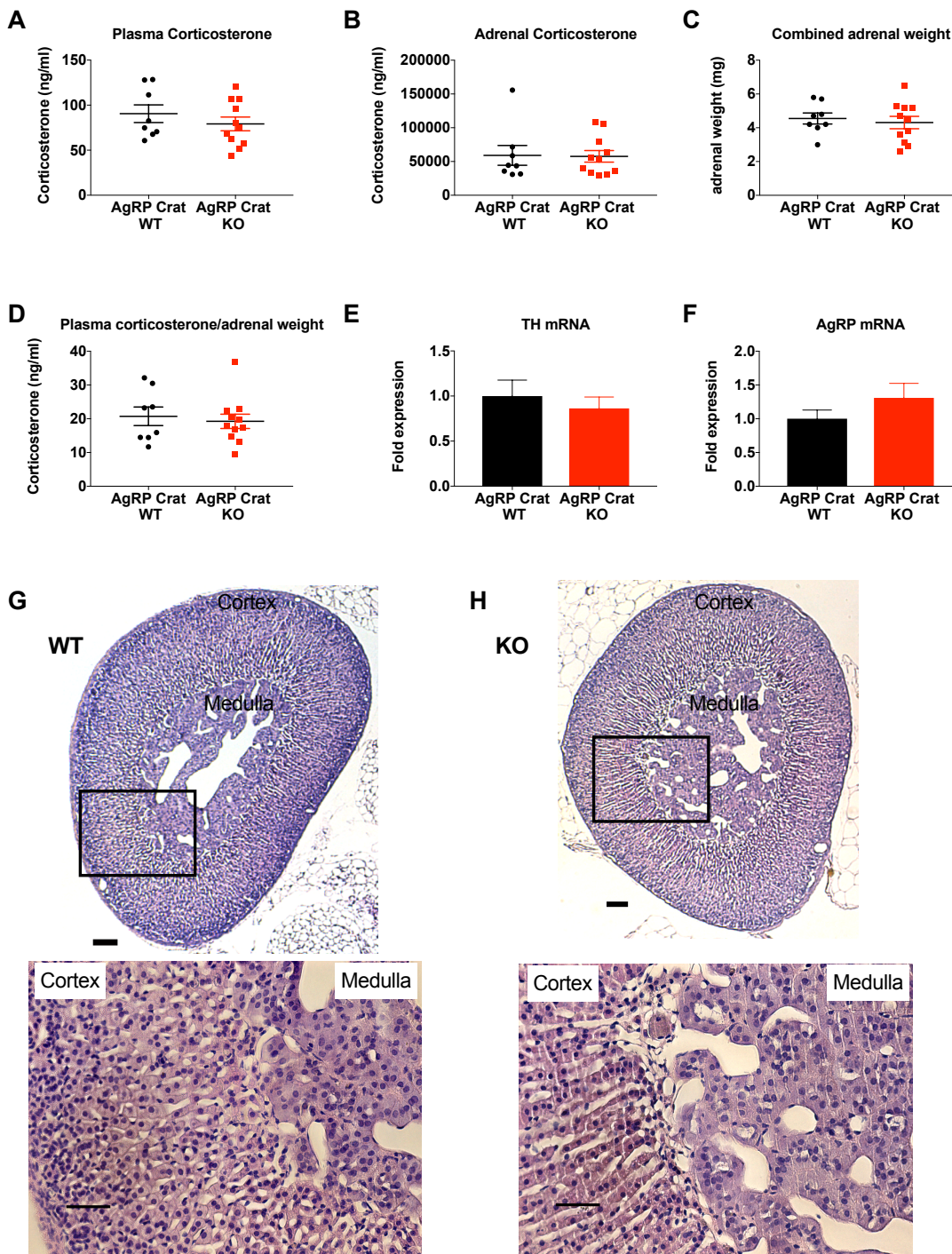


Figure 2.2 AgRP Crat deletion does not affect adrenal morphology and function

Plasma (A) and adrenal corticosterone (B) under basal ad libitum fed conditions. Weight of left and right adrenal (C) and ratio of corticosterone per mg adrenals (D). Gene expression of tyrosine hydroxylase (TH) and agouti related peptide (AgRP) in adrenals (E&F). Representative H&E staining of adrenals show no morphological differences (G&H); scale bar = 200 μm (2.5x magnification) and 100μm (20x magnification).

To confirm cre-recombination in the ARC nucleus, WT and KO mice were crossed to rosa(26) tdTomato reporter mice (Figure 2.1A-E) and we observed >90% of NPY GFP neurons expressing AgRP cre-dependent tdTomato reporter (Figure 2.1D). We used a Fluorescence Activated Cell Sorting (FACS) approach to isolate GFP positive NPY neurons in the ARC, coupled with nested PCR

to confirm the deletion of *Crat* in NPY (AgRP) GFP-positive neurons. NPY GFP neurons from WT (n=5) mice showed expected RNA transcripts for *Crat* at ~500bp whereas no *Crat* mRNA transcripts were observed in KO mice (n=5) (Figure 2.1F).

A stereological analysis showed no genotype differences in total NPY GFP neuronal number and cell volume at postnatal day 14 (P14), confirming there were no adverse developmental effects on the NPY cell number and volume in the ARC (Figure 2.1G-I).

No differences were observed in AgRP fibre density in the PVN, DMH or LH between WT and KO mice (Figure 2.1J-L). Likewise, we observed no differences in adrenal weight, adrenal histology, plasma corticosterone and adrenal *Tyrosine hydroxylase* and *Agrp* mRNA content between genotypes (Figure 2.2A-H), an important observation since AgRP is also expressed in adrenal glands (Gupta et al., 2017).

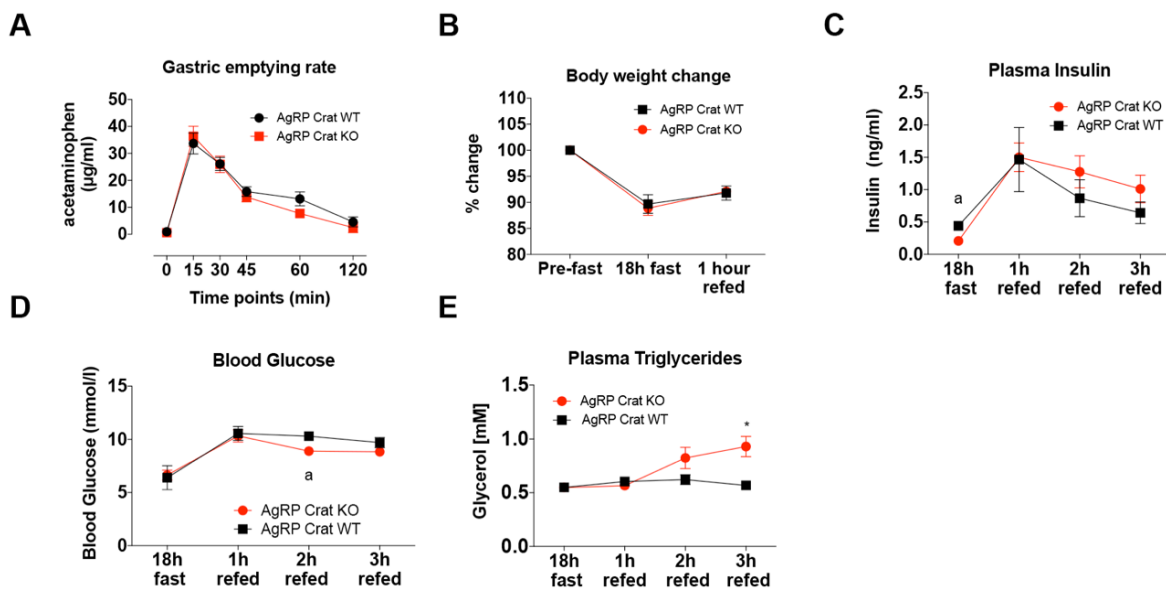
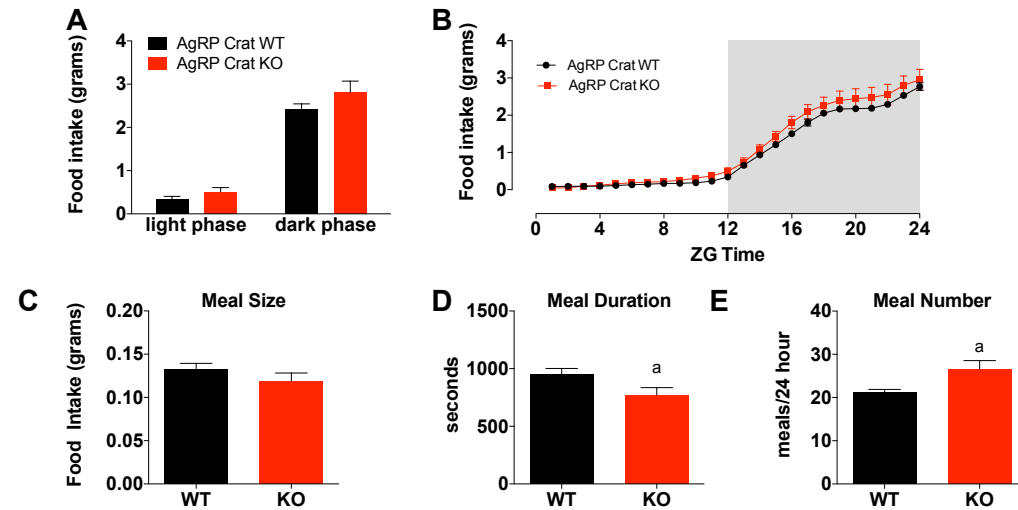


Figure 2.3 *AgRP Crat* deletion does not affect gastric emptying

KO mice show no differences in gastric emptying, as demonstrated by appearance of acetaminophen in blood of fasted mice after gavage of glucose/acetaminophen solution (A), as well as no differences in bodyweight change after fasting and refeeding (B). KO mice show slight alterations in plasma insulin (C), blood glucose (D) and plasma triglycerides (E) during the transition of fast to fed compared to WT controls.

Feeding behaviour: Ad libitum

Figure 2



Feeding behaviour: Fast/refeeding

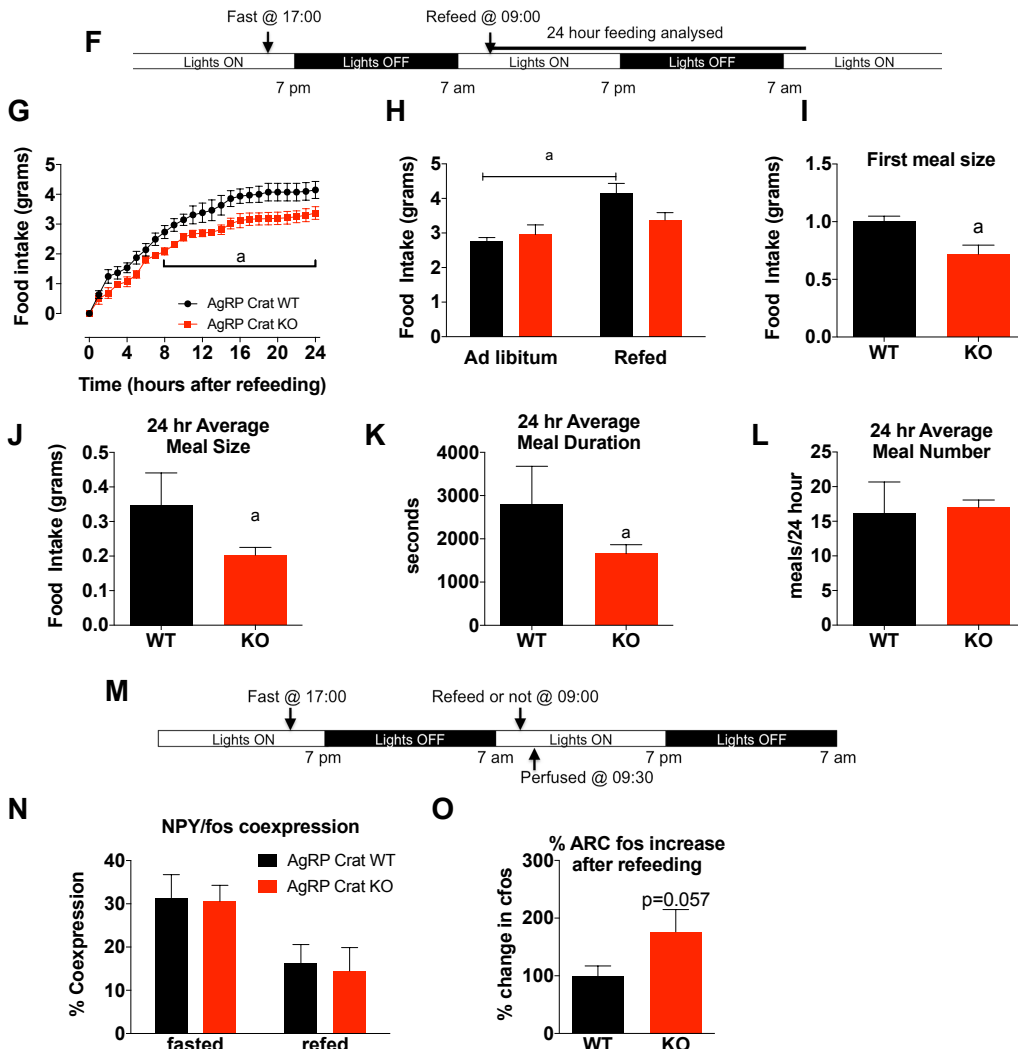


Figure 2.4 Deletion of *Crat* in *AgRP* neurons affects feeding behaviour and food intake in response to fasting.

Deletion of *Crat* in *AgRP* neurons does not affect total food intake (A), cumulative food intake over a 24-hour period (B) and meal size (C), however meal duration is reduced (D) and an increase in

meal number (E) accounts for reduced meal duration. In response to fasting-refeeding (F), KO mice eat less than WT mice (G), and KO mice do not increase food intake relative to ad libitum fed mice (H). KO mice had smaller first (I) and average meal size (J), and reduced meal duration (K), and no difference in meal number (L). Analysis of Fos expression (M) demonstrated AgRP/NPY neurons from KO mice had a similar Fos response to fasting refeeding (N), whereas overall Fos activity in response to refeeding in the ARC was significantly increased in KO compared to WT (O). All data are expressed as mean \pm sem; n=5-8. Two-way (repeated measured; where appropriate) ANOVA with Tukey's posthoc analysis; a, significant at $p < 0.05$.

Ad libitum and fasting-induced feeding behaviour

Under conditions of *ad libitum* access to food, there was no difference in average 24-hour food intake (Figure 2.4A-B). Intriguingly, despite no difference in total 24-hour food intake, the microstructure of feeding behaviour was altered in KO mice with significantly shorter meal duration compared to WT mice but increased meal number to compensate (Figure 2.4C-E). As AgRP neurons promote food seeking behaviour during states of negative energy balance, we examined refeeding in response to an overnight fast. KO mice exhibited significantly reduced cumulative food intake over a 24-hour period compared to WT control mice (Figure 2.4G-H), indicating an impaired feeding response after an overnight fast. Analysis of the microstructure of feeding behaviour indicated the first meal after refeeding was significantly smaller and both average meal duration and meal size were significantly smaller compared to WT mice (Figure 2.4J-K). Collectively, these results show that deletion of *Crat* in AgRP neurons impairs refeeding after fasting and affects the microstructure of feeding behaviour. There was no difference in body weight change or gastric emptying (Figure 2.3A-B) in WT and KO mice during fasting and refeeding.

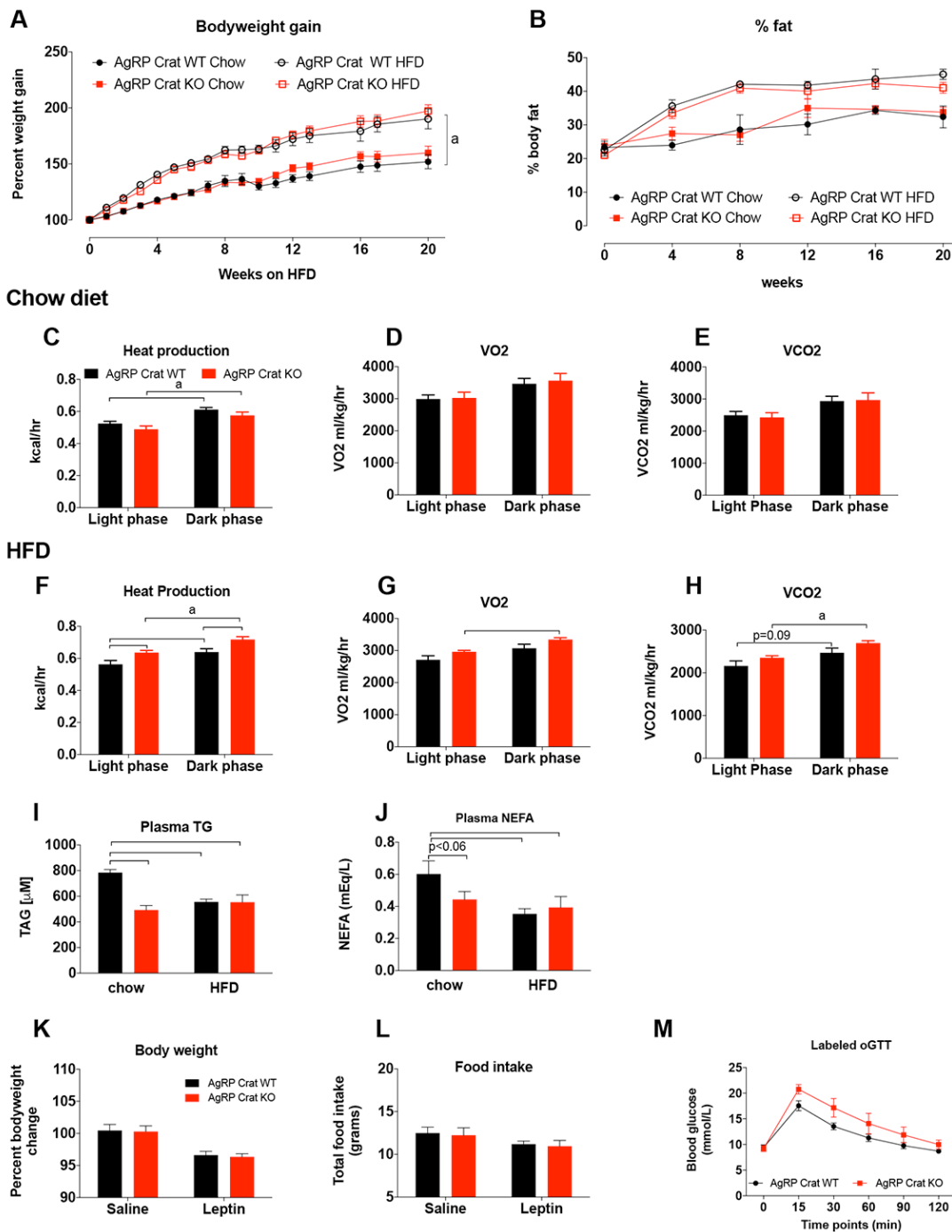


Figure 2.5 Crat in AgRP neurons is not required for sensing positive energy balance

No difference in body weight gain (A) or body fat mass (B) was observed in WT or KO mice on a chow or high fat diet (HFD). Analysis of metabolic parameters on a chow diet revealed no genotype differences in heat, VO₂ or VCO₂ (C-E). HFD exposure resulted in greater heat production in KO mice compared to WT controls but no genotype differences were observed in VO₂ or VCO₂ (F-H). Plasma triglyceride (I) and non-esterified fatty acids (J) on a high fat or chow diet. Percent body weight change in response to leptin injections over 5 days and total average food intake over the 5-day injection period (K&L). Oral glucose tolerance test using stable labelled 6,6D₂ glucose (M) All data are expressed as mean ± sem; n=6-11. Two-way (repeated measured; where appropriate) ANOVA with Tukey's posthoc analysis; a, significant at p<0.05.

Interestingly, there was no difference in the percentage of activated NPY neurons in WT or KO mice in fasted or refeed conditions (Figure 2.4N) using *Fos* as a surrogate marker for activation in NPY GFP labelled neurons. However, an increase in *Fos* positive neurons in non-NPY ARC neurons during refeeding (Figure 2.4O), suggests a greater sensitivity to potential satiety factors associated with refeeding.

Body weight gain or fat mass over a 20-week chow diet or HFD feeding period did not differ between genotypes (Figure 2.5A-B). Analysis of metabolic parameters revealed no genotype differences in heat production, VO₂ or VCO₂ on a chow diet (Figure 2.5C-E). High-fat fed KO mice had an increase in heat production during both the light and dark phase relative to WT controls (Figure 2.5F), but this was not sufficient to influence adiposity. There were no genotype differences in VO₂ or VCO₂ (Figure 2.5G-H). There were also no differences in body weight change or total food intake after 5 days of leptin injections (Figure 2.5K-L).

Feeding behaviour in response to i.p. CCK and ICV insulin

Given that deletion of *Crat* in AgRP neurons decreased meal duration in ad libitum conditions, the possibility arises that KO mice were more sensitive to satiety signals. An injection of CCK (0.25µg/kg, i.p.) immediately before the dark phase (Figure 2.6A) highlighted that KO mice were more sensitive to i.p. CCK. KO mice exhibited reduced meal size and meal duration relative to WT mice (Figure 2.6B-C), but meal number was significantly increased to compensate (Figure 2.6D). Hence, there was no overall difference in total food intake over the 24-hour period after CCK injection (Figure 2.6E).

Central insulin suppresses food intake (Bruning et al., 2000; Niswender et al., 2003) so we also injected insulin (0.025µU, ICV) into WT and KO mice and examined food intake and feeding behaviour over a 24-hour period (Figure 2.6F). ICV insulin suppressed food intake in KO mice 2 hours post injection, an effect that was no longer evident by 6 hours or thereafter (Figure 2.6G-H). Analysis of 24-hour feeding behaviour revealed that ICV insulin reduced meal size and meal duration, and increased meal number in KO mice to compensate (Figure 2.6I-K), resulting in no difference in 24-hour food intake between genotypes. These results are in accord with those of others (Campos et al., 2016), which highlight the ability of mice to adjust meal number in order to ensure constant 24-hour food intake (under *ad libitum* conditions), despite reduced meal size and duration.

Feeding behaviour: ip CCK

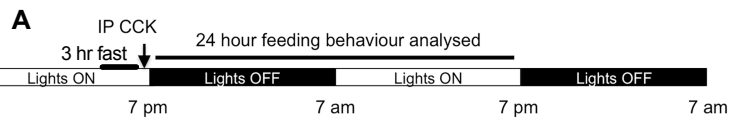


Figure 3

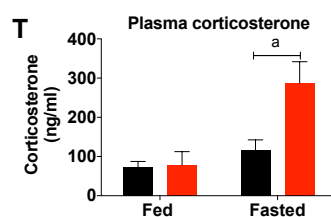
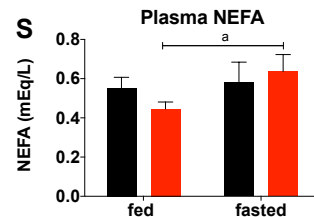
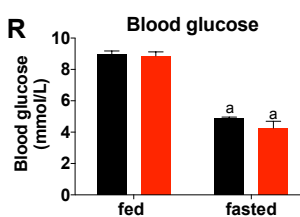
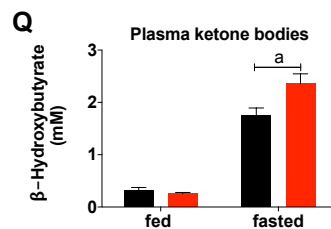
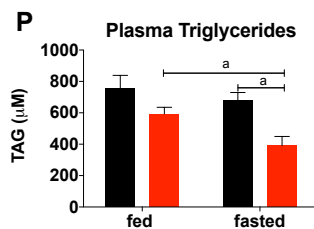
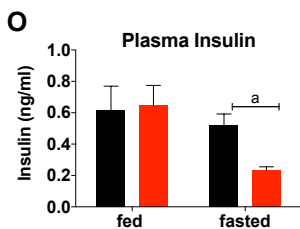
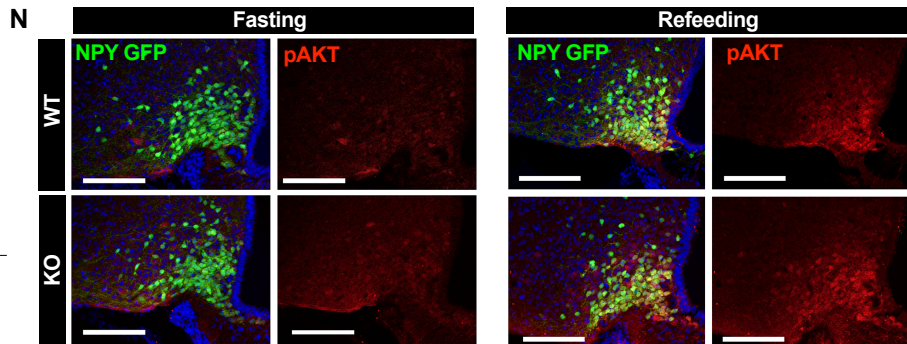
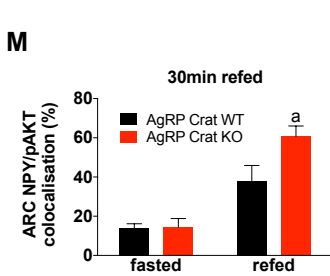
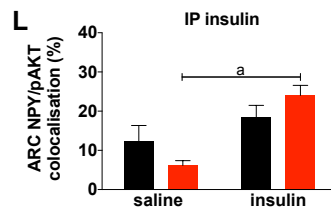
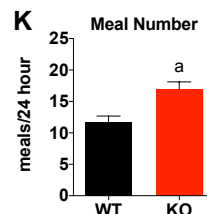
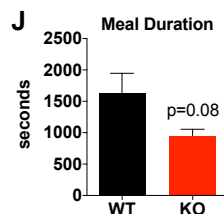
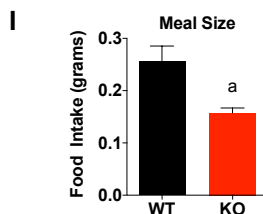
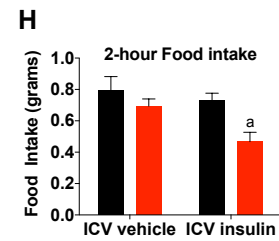
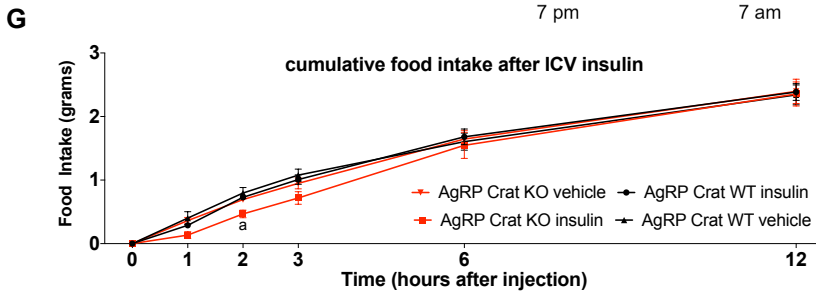
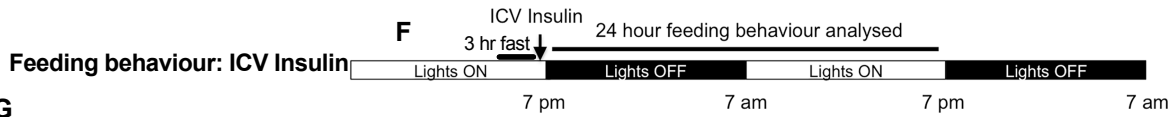
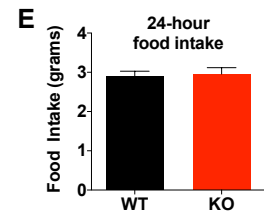
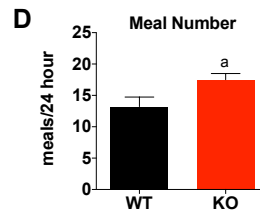
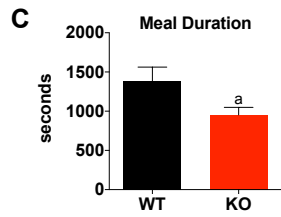
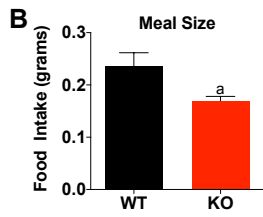


Figure 2.6 Sensitivity to insulin and CCK

CCK (0.25µg/kg, i.p.) (A) or insulin (0.025uU, ICV) (F) produced smaller meal size (B;I), shorter meal duration (C;J) with a compensatory increase in meal number (D;K) in KO mice compared to WT controls. As a result, there were no differences in overall food intake 24 hours after CCK injections (E) and no differences 6 hours after insulin injections (G), although KO mice had significantly lower food intake 2 hours after ICV insulin administration (H). Analysis of pAKT staining in AgRP/NPY neurons 10 min after exogenous insulin injection (0.75U/kg, i.p.) (L) or 30 min after refeeding (M) showed that KO have a higher sensitivity to circulating insulin. Representative micrographs of NPY/pAKT coexpression ARC sections during fasting and 30 minutes after refeeding (white bar represents 100µm) (N). Analysis of plasma insulin (O), triglycerides (P), ketone bodies (Q), glucose (R), NEFA (S) and corticosterone (T) from fed and fasted AgRP Crat mice. All data are expressed as mean ± sem; n=7, a, significant at p<0.05.

In line with the feeding response to insulin, NPY (AgRP) neurons from KO mice showed greater sensitivity to exogenous insulin (i.p. 0.75U/kg bodyweight) with a significant increase in insulin-induced pAKT staining in NPY (AgRP) neurons when compared to saline (Figure 2.6L). To further examine the physiological sensitivity of NPY (AgRP) neurons to insulin, we measured pAKT in NPY neurons 30 minutes after refeeding and observed significantly more NPY neurons expressing pAKT in KO mice compared to WT controls (Figure 2.6M).

AgRP Crat deletion causes a metabolic adaptation in liver function

Analysis of plasma in fed and fasted states revealed significantly lower concentrations of insulin and triglyceride (TG) in fasted KO mice compared to WT mice (Figure 2.6O&P). Fasting significantly increased plasma corticosterone, NEFA and ketone bodies in KO mice, yet we found no significant genotype effect on blood glucose (Figure 2.6Q-T). Although blood glucose was not different during fasting, the increased circulating ketone bodies indicated increased fatty acid oxidation and altered hepatic liver function in KO mice during fasting. In the fasted state, KO mice had significantly lower liver glycogen and higher triglyceride concentrations relative to WT mice (Figure 2.7A-C). The hepatic gluconeogenic genes, *Pck1*, *Pck2* and *G6pc*, were significantly increased in fasted KO mice relative to fasted WT mice (Figure 2.7D) and consistent with increased breakdown of liver glycogen, liver glycogen phosphorylase (*Pygl*) gene expression was significant increased (Figure 2.7D).

The accumulation of triglyceride in the liver was unlikely to be due to increased *de novo* lipid synthesis, since fatty acid synthase (*Fasn*) and stearoyl CoA desaturase (*Scd1*), were significantly suppressed in the fed state with no differences in the fasted state. Adipose triglyceride lipase (*Atgl*), a marker of lipolysis, and carnitine palmitoyltransferase 1a (*Cpt1a*), rate-limiting enzyme for acyl-CoA delivery into the mitochondria matrix for oxidation, were elevated in fasted KO mice relative to fasted WT (Figure 2.7D). Liver fatty acid oxidation was also increased in KO mice (Figure 2.7 E-F), which would account for the increased ketone bodies in the blood (Figure 2.7Q). Using a norepinephrine (NE) turnover approach (Joly-Amado et al., 2012), we showed little to no NE turnover

in fasted KO mice and impaired NE turnover in the refed state (Figure 2.7G-H), suggesting inappropriate AgRP function in KO mice alters liver function by diminished sympathetic activity.

The differences in liver glycogen and gluconeogenic genes in fasted KO mice suggest alterations in glycogenolysis and gluconeogenesis. In support of this, *Glycerol kinase* mRNA, the enzyme required to facilitate gluconeogenesis from glycerol, was significantly elevated in fasted KO mice (Figure 2.7D). Moreover, we investigated the fractional contribution of glycogenolysis and gluconeogenesis during fasting by employing a tracer-based approach to measure the sources of endogenous glucose production (EGP). KO mice showed increased glycerol-driven gluconeogenesis after 3 hours fasting with a corresponding decrease in gluconeogenesis from phosphoenolpyruvate (Figure 2.7K-L). Moreover, blood glucose was significantly higher in KO mice compared with WT mice 15 min after an i.p. glycerol injection, indicating greater glycerol utilisation for glucose production (Figure 2.7M). Collectively, our results suggest that the deletion of *Crat* from AgRP neurons affects the output of the sympathetic nervous system, which shifts liver metabolism to preferentially utilise glycerol as a substrate for gluconeogenesis.

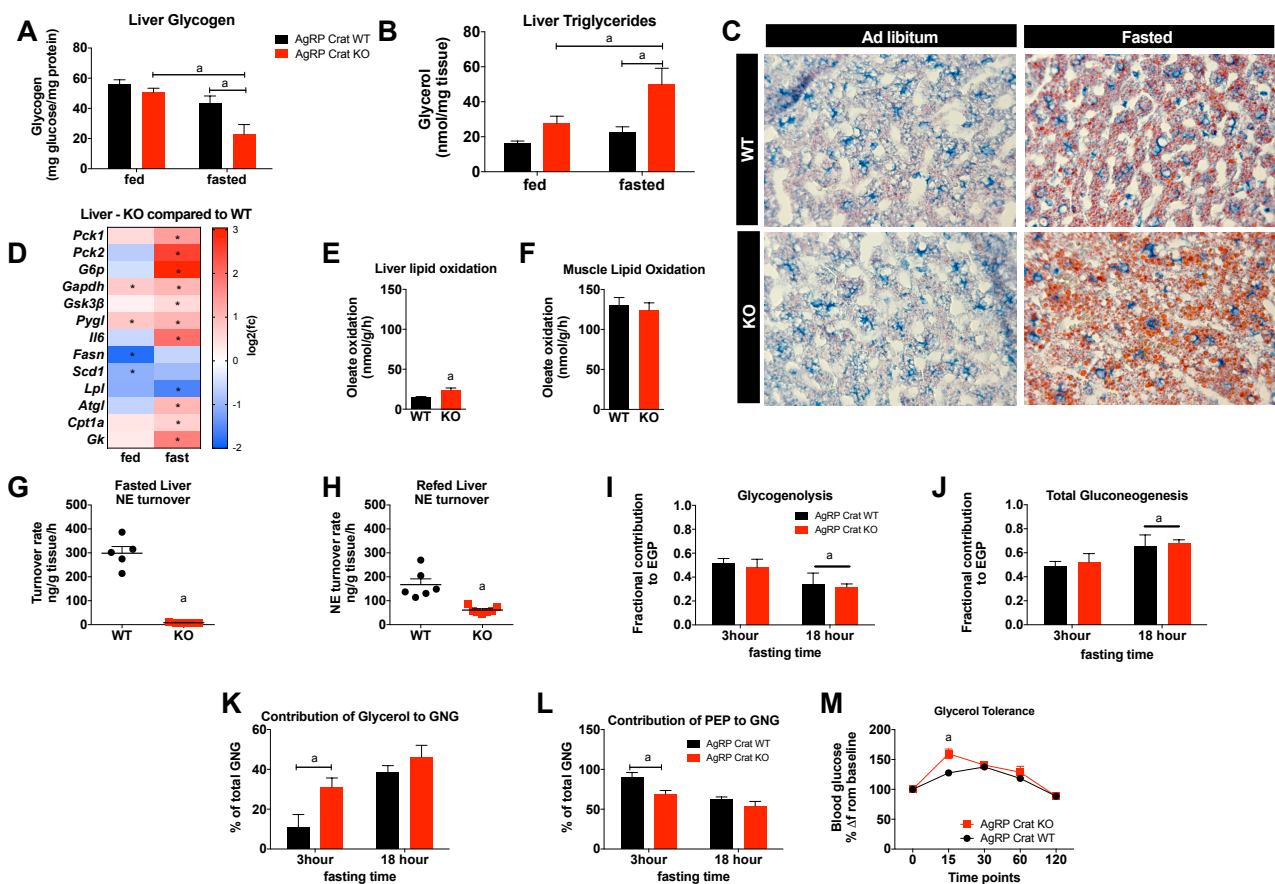


Figure 2.7 Deletion of *Crat* in AgRP neurons affects peripheral metabolism.

Liver glycogen was significantly reduced in KO mice relative to WT mice during fasting (A). Liver triglycerides (B) were significantly increased in fasted KO mice compared with WT mice (C); Scale bars in C=100 μm. KO liver mRNA levels as log₂ fold expression relative to WT controls (D). Ex vivo analysis of fasted liver (E) and soleus muscle (F) oleate oxidation. Noradrenaline turnover in fasted (G) and refed liver (H). Analysis of the fractional contribution of glycogenolysis (I) and

gluconeogenesis (J) to endogenous glucose production, as well as the contribution of glycerol (K) and PEP (L) to gluconeogenesis, during fasting using heavy water coupled with mass spectrometry. Blood glucose measurements after i.p. glycerol injection to assess glycerol tolerance (M). Abbreviations: atgl, adipose triglyceride lipase; Cpt1a, carnitine palmitoyltransferase 1a; Fasn, Fatty acid synthase; G6p, glucose-6-phosphatase, catalytic; Gapdh, glyceraldehyde-3-phosphate dehydrogenase; Gk, Glycerol kinase, transcript variant 1; Gsk3 β , glycogen synthase kinase 3 beta; Il6, interleukin 6; Lpl, Lipoprotein Lipase; Pck1, Phosphoenolpyruvate Carboxykinase 1 (cytosol) ; Pck2, Phosphoenolpyruvate Carboxykinase 2 (mitochondrial); Pygl, glycogen phosphorylase, liver; Scd1, Stearoyl-Coenzyme A desaturase 1. All data are expressed as mean \pm sem; n=7-10. Two-way (repeated measured; where appropriate) ANOVA with Tukey's posthoc analysis; a, significant at $p < 0.05$.

AgRP Crat deletion acutely impairs glucose tolerance

Initial experiments highlighted a greater increase in plasma glucose in KO compared with WT mice at 15 and 30 minutes after oral glucose gavage (Figure 2.8A). Notably, blood glucose was not different between genotypes after 60 minutes, suggesting that effects of AgRP Crat deletion may impact acute glycaemic control rather than long-term regulation. Next, we performed oGTTs with stable isotope labelled glucose (6,6D2 glucose) allowing the distinction between exogenous labelled glucose and unlabelled endogenous glucose in the blood. Our results showed significantly higher levels of labelled (exogenous) glucose in the plasma of KO mice, indicating reduced glucose disposal during the oGTT (Figure 2.8C-D). While there was no difference in the glucose concentration from endogenous sources over the course of 120 minutes, the rate of change from 0-15 minutes was significantly reduced in KO mice relative to WT mice (Figure 2.8E-F), indicating a diminished ability to suppress endogenous glucose production in that time. In addition, plasma insulin levels at 5 and 10 minutes post glucose gavage were reduced compared to WT mice (Figure 2.8G), underpinning reduced glucose disposal and reduced ability to suppress endogenous glucose production observed in KO mice.

We then performed a glucose uptake assay in various tissues to determine the capacity of the endogenous response to oral glucose to regulate glucose uptake. At 15 minutes post glucose load, glucose uptake was lower in WAT and skeletal muscle, with a paradoxical increase in the hypothalamus (Figure 2.8H). By 30 minutes post glucose load, all tissues showed greater glucose uptake in KO compared with WT mice (Figure 2.8I). *Fos* co-expression within ARC NPY GFP neurons was examined 10 minutes after an oral glucose load, which should reduce *Fos* co-expression in NPY neurons, as their activity is reduced. The results showed more *Fos* expressing NPY (AgRP) neurons in KO compared to WT mice (Figure 2.8J-L), consistent with lack of suppression of *Fos* activity in response to a glucose load. Collectively, these results suggest, that the deletion of Crat from AgRP neurons attenuates their ability to acutely sense glucose and engage the appropriate mechanisms to clear plasma glucose within a 30-minute time frame.

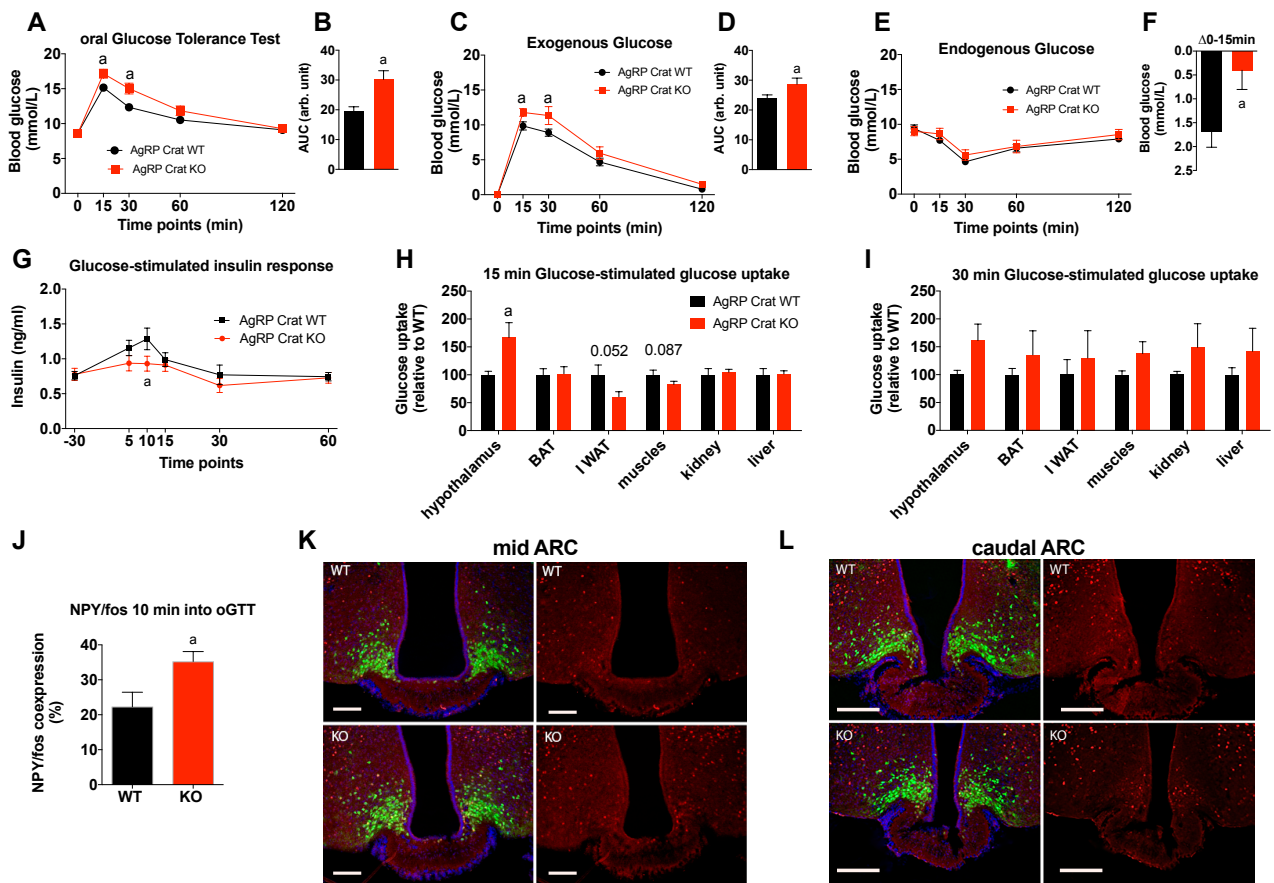


Figure 2.8 Deletion of Crat in AgRP neurons affects glucose homeostasis.

- Oral glucose tolerance test (oGTT, 1.5 g/kg) after 5 hr of fasting (A) and area under the curve analysis (AUC) (B). Labelled oGTT allows an estimate of exogenous glucose from gavage (C), with AUC (D), versus endogenous glucose from hepatic gluconeogenesis (E). The rate of decline of endogenous blood glucose after 15 minutes (Δ 0-15 mins; F). Glucose-stimulated insulin release during the oGTT (G). Glucose-stimulated glucose uptake after 15 min (H) and 30 min (I). Analysis of Fos-positive AgRP/NPY neurons 10 min after glucose gavage (J). Representative micrographs of mid ARC (K) and caudal ARC (L) sections, left panel showing an overlay of green channel (NPY-GFP) with the red (cos) from the right panel, top panels show WT, bottom panels show KO; scale bar = 100 μ m. All data are expressed as mean \pm sem; n=7-10. Two-way (repeated measured; where appropriate) ANOVA with Tukey's posthoc analysis; a, significant at $p < 0.05$.

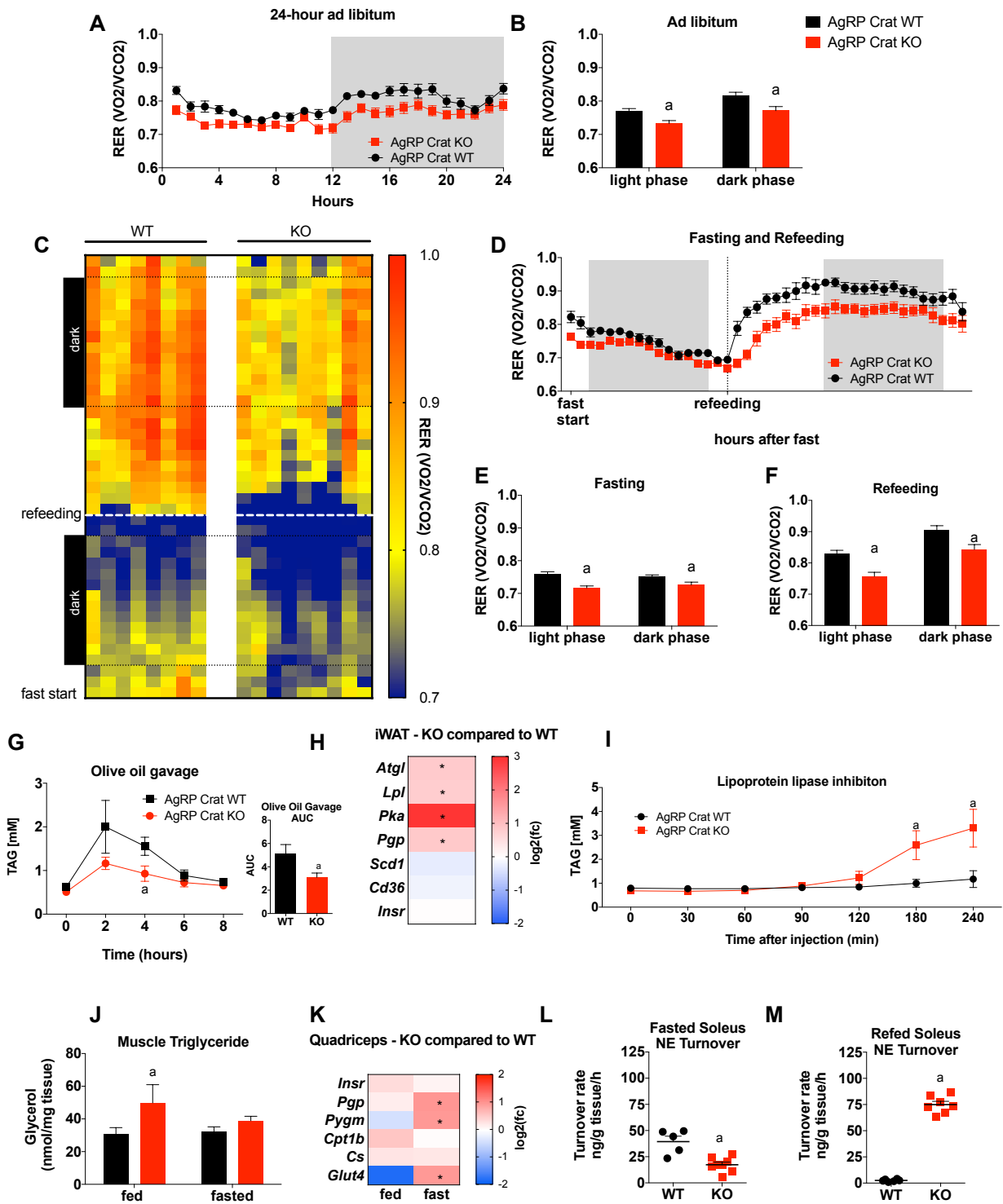


Figure 2.9 AgRP Crat deletion impairs peripheral nutrient partitioning

KO mice have lower respiratory quotient (RER) under ad libitum conditions (A&B) and during fasting and refeeding (C-F). Each column of the heat map represents one animal and each row represents the average RER per hour; black boxes on the left side represent dark phase with black dotted lines indicating the change in light conditions. White line represents time point of refeeding. KO mice have a delayed switch from fatty acid to glucose utilisation. KO mice showed greater triglyceride clearance after olive oil load (G). KO iWAT mRNA levels as log₂ fold expression relative to WT controls (H). KO mice exhibit greater plasma triglyceride levels after inhibiting LPL with tyloxapol (300mg/kg bodyweight) (I). Muscle triglycerides are significantly increased in fed KO mice compared to WT mice (J). KO muscle mRNA levels as log₂ fold expression relative to WT controls (K). Noradrenaline turnover in fasted and re-fed muscle (L&M). Abbreviations: *Atgl*, adipose triglyceride lipase; *CD36*,

CD36 antigen, transcript variant 1; *Cpt1b*, carnitine palmitoyltransferase 1b; *Cs*, citrate synthase; *Glut4*, Glucose Transporter 4; *InsR*, Insulin receptor; *Lpl*, Lipoprotein Lipase; *Pgp*, phosphoglycolate phosphatase; *Pka*, protein kinase A; *Pygm*, glycogen phosphorylase, muscle; *Scd1*, Stearoyl-Coenzyme A desaturase 1. All data are expressed as mean \pm sem; n=7-10. Two-way (repeated measured; where appropriate) ANOVA with Tukey's posthoc analysis; a, significant at $p < 0.05$.

AgRP Crat deletion impairs peripheral nutrient partitioning.

KO mice showed a shift towards increased fatty acid utilisation with a lower respiratory exchange ratio (RER) during both light and dark phases of the day (Figure 2.9A-B) when fed *ad libitum* chow diet. In addition, heat map analysis of RER values from individual mice clearly show reduced RER values during fasting and refeeding (Figure 2.9C-D). Importantly, the change in RER in response to refeeding was delayed in KO mice, suggesting the deletion of Crat from AgRP neurons influences peripheral nutrient partitioning to incoming nutrient availability. In line with greater fatty acid utilisation, KO mice show a greater clearance of lipids from the plasma following an olive oil gavage (Figure 2.9G). Moreover, we observed an adipose tissue (inguinal white fat) gene expression profile that would predict increased lipolysis in a fasted state (Figure 2.9H), which is consistent with increased plasma NEFA levels during fasting in KO mice (Figure 2.6S). Specifically, we observed an increase in KO mice in *Atgl*, and lipoprotein lipase (*Lpl*), which hydrolyse TGs in intracellular lipid droplets and lipoproteins respectively. Similarly, protein kinase A (*Pka*), an enzyme induced by adrenergic stimulation that increases lipolysis and phosphoglycolate phosphatase (*Pgp*), an enzyme required to liberate glycerol by dephosphorylating glycerol-3-phosphate (Mugabo et al., 2016), were both increased in KO mice. We also performed a lipoprotein lipase inhibition assay using tyloxapol (300mg/kg bodyweight, i.p. after a 5-hour fast) (Schotz et al., 1957) and observed a significant increase in plasma TG in KO mice (Figure 2.9I) suggesting greater efflux from the liver for utilisation in peripheral tissues such as muscle. Indeed, the increased muscle TG concentration in the fed state in (Figure 2.9J) and increased plasma TG concentration in KO mice 3 hours after refeeding (Figure 2.3E), support this idea as a mechanism to restock muscle lipid content. We also observed that fasting increased *Pgp* mRNA expression, muscle glycogen phosphorylase (*Pygm*) and *Glut4*, whereas there was no increase in *Cpt1b* (Figure 2.9K). NE turnover was reduced in fasted KO mice but significantly increased in refed KO mice, compared to WT controls (Figure 2.9L&M) underlying altered communication between the central nervous system and muscle in KO mice. Collectively, these studies show that Crat is required in AgRP neurons to regulate nutrient partitioning by regulating fatty acid utilisation, gene expression and metabolism.

Crat deletion changes the AgRP proteomic response to fasting and refeeding.

To examine how Crat deletion in AgRP neurons affects intracellular protein expression during fasting and refeeding, we used a FACS approach to collect NPY GFP neurons from WT and KO mice under fed, fasted and refed conditions and analysed protein abundance using mass spectrometry (Figure

2.10A). A comparison of WT vs. KO mice under fed conditions revealed 32 proteins with a significant difference in abundance. Of these 32, 7 were >2-fold higher in NPY neurons and 3 were >2-fold lower in NPY neurons from KO vs. WT mice (Figure 2.10B, Table 3). Of the 32 proteins, 10 were grouped into metabolic pathways (KEGG pathways ID 1100) (Figure 2.10C) and 3 were grouped to glycolysis (KEGG pathway ID 10). Two proteins within the metabolic KEGG pathway that were more than 2-fold higher in KO were NADH dehydrogenase 1 alpha subcomplex subunit 2 (Ndufa2) and methylenetetrahydrofolate dehydrogenase (Mthfd1), an oxidoreductase that can use NAD⁺ or NADP⁺ as acceptors.

In the fasted state, we identified 131 significantly different proteins in KO compared to WT NPY neurons. Of these 131, 84 were >2-fold higher and 17 were >2-fold decreased (Table 4). KEGG identified 79 enriched pathways with metabolic pathways (32/131) the most enriched (Figure 2.10D). The two most significantly increased proteins in KO vs. WT NPY neurons in the fasted state were mitochondrial cytochrome b-c1 complex subunit 6 (Uqcrh) and ATP-dependent 6-phosphofructokinase, platelet type (Pfkp), which catalyses the 3rd step of glycolysis. The 2 most significantly decreased proteins in NPY neurons from KO vs. WT mice were NADH dehydrogenase (ubiquinone) Fe-S protein 6 (Ndufs6) and ATP synthase, H⁺ transporting, mitochondrial F1F0 complex, subunit e (Atp5K).

During refeeding, we observed 190 significantly different proteins in KO vs. WT NPY neurons. Of these 190, 39 were >2-fold increased and 47 were >2-fold decreased in NPY neurons from KO vs. WT mice. KEGG identified 59 enriched pathways, many of which were similar to those reported in the fasted group, including the enrichment of the metabolic pathway (50/190) (Figure 2.10E; Table 5). The 2 most significantly increased metabolic pathway proteins in NPY neurons from KO vs. WT mice were NADH dehydrogenase (ubiquinone) 1 subunit C2 (Ndufc2) and Dolichyl-diphosphooligosaccharide protein (Rpn1). The 3 most significantly decreased proteins in NPY neurons from KO vs. WT mice were ATP synthase protein 8 (Mtatp8), arginase 1 (Arg-1) and NADH dehydrogenase (ubiquinone) Fe-S protein 6 (Ndufs6).

Since acetyl CoA is the sole donor of acetyl groups for acetylation (Pietrocola et al., 2015), Crat may play an important indirect role in intracellular acetylation of proteins. Therefore, we examined whether Crat deletion affected the protein acetylation signature within NPY neurons from KO vs. WT mice. Our results indicated that under fed conditions, 14.15% vs. 13.80% of proteins were acetylated in WT and KO NPY neurons, respectively (Figure 2.10F). However, under conditions of fasting, 15.03% of proteins in WT NPY neurons were acetylated whereas this was significantly lower at 13.88% in KO NPY neurons ($p < 0.05$). In refed conditions, 15.06% and 13.61% of proteins were acetylated from WT and KO NPY neurons ($p < 0.05$), respectively (Figure 2.10F).

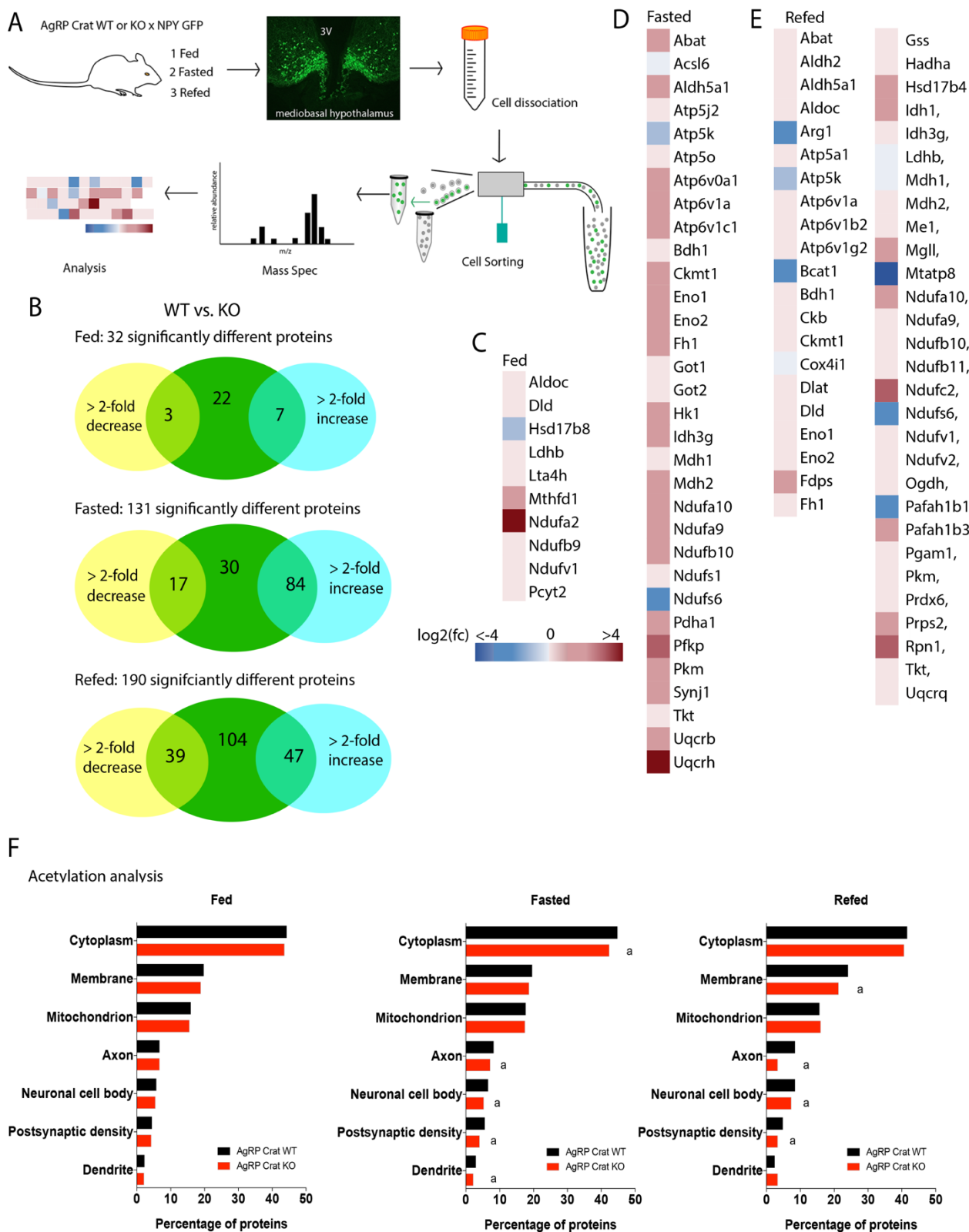


Figure 2.10 Crat deletion affects protein regulation in AgRP neurons.

Hypothalami of mice in fed, fast and refed conditions were dissociated and NPY GFP-positive cells were FAC sorted for proteomic analysis (A). Significantly changed proteins (B) were subjected to enrichment analysis using string database 10.0. KEGG metabolic pathway had the highest enrichment in fed (C), fasted (D) and refed condition (E). Enrichment analysis of acetylated proteins using FunRich 3.0 revealed that less proteins in KO are acetylated in fasted and refed state (F). Abbreviations; Abat, 4-aminobutyrate aminotransferase; Acsl6, acyl-CoA synthetase long-chain

family member 6; Aldh2, aldehyde dehydrogenase 2, mitochondrial; Aldh5a1, aldehyde dehydrogenase family 5, subfamily A1; Aldoc, aldolase C, fructose-bisphosphate; Arg1, arginase, liver; Atp5a1, ATP synthase, H⁺ transporting, mitochondrial F1 complex, alpha subunit 1; Atp5j2, ATP synthase, H⁺ transporting, mitochondrial F0 complex, subunit F2; Atp5k, ATP synthase, H⁺ transporting, mitochondrial F1F0 complex, subunit e; Atp5o, ATP synthase, H⁺ transporting, mitochondrial F1 complex, O subunit; Atp6v0a1, ATPase, H⁺ transporting, lysosomal V0 subunit A1; Atp6v1a, ATPase, H⁺ transporting, lysosomal V1 subunit A; Atp6v1b2, ATPase, H⁺ transporting, lysosomal V1 subunit B2; Atp6v1c1, ATPase, H⁺ transporting, lysosomal V1 subunit C1; Atp6v1g2, ATPase, H⁺ transporting, lysosomal V1 subunit G2; Bcat1, branched chain aminotransferase 1, cytosolic; Bdh1, 3-hydroxybutyrate dehydrogenase, type 1; Ckb, creatine kinase, brain; Ckmt1, creatine kinase, mitochondrial 1, ubiquitous; Cox4i1, cytochrome c oxidase subunit IV isoform 1; Dlat, dihydrolipoamide S-acetyltransferase (E2 component of pyruvate dehydrogenase complex); Dld, dihydrolipoamide dehydrogenase; Eno1, enolase 1, alpha non-neuron; Eno2, enolase 2, gamma neuronal; Fdps, farnesyl diphosphate synthetase; Fh1, fumarate hydratase 1; Got1, glutamate oxaloacetate transaminase 1, soluble; Got2, glutamate oxaloacetate transaminase 2, mitochondrial; Gss, glutathione synthetase; H2-Ke6, H2-K region expressed gene 6; Hadha, hydroxyacyl-Coenzyme A dehydrogenase/3-ketoacyl-Coenzyme A thiolase/enoyl-Coenzyme A hydratase (trifunctional protein), alpha subunit; Hk1, hexokinase 1; Hsd17b4, hydroxysteroid (17-beta) dehydrogenase 4; Idh1, isocitrate dehydrogenase 1 (NADP⁺), soluble; Idh3g, isocitrate dehydrogenase 3 (NAD⁺), gamma; Ldhb, lactate dehydrogenase B; Lta4h, leukotriene A4 hydrolase; Mdh1, malate dehydrogenase 1, NAD (soluble); Mdh2, malate dehydrogenase 2, NAD (mitochondrial); Me1, malic enzyme 1, NADP(+)-dependent, cytosolic; Mgll, monoglyceride lipase; mt-Atp8, mitochondrially encoded ATP synthase 8; Mthfd1, methylenetetrahydrofolate dehydrogenase (NADP⁺ dependent), methenyltetrahydrofolate cyclohydrolase, formyltetrahydrofolate synthase; Ndufa10, NADH dehydrogenase (ubiquinone) 1 alpha subcomplex 10; Ndufa2, NADH dehydrogenase (ubiquinone) 1 alpha subcomplex, 2; Ndufa9, NADH dehydrogenase (ubiquinone) 1 alpha subcomplex, 9; Ndubf10, NADH dehydrogenase (ubiquinone) 1 beta subcomplex, 10; Ndubf11, NADH dehydrogenase (ubiquinone) 1 beta subcomplex, 11; Ndubf9, NADH dehydrogenase (ubiquinone) 1 beta subcomplex, 9; Ndufc2, NADH dehydrogenase (ubiquinone) 1, subcomplex unknown, 2; Ndufs1, NADH dehydrogenase (ubiquinone) Fe-S protein 1; Ndufs6, NADH dehydrogenase (ubiquinone) Fe-S protein 6; Ndufv1, NADH dehydrogenase (ubiquinone) flavoprotein 1; Ndufv2, NADH dehydrogenase (ubiquinone) flavoprotein 2; Ogdh, oxoglutarate dehydrogenase (lipoamide); Pafah1b1, platelet-activating factor acetylhydrolase, isoform 1b, subunit 1; Pafah1b3, platelet-activating factor acetylhydrolase, isoform 1b, subunit 3; Pcyt2, phosphate cytidyltransferase 2, ethanolamine; Pdha1, pyruvate dehydrogenase E1 alpha 1; Pfkfb, phosphofructokinase, platelet; Pgam1, phosphoglycerate mutase 1; Pkm, pyruvate kinase, muscle; Prdx6, peroxiredoxin 6; Prps2, phosphoribosyl pyrophosphate synthetase 2; Rpn1, ribophorin I; Synj1, synaptojanin 1; Tkt, transketolase; Uqcrb, ubiquinol-cytochrome c reductase binding protein; Uqcrrh, ubiquinol-cytochrome c reductase hinge protein; Uqcrcq, ubiquinol-cytochrome c reductase, complex III subunit VII

2.5 Discussion

AgRP activation engages neural circuits to prevent and/or adapt to states of hunger by promoting energy conservation and euglycaemia. However, the ability of AgRP neurons to acutely respond to signals of incoming energy availability is also important to conserve energy, as illustrated by increased fatty acid utilisation and attenuated body weight gain on a HFD in AgRP neonatally ablated mice (Joly-Amado et al., 2012). This nutrient partitioning involves effectively and rapidly switching off peripheral fatty acid oxidation in favour of storage, characteristic of the transition from a fasted to refeed state. Our current studies suggest that Crat affects AgRP neuronal function predominantly during fasting and the transition to refeeding. This is based on observations in which the deletion of Crat in AgRP neurons changes 1) food intake and feeding behaviour after fasting; 2) hepatic function during fasting, which includes a shift to glycerol as a preferred gluconeogenic substrate; 3) peripheral glucose clearance in response to an acute glucose load; 4) peripheral fatty acid oxidation during fasting and in response to refeeding and 5) the intracellular protein abundance and acetylation status within AgRP neurons particularly during fasting and refeeding. Thus, the influence of Crat on AgRP neuronal function is most relevant during fasting and in the transition to refeeding. This occurs at a time when metabolic processing in AgRP neurons is most relevant to control nutrient partitioning in order to promote maximal energy conservation.

Although a large amount of literature has focused on the important role of AgRP neurons to increase energy conserving mechanisms during fasting, little research has focused on the mechanisms that enable AgRP neurons to respond to acute refeeding. In muscle, Crat regulates metabolic flexibility by facilitating the substrate switch during the transition from fasting to refeeding (Muoio et al., 2012; Seiler et al., 2015). These actions attenuate the development of metabolic diseases such as obesity and type-2 diabetes. Our results show that Crat in AgRP neurons is required to maintain metabolic flexibility during the transition from fasting to refeeding and suggest a distinct function of Crat in substrate switching, irrespective of tissue type. KO mice not only showed increased fatty acid utilisation during ad libitum and fasted conditions, as indicated by the lower RER, they also showed a blunted switch from fatty acid to glucose utilisation during the fasting to refeeding transition. Moreover, the deletion of Crat in AgRP neurons improves whole body glycerol and triglyceride handling and the response to lipoprotein lipase inhibition in the same manner as AgRP-ablation (Joly-Amado et al., 2012). Although this did not influence body fat loss during a single bout of fasting, we predict this would affect energy homeostasis during a model of chronic energy deficit such as calorie restriction or feeding entrainment, when AgRP neurons are most important to restore energy homeostasis (Andermann and Lowell, 2017).

The importance of Crat in AgRP neurons to maintain metabolic flexibility and nutrient partitioning was also observed after glucose administration, as blood glucose was significantly higher in KO mice

at 15 and 30 minutes post gavage primarily due to impaired glucose clearance, but returned to levels in WT mice at 60 and 120 minutes. Together with RER changes, these results show that Crat blunts, but does not prevent, the responsiveness of AgRP neurons. This observation is supported by measures of glucose-stimulated glucose uptake, which shows deficits in glucose uptake in iWAT and muscle at 15 minutes but not at 30 minutes. Interestingly, it is after this 30-minute time point that glucose clearance is no longer different in WT and KO mice during an oGTT.

Crat deletion affected the acetylation profile of proteins within AgRP neurons during fasting and refeeding but not in the fed state, which further highlights the important role of Crat in AgRP neurons during fasting to refeeding transition. This is consistent with others that show Crat plays an important role in intracellular acetylation of proteins (Davies et al., 2016; Madiraju et al., 2009) by regulating acetyl group availability for acetylation (Pietrocola et al., 2015). Further analysis of proteomic data highlighted that Crat regulates metabolic processing primarily during fasting and refeeding. Differentially regulated proteins included those involved in SIRT activity, NADH metabolism, uncoupling activity, glycolysis and mitochondrial dynamics. We also noted a number of differences related to proteins involved in synaptic function and endocytosis. This supports the concept that increased synaptic activity requires greater energetic demands via mitochondrial transport (Li et al., 2004), dynamics (Dietrich et al., 2013) and appropriate mitochondrial processing. Although a number of proteins regulating mitochondrial function are known to influence AgRP function and energy homeostasis, including mitofusins (Dietrich et al., 2013), AMPK (Claret et al., 2007), SIRT (Dietrich et al., 2010), PGC1a (Gill et al., 2016) and uncoupling protein-2 (Andrews et al., 2008), none of these studies have illustrated the importance of AgRP metabolic pathways during fasting and the refeeding transition.

Since AgRP neurons play a fundamental role in food intake, we examined the effects of Crat deletion on food intake and feeding behaviour. In *ad libitum* conditions, meal duration was significantly reduced, however, animals increased meal number such that overall food intake was not different between genotypes. These results are consistent with Campos et al. (Campos et al., 2016), in which inactivation of a subpopulation of AgRP to parabrachial CGRP neurons (AgRP→CGRP^{PBeI}) reduced meal duration but mice were able to increase meal number to maintain appropriate food intake. Moreover, this study showed the inability to engage the AgRP→CGRP^{PBeI} pathway heightened sensitivity to satiety cues (Campos et al., 2016), consistent with our observations that KO mice are more sensitive to feedback signals of satiety (i.p. CCK and ICV insulin). AgRP neurons projecting to the lateral hypothalamus, anterior bed nucleus of the stria terminalis, PVN and paraventricular thalamus also increase the drive to eat (Betley et al., 2013) independent from the AgRP→CGRP^{PBeI} pathway and elevated AgRP neuronal activity during fasting is required to elicit positive valence after MC4R^{PVN} activation (Garfield et al., 2015). Thus, under conditions of hunger, as seen in fasted mice, AgRP neurons promote energy intake by simultaneously increasing food intake and suppressing the

actions of satiety signals. Indeed, Crat deletion occurs in 90% of ARC NPY neurons, suggesting impaired pathways driving food intake and the AgRP→CGRP^{PBel} pathway that suppresses meal termination. Consistent with this, fasted KO mice exhibit reduced food intake during refeeding and smaller meal size and duration.

Although there was no difference in fasting blood glucose between genotypes, our results indicate that during fasting, the deletion of Crat from AgRP neurons forces the liver to generate glucose using glycerol as a substrate for gluconeogenesis. Hepatic glycogen depletion during fasting in humans increases glycerol as a substrate for gluconeogenesis, an effect dependent on an increase in lipolysis (Jahoor et al., 1992). Indeed, we observed greater glycogen depletion in fasted KO mice, supporting the concept that KO mice shift more quickly to glycerol as a gluconeogenic substrate, and show greater fatty acid oxidation. This change occurs without affecting rates of glycogenolysis and total gluconeogenesis and suggests a simple endpoint measurement of blood glucose is not sufficient to address the biological adaptive mechanisms that ensure euglycaemia. Importantly, gluconeogenesis from glycerol requires a constant rate of glycerol supply (Samuel and Shulman, 2016) and we observed significantly greater triglyceride concentrations in the liver and plasma NEFA in fasted KO mice, a phenomenon also witnessed in AgRP-ablated mice (Joly-Amado et al., 2012). Our data indicate greater hepatic fatty acid oxidation (gene expression, functional enzyme activity, and ketone bodies) in fasted KO mice reflects the need to breakdown TG to supply glycerol for gluconeogenesis. We also observed an increase in phosphoglycolate phosphatase (*pgp*) mRNA in adipose tissue, the enzyme required for glycerol release from adipocytes (Mugabo et al., 2016).

In summary, our studies show that AgRP neurons require Crat to regulate metabolic flexibility and peripheral nutrient partitioning during fasting and the transition to refeeding, similar to a known role of Crat in skeletal muscle (Muoio et al., 2012; Seiler et al., 2015). The metabolic flexibility required to acutely switch from fatty acid to glucose utilisation during refeeding represents an important mechanism that helps store energy-rich fatty acids and maximises energy conservation until required. We suggest that Crat in AgRP neurons is required for metabolic processing, as shown by a number of intracellular proteomic changes, to allow AgRP neurons to respond to changing metabolic states, particularly during “active” fasting states and during the transition to refeeding, which requires “acute inhibition” of AgRP neurons (Wu et al., 2014). Moreover, Crat within AgRP neurons engages sympathetic outflow in response to changing metabolic states, which in turn coordinates peripheral organs to optimise nutrient partitioning. The inability to properly adapt to changing metabolic substrates is clearly an important mechanism impacting the development of obesity-related diseases including diabetes and dyslipidaemia. Beyond calorie intake, it is becoming clear that the inappropriate handling of nutrient ‘fate’ is largely responsible for metabolic disease and this study shows that Crat in AgRP neurons has an unappreciated role in this process.

Supplemental Items In Appendix

1. Table 3 - MSprotein_enrichment_KOvsWT_fed. All proteins in the spreadsheet are significantly different between genotypes. Proteins highlighted in blue are listed as 2-fold higher, whereas those highlighted in yellow are listed as 2-fold lower expression, in KO mice relative to WT mice. Related to figure 2.10
2. Table 4 - MSprotein_enrichment_KOvsWT_fast. All proteins in the spreadsheet are significantly different between genotypes. Proteins highlighted in blue are listed as 2-fold higher, whereas those highlighted in yellow are listed as 2-fold lower expression, in KO mice relative to WT mice. Related to figure 2.10
3. Table 5 - MSprotein_enrichment_KOvsWT_refed. All proteins in the spreadsheet are significantly different between genotypes. Proteins highlighted in blue are listed as 2-fold higher, whereas those highlighted in yellow are listed as 2-fold lower expression, in KO mice relative to WT mice. Related to figure 2.10

Acknowledgements

We thank Minh Deo technical assistance. Authors acknowledge Monash FlowCore for sorting of cells using FACS. The authors acknowledge use of the facilities at the Monash Biomedical Proteomics Facility and the Monash Histology Platform. We thank Doug Compton from Research Diets for helping setup and establish BioDAQ feeding cages. This study was supported by an Australian NHMRC grant and fellowship to ZBA (1126724, 1084344) and MJW (APP1077703). This work used the PBRC Transgenic Core which is supported in part by COBRE (NIH 8P20GM103528) and the NORC (NIH 2P30-DK072476-11A1) center grants from the National Institutes of Health. AR is supported through an Australian Government Research Training Program Scholarship. JFG was a recipient of a funding from Conselho Nacional de Desenvolvimento Cientifico e Tecnologico-CNPq Brazil.

Author Contribution

A.R. and Z.B.A. conceived the idea, designed and performed the experiments, analysed data, and wrote the manuscript. Z.B.A. supervised and coordinated the project. G.M.K., C.R.B., R.B.S., B.J.O., S.L., and M.J.W. helped design experiments. R.S., R.E.C., S.H.L., C.H., M.B.L., J.F.G., G.M.K., C.R.B., M.M., S.L., R.R.G.D., and M.J.W. contributed to performing experiments. R.L.M. provided the Crat floxed mouse model. A.R., M.J.W., S.L., and Z.B.A. discussed the results and edited the manuscript. All authors read and approved the manuscript.

Declaration Of Interests

The authors have nothing to disclose.

2.6 Summary Chapter 2

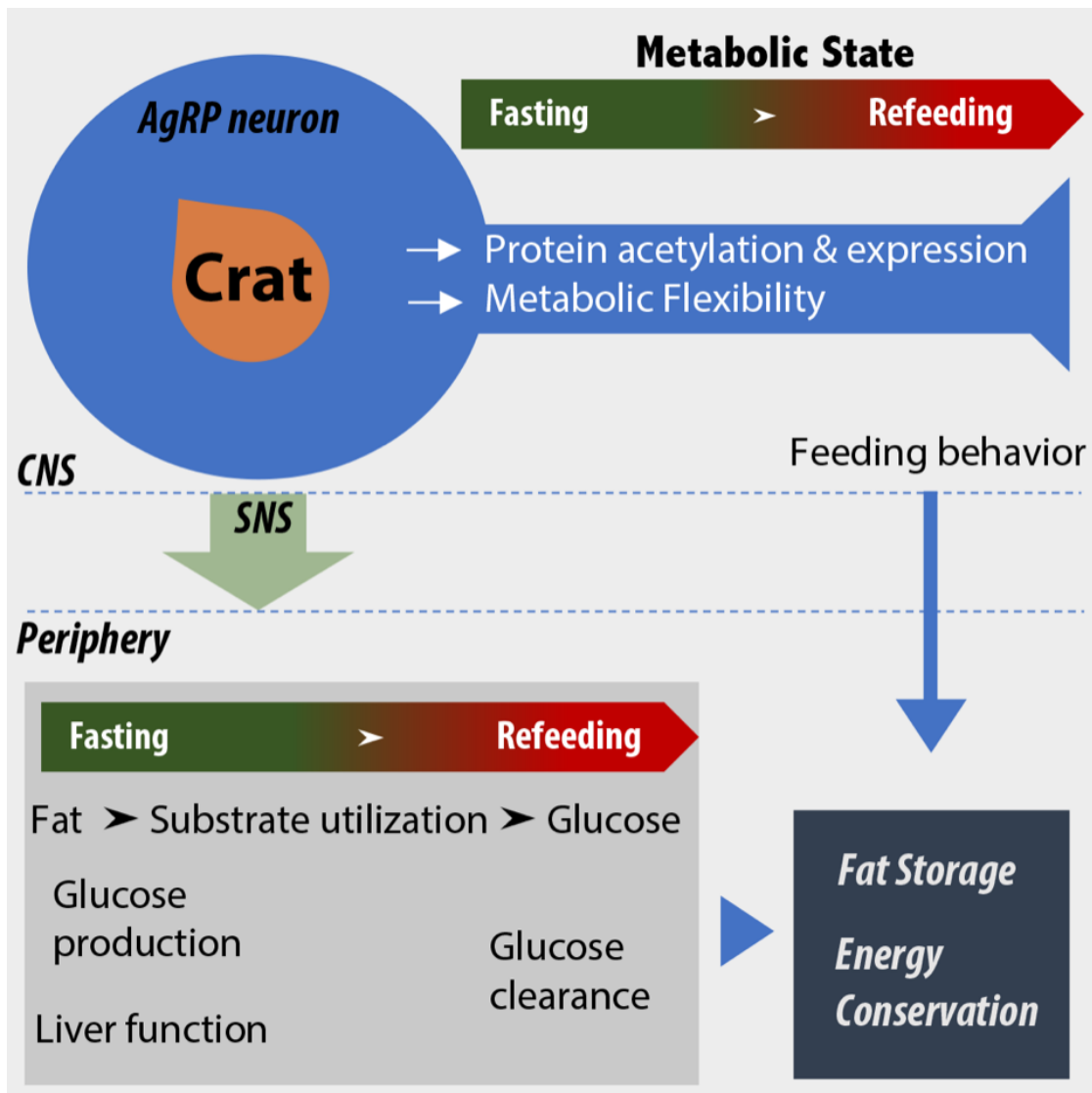


Figure 2.11 Summary of results from Chapter 2.

AgRP neurons require Crat to regulate peripheral substrate switching from fatty acid to glucose utilisation during fasting and the transition to refeeding. This mechanism preserves fatty acids, when glucose from food becomes available, and maximises energy conservation for future periods of energy deficit.

Highlights

- Crat in AgRP neurons helps nutrient replenishment as food is available after fasting.
- Crat in AgRP helps to maintain appropriate hepatic glucose production during fasting.
- Crat in AgRP neurons facilitates peripheral substrate switching upon acute refeeding.
- Crat regulates protein expression and acetylation in AgRP cells in fasting and refeeding.

Chapter 3: Carnitine acetyltransferase (Crat) in AgRP neurons permits adaptation to calorie restriction by regulating nutrient partitioning

The results presented in this Chapter are submitted for publication.

Carnitine acetyltransferase (Crat) in AgRP neurons permits adaptation to calorie restriction by regulating nutrient partitioning

Alex Reichenbach^{1,2}, Romana Stark^{1,2}, Mathieu Mequinion^{1,2}, Sarah H Lockie^{1,2}, Moyra B Lemus^{1,2}, Randall Mynatt^{3,4}, Serge Luquet⁵, Zane B Andrews^{1,2}

1. Monash Biomedicine Discovery Institute, Monash University, Clayton 3800, Victoria, Australia

2. Department of Physiology, Monash University, Clayton 3800, Victoria, Australia

3. Gene Nutrient Interactions Laboratory, Pennington Biomedical Research Center, Louisiana State University System, Baton Rouge, Louisiana, USA.

4. Transgenic Core Facility, Pennington Biomedical Research Center, Louisiana State University System, Baton Rouge, Louisiana, USA

5 Université of Paris Diderot, Sorbonne Paris Cité, Unité de Biologie Fonctionnelle et Adaptative, CNRS UMR 8251, F-75205 Paris, France.

Corresponding author and Lead Contact:

A/Prof Z. B. Andrews: Email: [REDACTED] Tel: [REDACTED]

Key words: substrate selection; rebound weight gain; body composition; RER; feeding behaviour; metabolic flexibility.

3.1 Abstract

Objective: Hunger-sensing AgRP neurons ensure survival by adapting metabolism and behaviour to low caloric environments. This is accomplished by consolidating food intake, suppressing energy expenditure and effectively partitioning energy upon food intake into storage to maximise energy preservation. We recently demonstrated that carnitine acetyltransferase (Crat) in AgRP neurons controls energy substrate utilisation during fasting and acute refeeding. Here we report the consequences of this impaired substrate utilisation in AgRP Crat KO mice under prolonged calorie restriction and with *ad libitum* feeding post CR.

Methods: Mice with an AgRP neuron specific deletion of Crat, or controls, were placed on a calorie restricted diet for 9 days and a number of metabolic parameters were examined including feeding behaviour, blood glucose, energy expenditure, substrate utilisation, body composition, brown adipose tissue temperature and locomotor behaviour. Following CR, all mice were monitored for 11 days to measure metabolic parameters associated with weight rebound.

Results: We found that Crat activity in AgRP neuron is essential for both, behavioural and metabolic adaptive response to energy deprivation. AgRP Crat KO mice exhibited impaired regulation of nutrient partitioning and increased fatty acid utilisation, which leads to greater fat loss after 9 days calorie restriction. Eleven days *ad libitum* feeding after CR results in greater food intake, rebound weight gain and adiposity in AgRP Crat KO mice compared to WT controls, as KO mice act to restore pre-CR fat mass.

Conclusions: Collectively, this study highlights the importance of Crat in AgRP neurons to regulate nutrient partitioning and fat mass during chronically reduced caloric intake. The increased food intake, body weight gain and adiposity in KO mice after the greater energy debt incurred during CR also highlights the detrimental metabolic consequence of impaired substrate utilisation and metabolic flexibility during the restriction phase. This may have significant implications for post dieting weight management in patients with metabolic diseases.

3.2 Introduction

The neural processing of peripheral energy state is indispensable for energy homeostasis and disturbances in this process are linked to the emergence of metabolic disorders including obesity and type 2 diabetes. (O'Rahilly and Farooqi, 2008). Neuronal populations within the hypothalamus are all implicated in the control of energy homeostasis, however Agouti-related peptide (AgRP) neurons in the ARC are arguably the most fundamentally important population to maintain body energy homeostasis.

AgRP neurons coexpress neuropeptide Y (NPY) and gamma-aminobutyric acid (GABA) and together with AgRP all three play an important role in regulating food intake and energy homeostasis (Krashes et al., 2013). The ablation of AgRP neurons during adulthood, which avoids development compensation, causes a dramatic loss of body weight and food intake to the point of starvation (Luquet et al., 2005). Moreover, AgRP ablation during the early postnatal period permits survival but results in increased peripheral lipid utilisation and lipolysis (Joly-Amado et al., 2012). In particular, AgRP/NPY neurons conserve energy by suppressing thermogenesis in white adipose tissue (WAT) (Dodd et al., 2017) and brown adipose tissue (BAT) (Ruan et al., 2014) and reducing energy expenditure (Shi et al., 2013) via the CNS and the sympathetic nervous system. These studies highlight the fundamental actions of AgRP neurons to signal hunger, as well as to preferentially store lipids particularly during energy deficit in order to promote survival.

AgRP itself is an endogenous antagonist at the melanocortin 4 receptor (MC4R) and central AgRP antagonism of the MC4R increased BAT temperature and glucose oxidation as indicated by the respiratory exchange ratio (RER), whereas stimulating MC receptor signalling increased lipolysis (Brito et al., 2007; Nogueiras et al., 2007). Moreover, NPY KO mice have increased fat loss caused by lipolysis during calorie restriction (Park et al., 2017). Collectively these results show that both AgRP and NPY peptides conserve energy by regulating nutrient partitioning and utilisation in peripheral tissues.

AgRP neurons are most active in response to a metabolic signature of negative energy balance that includes increased plasma ghrelin, free fatty acids, low glucose, low insulin, low leptin (Andermann and Lowell, 2017; Joly-Amado et al., 2014; Lockie and Andrews, 2013; Mandelblat-Cerf et al., 2015) and communicate with peripheral tissues through the SNS (Dodd et al., 2017; Nogueiras et al., 2009; Ruan et al., 2014; Shi et al., 2017). We recently discovered that carnitine acetyltransferase (Crat) in AgRP neurons is required to control food intake, feeding behaviour, glucose clearance, lipid utilisation and AgRP protein expression during fasting and refeeding. In particular, Crat in AgRP neurons regulated metabolic flexibility and facilitated a rapid switch from fatty acid to glucose oxidation upon nutrient replenishment after a single fast (Reichenbach et al., 2018), indicating

appropriate peripheral nutrient partitioning. These observations are consistent with studies deleting Crat in skeletal muscle, which increases fatty acid utilisation and reduces metabolic flexibility, or the ability to switch metabolic substrates, during the transition from fast to fed state (Muoio et al., 2012). This mechanism ensures that as glucose from food comes available for oxidation, such as during refeeding, fatty acid utilisation is acutely and rapidly switched off to conserve energy reserves.

Our previous study showed that Crat in AgRP neurons regulates metabolic flexibility and peripheral nutrient partitioning in response to a single fast (Reichenbach et al., 2018), however, the response to chronic calorie restriction remains unknown. Because calorie restriction involves multiple transitions from a fasted to fed state for a chronic period of time, we hypothesised that Crat in AgRP neurons would be critical for the adaptation to chronic energy deficit during calorie restriction. Moreover, we predict that increased fatty acid utilisation in a low caloric environment would increase fat loss in AgRP Crat KO mice. To test this hypothesis, we calorie-restricted mice with AgRP specific deletion of Crat (Reichenbach et al., 2018) and analysed changes in feeding behaviour, energy expenditure and body composition related to a low caloric environment.

3.3 Experimental Procedures

Animals

All experiments were conducted in compliance with the Monash University Animal Ethics Committee guidelines. Before starting calorie restriction experiments, mice were kept at standard laboratory conditions with free access to food (chow diet, cat no. 8720610 Barastoc stockfeeds, Victoria Australia) and water at 23 °C in a 12-hour light/dark cycle and were group-housed to prevent isolation stress.

Calorie restriction and *ad libitum* refeeding experiments

Male mice, 8-12 weeks of age, were singly housed in specialised feeding cages (BioDAQ; Research Diets, NJ, USA), fitted with computer controlled automatic gates to prevent access to feeding hoppers during calorie restriction experiments. This also allows stress-free intervention without human interaction. After twelve days *ad libitum* feeding (inclusive acclimation period) mice were subjected to 60% CR of their average food intake during *ad libitum* conditions for nine days. Mice gained access to food hoppers one hour before onset of dark phase and individual gates closed after mice consumed 1.8grams. Body weight and blood glucose (ACCU-CHEK® Active, Roche Diagnostics GmbH, Tokyo, Japan) of mice were measured daily 1-2 hours before refeeding (See Figure 1a for experimental protocol). After nine days calorie restriction, mice were allowed access to *ad libitum* chow for eleven days to assess changes in feeding behaviour.

Telemetry surgery

Mice were anaesthetised with isoflurane, and anaesthesia was maintained by constant nasal delivery of 2.5% isoflurane. Each animal received 50µL Metacam (0.25mg/mL Meloxicam; Boehringer Ingelheim) prior surgery in order to minimise post-surgery pain. Telemeter probes (Starr Life Science, Holliston, MA) were implanted into the interscapular brown adipose tissue (BAT), and mice were monitored for 48 hours. After one week recovery period, temperature and activity were recorded every minute with Vital View 2.0 (Starr Life Science, Holliston, MA) and data averaged over 15 minutes.

Body composition

Body composition of mice was assessed through EchoMRI™-100H Body Composition Analyzer (EchoMRI LLC, Houston, USA) by creating the average of 3 repeated scans. Body fat loss during calorie restriction was calculated as the difference of baseline (*ad libitum* fed) % body fat and after nine days calorie restriction. Loss and regain of body weight, lean and fat mass after 1, 4, 7 and 11 days *ad libitum* refeeding were calculated as % change from baseline.

Metabolic phenotyping

Energy expenditure and respiratory quotient were measured with Promethion metabolic cages (Sable systems) from day 7 to day 9 of calorie restriction and from day one to day eleven during *ad libitum* refeeding. During calorie restricted conditions, mice were subjected to the same protocol described above (access to 1.8 gram chow commencing one hour before onset of dark phase).

Analysis of blood chemistry

Plasma Insulin concentration was determined through an in-house ELISA assay.

Plasma concentration of acylated and des-acylated ghrelin (Mitsubishi Chemical Medience Corp), glucagon (Yanaihara Institute, Inc) and corticosterone (Abnova, Heidelberg, Germany) were measured with ELISA according to manufacturer's instructions.

Non-esterified fatty acid concentration, ketone bodies and triglycerides levels in plasma were measured using a NEFA C assay kit (Wako Pure Chemical Industries, Ltd. 1-2, Doshomachi 3-Chome, Chuo-Ku, Osaka 540-8605, Japan), β -hydroxybutyrate colorimetric assay kit (Cayman chemical company, Ann Arbor, Mi, USA) or triglyceride assay kit (Roche/Hitachi, Roche Diagnostics GmbH) respectively.

Tissue collection

After nine days calorie restriction or 11 days *ad libitum* refeeding, animals were deeply anesthetised with isoflurane, and blood was collected via cardiac puncture and hypothalamus, gastrocnemius and soleus muscle, liver, kidney, and epididymal and inguinal fat pads were collected. Plasma collected from blood samples was stored at -80°C , and samples collected were snap frozen in liquid nitrogen.

Reverse transcription-polymerase chain reaction

Total RNA was extracted from tissue with Qiazol (Qiazol Sciences) as described previously (Reichenbach 2017). Following SYBR Green Mastermix. Primers were obtained from GeneWorks Amplifications: Phosphoenolpyruvate Carboxykinase 1 (cytosol), PCK1 (TGCCCAAGGCAACTTAAGGG, CAGTAAACACCCCCATCGCT); glucose-6-phosphatase, catalytic, G6Pc (AGTCTTGTCAGGCATTGCTGT, AAAGTCCACAGGAGGTCCAC); glycogen phosphorylase, liver, Pygl (AAGAAGGGGTATGAGGCCAAA, GACACTTGACATAGGCTTCGT); glycogen synthase 2, liver, Gys2 (AATGTGAGCCCACCAACGAT, CTTCCAAAATGCACCTGGCA); glycerol kinase, GK (GCAACCAGAGGGAAACCACA, TAGGTCAAGCCACACCACG); Patatin-like phospholipase domain containing 2 (Pnpla2), transcript variant 1, Atgl (AGAGCCCATGGTCTCCGA, AGCAAAGGGTTGGGTTGGTT); Diacylglycerol acyltransferase , DGAT (TAGAAGAGGACGAGGTGCGA, GTCTTTGTCCCGGGTATGGG) Glycerol-3-phosphate acyltransferase, mitochondrial, GPAT (CCAGTGAGGACTGGGTTGAC, CTCTGTGGCGTGCAGGAATA); fatty acid synthase FASN (TGGGTGTGGAAGTTCGTCAG, CTGTCTGTGTCAGTAGCCGAG); carnitine palmitoyltransferase 1a CPT1

(ATCGCTTTGGGAGTCCACAT, CCATCGTTAAGGCACTGGGT); citrate synthase CS (TGTAGCTCTCTCCCTTCGGT, ACGAGGCAGGATGAGTTCTTG); 18S Ribosomal RNA 18S (TTCCGATAACGAACGAGACTCT, TGGCTGAACGCCACTTGTC) Quantitative real time PCR were performed using a Real Plex4 Mastercycler (Eppendorf).

Liver glycogen and triglycerides

Liver glycogen and triglyceride concentrations were measured as described previously (Reichenbach et al., 2018) with glucose oxidase assay kit (Sigma Aldrich, Saint Louis, Missouri 63103 USA) or Triglyceride assay kit (Roche/Hitachi, Roche Diagnostics GmbH) respectively.

Statistical Analysis

Statistical analyses were performed using GraphPad Prism for MacOS X (version 7.0b) All data are represented as mean \pm standard error of the mean (SEM). Two-Way ANOVAs with post hoc tests were used to determine statistical significance between treatment and genotype. A two-tailed Student's unpaired t-test was used when comparing genotype only. Linear regression analyses were performed to establish relationships between BAT temperature or locomotor activity and time. To determine relationships between two continuous variables we performed correlation analysis. $p < 0.05$ was considered statistically significant.

3.4 Results

Crat in AgRP neurons is required for adaption of feeding behaviour in response to calorie restriction

Our previous study confirmed Crat deletion in AgRP neurons and showed that Crat in AgRP neurons is required to regulate food intake, feeding microstructure, fatty acid metabolism and energy substrate utilisation after fasting. To determine if this predisposes to metabolic impairments in models of chronic energy deficit we exposed AgRP Crat WT and KO mice to a calorie restriction schedule (Figure 3.1a). Both AgRP Crat WT and KO mice were allowed to eat 1.8g, which was assessed as ~60% of *ad libitum* food intake during a baseline period.

After mice consumed 1.8g computer controlled gates closed and prevented access to the food hopper for the remainder of the 24-hour period. This approach allowed calorie restriction without human intervention and additional stressors unrelated to the experimental paradigm. Interestingly, caloric restriction for nine days did not produce a difference in body weight or blood glucose (Figure 3.1b&c), however body composition analysis before and after caloric restriction in the same mice revealed that AgRP Crat KO mice lost a significantly greater percentage body fat (Figure 3.1d), while preserving lean mass (Figure 3.1e).

Although all mice were allowed only to eat 1.8g, AgRP Crat KO displayed significant differences in meal feeding microstructure, consistent with results from fasting and *ad libitum* feeding behaviour (Reichenbach et al., 2018). All mice started to consume chow within a few minutes after gaining access, however AgRP Crat KO mice took significantly longer (~8 hours vs ~4 hours in WT mice) to consume most of the 1.8g ration (Figure 3.1f-h), had fewer feeding bouts, but spent more time in a feeding bout (Figure 3.1i+j). Overall, WT mice adapted to the feeding regime and changed feeding behaviour accordingly by progressively consolidating their food intake into a smaller feeding window (Figure 3.1h), whereas KO mice did not by the end of nine-day calorie restriction.

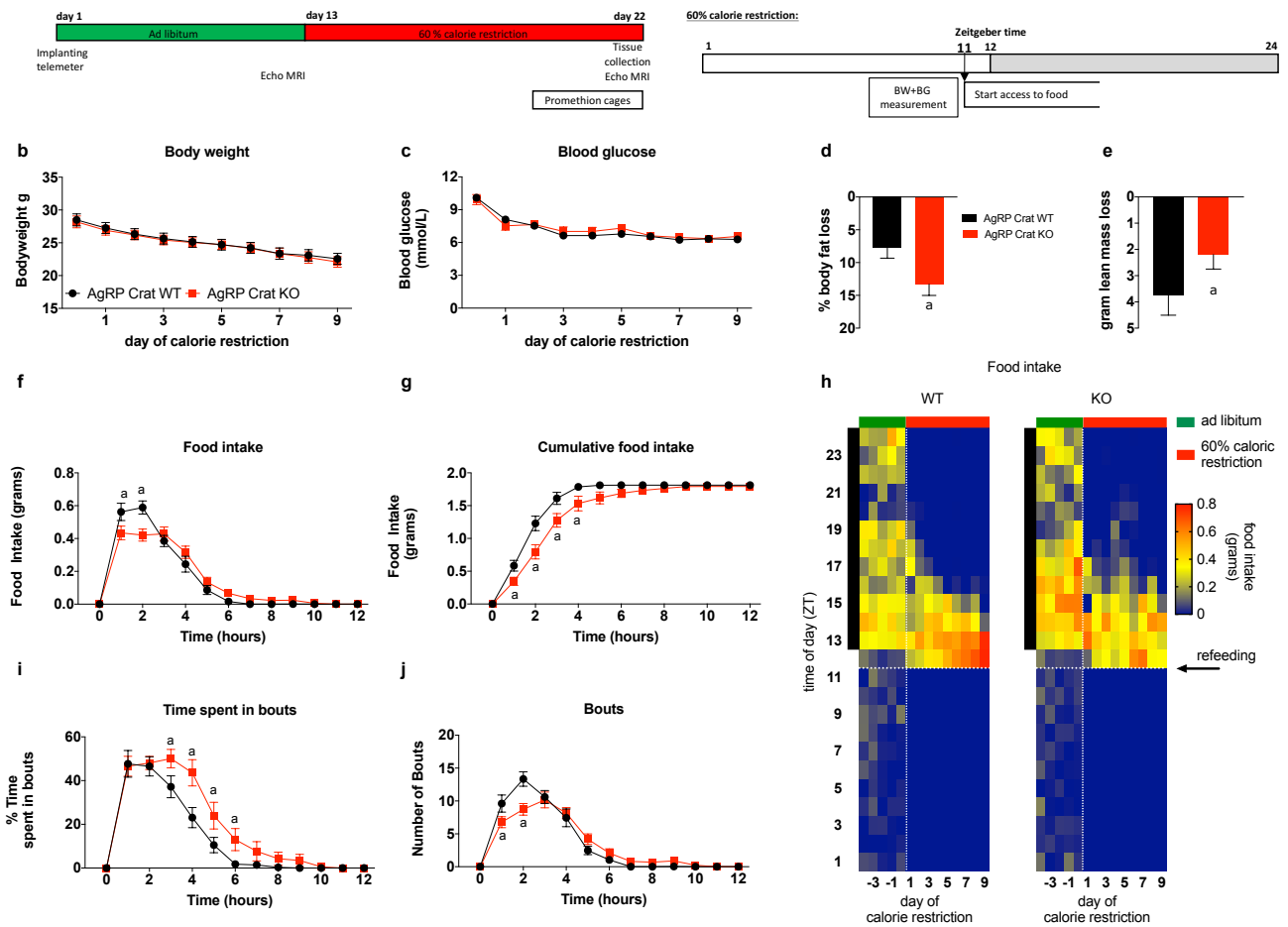


Figure 3.1: Crat in AgRP neurons is required for adaption of feeding behaviour in response to calorie restriction

Experimental timeline of calorie restriction in BioDaq feeding cages. Three cohorts were subjected to the same feeding schedule, BAT temperature and locomotor activity were measured in Cohort 1, body composition assessed in cohort 2 and metabolic phenotype analysed in cohort 3 (a). There were no differences in body weight development (b) nor blood glucose development (c) between genotypes. Body composition examination was performed before and after the experiment, and revealed greater loss of relative fat mass (d) and less loss of lean mass (e) in KO during calorie restriction. Food intake (f), cumulative food intake during calorie restriction (g) and food intake under ad libitum fed and CR conditions shown as heat map (h). Each voxel represents food intake of one hour, each column represents a day, black bar on left hand side indicates dark phase, green bar on top of heat map indicates ad libitum access to food, red bar restricted access to 1.8gram per 24 hours starting at 11 ZT, indicated by horizontal dotted line. Time spent in bouts (i) and bouts (j) averaged over nine days of calorie restriction quantify the deficits in feeding behaviour. All data are expressed as mean \pm sem; $n=9-11$. Two-way (repeated measured; where appropriate) ANOVA with Sidak posthoc analysis; a, significant at $p<0.05$.

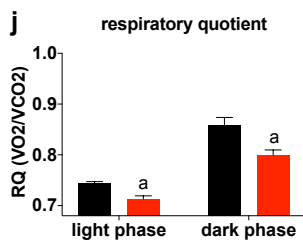
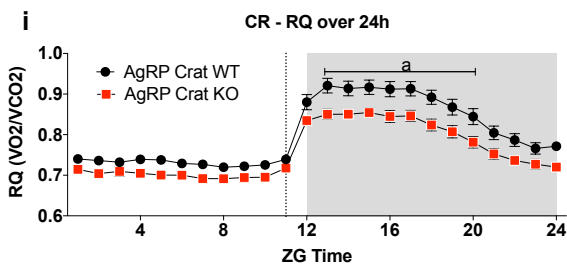
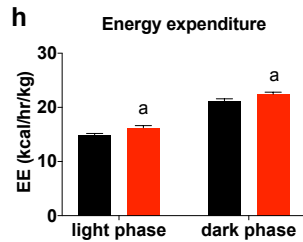
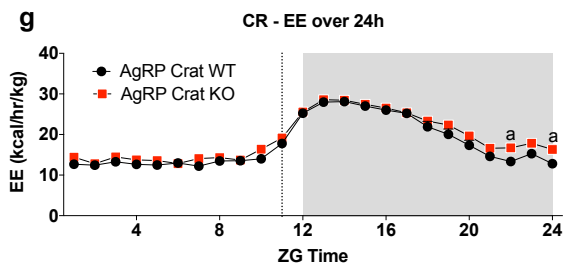
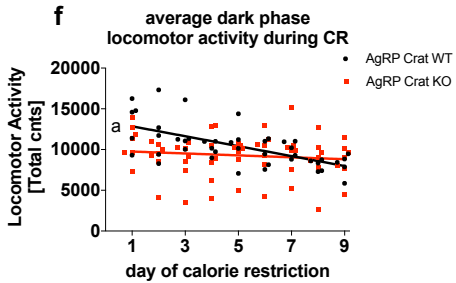
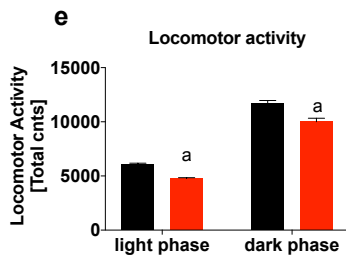
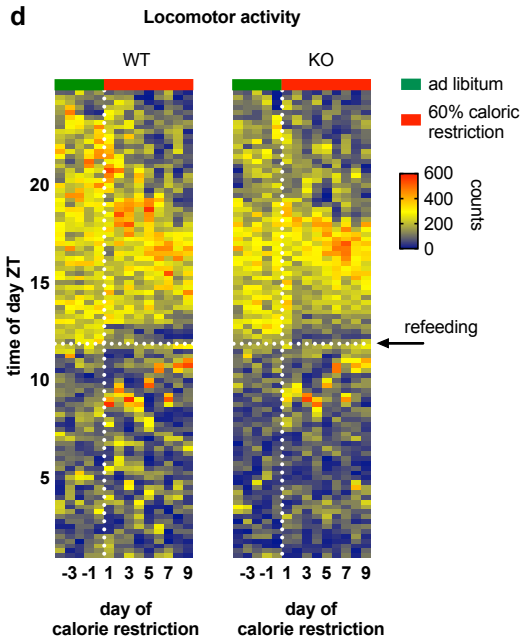
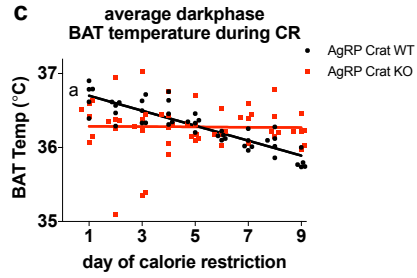
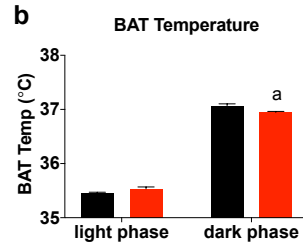
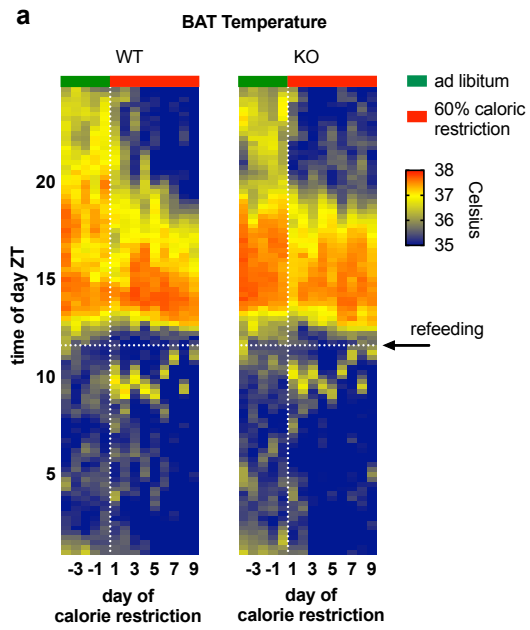


Figure 3.2. *Crat* in AgRP neurons is needed to regulate nutrient partitioning and energy expenditure in response to calorie restriction

Brown adipose tissue (BAT) temperature (a) and locomotor activity (d) under ad libitum fed and CR conditions shown as heat map. Each voxel represents average BAT temperature or cumulative locomotor activity of 15 min intervals, each column represents a day, black bar on left hand side indicates dark phase, green bar on top of heat map indicates ad libitum access to food, red bar restricted access to 1.8gram per 24 hours starting at 11 ZT, indicated by horizontal dotted line. Average BAT temperature during light and dark phase of ad libitum fed animals (b) and regression analysis of average BAT temperature during dark phase of nine consecutive days calorie restriction (c). Total locomotor activity during light and dark phase of ad libitum fed animals (e) and regression analysis of total dark phase locomotor activity under CR conditions (f). Average 24-hour profile of energy expenditure (g) and respiratory quotient (i) of calorie restriction day 7-9, and light and dark phase average of energy expenditure (h) and respiratory quotient (j) of this period. All data are expressed as mean \pm sem; n=5-7. Two-way (repeated measured; where appropriate) ANOVA with Sidak posthoc analysis; a, significant at $p < 0.05$.

Crat in AgRP neurons is needed to regulate nutrient partitioning and energy expenditure in response to calorie restriction

Implanting temperature probes into the interscapular brown adipose tissue (BAT) of mice allowed us to record real-time BAT temperature changes as well as locomotor activity in response to calorie restriction. KO mice had slightly lower average BAT temperature during the dark phase under ad lib conditions (Figure 3.2a+b) and failed to reduce average BAT temperature during the dark phase in response to calorie restriction (Figure 3.2a+c). A similar effect was observed for locomotor activity in which WT mice exhibit greater locomotor activity during *ad libitum* conditions (Figure 3.2d+e), with a 40% reduction from the first to last day of calorie restriction. KO mice showed a non-significant reduction in their locomotor activity by about 20% during this period (Figure 3.2d+f), collectively suggesting greater energy conservation in WT mice during calorie restriction. To estimate energy expenditure under these advanced CR conditions we placed mice in metabolic cages on days 7-9 of the calorie restriction protocol. We found that KO mice have increased average energy expenditure during this period (Figure 3.2g+h), matching the discrepancy observed in BAT temperature (Figure 3.2c), and lower RER (Figure 3.2i+j) compared to WT litter mates. The lower RER indicates that KO mice are preferentially utilising fatty acids as an energy substrate, which accounts for the greater loss of fat mass during calorie restriction (Figure 3.1d). This increase in fatty acid utilisation during CR is consistent with results during acute fasting (Reichenbach et al., 2018).

Crat in AgRP neurons affects hepatic function in response to calorie restriction

In previous fasting studies, we observed no differences measurable in blood glucose in WT and KO mice; however, there were significant adaptive changes in the liver of KO mice to support ongoing glucose production (Reichenbach et al., 2018). This included reduced liver glycogen and elevated liver triglyceride as well as changes in gene expression and the substrate contributing to gluconeogenesis. To test if similar changes occur in the calorie restricted state, we measured liver glycogen and triglyceride at the end of the 9-day restriction protocol. Liver analysis revealed a non-

significant trend towards lower glycogen (Figure 3.3a), but equal triglyceride (Figure 3.3b) concentrations in AgRP Crat KO relative to WT mice. Liver gene expression revealed an increase in gene transcripts involved in gluconeogenesis (*Pck1*, *G6pc*) and glycogen breakdown (*Glycogen phosphorylase*), as well as carnitine palmitoyltransferase 1a (*Cpt1a*) and citrate synthase (*Cs*) suggesting increased liver fatty acid oxidation and mitochondrial biogenesis in KO relative to WT mice (Figure 3.3c). Interestingly, we observed an increase in *Fasn* suggesting a possible compensatory attempt to increase *de novo* lipid synthesis due to low liver triglyceride after nine days of calorie restriction, as described elsewhere (Bruss et al., 2010).

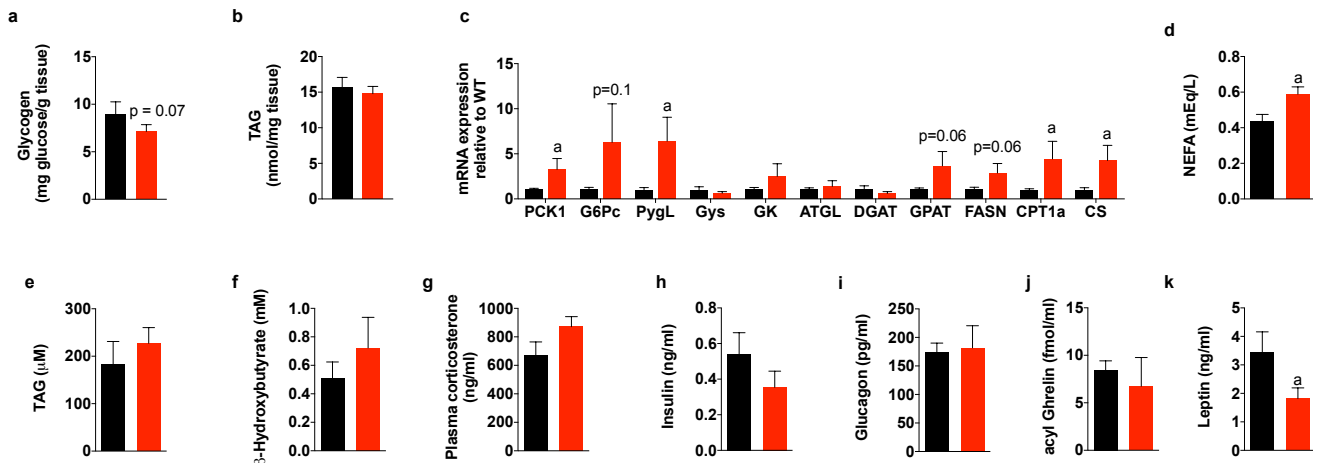


Figure 3.3. Crat in AgRP neurons affects hepatic function in response to calorie restriction

Liver glycogen (a) and triglycerides (b) after nine days of calorie restriction. Hepatic gene expression of enzymes involved in gluconeogenesis, glycogenolysis, lipogenesis, and lipolysis (c). Plasma profiles after calorie restriction of metabolites: NEFA (d), triglycerides (e), and ketone bodies (f), and hormones: corticosterone (g) insulin (h) glucagon (i), acyl-ghrelin (j), and leptin (k) All data are expressed as mean \pm sem; n=6-9. two-tailed Student's unpaired t-test; a, significant at $p < 0.05$

Plasma NEFAs (Figure 3.3d) were significantly higher in AgRP Crat KO mice reflecting greater lipolytic rates yet plasma triglycerides and ketone bodies were not significantly increased (Figure 3.3e&f). No differences were observed in corticosterone, acyl ghrelin, insulin, and glucagon between AgRP Crat WT and KO mice at the end of caloric restriction (Figure 3.3g-j), but leptin levels were significantly lower in calorie-restricted KO mice (Figure 3.3k), reflecting reduced adiposity.

Crat in AgRP neurons influences rebound weight gain, food intake, and adiposity after cessation of calorie restriction.

At the end of calorie restriction, body weight and blood glucose did not differ between genotypes, however, due to changes in nutrient partitioning, KO mice had a significantly greater fat loss and less lean muscle loss. In order to determine if this change in body composition affected rebound weight gain, food intake or adiposity we followed mice for 11 days after the cessation of calorie restriction.

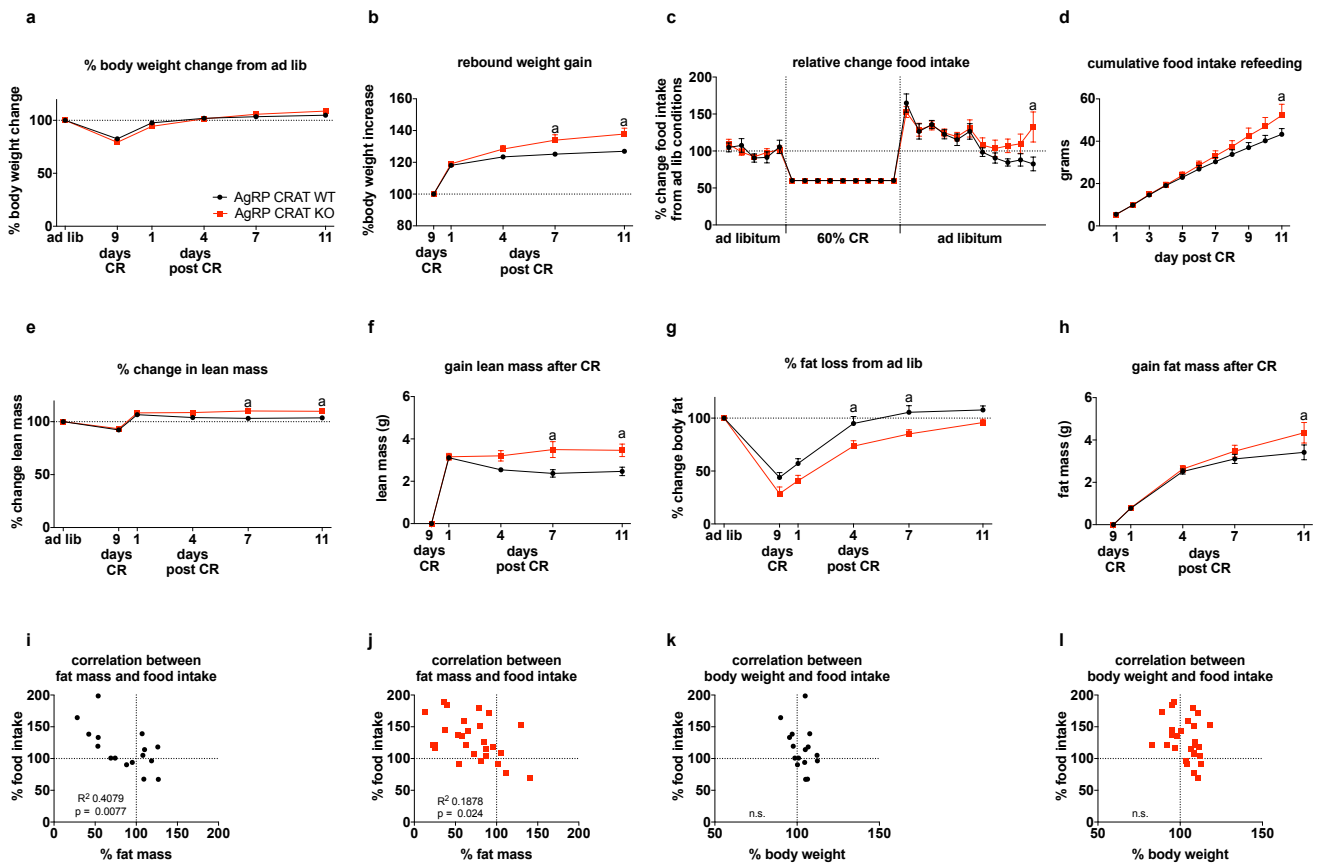


Figure 3.4. *Crat* in AgRP neurons influences rebound weight gain, food intake and adiposity after cessation of calorie restriction.

Relative changes to baseline in bodyweight after calorie restriction and ad libitum refeeding (b) and rebound weight gain during ad libitum refeeding (b). Changes in average 24hour food intake relative to baseline ad libitum fed conditions (c) and cumulative food intake during ad libitum refeeding (d). Changes relative to baseline in lean mass (e) and fat mass (g) after calorie restriction and ad libitum refeeding and gain in lean mass (f) and fat mass (h) during ad libitum refeeding. Correlation between changes in food intake and changes in fat mass (i+j) and correlation between changes in food intake and changes in body weight (k+l). All data are expressed as mean \pm sem; n=9-11. Two-way (repeated measured; where appropriate) ANOVA with Sidak posthoc analysis; a, significant at $p < 0.05$.

When compared to pre-CR body weight, WT and KO mice rapidly recover body weight reaching their baseline weight after 4 days refeeding and continue to moderately gain weight (WT 105%, KO 109%; Figure 3.4a). However, weight gain after CR significantly increased in KO mice when compared with body weight at the end of CR (Figure 3.4b). Intriguingly, after the cessation of CR, both WT and KO mice dramatically increased their 24-hour food intake to approximately 165% and 150% of baseline *ad libitum* food intake respectively. With time, WT mice reduced their daily food intake to below baseline levels after 7 days *ad libitum* refeeding but KO mice continued to consume more compared to *ad libitum* food intake resulting in significantly greater chow consumption at the end of the experimental period (Figure 3.4c+d).

Body composition analysis with ECHO MRI dissociated weight gain in lean mass from that in fat mass (Figure 3.5a). This showed that the increase in body weight the first day after cessation of CR

is due to complete restoration of pre-calorie-restriction lean mass (Figure 3.4e). While WT mice slightly reduce lean mass thereafter, KO mice maintain the increased lean mass to the end of the experiment (Figure 3.4f). The restoration of fat mass after calorie restriction takes longer, with WT mice reaching pre-calorie-restriction adiposity between 4-7 days *ad libitum* refeeding. Despite gaining more absolute fat mass (Figure 3.4h), KO mice did not reach their pre-CR adiposity level until after 11 days ad lib refeeding (Figure 3.4g), due to the greater fat loss during calorie restriction (Figure 3.4g, compare Figure 3.1d). Dulloo et al suggest the interplay between mechanisms regulating fat and protein mass, including the ratio of secreted adipokines and myokines, may regulate body composition (Dulloo et al., 2015) and determine food intake in order to regain fat and lean mass. In our studies, KO mice gained more relative fat and lean mass compared to WT control and also consumed more food. Furthermore, the significant inverse correlation between the relative change in fat mass and change in food intake (Figure 3.4i+j) suggests that elevated food intake in KO mice in the post CR period is to restore adiposity levels to pre-CR levels and not body weight per se (Figure 3.4k+l). This is in line with leptin from adipose tissue as an endocrine signal that communicates long-term energy availability to the brain (Rosen and Spiegelman, 2014; Stern et al., 2016).

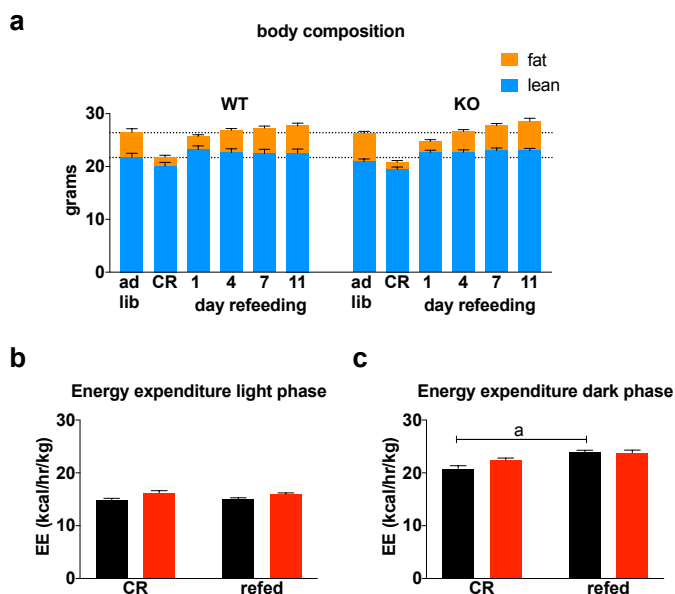


Figure 3.5 Influence of calorie restriction and refeeding on body composition and energy expenditure.

Body composition measured by Echo MRI before and after calorie restriction and during refeeding (a). Average light (b) and dark phase (c) energy expenditure measured during calorie restriction day 7-9 and during ad libitum refeeding. All data are expressed as mean \pm sem; $n=9-11$. Two-way (repeated measured; where appropriate) ANOVA with Sidak posthoc analysis; a, significant at $p<0.05$.

Therefore, we analysed circulating leptin from plasma of refeed mice (Figure 3.6a) and found no difference between genotypes for leptin levels or for the correlation between circulating leptin levels and fat mass (Figure 3.6d+e). Measuring insulin (Figure 3.6b) and NEFA (Figure 3.6c) from the same animals also did not reveal differences between genotypes. Metabolic analysis during *ad libitum* refeeding reveals that there are no genotype differences in energy expenditure (Figure 3.6g). Also, comparing energy expenditure between CR and post CR *ad libitum* feeding (Figure 3.5b,c) shows that WT mice reduced EE during CR in the dark phase, but not light phase, and KO maintained high EE during calorie restriction. Furthermore, KO mice have lower RER compared to WT controls (Figure 3.6f+h) showing a persistent increase in fatty acid utilisation 11 days post CR. Despite this persistent increase in lipid utilisation, mice consume more food and gain fat mass compared to WT in order to restore pre-CR adiposity levels.

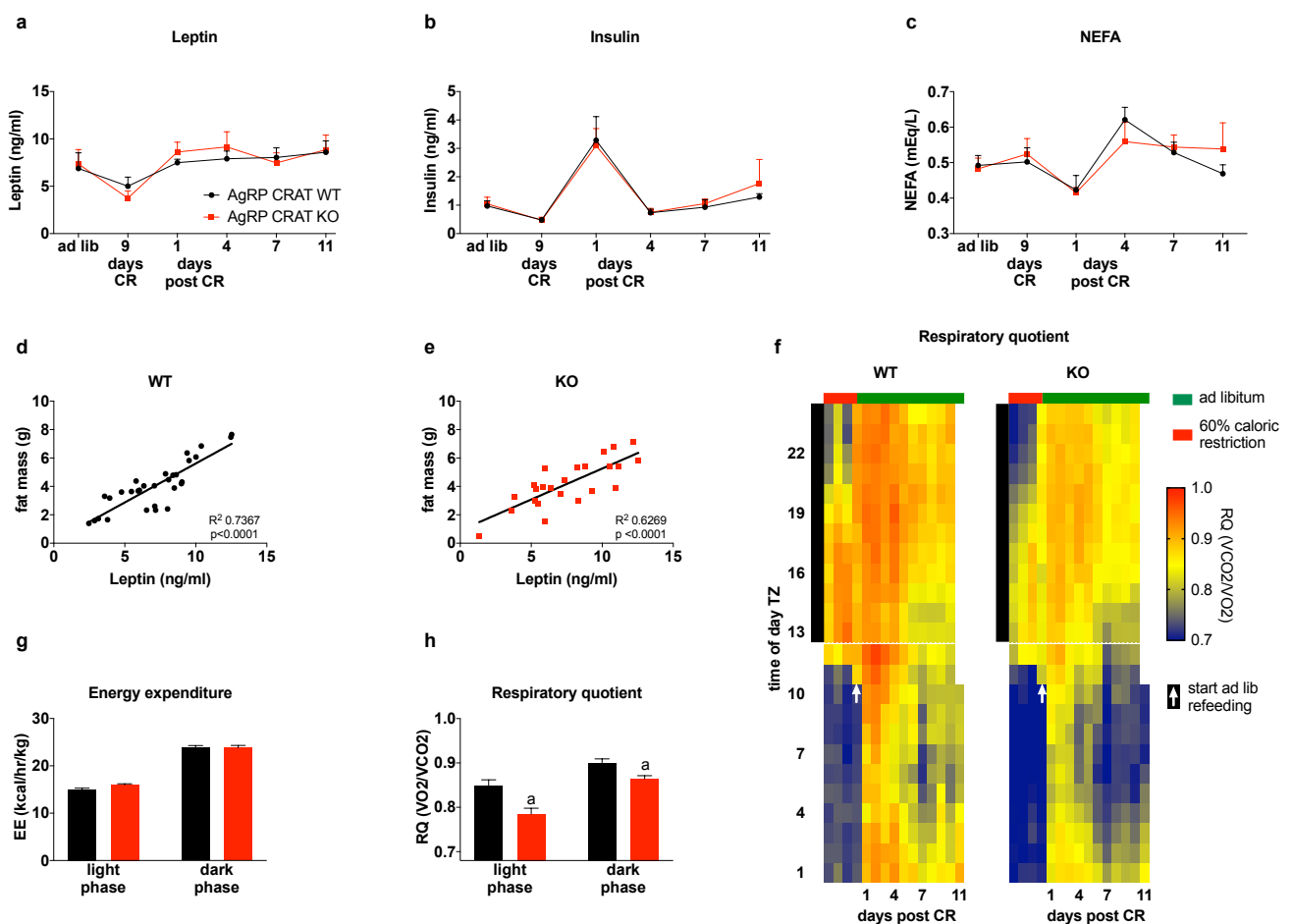


Figure 3.6. *Crat* in AgRP neurons regulates substrate selection during *ad libitum* refeeding

Plasma leptin (a) insulin (b) and free fatty acids (NEFA) (c) during *ad libitum* refeeding, and correlation between leptin levels and fat mass (d+e). Heat map depicting temporal changes in respiratory quotient during transition from calorie restricted to *ad libitum* refeed conditions (f). Each voxel represents average RQ of one hour, each column represents a day, black bar on left side indicates dark phase, red bar on top indicates restricted access to 1.8gram per 24 hours starting at 11 ZT, indicated by horizontal white line, *ad libitum* access to food is indicated by green bar on top of heat map and start of *ad libitum* refeeding is indicated by white arrow. Average Energy expenditure (g) and respiratory quotient (h) of light and dark phase during *ad libitum* refeeding. All data are expressed as mean \pm sem; $n=9-11$. Two-way (repeated measured; where appropriate) ANOVA with Sidak posthoc analysis; a, significant at $p<0.05$.

3.5 Discussion

The metabolic flexibility to acutely switch fatty acid to glucose utilisation during refeeding represents an important mechanism referred to as “nutrient partitioning” that helps store energy-rich fatty acids and maximises energy conservation until required. Our previous studies show that Crat in AgRP neurons is important to regulate metabolic flexibility and peripheral nutrient (Reichenbach et al., 2018). Here we demonstrate that crat-mediated metabolic signalling in AgRP neurons regulates metabolic adaptation to a chronic state of low caloric intake (60% CR) by regulating meal feeding structure, BAT thermogenesis, peripheral energy expenditure and energy substrate utilisation.

Although Crat deletion from AgRP neurons does not affect body weight loss or blood glucose during CR, it causes a greater loss of body fat. Intriguingly, rebound weight gain, lean and fat mass as well as food intake all increased and fatty acid utilisation remained high after the cessation of CR in KO mice compared to WT controls. These studies suggest that Crat in AgRP neurons regulates peripheral nutrient partitioning to preserve lipid stores and suppress energy expenditure during chronic nutrient shortfall associated with CR. These studies also highlight that chronic impairment in nutrient partitioning during calorie restriction can impact rebound weight gain, rebound food intake and rebound adiposity. Such an observation may have implications for rebound weight gain after diet-restricted weight loss interventions in humans. This is especially important considering metabolic diseases such as diabetes, NAFLD, and dyslipidaemia can develop due to inappropriate nutrient “fate” without significant changes in body weight (Darabian et al., 2016; Gastaldelli, 2017; Goodpaster and Sparks, 2017; Padwal et al., 2016).

In terms of meal feeding structure, WT mice adapt over the course of the calorie restriction protocol to quickly consume food, which was always introduced at the same time of the day during CR, an effect that is supported by previous studies (Acosta-Rodriguez et al., 2017). The finding that AgRP Crat KO mice do not show the same temporal adaptation over the course of CR infers that Crat in AgRP neurons is crucial for assessment of food availability and may be involved in a food-entrainable oscillator (FEO) (Carneiro and Araujo, 2009). Tan et al demonstrated that ablating AgRP neurons delays food intake under a day-time restricted feeding regime, as well as abolishes the food-anticipatory activity, an important feature of the FEO (Tan et al., 2014). In support of this, KO mice did not exhibit a similar temporal adaptation in BAT temperature, locomotor activity or energy expenditure, all of which are important functions controlled by AgRP neurons (Brito et al., 2007; Ruan et al., 2014; Shi et al., 2013). Given that Crat in AgRP neurons is required for metabolic flexibility and peripheral nutrient partitioning, it is tempting to speculate that the metabolic processing of incoming nutrients via Crat is a key component of the FEO. There is evidence to support this claim since feeding time influences metabolism (Mauvoisin et al., 2017; Shamsi et al., 2014; Zwihaft et al., 2015) and circadian cycles influence mitochondrial rate-limiting enzymes and nutrient utilisation (Neufeld-Cohen et al., 2016). In a proteomic screen of AgRP neurons from WT and KO mice, we

observed numerous differences in mitochondrial enzymes, NAD⁺-regulating enzymes and differences in protein acetylation (Reichenbach et al., 2018), all of which affect NAD⁺ bioavailability and modulate mitochondrial oxidative function across cycles of fasting and feeding (Peek et al., 2013). Collectively these results suggest Crat in AgRP neurons may be vital for the accurate assessment of peripheral nutrient availability and subsequent nutrient partitioning, which enables behavioural and metabolic adaptation to chronic low caloric environments to ensure and maximise energy conservation.

In previous experiments, we demonstrated that AgRP Crat KO mice exhibit a shift towards increased fatty acid utilisation and an attenuated switch to glucose oxidation with nutrient replenishment after fasting (Reichenbach et al., 2018). Our observations herein show that prolonged preferential fatty acid utilisation and increased lipolysis, as indicated by lower RER and increased NEFAs respectively, during chronic low-caloric conditions results in increased body fat loss. This shift towards fatty acid utilisation might be facilitated by reduced AgRP-mediated antagonism of melanocortin 4 receptors (MC4R) resulting in augmented MC4R signalling and increased lipolysis (Brito et al., 2007; Nogueiras et al., 2007). Nevertheless, our results are consistent with the ablation of AgRP or NPY neurons on substrate utilisation and nutrient partitioning (Joly-Amado et al., 2012; Park et al., 2017).

Consistent with our previous report (Reichenbach et al., 2018) we observed a hepatic mRNA profile with increased gluconeogenic and glycogenolytic genes as well as genes suggesting increased liver fatty acid oxidation and mitochondrial biogenesis in KO to feed gluconeogenesis (Jackowski and Leonardi, 2014). The differences in hepatic gene profile are supported by a lower glycogen concentration in KO mice. Furthermore, we observed an increase in *Fasn* suggesting an increase in *de novo* lipid synthesis. Indeed, it has been reported that *de novo* lipid synthesis is elevated to meet the lipid demand during calorie restriction (Bruss et al., 2010).

Although the integrated neural circuit responsible for the effect of CR on lipolysis and fat utilisation remains unknown, it presumably involves impaired SNS-mediated communication with peripheral tissues as seen in previous studies on AgRP function (Kuperman et al., 2016; Reichenbach et al., 2018; Ruan et al., 2014; Shi et al., 2017). Furthermore, AgRP->PVN pathway subpopulation is required to drive positive reinforcement after food intake in caloric depleted mice (Chen et al., 2016; Garfield et al., 2015). Moreover, food ingestion also alleviates a negative valence signal conferred by persistent AgRP neurons (Betley et al., 2015). Thus, these combined actions in WT mice presumably underlie the temporal adaptation to consume quickly over the 9-day restriction protocol. That KO mice take longer to consume the same amount suggests altered processing in response to these valence cues, which may affect motivational aspects of food intake during a state of homeostatic need (Betley et al., 2015). Indeed, fewer feeding bouts 4 hours after food access and

reduced food consumption despite more time in a given feeding bout, suggests that deletion of Crat in AgRP neurons affects the motivation for food intake. Future studies are required to address this suggestion.

We propose that Crat may be a critical enzyme, which enables AgRP neurons to act as “energy calculators”, as proposed by Beutler et al (Beutler et al., 2017) integrating information on acute changes in energy balance and regulating substrate utilisation in response. Indeed, we have previously shown, that deleting Crat in AgRP neurons impairs the switch in substrate utilisation upon refeeding, but does not disturb energy homeostasis under *ad libitum* fed conditions (Reichenbach et al., 2018). Furthermore, we found no differences in the orexigenic hormone ghrelin and lower levels of leptin in calorie-restricted animals, supporting the notion that AgRP neurons regulate energy homeostasis through multiple mechanisms on different time scales. In our view, Crat activity in AgRP neurons would allow a temporally regulated response allowing for the proper orchestration of peripheral organ activity through the autonomic nervous system (Joly-Amado et al., 2012; Reichenbach et al., 2018), in that view perception of food quality and availability and later on calorie intake would have a dynamic action onto AgRP neuron activity through Crat activity allowing for adaptive nutrient partitioning.

Our post CR *ad libitum* refeeding experiments demonstrate that AgRP Crat KO mice, despite losing more fat under calorie restricted conditions, are capable of regenerating fat mass by increasing food intake until pre-diet-adiposity is reached, similar to WT controls. Surprisingly, despite the greater loss of body fat at the end of CR, KO mice had no difference in body weight due to a preservation of lean mass and even increase their relative lean mass during post CR *ad libitum* feeding, leading to greater rebound body weight compared to WT. In support of this, AgRP activation is associated with increased circulating plasma myostatin (Steculorum et al., 2016), which is a negative regulator of muscle mass. Since the inhibition of myostatin increases muscle mass in mice (Whittemore et al., 2003), any influence on the ability of AgRP neurons to regulate myostatin may affect the preservation or restoration of lean mass; we suggest the deletion of Crat in AgRP neurons represents one such influence over AgRP neurons. This finding might have implications for muscle degenerative diseases such as cachexia or muscle dystrophy, but further research is needed, as CR has differential effects on muscle dependent on strain, sex and time (Boldrin et al., 2017). Recent studies suggest also osteocytes as body weight sensor, regulating food intake independent of leptin in order to maintain bodyweight (Jansson et al., 2017) The relative increase in lean mass elevates basal metabolic rate (Hopkins et al., 2016; Weise et al., 2015), which is known to influence food intake (Kennedy, 1953), offering an explanation for increased food intake in AgRP Crat KO during *ad libitum* refeeding.

In summary, Crat deletion in AgRP neurons promotes a shift towards increased fatty acid utilisation, which persists during the post CR feeding period. This chronic impairment in nutrient partitioning

affects food intake, body composition, adiposity and rebound weight gain after a period of CR, which has significant implications for people in weight loss programs, especially considering metabolic inflexibility in obesity (Goodpaster and Sparks, 2017). Collectively our results demonstrate that Crat in AgRP neurons is crucial for adaptation to low caloric environments. In particular, this is achieved by adjusting feeding behaviour to consume food quickly, control nutrient partitioning and substrate selection to preserve fat stores, and regulate energy expenditure to conserve energy. Furthermore, our results demonstrate the importance of substrate selection and metabolic flexibility during refeeding in light of weight management after dieting. This highlights the fact that Crat in AgRP neurons acts as an integrator of acute changes to adapt metabolism and behaviour by regulating nutrient partitioning, and that defects of this mechanism impact body weight and adiposity with implications for metabolic diseases.

Acknowledgements

We thank Doug Compton from Research Diets for helping setup and establish BioDAQ feeding cages. This study was supported by an Australian NHMRC grant and fellowship to ZBA (1126724, 1084344). This work used the PBRC Transgenic Core which is supported in part by COBRE (NIH 8P20GM103528) and the NORC (NIH 2P30-DK072476-11A1) center grants from the National Institutes of Health. AR is supported through an Australian Government Research Training Program Scholarship. SHL and RS are supported by an Australian NHMRC early career research fellowship.

Author Contribution

AR and ZBA conceived the idea, designed and performed the experiments, analysed data, and wrote the manuscript. ZBA supervised and coordinated the project., SL helped design experiments. MM, MBL, SHL, RS contributed to perform experiments. RM provided Crat floxed mouse model. AR, SL, ZBA discussed results and edited the manuscript. All authors read and approved the manuscript.

CONFLICT OF INTEREST:

The authors declare no conflicts of interest.

3.6 Summary Chapter 3

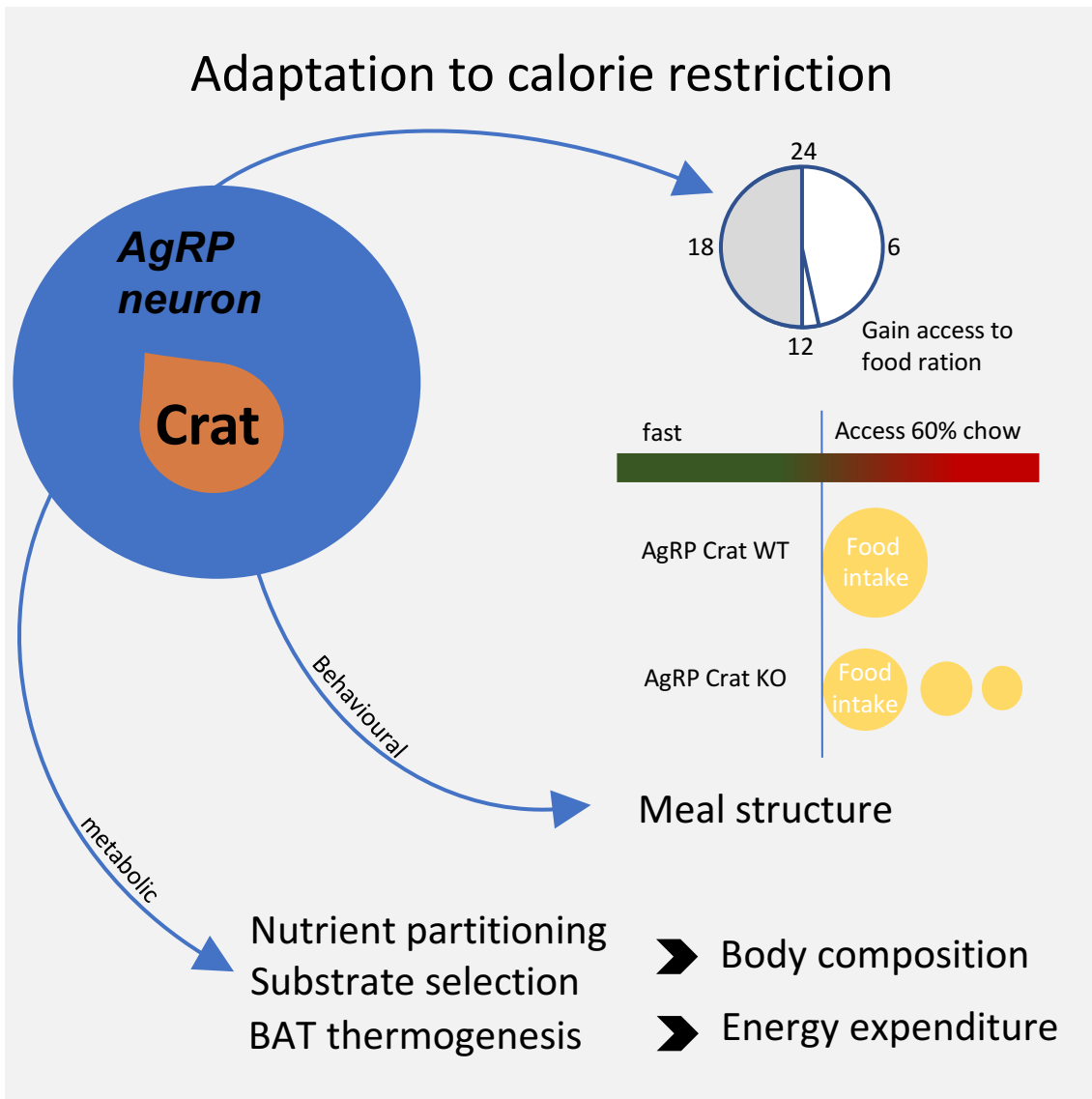


Figure 3.7 Summary of results from Chapter 3

Crat in AgRP neurons is essential for both, behavioural and metabolic adaptive response to calorie restriction. Crat activity ensures appropriate substrate utilisation to preserve fat stores and reduce energy expenditure during energy deprivation

Highlights

Crat in AgRP cells allows the adaptation of feeding behaviour during CR.

Crat in AgRP cells regulates nutrient partitioning and body composition during CR

Crat in AgRP cells enables adaptive changes in energy expenditure and BAT during CR

Crat in AgRP cells regulates substrate selection after the cessation of CR

Body composition during CR affects weight gain, food intake and adiposity after CR

Chapter 4: Carnitine acetyltransferase in AgRP neurons is required for the adaptation to restricted feeding

The results presented in this Chapter are submitted for publication.

Carnitine acetyltransferase in AgRP neurons is required for the adaptation to restricted feeding.

Alex Reichenbach¹, Mathieu Mequinion¹, Jacqueline A Bayliss¹, Sarah H Lockie¹, Moyra B Lemus¹, Randall Mynatt^{2,3}, Romana Stark¹, Zane B. Andrews¹

1. Monash Biomedicine Discovery Institute and Department of Physiology, Monash University, Clayton 3800, Victoria, Australia

2. Gene Nutrient Interactions Laboratory, Pennington Biomedical Research Center, Louisiana State University System, Baton Rouge, Louisiana, USA.

3. Transgenic Core Facility, Pennington Biomedical Research Center, Louisiana State University System, Baton Rouge, Louisiana, USA

Corresponding author:

A/Prof Z. B. Andrews: Email: [REDACTED] Tel: [REDACTED]

Key words: acetyl CoA, energy calculator, restricted feeding, food anticipatory activity

4.1 Abstract

Behavioural adaptation to times when food sources are available is crucial for survival and AgRP neurons have been associated with entrainment to temporal restricted feeding. We have previously shown that Crat in AgRP neurons enables metabolic flexibility, appropriate nutrient partitioning and is crucial for adaptation to caloric restriction. Here, we examined whether Crat is a component of a food entrainable oscillator (FEO) that helps link behaviour to food availability by restricting food availability to 3 hours per day during the light phase. AgRP Crat KO mice consumed less food, regained less body weight but maintained blood glucose levels during the 25-day restricted feeding protocol. Importantly, we observed no difference in meal latency, food anticipatory activity (FAA) or brown adipose tissue temperature during the first days of restricted feeding. However, as the restricted feeding paradigm progressed we noticed an increased FAA in AgRP Crat KO mice. The increase in FAA, which developed during restricted feeding, corresponded with elevated plasma corticosterone and non-esterified fatty acids at the end of the paradigm indicating it resulted from greater energy debt incurred by KO mice over the course of the experiment. These experiments highlight the importance of Crat in AgRP neurons to regulate feeding behaviour and body weight gain during restricted feeding, but not synchronising behaviour to food availability. Thus, Crat within AgRP neurons forms a component of the homeostatic response to restricted feeding but is not likely to be a molecular component of FEO.

4.2 Introduction

In an environment with limited food resources, it is crucial to synchronise behaviour and metabolism to times when food is available to maximise energy intake and storage. The field of chronobiology describes a food entrainable oscillator (FEO), made up of several neuronal populations throughout the brain, which are broadly responsible for energy homeostasis, wakefulness and reward, adjust physiology and metabolism to temporally match available food sources (Andermann and Lowell, 2017; Carneiro and Araujo, 2009; Kosse et al., 2015). Indeed, various brain regions, including arcuate nucleus, dorsomedial hypothalamus, parabrachial nucleus and the nucleus of the solitary tract, show *c-Fos* activation in food entrained mice prior to the expected meal, even after they returned to *ad libitum* feeding (Blum et al., 2012).

The FEO provides a mechanism, based on the integration of metabolic feedback information, to predict future meals and allow the effective metabolism of incoming nutrients and the maintenance of energy homeostasis (Andermann and Lowell, 2017; Kosse et al., 2015). The integration of feedback is in part provided by AgRP neurons, which adjust their activity in a feeding- and nutrient dependent manner (Betley et al., 2015; Beutler et al., 2017; Chen et al., 2016; Garfield et al., 2016; Su et al., 2017). AgRP neurons are active during energy deficit and drive behavioural changes in a low caloric environment by increasing food intake when available, motivation for food and food seeking locomotor activity (Burnett and Krashes, 2016; Krashes et al., 2011). Therefore, it is not surprising, that ablating AgRP neurons diminished food anticipatory activity (FAA) and impaired the adaptation to restricted feeding (Tan et al., 2014). These studies indicate that AgRP neurons function as an FEO, however, how AgRP neurons identify a state of metabolic need at a molecular level is not fully explored. This function involves the efficient substrate switching from fatty acid to glucose oxidation during the transition from fasting to refeeding, as this represents an acute metabolic change associated with food availability. This is particularly important in a restricted feeding paradigm, when food availability is defined by set times.

Carnitine acetyltransferase (Crat) controls mitochondrial acetyl-CoA levels, a common metabolic intermediate from glucose catabolism and fatty acid oxidation. This is crucial for the normal processing of incoming glucose, such as that occurs during refeeding after a fast, since the inability to regulate intracellular acetyl CoA inhibits pyruvate dehydrogenase and reduces intracellular glucose metabolism (Koves et al., 2008; Muoio, 2014). Indeed, Crat deletion in skeletal muscle impairs substrate switching from fatty acid oxidation to glucose oxidation during a fast/refeeding transition in mice due to decreased pyruvate dehydrogenase activity (Muoio et al., 2012). We described recently that AgRP neurons require Crat to mediate adaptive changes during fasting and refeeding and subsequently control peripheral nutrient partitioning (Reichenbach et al., 2018). These studies show that mice lacking Crat in AgRP neurons (KO mice) lack the metabolic flexibility to

effectively switch from fatty acid utilisation to glucose utilisation during the transition from fasting to refeeding, as seen in WT mice. As a result, Crat deletion in AgRP neurons causes persistently greater fatty acid oxidation, energy expenditure and greater loss of fat mass during calorie restriction (Chapter 3). Furthermore, we demonstrated that Crat in AgRP neurons regulates feeding behaviour since WT mice adapt over time to quickly consume their food ration within the first 4 hours after presentation. KO mice, on the other hand, do not adapt to quickly consume their food, such that consumption of the food ration was significantly slower in KO mice taking ~8 hours after food presentation (Chapter 3).

The actions of Crat to regulate cellular function during a fast/refeeding transition make it an ideal enzyme to convey information about nutrient availability to AgRP neurons, which underlies a potential role as a FEO. AgRP neurons have recently been described as “energy calculators” (Beutler et al., 2017), which function to pass on metabolic information to various parts of the brain to influence physiology and behaviour. Given that AgRP neurons can act as FEOs (Tan et al., 2014), it is not surprising that AgRP neurons communicate a rise in glucose levels to the suprachiasmatic nucleus (SCN), the master clock regulating circadian rhythms (Buijs et al., 2017). However, the molecular mechanisms within AgRP neurons to enable them to act as a FEO have not been addressed. We hypothesise that the handling of incoming nutrients associated with the fast/refeeding transition via Crat provides a mechanism to integrate metabolic feedback for circadian entrainment and FEO function in AgRP neurons. Here we report that deleting Crat in AgRP neurons affects adaptation to restricted feeding by reducing food intake, which results in lower body weight and BAT temperature, and increased food anticipatory activity.

4.3 Experimental Procedures

Animals

All experiments were conducted in compliance with the Monash University Animal Ethics Committee guidelines. Male mice were kept at standard laboratory conditions with free access to food (chow diet, cat no. 8720610 Barastoc stockfeeds, Victoria Australia), and water at 23 °C in a 12-hour light/dark cycle and were group-housed to prevent isolation stress, unless otherwise stated. AgRP-ires-cre mice were obtained from Jackson Laboratory AgRP^{tm1(cre)Low/J} (stock no. 012899) and bred with NPY GFP mice (B6.FVB-Tg(Npy-hrGFP)1Low/J; stock number 006417; The Jackson Laboratory, Maine, USA). AgRP-ires-cre::NPY GFP mice were then crossed with Crat^{fl/fl} mice donated by Randall Mynatt (Pennington Biomedical Research Center, LA, USA) in order to delete Crat from AgRP neurons (AgRP Crat KO). These mice were also crossed to B6.Cg-Gt(Rosa)26Sor^{tm14(CAG-td-Tomato)Hze/J} to visualise cre-mediated recombination in AgRP neurons.

Surgery

Telemeter surgery: Single housed mice were anaesthetised with isoflurane, and anaesthesia was maintained by constant nasal delivery of 2.5% isoflurane. Each animal received 50µL Metacam (0.25mg/mL Meloxicam; Boehringer Ingelheim) before the surgery in order to minimise post-surgery pain. Telemeter probes were inserted into the scBAT and fixated in the surrounding fat tissue. Telemetric data was recorded with VitalView (STARR life science Corp). After 7 days recovery, mice were transferred into BioDAQ feeding cages.

Feeding experiment

After 48 hours acclimation to feeding cage environment, ad libitum food intake was monitored for 6 days before restricting access to food to three hours during the light phase (4-7 Zeitgeber time). Body weight and blood glucose was measured daily before feeding period. After 26 days mice were culled one hour before or 2 hours after access to food, tissues dissected and frozen at -80 degrees.

Analysis of blood chemistry

Acylated and des-acylated ghrelin (Mitsubishi Chemical Medience Corp), glucagon (Yanaihara Institute, Inc), corticosterone (Abnova, Heidelberg, Germany), non-esterified fatty acid concentration (NEFA C Assay Kit, Wako Pure Chemical Industries, Japan), and triglycerides (triglyceride Assay kit, Roche/Hitachi, Roche Diagnostics GmbH) were all measured according to manufacturers instructions.

Glucose extraction

The crushed and weight frozen tissue was digested in KOH at 70°C for 20 minutes. Saturated NaSO₄ and 95% ethanol were added, mixed and centrifuged for 10 minutes. The pellet was resuspended in

deionised water and digested at 70°C for 10 minutes, before adding 95% ethanol, mixing and centrifuging. The precipitate was resuspended in amyloglucosidase buffer (0.3mg/ml amyloglucosidase in 0.25M acetate) and incubated at 37°C overnight. Liver glycogen concentrations were determined with glucose oxidase assay kit (Sigma Aldrich, Saint Louis, Missouri 63103 USA) after glucose extraction.

Liver Triglycerides

The crushed and weight frozen tissue was incubated with a chloroform:methanol (2:1) solution overnight. Then, pure chloroform and 0.9% NaCl were added and 10 minutes incubated on a shaker, followed by a 10-minute centrifugation step at 2000 rpm. The chloroform phase was transferred to a fresh glass tube and evaporated to complete dryness under N₂ at 40°C. The dried extract was dissolved in absolute ethanol and triglycerides were determined with Triglyceride assay kit (Roche/Hitachi, Roche Diagnostics GmbH).

Real time PCR

RNA was extracted using Qiazol (Qiazol Sciences). Briefly, frozen, crushed tissue was dispersed in Qiazol and incubated for 5 minutes, before adding chloroform and 15 seconds mixing using a Vortexer. After centrifuging the samples, the upper aqueous phase was transferred to a new tube and incubated with isopropanol for 10 minutes to form a precipitate. The samples were centrifuged and the pellet washed with 75% ethanol and then air dried. The dry RNA pellets were dissolved in Tris-EDTA buffer, and the concentration was measured with a Nano Drop 1000 (Thermo Scientific). cDNA was synthesised using iScript cDNA synthesis kit (170-8890; Bio-Rad Laboratories). Real-time quantitative PCR was performed using SYBR Green Mastermix using a Real Plex4 Mastercycler (Eppendorf). Following SYBR Green Mastermix. Primers were obtained from GeneWorks Amplifications: 18S Ribosomal RNA 18S (TTCCGATAACGAACGAGACTCT, TGGCTGAACGCCACTTGTC); Phosphoenolpyruvate Carboxykinase 1 (cytosol), PCK1 (TGCCCAAGGCAACTTAAGGG, CAGTAAACACCCCCATCGCT); glucose-6-phosphatase, catalytic, G6Pc (AGTCTTGTCAGGCATTGCTGT, AAAGTCCACAGGAGGTCCAC); glycogen phosphorylase, liver, Pygl (AAGAAGGGGTATGAGGCCAAA, GACACTTGACATAGGCTTCGT); glycogen synthase 2, liver, Gys2 (AATGTGAGCCCACCAACGAT, CTTCCAAAATGCACCTGGCA); glycerol kinase, GK (GCAACCAGAGGGAAACCACA, TAGGTCAAGCCACACCACG); Patatin-like phospholipase domain containing 2 (Pnpla2), transcript variant 1, Atgl (AGAGCCCATGGTCCTCCGA, AGCAAAGGGTTGGGTTGGTT); Glycerol-3-phosphate acyltransferase, mitochondrial, GPAT (CCAGTGAGGACTGGGTTGAC, CTCTGTGGCGTGCAGGAATA); fatty acid synthase, FASN (TGGGTGTGGAAGTTCGTCAG, CTGTCTGTGTCAGTAGCCGAG); citrate synthase, CS (TG TAGCTCTCTCCCTTCGGT, ACGAGGCAGGATGAGTTCTTG); neuropeptide Y, NPY (CCGCCACGATGCTAGGTAAC, CAGCCAGAATGCCCAAACAC); agouti related protein, AgRP

(AAGTCTGAATGGCCTCAAGAAGA, GACTCGTGCAGCCTTACACAG); growth hormone secretagogue receptor, GHSR (ATGGGTGTCGAGCGTCTTCTTCTT, CAAACACCACCACAGCAAGCATCT); pro-opiomelanocortin-alpha, POMC (GCGACGGAAGAGAAAAGAGGT, ATTGGAGGGACCCCTGTCTG); glucokinase, Gck (ATGTGCTCAGCAGGACTAGC, AACCGCTCCTTGAAGCTCG); glyceraldehyde-3-phosphate dehydrogenase, Gapdh (TCAAGCTCATTTCCTGGTATGACA, TCTTGCTCAGTGTCTTGGCT); pyruvate dehydrogenase E1 alpha 1, PDH1 (TGCTGGTTGCTTCCCGTAAT, AGCCGATGAAGGTACATTTCTTA); acetyl-CoA carboxylase alpha, ACC1 (GCTAAACCAGCACTCCCGAT, GCTGGATCTCATGTGAAAGGC); acetyl-CoA carboxylase beta, ACC2 (GAACACAAGTGATCCTGAATCTCAC, ATGAGCACCTTCTCTATGACCC). Quantitative real time PCR were performed using a Real Plex4 Mastercycler (Eppendorf). All reactions confirmed a single product of the expected size by melting curve and agarose gel electrophoresis. Reaction efficiencies for primers were greater than 1.90. mRNA levels were expressed as the $\Delta\Delta C(t)$ normalised to the house keeping gene, where C(t) is the cycle threshold.

Statistical Analysis

All data are represented as mean \pm standard error of the mean (SEM). Two-Way ANOVAs with Tukey's *post hoc* tests were used to determine statistical significance between treatment and genotype. A two-tailed Student's unpaired *t*-test was used when comparing genotype only. $p < 0.05$ was considered statistically significant.

4.4 Results

Crat in AgRP neurons is required for adaptation of feeding behaviour to restricted feeding

Our previous findings demonstrate that Crat is required for AgRP neurons to acutely and chronically sense states of energy deficit including fasting and caloric restriction (Chapter 3, Reichenbach et al., 2018). Moreover, AgRP neurons are required for the appropriate adaptation to a state of restricted feeding and to integrate circadian and metabolic cues to facilitate appropriate adaptation (Tan et al., 2014). To test if Crat in AgRP neurons facilitates adaptation to states of restricted food availability, we placed AgRP Crat WT and KO mice on a restricted feeding paradigm in feeding cages with computer-controlled gating system without the need for human intervention (BioDAQ, Research Diets, NJ, USA), whereby they only had access to food for 3 hours per day from 4-7 hours into the light cycle (Figure 4.1a+b).

Analysing feeding behaviour (Figure 4.1c), we found that adaptation to altered food availability occurs in 3 stages. Phase one (= day 0-5) is marked by very low food intake causing the rapid body weight loss (Figure 4.2a). During phase two (= day 6-12) mice adapt to day time feeding, increase food intake, feeding time and consequently begin to restore body weight. In phase three (day 13-25), mice are fully adjusted to the new feeding paradigm and food intake in mice plateaus, although mice continue to restore body weight (Figure 4.2a).

Throughout the experiment, we found no differences in meal latency, defined as the time passed between opening of the feeding window and meal initiation (Figure 4.1h+i), but AgRP Crat KO mice ate on average less during the 3-hour feeding window over the course of the restricted feeding paradigm (Figure 4.1d-f). This was mostly due to shorter meal duration (Figure 4.1j) and smaller meal size (Figure 4.1k) of the initial meal, resulting in less food intake from 90-180 minutes of the 3-hour feeding window (Figure 4.1g).

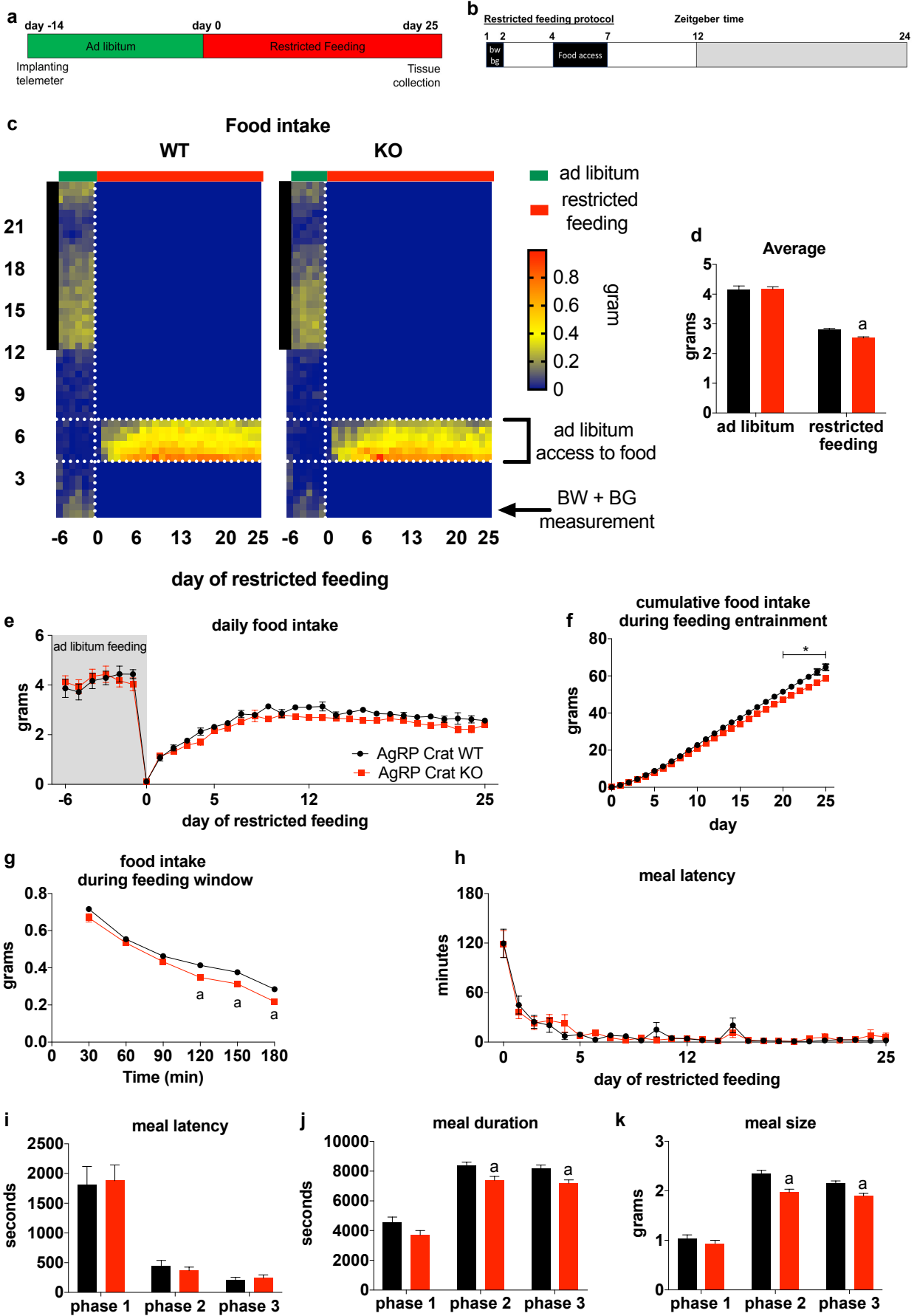


Figure 4.1. AgRP Crat KO mice adjust to feeding entrainment, but show altered feeding behaviour.

Schematic of the experimental design (a) and the restricted feeding protocol (b). Heat map depicting food intake in 30 minutes bins for six days ad libitum and 25 days restricted feeding; black bar on left indicates dark phase, vertical white dashed line indicates start of restricted feeding, horizontal white dashed lines frame the feeding window during restricted feeding (c). Total daily food intake and average food intake during ad libitum and food restriction (d) and cumulative food intake during restricted feeding (e). Average food intake during the feeding window from day 5-25 of restricted feeding (f). Daily meal latency during the restricted feeding (g) and average latency (h) duration (i) and size (j) of the first meal from phase 1 (day 0-5), phase 2 (day 6-12) and phase 3 (day 13-25) of restricted feeding. All data are expressed as mean \pm sem; $n=18-20$. Two-way (repeated measured; where appropriate) ANOVA with Sidak posthoc analysis; a, significant at $p<0.05$.

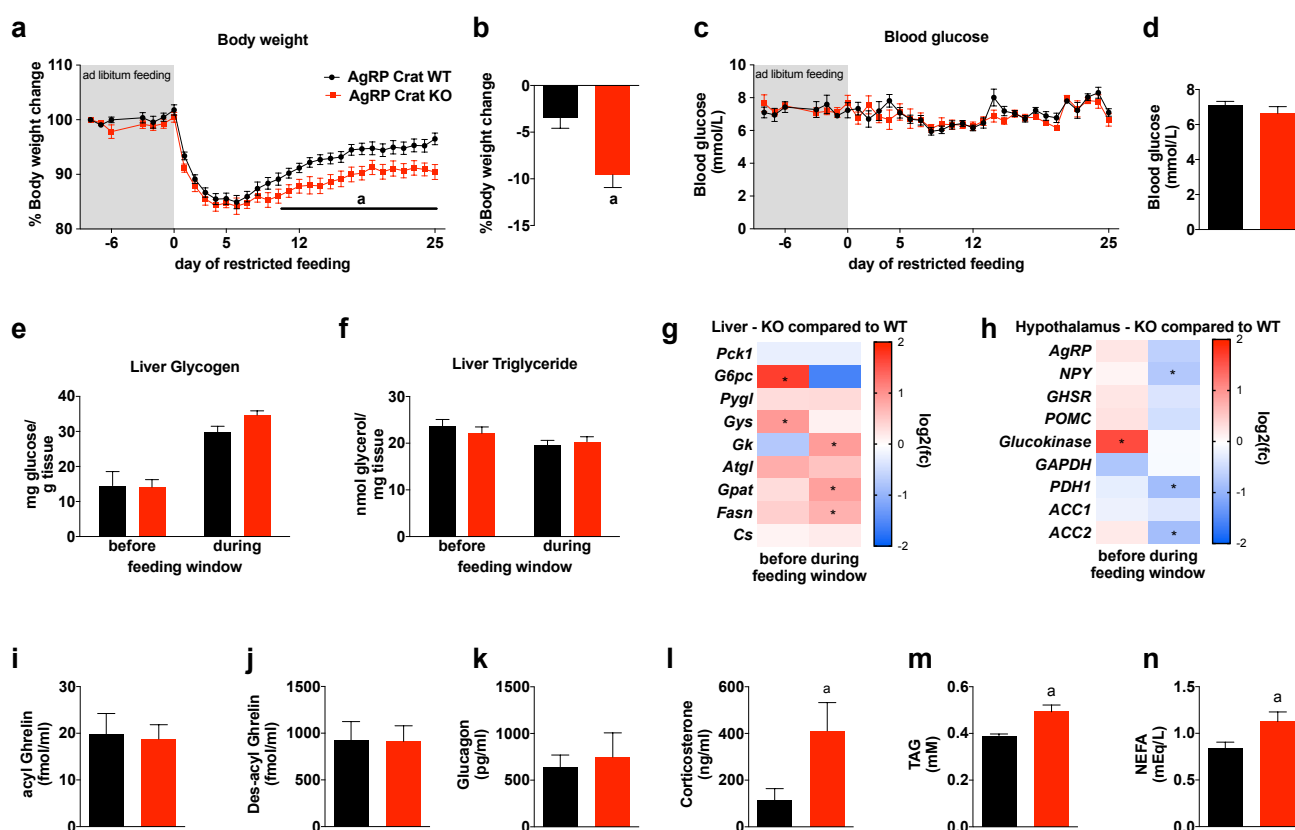


Figure 4.2. AgRP Crat KO mice exhibit slower body weight regain on restricted feeding schedule.

Body weight development (a), and relative body weight loss during the restricted feeding (b). Daily blood glucose measured prior to feeding (c). Plasma glucose (d), Liver glycogen (e), triglycerides (f) and liver gene expression (g) from mice after 25 days of restricted feeding before (fast) or 2 hours after access to food (fed). Phosphoenolpyruvate kinase1 (*Pck1*), glucose-6-phosphatase (*G6pc*), glycogen phosphorylase L (*Pygl*), glycogen synthase (*Gys*), glycerol kinase (*Gk*), Triglyceride lipase (*Atgl*), (i), glycerol-3-phosphate acyltransferase (*Gpat*), and fatty acid synthase (*Fasn*) citrate synthase (*Cs*). Hypothalamic gene expression profiles of agouti related peptide (*AgRP*), neuropeptide Y (*NPY*), growth hormone secretagogue receptor (*GHSR*), pro-opiomelanocortin (*POMC*), glucokinase, Glyceraldehyde 3-phosphate dehydrogenase (*GAPDH*), Pyruvate Dehydrogenase alpha 1 (*PDH1*), acetyl-CoA carboxylase alpha (*ACC1*), and acetyl-CoA carboxylase beta (*ACC2*) from mice after 25 days of restricted feeding before or 2 hours into feeding window (h). Acyl ghrelin (i), des-acyl ghrelin (j), glucagon (k), corticosterone (l), plasma triglyceride levels (m) non-esterified fatty acid (NEFA) (n) at the end of the experiment (day 25) 1 hour before feeding window. All data are expressed as mean \pm sem; $n=8-12$. Two-way (repeated measured; where appropriate) ANOVA with Sidak posthoc analysis or unpaired *t* tests; a, significant at $p<0.05$.

Crat in AgRP neurons affects physiological adaptation to restricted feeding

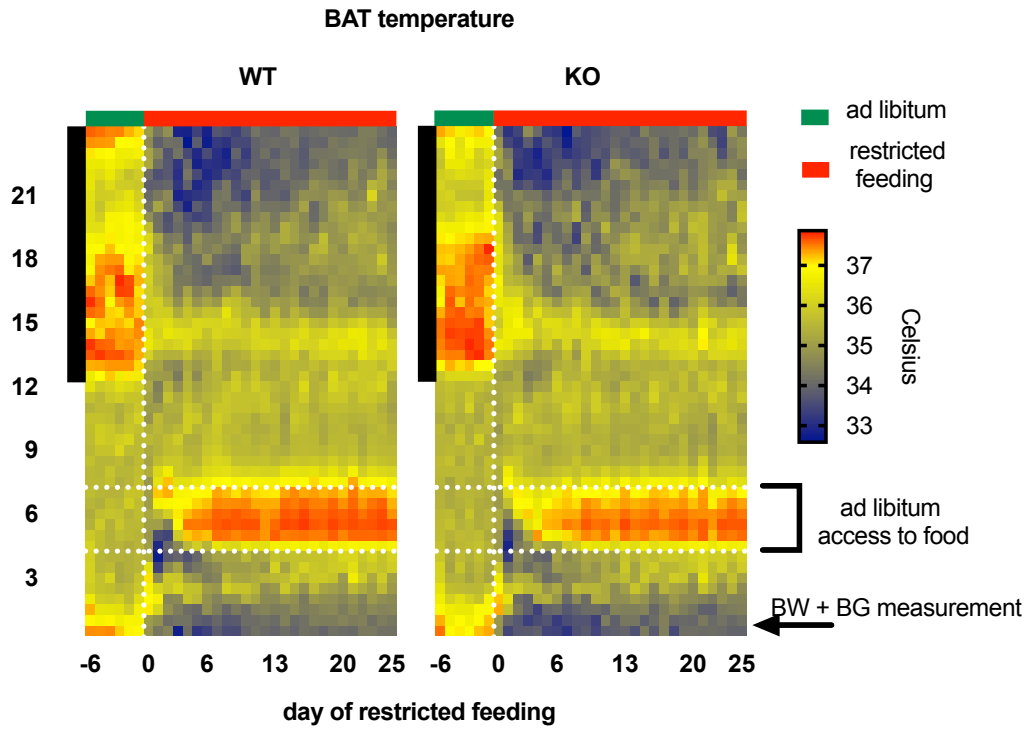
There was no difference in body weight during the 8-day ad libitum acclimation period, however restricted feeding during the light phase caused a rapid reduction in body weight from day 0 to day 5, at which time the fall in body weight plateaued. By day 8 of restricted feeding both AgRP Crat WT and KO mice started to display adaptation to day time feeding and restore lost body weight. Although both genotypes restored lost body weight, AgRP Crat KO gained less body weight from day 10 until the end of the experiment at day 25 (Figure 4.2a) and the change in body weight from the beginning of the experiment was significantly greater in KO versus WT mice (Figure 4.2b).

Despite the loss in body weight, blood glucose levels remained similar in both genotypes (Figure 4.2c,d). Our previous studies showed that AgRP Crat KO mice maintain blood glucose levels during fasting through adaptation of liver metabolism (Reichenbach et al., 2018). Therefore, we sought next to examine if there are changes in liver at the end of the experiment and compared glycogen and triglyceride content and hepatic gene expression before and two hours into the feeding window. We found low glycogen levels in fasted mice, which were replenished in the fed state, without differences in genotype (Figure 4.2e). Also, liver triglycerides were not different between genotype and did not change (Figure 4.2f)

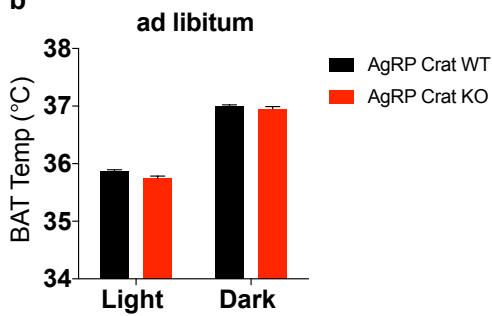
Under fasted conditions before the feeding window, AgRP Crat KO mice had greater mRNA levels of Glucose-6-phosphatase (*G6pc*), a key enzyme in gluconeogenesis, but we found no genotype differences in other genes involved in endogenous glucose production (Figure 4.2g). Interestingly, glycogen synthase (*Gys*) was significantly elevated before, but not during feeding in KO relative to WT. Gene expression of enzymes involved in lipid synthesis (*Gk*, *Gpat*, *Fasn*) were significantly elevated in AgRP Crat KO mice during feeding compared to WT mice (Figure 4.2g).

Hypothalamic neurons, including AgRP and MC3R-containing neurons, are crucial for food entrainable behaviour (Begrache et al., 2012; Girardet et al., 2014; Tan et al., 2014). Hence, we also examined mRNA expression of the hypothalamus immediately before and during the feeding window. We found no differences in *Agrp*, *Ghsr* or *Pomc* mRNA levels between genotypes. *Npy* mRNA levels were not significantly different before feeding window, however, there was a significant decrease in *Npy* mRNA expression in AgRP Crat KO mice during feeding compared to WT mice (Fig 2h). Gene expression of *Glucokinase*, well described as glucose sensor (Burdakov et al., 2005; Dunn-Meynell et al., 2002; Kang et al., 2006; Levin et al., 2008; Lynch et al., 2000), was significantly elevated in KO before but not during feeding window compared to WT littermates. Pyruvate dehydrogenase (*Pdha1*), Acetyl-CoA carboxylase B (*Acc2*) were not significantly different between genotypes before feeding, but were significantly reduced in KO during feeding window, Glyceraldehyde-3-phosphate dehydrogenase (*Gapdh*) and Acetyl-CoA carboxylase A (*Acc1*) were not different between genotype and not affected by feeding (Figure 4.2h).

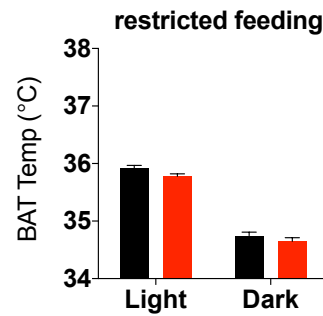
a



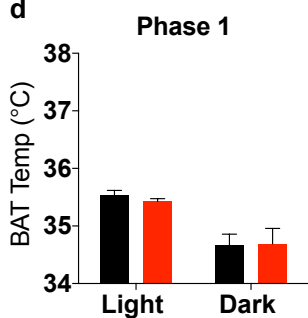
b



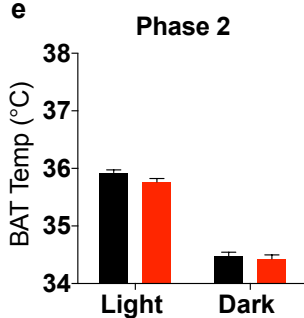
c



d



e



f

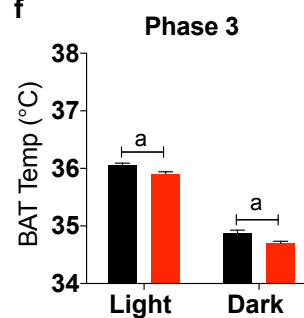


Figure 4.3 Changes in BAT temperature

Heat map depicting brown adipose tissue temperature in 30-minute bins during ad libitum and restricted feeding; black bar on left indicates dark phase vertical white dashed line indicates start of restricted feeding, horizontal white dashed lines frame the feeding window during restricted feeding (a). Average BAT temperature during ad libitum (b) and restricted feeding conditions (c) and average BAT temperature during restricted feeding separated into phase 1 (d), phase 2 (e) and phase 3 (f). All data are expressed as mean \pm sem; $n=8-10$. Two-way (repeated measured; where appropriate) ANOVA with Sidak posthoc analysis; a, significant at $p<0.05$.

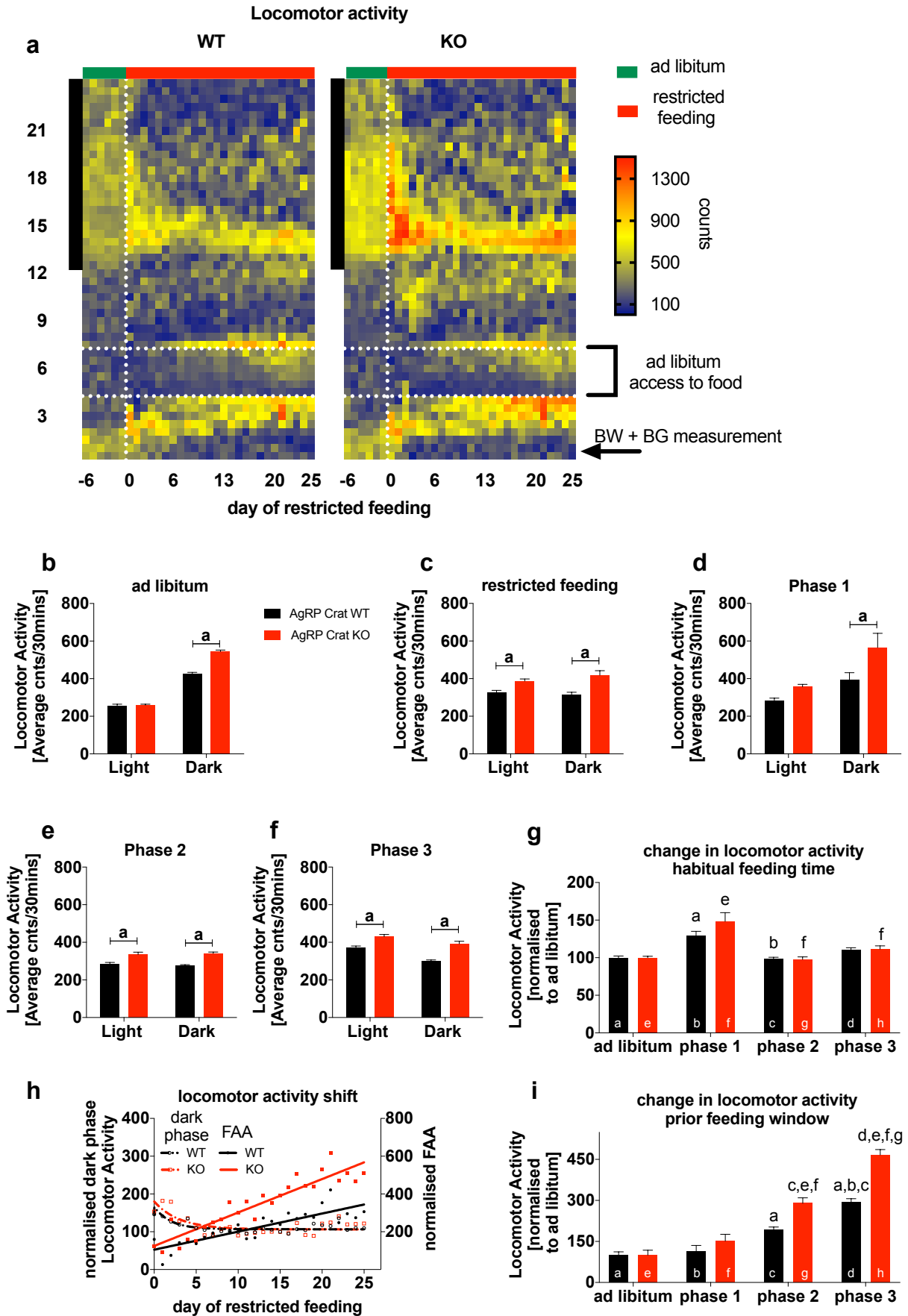


Figure 4.4. AgRP Crat KO mice exhibit greater food anticipatory activity

Heat map depicting locomotor activity in 30 minute bin during ad libitum and restricted feeding, black bar on left indicates dark phase, dashed lines frame feeding window during restricted feeding (a). Average locomotor activity during ad libitum (b) and restricted feeding conditions (c) and average locomotor activity during restricted feeding separated into phase 1 (d), phase 2 (e) and phase 3 (f). Change of total locomotor activity during first 4 hours of dark phase relative to ad libitum conditions (g). change in activity per day during ZT 3-4 (prior feeding window) and ZT 12-16 (beginning dark phase) relative to ad libitum conditions (h). Food anticipatory activity defined as the total activity one hour prior feeding window relative to ad libitum conditions (i). All data are expressed as mean \pm sem; n=8-10. Two-way (repeated measured; where appropriate) ANOVA with Sidak posthoc analysis; a, significant at $p < 0.05$. except Figure g and h: letter above bars indicate significant difference between genotype and phase.

As previous studies show a FEO responds to signals from the periphery (Carneiro and Araujo, 2009) we analysed plasma at the end of the experiment, 1 hour before commencing the feeding period and found no differences in blood glucose (Figure 4.2d), acyl ghrelin (Figure 4.2i), des-acyl ghrelin (Figure 4.2j) or glucagon (Figure 4.2k), but AgRP Crat KO have significantly greater corticosterone (Figure 4.2l), triglyceride (Figure 4.2m) and non-esterified fatty acid levels (Figure 4.2n).

Crat in AgRP neurons regulates food seeking activity during restricted food availability

To further investigate adaptive changes in response to the temporal food availability we implanted telemeter probes into the interscapular brown adipose tissue (BAT) to monitor BAT thermogenesis (Figure 4.3a) and locomotor activity (Figure 4.4a). BAT temperature only diverged after animals adjusted to restricted feeding, in the third phase of the feeding entrainment when both genotypes were regaining body weight (Figure 4.3b-f), most likely a consequence of lower body weight during this phase. KO mice under ad libitum conditions show increased locomotor activity during the dark phase, but no differences during the light phase (Figure 4.4b). Once food availability is restricted to a few hours during the light phase, mice shift their activity pattern towards the new feeding time, reduce their activity during the dark phase and increase activity during the light phase progressively, with KO showing greater locomotor activity (Figure 4.4c-f).

To account for these differences, we normalised locomotor activity to baseline activity, to be able to specifically compare changes in locomotor activity provoked by the change in feeding time. Although both develop food anticipatory activity (FAA), AgRP Crat KO mice exhibit significantly increased FAA compared to WT controls (Figure 4.4i) after 5 days restricted feeding in phase 2 and 3. Interestingly, mice show initially increased locomotor activity during the beginning of the dark phase, suggesting increased food seeking behaviour during their habitual feeding period (Figure 4.4g), which is in line with previous studies (Krashes et al., 2011). As the restricted feeding paradigm develops, mice progressively reduce dark phase activity and increase FAA (Figure 4.4h), representing an active learning process.

4.5 Discussion

AgRP neurons primarily function to conserve energy during periods of food scarcity and replenish energy stores during food availability and play an important role to maintain energy homeostasis. Recent evidence also suggests that AgRP neurons are a component of the FEO (Blum et al., 2012; Tan et al., 2014). To effectively function as an FEO, AgRP neurons need to accurately integrate and respond to information about energy deficit and energy availability. We have recently shown that Crat in AgRP neurons is important to regulate the fasting/refeeding transition by effectively enabling substrate switching from fatty acid utilisation to glucose utilisation. This enables the preservation of fatty acids for storage as soon as glucose from food consumption becomes available and represents not only an important mechanism of energy conservation but might also be an important component of an FEO. Tan et al. showed that mice lacking AgRP neurons take longer to adapt to a restricted feeding paradigm causing reduced food intake and reduced body weight during the first 10 days of the restricted feeding paradigm (Tan et al., 2014), but eventually anticipate day time feeding, and increase food intake and gain body weight similar to WT. Our results show AgRP Crat KO mice have shorter and smaller meals during restricted day time feeding similar to our previous findings after overnight fast/refeeding and calorie restriction experiments (Chapter 3, Reichenbach et al., 2018). This results in reduced food intake, slower body weight gain and increased FAA after 25 days restricted feeding, however it is important to note that unlike AgRP neuronal ablation (Tan et al., 2014), AgRP Crat KO display no deficit in FAA or importantly meal latency. Thus, Crat within AgRP neurons form a component of the homeostatic response to restricted feeding but is not likely to be a molecular component of FEO.

Food availability and consumption during the light phase shifts the periodicity of circadian gene expression, hormonal secretion and circulating metabolites, alters brain activity, sleep and physical activity as well as meal patterns (Bray et al., 2013; de Vasconcelos et al., 2006; Girotti et al., 2009; Marcheva et al., 2013; Oosterman et al., 2015; Verhagen et al., 2011; Wiater et al., 2011; Yasumoto et al., 2016). Rodents entrained to day time feeding show increased locomotor activity prior to anticipated meal time (Patton et al., 2014; Rastogi and Mintz, 2017) and this FAA is a crucial adaptation to predicted feeding opportunities (Lo et al., 2016; Shamsi et al., 2014). Several studies demonstrate that brain regions regulating food intake and energy homeostasis are required for expression of FAA (Begrache et al., 2012; Girardet et al., 2014; Lo et al., 2016; Merkestein et al., 2014; Patton and Mistlberger, 2013) and peripheral metabolic signals can modulate and entrain FAA including ketone bodies, free fatty acids, glucose, ghrelin, leptin and corticosterone (Chavan et al., 2016; Escobar et al., 1998; Namvar et al., 2016; Shamsi et al., 2014; Stephan and Davidson, 1998; Wiater et al., 2013; Wortley et al., 2004) of which some signal energy deficit (Lockie and Andrews, 2013). Previous studies show that AgRP ablation reduces FAA during the first 3 days of restricted feeding (Tan et al., 2014), however AgRP Crat KO mice show no deficit in FAA at any time of our

restricted feeding regime and in fact KO mice exhibit increased FAA during the second and 3rd phase of restricted feeding (day 6-25). Moreover, KO mice exhibit lower food intake and show reduced body weight gain, particularly in the 3rd phase, and therefore we predict the increased FAA manifests due to the greater energy deficit incurred in KO mice at this time. In support of this, greater energy deficit and body weight loss during calorie restriction elicits greater food anticipatory activity (Gallardo et al., 2014; Mitchell et al., 2016; Vaanholt et al., 2015). Moreover, greater corticosterone and NEFA levels prior to the feeding window, as seen in our KO mice, correspond with a progressively increasing FAA (Escobar et al., 1998; Namvar et al., 2016).

Furthermore, KO mice commence feeding in a similar timeframe to WT when challenged with restricted food availability, indicating that Crat deletion in AgRP neurons does not affect behavioural synchronisation to altered food availability. Also, during the first days of restricted feeding before the development of FAA both, WT and KO mice increase food seeking activity at the beginning of the dark phase, their habitual feeding time. This reflects findings from Krashes et al, where AgRP neuronal activation in the absence of food increases locomotor activity (Krashes et al., 2011). Additionally, we found in our previous study in a proteomic screen of AgRP neurons significantly increased levels of proteins associated with circadian entrainment (KEGG pathway 4713) during fasting (Reichenbach et al., 2018) including Mitogen activated protein kinase (Mapk1, also known as ERK), a marker for cellular activity and associated with FAA (Akashi et al., 2008; Delezie et al., 2016; Goldsmith and Bell-Pedersen, 2013). Together these findings suggest that deleting Crat in AgRP neurons does not impair synchronisation to day time feeding, but sensitises AgRP neurons to energy deficit.

Despite no deficit anticipating day time feeding, KO mice have reduced meal size and duration leading to reduced overall food intake during the feeding window, a phenomenon we also observed previously during fasting/refeeding experiments (Reichenbach et al., 2018). Here, we observed lower *Npy* gene expression in KO mice during feeding, suggesting that the impaired feeding response might be due to a greater reduction of NPY signalling upon refeeding. That rats under a restricted feeding paradigm have high *Npy* gene expression prior to feeding and reduce *Npy* gene expression upon refeeding (Yoshihara et al., 1996) supports this idea. Additionally, gene expression of *Pdha1* and *Acc2*, both enzymes dependent on proper functioning of Crat were significantly reduced during refeeding, demonstrating the importance of Crat in AgRP neurons during refeeding. Hypothalamic gene expression of *Glucokinase*, the enzyme phosphorylating glucose during the initial step of glycolysis was significantly elevated in KO prior the feeding window and suggests dysregulated glucose metabolism in AgRP neurons at this time. Indeed, our previous glucose-stimulated glucose uptake experiments showed significantly increased glucose uptake in the hypothalamus 15 minutes after glucose administration in AgRP Crat KO mice (Reichenbach et al., 2018). Together, this emphasises the inability of AgRP Crat KO mice to accurately calculate the caloric value of incoming nutrients and highlights that Crat is crucial for integrating acute changes in

metabolic state. The resulting lower food intake represents an impairment to restricted feeding and underlines that Crat in AgRP neurons is a component of the energy-calculating mechanism specifically promoting energy replenishment when food is available.

Increased plasma triglycerides and NEFA indicate greater fatty acid utilisation prior feeding, mimicking our previous findings during fasting/refeeding and calorie restriction (Chapter 3, Reichenbach et al., 2018). Therefore, we predict that the lower body weight seen in KO is due to lower fat mass owing the greater fatty acid utilisation and smaller food intake during the 25-day restricted feeding paradigm. The lower BAT temperature at the end of the experiment is presumably a consequence of lower body weight during this phase, particularly because no difference in BAT temperature was recorded until well after the body weight differences were observed. This suggests the reduced BAT temperature towards the end of the experiment is an indirect effect to spare energy reserves consistent with other studies showing thermal adaptation to calorie restriction (Redman et al., 2008; Soare et al., 2011).

Peripheral organs are also under circadian control (Krishnaiah et al., 2017) and time restricted feeding aligns circadian rhythm of liver gene expression, acetylome, glycogen and triglycerides stores to feeding times (Diaz-Munoz et al., 2010; Mauvoisin et al., 2017; Shamsi et al., 2014) and improves metabolic flexibility (Bray et al., 2013; Hatori et al., 2012). Our previous experiment with AgRP Crat KO mice showed differences in hepatic glycogen and triglyceride management after a single fast and increased liver fatty acid oxidation resulting in impaired metabolic flexibility and nutrient partitioning (Reichenbach et al., 2018) and showed that increased fatty acid utilisation during calorie restriction causes greater body fat loss (Chapter 3). Here, after 25 days of time restricted feeding we found no genotype differences in liver triglycerides and glycogen suggesting that circadian entrainment of liver metabolism enables appropriate adaptation in AgRP Crat KO mice. In support of this, KO mice have increased hepatic mRNA expression of lipogenic genes, which favours energy storage upon refeeding (Bruss et al., 2010).

In summary, our results show that Crat in AgRP neurons assesses alterations in metabolic state, gauges food intake and forms a critical component of an energy calculating mechanism that allows an appropriate homeostatic response to restricted feeding. However, because KO mice commence feeding in a similar timeframe to WT without any deficit in FAA, we conclude that Crat deletion in AgRP neurons does not affect behavioural synchronisation to altered food availability and is not likely to form a component of a FEO mechanism in AgRP neurons.

Acknowledgements

We thank Doug Compton from Research Diets for helping setup and establish BioDAQ feeding cages. This study was supported by an NHMRC grant and fellowship to ZBA (1126724, 1084344). This work used the PBRC Transgenic Core which is supported in part by COBRE (NIH 8P20GM103528) and the NORC (NIH 2P30-DK072476-11A1) center grants from the National Institutes of Health. AR is supported through an Australian Government Research Training Program Scholarship.

Author Contribution

AR and ZBA conceived the idea, designed and performed the experiments, analysed data, and wrote the manuscript. ZBA supervised and coordinated the project., MM, JAB, MBL, SHL, RS contributed to perform experiments. RM provided Crat floxed mouse model. AR, ZBA discussed results and edited the manuscript. All authors read and approved the manuscript.

Declaration Of Interests

The authors have nothing to disclose

4.6 Summary Chapter 4

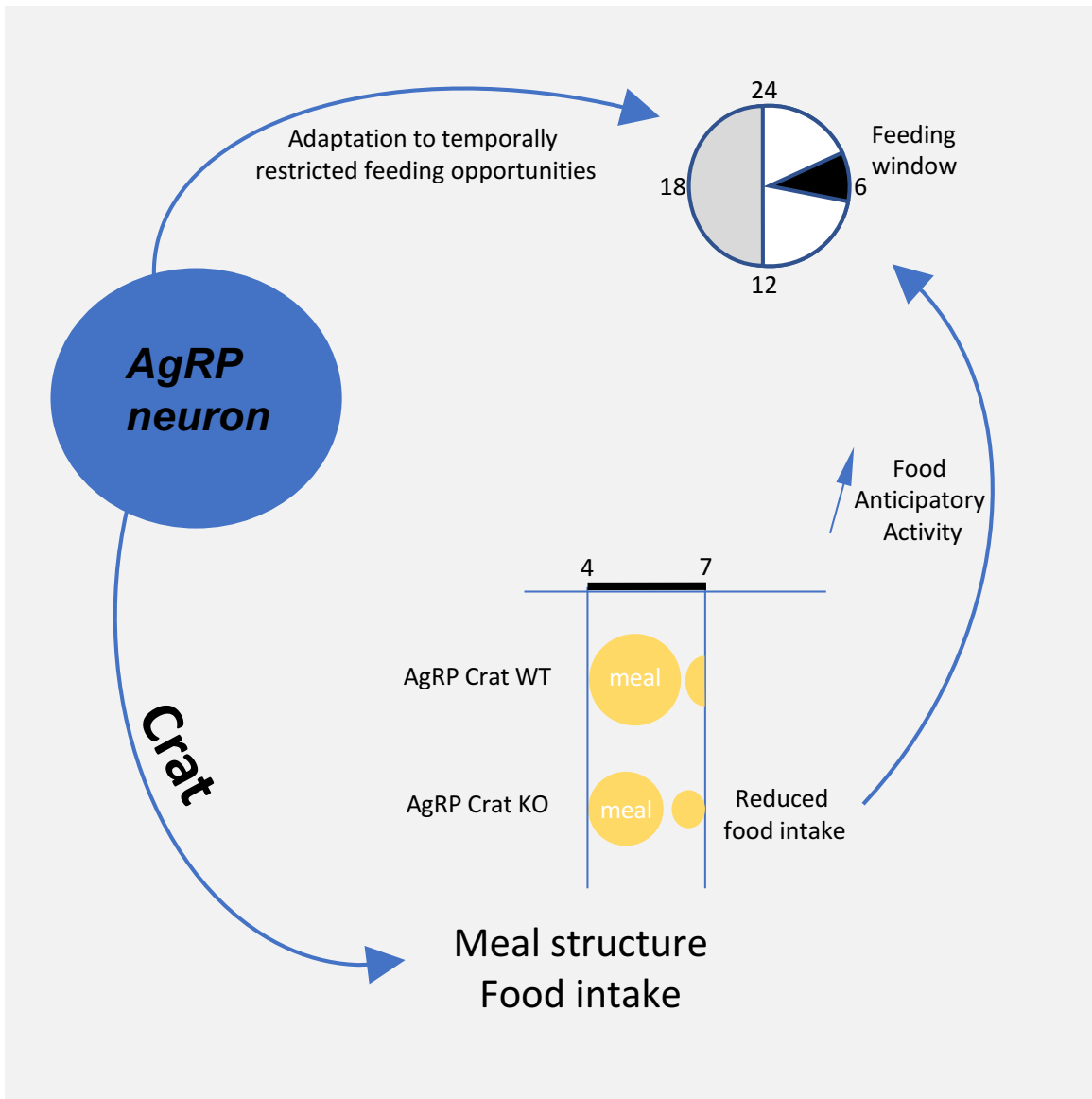


Figure 4.5 Summary of results from Chapter 4

Crat within *AgRP* neurons forms a component of the homeostatic response to restricted feeding by regulating meal structure and food intake. *AgRP* specific *Crat* deletion results in lower food intake and greater energy debt during restricted feeding, which leads to increased FAA. Therefore, *Crat* in *AgRP* neurons is not likely to be a molecular component of FEO.

Highlights

Crat in *AgRP* neurons regulates feeding behaviour during restricted feeding.

Crat in *AgRP* helps to regain body weight during restricted feeding.

Crat is not likely to be a molecular component of FEO mechanism in *AgRP* neurons.

Chapter 5: Conclusion and future directions

Data herein focused on carnitine acetyltransferase in AgRP neurons and its role in substrate selection and nutrient partitioning in order to maintain whole body energy homeostasis. We presented compelling evidence suggesting that Crat in AgRP neurons regulates feeding behaviour and is crucial for metabolic flexibility. As a result, Crat in AgRP neurons is required for proper adaptive “energy conserving” responses to chronic energy deficient states, such as calorie restriction (Chapter 3) and restricted feeding (Chapter 4).

During energy deficient states AgRP neurons suppress energy expenditure (Brito et al., 2007; Ruan et al., 2014; Shi et al., 2013; Wu et al., 2017) and promote food intake when food becomes available (Krashes et al., 2011). Furthermore, AgRP neurons also facilitate a change from peripheral fatty acid oxidation to carbohydrate oxidation if food becomes available (Cavalcanti-de-Albuquerque et al., 2016; Joly-Amado et al., 2012). This switch in substrate utilisation is fundamental to energy homeostasis and needs to be as efficient as possible in order to store fatty acids and conserve maximal energy. To achieve this transition as fast as possible, AgRP neurons require a mechanism to rapidly detect and process changes in glucose and fatty acid availability.

Here we present Crat as a key enzyme of the carnitine metabolism providing the metabolic flexibility at cellular level in AgRP neurons required for peripheral nutrient partitioning and whole body energy homeostasis (Moreno et al., 2013). We used a cre-lox approach to delete Crat specifically from AgRP neurons. Although brain-specific Crat deficiency causes severe neurodegeneration (DiDonato et al., 1979; Melegh et al., 1999; Przyrembel, 1987), AgRP specific deletion of Crat did not affect AgRP neuronal development or fibre density as described in Chapter 2. Also, proteomic analysis of AgRP neurons showed that Crat deletion causes only minor changes under *ad libitum* fed conditions.

In Chapter 2 we describe the metabolic inflexible phenotype of AgRP Crat KO mice during the transition from an energy depleted (fasted) to an energy restored (fed) state. This metabolically inflexible phenotype was marked by a delayed and blunted switch in peripheral substrate utilisation and an altered protein landscape in AgRP neurons of fasted and acute refeed, but not *ad libitum* fed mice. These results highlight that Crat in AgRP neurons is of central importance during fasting and the transition to refeeding, when metabolic processing in AgRP neurons is most relevant to shut off lipid utilisation, control peripheral nutrient partitioning, and maximise energy conservation.

Furthermore, we presented evidence that the immediate response to a glucose load is processed by Crat in AgRP neurons but not long term glucose homeostasis, further highlighting the importance of Crat specifically during the dynamic shift from an energy deplete to an energy replete state.

Crat deletion also affected food intake and feeding behaviour, the best-known function of AgRP neurons. Although there was no difference in total food intake in KO vs WT under *ad libitum* fed conditions, the meal microstructure varied between genotypes. For example, meal duration was significantly shorter in KO mice but was compensated by increasing meal number in *ad libitum* but

not fasted state leading to lower refeeding food intake, further highlighting that current metabolic state is important to the function of Crat in AgRP neurons.

Chapter 3 and 4 echo findings from Chapter 2 when we investigate the consequences of Crat deletion under prolonged calorie shortfall. Crat within AgRP neurons allows the adaptation to low caloric environments, particularly by adjusting feeding behaviour to consuming food quickly and increasing meal size. Restricting access to the amount of food (CR, Chapter 3) highlights that KO mice compensate shorter meals by having more meals, prolonging the active feeding time. Whereas restricting temporal access to food (RF, Chapter 4) emphasises that KO mice cannot effectively increase meal size after fasting, resulting in reduced food intake.

Chapter 3 describes the effect of increased lipid utilisation under chronic calorie restriction, further highlighting that Crat in AgRP neurons controls nutrient partitioning and substrate selection to preserve fat stores, and regulates energy expenditure to conserve energy. Furthermore, we showed that after a period of calorie restriction, mice increase food intake under *ad libitum* post calorie restriction conditions to restore depleted fat depots irrespectively of total body weight gain and independent of genotype. This highlights the fact that Crat in AgRP neurons is most important during energy deficit and acts primarily to integrate sudden changes in metabolic state to adapt metabolism and behaviour in low caloric settings. That we found little or no differences under *ad libitum* fed and high-fat-fed conditions suggests that long-term homeostatic regulation of *ad libitum* food intake is regulated by other means.

Chapter 4 discriminates between homeostatic adaption as described in Chapter 3 and adaptation to temporally restricted feeding. AgRP neurons are required for the feeding rhythmicity (Blasiak et al., 2017; Li et al., 2012), and ablating AgRP neurons impairs also adaptation to restricted feeding (Tan et al., 2014). Moreover, Crat deletion in AgRP neurons prevented the adaptation of feeding behaviour to calorie restriction, therefore we investigated if AgRP Crat KO mice can adapt to restricted feeding. Although KO mice showed reduced food intake and lower body weight, we did not find any sign of impaired FEO function: Meal latency did not differ and food anticipatory activity was actually greater in KO during the second half of the restricted feeding protocol. Thus, we conclude that although Crat is required to maintain energy homeostasis during restricted feeding, it is not required for circadian entrainment of food intake. This is explicated by a similar learning curve adjusting activity patterns in response to altered food availability, demonstrating that Crat deletion in AgRP neurons does not affect the physiological adaptation to day-time feeding.

Together, these experiments show that Crat in AgRP neurons provides the ability to sense acute changes in metabolic state and mount appropriate responses by adapting metabolism and behaviour. Indeed, the greater loss of fat mass during calorie restriction in KO mice illustrates how Crat in AgRP neurons allows maximal energy conservation by effectively switching substrates during the transition from an energy depleted to an energy repleted state.

In aggregate, the presented data suggest a critical role for Crat processing metabolic information in AgRP neurons. However, the cellular mechanism and signalling cascade around Crat has not been elucidated in this thesis and will be the subject of future investigation. The following sections describe future directions that might give insights to unanswered questions and suggests a molecular mechanism for nutrient sensing implicated by the known properties of Crat.

5.1 Motivation for food

The motivation to eat depends on the palatability of the food object, but also on the metabolic state (Simon et al., 2017; Sun et al., 2014). Hunger/energy deficit increases the motivation to work for food with numerous studies showing that AgRP neuronal activation increases the willingness to nose poke (Krashes et al., 2011) or press a lever (Atasoy et al., 2012; Betley et al., 2015; Chen et al., 2016) in order to obtain food. The intensity of lever-pressing during continuous stimulation of AgRP neurons diminishes over time, suggesting AgRP neuronal activity conveys a negative valence signal that the mice seek to quench (Betley et al., 2015). Simultaneously, brief pre-stimulation of AgRP neurons before feeding provokes food intake in the absence of AgRP neuronal activity (Chen et al., 2016) demonstrating that AgRP neurons contain a “Flip-Flop memory circuit” to positively enforce food intake (Yang et al., 2011).

Calorie restriction is a model of energy deficit and is known to increase the incentive salience of food (Lockie and Andrews, 2013). Because energy deficit increases motivation to consume food (Cansell et al., 2012) and because Crat function in AgRP neurons is most important at this time, it seems reasonable to assume that Crat in AgRP neurons could translate metabolic information about energy state into neural circuits controlling motivational properties of food “goal” directed behaviours.

Indeed, there is evidence within this thesis to suggest that AgRP Crat KO mice have impaired motivational drive to obtain food. This can be seen under ad libitum conditions, when KO mice have shorter meals suggesting that satiation signals are stronger than motivation (Thomas et al., 2015), as well as in energy-depleted states, since refeeding after fast and restricted feeding results in lower food intake due to shorter meals. But it is most apparent during calorie restriction when we can compare feeding time for the same amount of food. KO mice spend more time in feeding bouts but eat less, taking longer to eat the daily food ration seemingly having reduced appetitive drive (like somebody without appetite poking with the fork at the dinner plate).

A recent study demonstrates that ingestion of calories is required to sustainably reduce AgRP neuronal activity (Su et al., 2017). Ingestion of a novel non-nutritive, sweetened gel transiently reduces AgRP activity and repeated exposure diminishes the response. This is an important observation suggesting the pairing of sensory cues (e.g. taste) with the caloric value after exposure. In succeeding experiments, Su et al show also that reduction of AgRP neuronal activity correlates with the number of calories ingested (Su et al., 2017).

Mice lacking taste receptors cannot develop a preference to calorie-free sucralose and only show an increase in striatal dopamine release after ingestion of sucrose, but not sucralose (de Araujo et al., 2008) demonstrating that calories are inherently rewarding irrespective of taste. Furthermore, recent experiments show that the hedonic value (taste) and the caloric value of glucose are mediated by separate pathways and cause dopamine release in the ventral and dorsal striatum respectively (Tellez et al., 2016). Importantly, this study demonstrates that dopamine release in the dorsal striatum (simulating caloric value) can override taste aversion.

The motivation to obtain food is associated with dopaminergic reward pathways and is increased by ghrelin or activation of AgRP neurons (Dietrich et al., 2012; Skibicka et al., 2011). Moreover, NPY activates dopaminergic VTA neurons and increases the motivation for food (Skibicka et al., 2012; West and Roseberry, 2017). Of note, in Chapter 4, we found reduced NPY gene expression upon refeeding supporting the notion that AgRP neuron-specific Crat deletion curtails motivation for food during refeeding.

Based on the literature cited above and on the ability of Crat deletion from AgRP neurons to impair feeding and feeding behaviour, we investigated whether Crat deletion affects the rewarding properties of sucrose, using 2-bottle choice experiments (Figure 5.1). We show that Crat deletion in AgRP neurons affects the processing of the caloric value of sucrose. Initial experiments show that WT and KO mice prefer a non-caloric sweetened drink (0.1% saccharin) over water (Figure 5.1a).

Providing a choice between the non-caloric saccharin solution and a caloric 4% sucrose solution, WT mice shift their preference towards the sucrose solution, but KO mice do not show a preference (Figure 5.1b). Moreover, fasting increases the preference for sucrose in WT mice but does not affect the sucrose consumption in KO mice (Figure 5.1c).

Pairing the caloric solution with an unpalatable taste by lacing sucrose with the bitter tasting quinine shifts the preference to saccharin in KO, with WT mice showing no preference (Figure 5.1d). Strikingly, an overnight fast increases the preference for the quinine-laced sucrose solution in WT, but not in KO. This implies that WT mice can sense the energy deficit and sacrifice taste for caloric value by consuming more quinine-laced sucrose, whereas KO mice cannot (Figure 5.1e).

The information about the aversive taste received by lingual taste receptors and delayed processing of the caloric value of the drink might be computed separately from each other (Stauffer et al., 2016) so that the temporal separation of both cues creates a mismatch, which disables appropriate integration. The concept of temporal coherence and timing rules is already described for other brain functions including motor learning (Wang et al., 2000) and hearing (Lu et al., 2017). Moreover, it has been shown that temporal inhibition of GABAergic LH neurons during cues that predict food availability prevents rats from associating these cues with food, and prevents the cue's ability to elicit food-seeking behaviour after learning (Sharpe et al., 2017). Whether the concept of credit assignment (Iordanidou and Burdakov, 2016) is also true for pairing of caloric information with taste to ensure energy homeostasis needs to be empirically tested in future experiments employing

operant lever pressing to further explore the role of Crat in AgRP neurons for the motivational aspects of feeding.

In aggregate, our results suggest that Crat deletion affects the ability of AgRP neurons to accurately process the value/number of ingested calories curtailing the motivation for sucrose consumption.

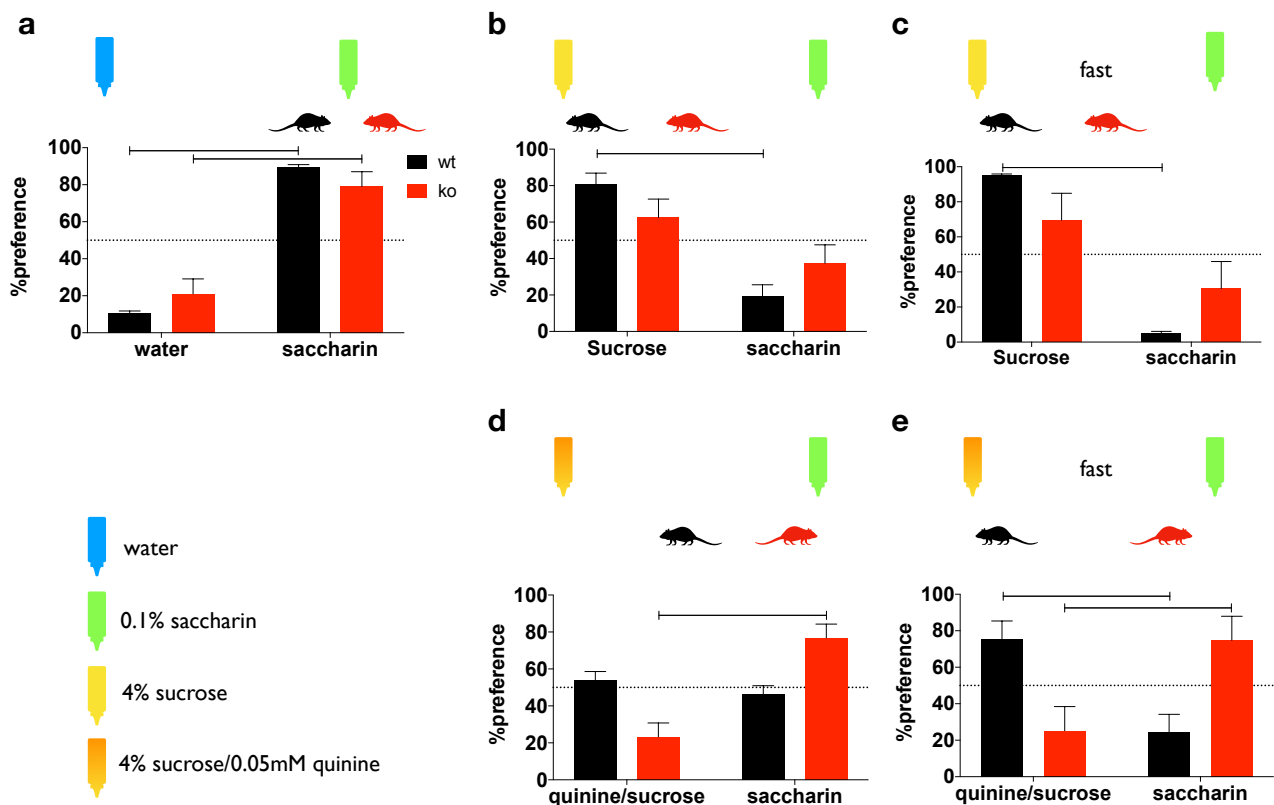


Figure 5.1. Two-bottle-choice test

AgRP Crat WT and KO mice housed in BioDAQ cages had ad libitum access to chow. Fluid intake from 2 bottles (water and saccharin; sucrose and saccharin, quinine/sucrose and saccharin) was monitored, left and right bottle were swapped over every day and the preference was calculated based on average ad libitum intake over 4 days (a,b,d) or 1 day, when mice were fasted and had no access to chow during fluid intake measurements (c,e). All data are expressed as mean \pm sem; $n=5-6$. Two-way (repeated measured; where appropriate) ANOVA with Sidak posthoc analysis; significant at $p<0.05$.

5.2 Reactive Oxygen Species as signalling molecule

Carnitine acetyltransferase is a critical regulator of glucose and fatty acid metabolism and functions as a molecular substrate switch facilitating glycolysis or beta-oxidation depending on substrate availability (Muio et al., 2012). Indeed, it has been shown that increased lipid availability and influx of these into the mitochondria for beta-oxidation diminishes glucose metabolism (Seiler et al., 2014) and overexpressing Crat (and therefore increasing acetyl-CoA-buffer capacity) in myocytes

promotes glucose uptake and alleviates lipid-induced suppression of glucose metabolism (Noland et al., 2009). Finally, deleting Crat in myocytes impairs their ability to switch from fatty acids to glucose as a substrate for energy production so that greater glucose levels are required to elicit the transition from fatty acid oxidation to glucose oxidation (Muoio et al., 2012).

Crat has an important function buffering mitochondrial acetyl CoA produced by glycolysis as well as beta-oxidation. Crat-mediated buffering of acetyl CoA in the mitochondria facilitates pyruvate dehydrogenase activity and therefore permits ongoing glucose metabolism and sensing (Koves et al., 2008; Muoio, 2014).

The lack of Crat is associated with increased mitochondrial stress on the electron transfer chain (ETC) and reactive oxygen species (ROS) production through electron leakage (Koves et al., 2008; Muoio, 2014; Sharma et al., 2012), when energy (ATP) demand is exceeded by nutrient catabolism providing redox equivalents NADH / FADH₂ (Muoio and Neufer, 2012), which occurs by sudden inactivity or increased nutrient availability and creates a highly oxidative redox state in the mitochondria (Anderson et al., 2009).

Increased nutrient availability (e.g. during refeeding) results in increased glucose oxidation and oxidative phosphorylation including electron leak. Several studies demonstrated that a low ROS environment is crucial for normal AgRP function (Andrews et al., 2008; Dietrich et al., 2010) to drive food intake (Diano et al., 2011) and mitochondrial stress and excessive ROS production in AgRP neurons are related to impaired neuronal function (Diano and Horvath, 2012). Moreover, ROS have long been associated with nutrient sensing, especially in pancreatic beta cells and neurons (Benani et al., 2007; Leloup et al., 2006; Leloup et al., 2009), with high levels of ROS signalling nutrient abundance and vice versa (Colombani et al., 2009; Shadel and Horvath, 2015). Therefore, the absence of Crat, which is known to regulate ROS in other tissues (Koves et al., 2008; Muoio, 2014), may render AgRP neurons less functional, a hypothesis that will be tested in future experiments.

Furthermore, insulin-induced ROS production in neurons involves NADPH oxidase and the electron transfer chain and is required for the anorectic effect of insulin in fed mice (Jaillard et al., 2009; Storzhevskiy et al., 2007). Importantly, central antioxidant administration or fasting prevents insulin-induced ROS and reduction of food intake (Jaillard et al., 2009) suggesting that ROS is the signalling molecule and integrates nutritional and hormonal information about the metabolic state. Indeed, in Chapter 2 we described increased satiety in AgRP Crat KO mice after central insulin administration, an effect possibly caused by increased ROS production in Crat deficient AgRP neurons upon refeeding.

One cellular mechanism to manage high ROS levels is the expression of the transcriptional factor PGC1 α (Baldelli et al., 2014; St-Pierre et al., 2006) and downregulation of PGC1 α prevents antioxidant expression and results in a ROS burst (Baldelli et al., 2014). Increased ROS induce the expression of PGC1 α , and an AgRP specific deletion of PGC1 α produces a similar phenotype to the mice described here with lower RER, reduced food intake after fasting and increased fat to lean

mass ratio (Gill et al., 2016) suggesting increased ROS production in AgRP neurons upon refeeding as commonality producing the phenotype.

PGC1 α promotes expression of mitofusin 2 (Soriano et al., 2006) necessary for mitochondrial fusion to mitigate the effects of oxidative stress (Youle and van der Bliek, 2012). Indeed, Dietrich et al demonstrated an important role for mitofusins for AgRP neuronal activity (Dietrich et al., 2013) with mitochondrial fusion during the transition from fasted to fed state, the same time point Crat in AgRP neurons is most critical.

Moreover, respiration-related ROS are also combated through antioxidant enzymes to prevent oxidative damage (Schrepfer and Scorrano, 2016; Thirupathi and de Souza, 2017) and the thioredoxin/peroxiredoxin system is the most active antioxidant system in the brain (Drechsel and Patel, 2010). Intriguingly, we found in a proteomic screen of AgRP neurons from refeed AgRP Crat KO mice increased levels of peroxiredoxins (Prdx2, Prdx3, Prdx6) and enzymes involved in glutathione synthesis (Glutathione synthetase, glutathione S-transferase P1), presumably a result of increased ROS.

In aggregate, AgRP neuronal ROS signalling is most likely affected by deletion of Crat in AgRP neurons. The changes in ROS would be most apparent during the dynamic metabolic changes seen at the transition from periods of high AgRP activity (fasting) compared to lower AgRP activity associated with acute inhibition (refeeding). Indeed, this is when the greatest alterations in substrate flux occur and we have observed the greatest differences in RER, proteomic profile, and protein acetylation in Chapter 2 at this same time point.

5.3 Fine tuning ROS for glucose tolerance

As mentioned above, Crat deletion in myocytes causes a delay in substrate switch and requires approximately four times higher pyruvate concentrations (the product of glycolysis) to achieve the same change as WT myocytes (Muoio et al., 2012). Increasing hypothalamic glucose concentration and subsequent glucose oxidation increases ROS and results in rapid insulin secretion and reduced food intake (Carneiro et al., 2012; Leloup et al., 2006). In Chapter 2 we described a delayed response to a glucose load with initial higher glucose peak, delayed reduction in endogenous glucose production, and reduced glucose uptake into WAT and muscle 15 minutes after a glucose load, an effect that was not seen any longer after 30 minutes and in fact almost reversed. This was paralleled with a reduced insulin response to the glucose load.

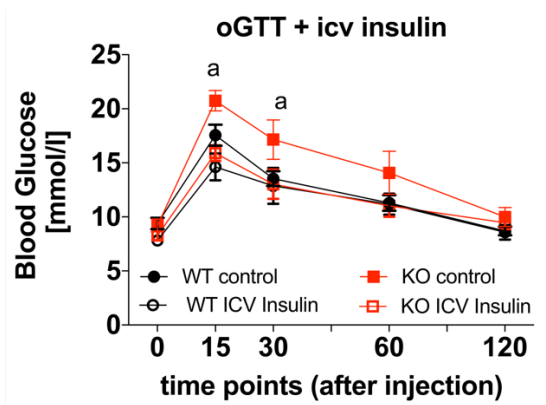


Figure 5.2. Oral Glucose Tolerance Test after ICV insulin administration

Mice received ICV surgery (see Chapter 2). After 1 week recovery, insulin (0.025uU in 1.5 μ l) was administered icv. just prior to oral glucose gavage (50mg/mouse, 200ul). Plasma samples were taken before insulin administration and 15, 30, 60 and 120 min after glucose gavage. data are expressed as mean \pm sem; n=5-8. Two-way (repeated measured; where appropriate) ANOVA with Sidak posthoc analysis; a significant at $p < 0.05$.

Additional experiments (Figure 5.2) showed that ICV administration of insulin prior to an oral glucose gavage normalised the glucose excursion to that of WT, further supporting that Crat deletion in AgRP neurons perturbs glucose stimulated insulin release.

It is conceivable that Crat deletion produces the same effect in AgRP neurons and AgRP Crat KO mice require a greater increase of the glucose level and take longer to shift metabolism from fatty acid to glucose oxidation and elicit ROS signalling to secrete insulin. This is supported by the greater glucose uptake in the hypothalamus 15 minutes after the glucose load. This delayed response to a glucose load might be the underlying reason why KO mice cannot associate the bitter tasting drink with acute ingested calories and do not prefer the unpalatable caloric drink after fasting (Figure 5.1).

5.4 Proposed role of Crat in AgRP neurons

Consequently, we propose a molecular mechanism in which Crat in AgRP neurons controls pyruvate import by regulating pyruvate dehydrogenase activity through buffering mitochondrial acetyl-CoA concentration, protein acetylation and so likely activity of other AgRP neuronal proteins affected by acetylation status. Furthermore, Crat influences ROS production and mitochondrial dynamics during the transition of fasting to refeeding (i.e. acute inhibition of AgRP neurons). Deletion of Crat in AgRP neurons specifically produces a phenotype that lacks accurate computation of ingested calories, marked by a delayed response (caused by the delayed switch from neuronal fatty acid to glucose oxidation) and followed by an overshoot (through increased ROS production) which causes hypersensitivity to an increase in nutrient availability (Figure 5.3).

sensing. Furthermore, it seems feasible to investigate acute changes in AgRP neuronal activity using *in vivo* calcium imaging techniques during the transition from fast to refeeding or during operant lever pressing experiments to further illuminate the change of timing and mode of action caused through AgRP neuronal Crat deletion. Ultimately, electrophysiological studies of AgRP Crat KO hypothalamic slice preparations should elucidate the effects of, and temporal changes elicited by glucose, fatty acids, and antioxidants on AgRP neuronal activity.

5.5 Summary

In summary, we demonstrated the importance of Crat in AgRP neurons for metabolic flexibility. Crat in AgRP neurons controls substrate utilisation, nutrient partitioning, feeding behaviour and adaptation to a low caloric environment. Moreover, we provided an unprecedented proteomic analysis of isolated AgRP neurons in various metabolic states, which will be a reference for further research. Additionally, we suggest a compelling cellular mechanism how Crat in AgRP neurons integrates peripheral information about nutrient availability, enables acute and precise adjusting of glucose metabolism to changes in metabolic state and affects the motivational aspect of food.

Although we presented a novel mechanism of processing and integrating changes in metabolic state and an alternative regulation of glucose homeostasis, more work is needed to explore and understand the exact pathway of nutrient sensing to correct deficiencies leading to metabolic complications. By influencing substrate utilisation and nutrient partitioning, Crat is a promising target candidate for obesity and type 2 diabetes therapies. We suggest that Crat in AgRP neurons represents a component of an energy calculator enabling AgRP neurons to compute multiple streams of information to mount appropriate metabolic and behavioural responses.

References

- Acosta-Rodriguez, V.A., de Groot, M.H.M., Rijo-Ferreira, F., Green, C.B., and Takahashi, J.S. (2017). Mice under Caloric Restriction Self-Impose a Temporal Restriction of Food Intake as Revealed by an Automated Feeder System. *Cell Metab* 26, 267-277 e262.
- Ainscow, E.K., Mirshamsi, S., Tang, T., Ashford, M.L., and Rutter, G.A. (2002). Dynamic imaging of free cytosolic ATP concentration during fuel sensing by rat hypothalamic neurones: evidence for ATP-independent control of ATP-sensitive K(+) channels. *J Physiol* 544, 429-445.
- Akashi, M., Hayasaka, N., Yamazaki, S., and Node, K. (2008). Mitogen-activated protein kinase is a functional component of the autonomous circadian system in the suprachiasmatic nucleus. *J Neurosci* 28, 4619-4623.
- Albert, V., Cornu, M., and Hall, M.N. (2015). mTORC1 signaling in *Agrp* neurons mediates circadian expression of *Agrp* and NPY but is dispensable for regulation of feeding behavior. *Biochem Biophys Res Commun* 464, 480-486.
- Anand, B.K., Chhina, G.S., Sharma, K.N., Dua, S., and Singh, B. (1964). Activity of Single Neurons in the Hypothalamic Feeding Centers: Effect of Glucose. *Am J Physiol* 207, 1146-1154.
- Anand, B.K., Chhina, G.S., and Singh, B. (1962). Effect of glucose on the activity of hypothalamic "feeding centers". *Science* 138, 597-598.
- Andermann, M.L., and Lowell, B.B. (2017). Toward a Wiring Diagram Understanding of Appetite Control. *Neuron* 95, 757-778.
- Anderson, E.J., Lustig, M.E., Boyle, K.E., Woodlief, T.L., Kane, D.A., Lin, C.T., Price, J.W., 3rd, Kang, L., Rabinovitch, P.S., Szeto, H.H., et al. (2009). Mitochondrial H₂O₂ emission and cellular redox state link excess fat intake to insulin resistance in both rodents and humans. *J Clin Invest* 119, 573-581.
- Anderson, K.A., and Hirschey, M.D. (2012). Mitochondrial protein acetylation regulates metabolism. *Essays Biochem* 52, 23-35.
- Andrews, Z.B. (2011). Central mechanisms involved in the orexigenic actions of ghrelin. *Peptides* 32, 2248-2255.
- Andrews, Z.B., Liu, Z.W., Wallingford, N., Erion, D.M., Borok, E., Friedman, J.M., Tschop, M.H., Shanabrough, M., Cline, G., Shulman, G.I., et al. (2008). UCP2 mediates ghrelin's action on NPY/AgRP neurons by lowering free radicals. *Nature* 454, 846-851.
- Aponte, Y., Atasoy, D., and Sternson, S.M. (2011). AGRP neurons are sufficient to orchestrate feeding behavior rapidly and without training. *Nat Neurosci* 14, 351-355.
- Atasoy, D., Betley, J.N., Su, H.H., and Sternson, S.M. (2012). Deconstruction of a neural circuit for hunger. *Nature* 488, 172-177.
- Baldelli, S., Aquilano, K., and Ciriolo, M.R. (2014). PGC-1 α buffers ROS-mediated removal of mitochondria during myogenesis. *Cell Death Dis* 5, e1515.
- Baskin, D.G., Breininger, J.F., and Schwartz, M.W. (1999). Leptin receptor mRNA identifies a subpopulation of neuropeptide Y neurons activated by fasting in rat hypothalamus. *Diabetes* 48, 828-833.
- Beall, C., Hamilton, D.L., Gallagher, J., Logie, L., Wright, K., Soutar, M.P., Dadak, S., Ashford, F.B., Haythorne, E., Du, Q., et al. (2012). Mouse hypothalamic GT1-7 cells demonstrate AMPK-dependent intrinsic glucose-sensing behaviour. *Diabetologia* 55, 2432-2444.
- Begrache, K., Marston, O.J., Rossi, J., Burke, L.K., McDonald, P., Heisler, L.K., and Butler, A.A. (2012). Melanocortin-3 receptors are involved in adaptation to restricted feeding. *Genes Brain Behav* 11, 291-302.
- Benani, A., Troy, S., Carmona, M.C., Fioramonti, X., Lorsignol, A., Leloup, C., Casteilla, L., and Penicaud, L. (2007). Role for mitochondrial reactive oxygen species in brain lipid sensing: redox regulation of food intake. *Diabetes* 56, 152-160.

- Betley, J.N., Cao, Z.F., Ritola, K.D., and Sternson, S.M. (2013). Parallel, redundant circuit organization for homeostatic control of feeding behavior. *Cell* 155, 1337-1350.
- Betley, J.N., Xu, S., Cao, Z.F.H., Gong, R., Magnus, C.J., Yu, Y., and Sternson, S.M. (2015). Neurons for hunger and thirst transmit a negative-valence teaching signal. *Nature* 521, 180-185.
- Beutler, L.R., Chen, Y., Ahn, J.S., Lin, Y.C., Essner, R.A., and Knight, Z.A. (2017). Dynamics of Gut-Brain Communication Underlying Hunger. *Neuron* 96, 461-475 e465.
- Blasiak, A., Gundlach, A.L., Hess, G., and Lewandowski, M.H. (2017). Interactions of Circadian Rhythmicity, Stress and Orexigenic Neuropeptide Systems: Implications for Food Intake Control. *Frontiers in neuroscience* 11, 127.
- Blum, I.D., Lamont, E.W., Rodrigues, T., and Abizaid, A. (2012). Isolating neural correlates of the pacemaker for food anticipation. *PLoS One* 7, e36117.
- Boldrin, L., Ross, J.A., Whitmore, C., Doreste, B., Beaver, C., Eddaoudi, A., Pearce, D.J., and Morgan, J.E. (2017). The effect of calorie restriction on mouse skeletal muscle is sex, strain and time-dependent. *Scientific reports* 7, 5160.
- Branstrom, R., Corkey, B.E., Berggren, P.O., and Larsson, O. (1997). Evidence for a unique long chain acyl-CoA ester binding site on the ATP-regulated potassium channel in mouse pancreatic beta cells. *J Biol Chem* 272, 17390-17394.
- Bray, M.S., Ratcliffe, W.F., Grenett, M.H., Brewer, R.A., Gamble, K.L., and Young, M.E. (2013). Quantitative analysis of light-phase restricted feeding reveals metabolic dyssynchrony in mice. *Int J Obes (Lond)* 37, 843-852.
- Briggs, D.I., and Andrews, Z.B. (2011). A Recent Update on the Role of Ghrelin in Glucose Homeostasis. *Current diabetes reviews*.
- Brito, M.N., Brito, N.A., Baro, D.J., Song, C.K., and Bartness, T.J. (2007). Differential activation of the sympathetic innervation of adipose tissues by melanocortin receptor stimulation. *Endocrinology* 148, 5339-5347.
- Broberger, C., Johansen, J., Johansson, C., Schalling, M., and Hokfelt, T. (1998). The neuropeptide Y/agouti gene-related protein (AGRP) brain circuitry in normal, anorectic, and monosodium glutamate-treated mice. *Proc Natl Acad Sci U S A* 95, 15043-15048.
- Brodie, B.B., Costa, E., Dlabac, A., Neff, N.H., and Smookler, H.H. (1966). Application of steady state kinetics to the estimation of synthesis rate and turnover time of tissue catecholamines. *J Pharmacol Exp Ther* 154, 493-498.
- Bruning, J.C., Gautam, D., Burks, D.J., Gillette, J., Schubert, M., Orban, P.C., Klein, R., Krone, W., Muller-Wieland, D., and Kahn, C.R. (2000). Role of brain insulin receptor in control of body weight and reproduction. *Science* 289, 2122-2125.
- Bruss, M.D., Khambatta, C.F., Ruby, M.A., Aggarwal, I., and Hellerstein, M.K. (2010). Calorie restriction increases fatty acid synthesis and whole body fat oxidation rates. *Am J Physiol Endocrinol Metab* 298, E108-116.
- Buijs, F.N., Guzman-Ruiz, M., Leon-Mercado, L., Basualdo, M.C., Escobar, C., Kalsbeek, A., and Buijs, R.M. (2017). Suprachiasmatic Nucleus Interaction with the Arcuate Nucleus; Essential for Organizing Physiological Rhythms. *eNeuro* 4.
- Burdakov, D., Luckman, S.M., and Verkhratsky, A. (2005). Glucose-sensing neurons of the hypothalamus. *Philos Trans R Soc Lond B Biol Sci* 360, 2227-2235.
- Burke, L.K., Darwish, T., Cavanaugh, A.R., Virtue, S., Roth, E., Morro, J., Liu, S.M., Xia, J., Dalley, J.W., Burling, K., et al. (2017). mTORC1 in AGRP neurons integrates exteroceptive and interoceptive food-related cues in the modulation of adaptive energy expenditure in mice. *Elife* 6.
- Burnett, C.J., and Krashes, M.J. (2016). Resolving Behavioral Output via Chemogenetic Designer Receptors Exclusively Activated by Designer Drugs. *J Neurosci* 36, 9268-9282.

- Burnett, C.J., Li, C., Webber, E., Tsaousidou, E., Xue, S.Y., Bruning, J.C., and Krashes, M.J. (2016). Hunger-Driven Motivational State Competition. *Neuron* 92, 187-201.
- Campos, C.A., Bowen, A.J., Schwartz, M.W., and Palmiter, R.D. (2016). Parabrachial CGRP Neurons Control Meal Termination. *Cell Metab* 23, 811-820.
- Cansell, C., Denis, R.G., Joly-Amado, A., Castel, J., and Luquet, S. (2012). Arcuate AgRP neurons and the regulation of energy balance. *Frontiers in endocrinology* 3, 169.
- Carneiro, B.T., and Araujo, J.F. (2009). The food-entrainable oscillator: a network of interconnected brain structures entrained by humoral signals? *Chronobiol Int* 26, 1273-1289.
- Carneiro, L., Allard, C., Guissard, C., Fioramonti, X., Tourrel-Cuzin, C., Bailbe, D., Barreau, C., Offer, G., Nedelec, E., Salin, B., et al. (2012). Importance of mitochondrial dynamin-related protein 1 in hypothalamic glucose sensitivity in rats. *Antioxid Redox Signal* 17, 433-444.
- Cavalcanti-de-Albuquerque, J.P., Zimmer, M.R., Bober, J., and Dietrich, M.O. (2016). Rapid shift in substrate utilization driven by hypothalamic Agrp neurons. *BioRxiv*.
- Chalmers, J.A., Jang, J.J., and Belsham, D.D. (2014). Glucose sensing mechanisms in hypothalamic cell models: glucose inhibition of AgRP synthesis and secretion. *Mol Cell Endocrinol* 382, 262-270.
- Chase, J.F. (1967). The substrate specificity of carnitine acetyltransferase. *Biochem J* 104, 510-518.
- Chavan, R., Feillet, C., Costa, S.S., Delorme, J.E., Okabe, T., Ripperger, J.A., and Albrecht, U. (2016). Liver-derived ketone bodies are necessary for food anticipation. *Nature communications* 7, 10580.
- Chen, Y., Lin, Y.C., Kuo, T.W., and Knight, Z.A. (2015). Sensory detection of food rapidly modulates arcuate feeding circuits. *Cell* 160, 829-841.
- Chen, Y., Lin, Y.C., Zimmerman, C.A., Essner, R.A., and Knight, Z.A. (2016). Hunger neurons drive feeding through a sustained, positive reinforcement signal. *Elife* 5.
- Cheng, A., Yang, Y., Zhou, Y., Maharana, C., Lu, D., Peng, W., Liu, Y., Wan, R., Marosi, K., Misiak, M., et al. (2016). Mitochondrial SIRT3 Mediates Adaptive Responses of Neurons to Exercise and Metabolic and Excitatory Challenges. *Cell Metab* 23, 128-142.
- Cheng, H., Isoda, F., Belsham, D.D., and Mobbs, C.V. (2008). Inhibition of agouti-related peptide expression by glucose in a clonal hypothalamic neuronal cell line is mediated by glycolysis, not oxidative phosphorylation. *Endocrinology* 149, 703-710.
- Chretien, C., Fenech, C., Lienard, F., Grall, S., Chevalier, C., Chaudy, S., Brenachot, X., Berges, R., Louche, K., Stark, R., et al. (2017). Transient Receptor Potential Canonical 3 (TRPC3) Channels Are Required for Hypothalamic Glucose Detection and Energy Homeostasis. *Diabetes* 66, 314-324.
- Claret, M., Smith, M.A., Batterham, R.L., Selman, C., Choudhury, A.I., Fryer, L.G., Clements, M., Al-Qassab, H., Heffron, H., Xu, A.W., et al. (2007). AMPK is essential for energy homeostasis regulation and glucose sensing by POMC and AgRP neurons. *J Clin Invest* 117, 2325-2336.
- Colombani, A.L., Carneiro, L., Benani, A., Galinier, A., Jaillard, T., Duparc, T., Offer, G., Lorsignol, A., Magnan, C., Casteilla, L., et al. (2009). Enhanced hypothalamic glucose sensing in obesity: alteration of redox signaling. *Diabetes* 58, 2189-2197.
- Cordente, A.G., Lopez-Vinas, E., Vazquez, M.I., Gomez-Puertas, P., Asins, G., Serra, D., and Hegardt, F.G. (2006). Mutagenesis of specific amino acids converts carnitine acetyltransferase into carnitine palmitoyltransferase. *Biochemistry* 45, 6133-6141.
- Cox, J., and Mann, M. (2008). MaxQuant enables high peptide identification rates, individualized p.p.b.-range mass accuracies and proteome-wide protein quantification. *Nature biotechnology* 26, 1367-1372.
- Dadak, S., Beall, C., Vlachaki Walker, J.M., Soutar, M.P.M., McCrimmon, R.J., and Ashford, M.L.J. (2017). Oleate induces KATP channel-dependent hyperpolarization in mouse hypothalamic glucose-excited neurons without altering cellular energy charge. *Neuroscience* 346, 29-42.

- Dai, Y., Wolfgang, M.J., Cha, S.H., and Lane, M.D. (2007). Localization and effect of ectopic expression of CPT1c in CNS feeding centers. *Biochemical and biophysical research communications* 359, 469-474.
- Darabian, S., Backlund, J.Y., Cleary, P.A., Sheidaee, N., Bebu, I., Lachin, J.M., Budoff, M.J., and Group, D.E.R. (2016). Significance of Epicardial and Intrathoracic Adipose Tissue Volume among Type 1 Diabetes Patients in the DCCT/EDIC: A Pilot Study. *PLoS One* 11, e0159958.
- Davies, M.N., Kjalarsdottir, L., Thompson, J.W., Dubois, L.G., Stevens, R.D., Ilkayeva, O.R., Brosnan, M.J., Rolph, T.P., Grimsrud, P.A., and Muoio, D.M. (2016). The Acetyl Group Buffering Action of Carnitine Acetyltransferase Offsets Macronutrient-Induced Lysine Acetylation of Mitochondrial Proteins. *Cell reports* 14, 243-254.
- de Araujo, I.E., Oliveira-Maia, A.J., Sotnikova, T.D., Gainetdinov, R.R., Caron, M.G., Nicoletis, M.A., and Simon, S.A. (2008). Food reward in the absence of taste receptor signaling. *Neuron* 57, 930-941.
- de Vasconcelos, A.P., Bartol-Munier, I., Feillet, C.A., Gormelen, S., Pevet, P., and Challet, E. (2006). Modifications of local cerebral glucose utilization during circadian food-anticipatory activity. *Neuroscience* 139, 741-748.
- Delezie, J., Dumont, S., Sandu, C., Reibel, S., Pevet, P., and Challet, E. (2016). Rev-erb α in the brain is essential for circadian food entrainment. *Scientific reports* 6, 29386.
- Diano, S., and Horvath, T.L. (2012). Mitochondrial uncoupling protein 2 (UCP2) in glucose and lipid metabolism. *Trends Mol Med* 18, 52-58.
- Diano, S., Liu, Z.W., Jeong, J.K., Dietrich, M.O., Ruan, H.B., Kim, E., Suyama, S., Kelly, K., Gyengesi, E., Arbiser, J.L., et al. (2011). Peroxisome proliferation-associated control of reactive oxygen species sets melanocortin tone and feeding in diet-induced obesity. *Nat Med* 17, 1121-1127.
- Diaz-Munoz, M., Vazquez-Martinez, O., Baez-Ruiz, A., Martinez-Cabrera, G., Soto-Abraham, M.V., Avila-Casado, M.C., and Larriva-Sahd, J. (2010). Daytime food restriction alters liver glycogen, triacylglycerols, and cell size. A histochemical, morphometric, and ultrastructural study. *Comp Hepatol* 9, 5.
- DiDonato, S., Rimoldi, M., Moise, A., Bertagnoglio, B., and Uziel, G. (1979). Fatal ataxic encephalopathy and carnitine acetyltransferase deficiency: a functional defect of pyruvate oxidation? *Neurology* 29, 1578-1583.
- Dietrich, M.O., Antunes, C., Geliang, G., Liu, Z.W., Borok, E., Nie, Y., Xu, A.W., Souza, D.O., Gao, Q., Diano, S., et al. (2010). Agrp neurons mediate Sirt1's action on the melanocortin system and energy balance: roles for Sirt1 in neuronal firing and synaptic plasticity. *J Neurosci* 30, 11815-11825.
- Dietrich, M.O., Bober, J., Ferreira, J.G., Tellez, L.A., Mineur, Y.S., Souza, D.O., Gao, X.B., Picciotto, M.R., Araujo, I., Liu, Z.W., et al. (2012). AgRP neurons regulate development of dopamine neuronal plasticity and nonfood-associated behaviors. *Nat Neurosci* 15, 1108-1110.
- Dietrich, M.O., Liu, Z.W., and Horvath, T.L. (2013). Mitochondrial dynamics controlled by mitofusins regulate Agrp neuronal activity and diet-induced obesity. *Cell* 155, 188-199.
- Dodd, G.T., Andrews, Z.B., Simonds, S.E., Michael, N.J., DeVeer, M., Bruning, J.C., Spanswick, D., Cowley, M.A., and Tiganis, T. (2017). A Hypothalamic Phosphatase Switch Coordinates Energy Expenditure with Feeding. *Cell Metab* 26, 375-393 e377.
- Dolezal, V., and Tucek, S. (1981). Utilization of citrate, acetylcarnitine, acetate, pyruvate and glucose for the synthesis of acetylcholine in rat brain slices. *J Neurochem* 36, 1323-1330.
- Drechsel, D.A., and Patel, M. (2010). Respiration-dependent H₂O₂ removal in brain mitochondria via the thioredoxin/peroxiredoxin system. *J Biol Chem* 285, 27850-27858.
- Dulloo, A.G., Jacquet, J., Montani, J.P., and Schutz, Y. (2015). How dieting makes the lean fatter: from a perspective of body composition autoregulation through adipostats and proteinstats awaiting discovery. *Obes Rev* 16 Suppl 1, 25-35.

- Dunn-Meynell, A.A., Routh, V.H., Kang, L., Gaspers, L., and Levin, B.E. (2002). Glucokinase is the likely mediator of glucosensing in both glucose-excited and glucose-inhibited central neurons. *Diabetes* 51, 2056-2065.
- Enriori, P.J., Evans, A.E., Sinnayah, P., Jobst, E.E., Tonelli-Lemos, L., Billes, S.K., Glavas, M.M., Grayson, B.E., Perello, M., Nillni, E.A., et al. (2007). Diet-induced obesity causes severe but reversible leptin resistance in arcuate melanocortin neurons. *Cell Metab* 5, 181-194.
- Escobar, C., Diaz-Munoz, M., Encinas, F., and Aguilar-Roblero, R. (1998). Persistence of metabolic rhythmicity during fasting and its entrainment by restricted feeding schedules in rats. *Am J Physiol* 274, R1309-1316.
- Essner, R.A., Smith, A.G., Jamnik, A.A., Ryba, A.R., Trutner, Z.D., and Carter, M.E. (2017). AgRP Neurons Can Increase Food Intake during Conditions of Appetite Suppression and Inhibit Anorexigenic Parabrachial Neurons. *J Neurosci* 37, 8678-8687.
- Ferreira, G.C., and McKenna, M.C. (2017). L-Carnitine and Acetyl-L-carnitine Roles and Neuroprotection in Developing Brain. *Neurochem Res* 42, 1661-1675.
- Freo, U., Dam, M., and Ori, C. (2009). Cerebral metabolic effects of acetyl-l-carnitine in rats during aging. *Brain Res* 1259, 32-39.
- Gallardo, C.M., Hsu, C.T., Gunapala, K.M., Parfyonov, M., Chang, C.H., Mistlberger, R.E., and Steele, A.D. (2014). Behavioral and neural correlates of acute and scheduled hunger in C57BL/6 mice. *PLoS One* 9, e95990.
- Garfield, A.S., Li, C., Madara, J.C., Shah, B.P., Webber, E., Steger, J.S., Campbell, J.N., Gavrilova, O., Lee, C.E., Olson, D.P., et al. (2015). A neural basis for melanocortin-4 receptor-regulated appetite. *Nat Neurosci* 18, 863-871.
- Garfield, A.S., Shah, B.P., Burgess, C.R., Li, M.M., Li, C., Steger, J.S., Madara, J.C., Campbell, J.N., Kroeger, D., Scammell, T.E., et al. (2016). Dynamic GABAergic afferent modulation of AgRP neurons. *Nat Neurosci* 19, 1628-1635.
- Gastaldelli, A. (2017). Insulin resistance and reduced metabolic flexibility: cause or consequence of NAFLD? *Clinical science* 131, 2701-2704.
- Gill, J.F., Delezie, J., Santos, G., and Handschin, C. (2016). PGC-1alpha expression in murine AgRP neurons regulates food intake and energy balance. *Molecular metabolism* 5, 580-588.
- Girardet, C., Mavrikaki, M., Southern, M.R., Smith, R.G., and Butler, A.A. (2014). Assessing interactions between Ghrelin and Mc3r reveals a role for AgRP in the expression of food anticipatory activity in male mice. *Endocrinology* 155, 4843-4855.
- Girotti, M., Weinberg, M.S., and Spencer, R.L. (2009). Diurnal expression of functional and clock-related genes throughout the rat HPA axis: system-wide shifts in response to a restricted feeding schedule. *Am J Physiol Endocrinol Metab* 296, E888-897.
- Goldsmith, C.S., and Bell-Pedersen, D. (2013). Diverse roles for MAPK signaling in circadian clocks. *Adv Genet* 84, 1-39.
- Goodpaster, B.H., and Sparks, L.M. (2017). Metabolic Flexibility in Health and Disease. *Cell Metab* 25, 1027-1036.
- Gropp, E., Shanabrough, M., Borok, E., Xu, A.W., Janoschek, R., Buch, T., Plum, L., Balthasar, N., Hampel, B., Waisman, A., et al. (2005). Agouti-related peptide-expressing neurons are mandatory for feeding. *Nature Neuroscience* 8, 1289-1291.
- Guillod-Maximin, E., Lorsignol, A., Alquier, T., and Penicaud, L. (2004). Acute intracarotid glucose injection towards the brain induces specific c-fos activation in hypothalamic nuclei: involvement of astrocytes in cerebral glucose-sensing in rats. *J Neuroendocrinol* 16, 464-471.
- Gupta, R., Ma, Y., Wang, M., and Whim, M.D. (2017). AgRP-Expressing Adrenal Chromaffin Cells Are Involved in the Sympathetic Response to Fasting. *Endocrinology*.

- Gyengesi, E., Liu, Z.W., D'Agostino, G., Gan, G., Horvath, T.L., Gao, X.B., and Diano, S. (2010). Corticosterone regulates synaptic input organization of POMC and NPY/AgRP neurons in adult mice. *Endocrinology* 151, 5395-5402.
- Hahn, T.M., Breininger, J.F., Baskin, D.G., and Schwartz, M.W. (1998). Coexpression of *Agrp* and *NPY* in fasting-activated hypothalamic neurons. *Nat Neurosci* 1, 271-272.
- Hatori, M., Vollmers, C., Zarrinpar, A., DiTacchio, L., Bushong, E.A., Gill, S., Leblanc, M., Chaix, A., Joens, M., Fitzpatrick, J.A., et al. (2012). Time-restricted feeding without reducing caloric intake prevents metabolic diseases in mice fed a high-fat diet. *Cell Metab* 15, 848-860.
- He, W., Lam, T.K., Obici, S., and Rossetti, L. (2006). Molecular disruption of hypothalamic nutrient sensing induces obesity. *Nat Neurosci* 9, 227-233.
- Hopkins, M., Finlayson, G., Duarte, C., Whybrow, S., Ritz, P., Horgan, G.W., Blundell, J.E., and Stubbs, R.J. (2016). Modelling the associations between fat-free mass, resting metabolic rate and energy intake in the context of total energy balance. *Int J Obes (Lond)* 40, 312-318.
- Iordanidou, P., and Burdakov, D. (2016). Brain glucose feedback predicts food choice (Commentary on Wakabayashi et al.). *Eur J Neurosci* 43, 1420-1421.
- Jackowski, S., and Leonardi, R. (2014). Deregulated coenzyme A, loss of metabolic flexibility and diabetes. *Biochem Soc Trans* 42, 1118-1122.
- Jahoor, F., Klein, S., and Wolfe, R. (1992). Mechanism of Regulation of Glucose-Production by Lipolysis in Humans. *American Journal of Physiology* 262, E353-E358.
- Jaillard, T., Roger, M., Galinier, A., Guillou, P., Benani, A., Leloup, C., Casteilla, L., Penicaud, L., and Lorsignol, A. (2009). Hypothalamic reactive oxygen species are required for insulin-induced food intake inhibition: an NADPH oxidase-dependent mechanism. *Diabetes* 58, 1544-1549.
- James, A.M., Hoogewijs, K., Logan, A., Hall, A.R., Ding, S., Fearnley, I.M., and Murphy, M.P. (2017). Non-enzymatic N-acetylation of Lysine Residues by AcetylCoA Often Occurs via a Proximal S-acetylated Thiol Intermediate Sensitive to Glyoxalase II. *Cell reports* 18, 2105-2112.
- Jansson, J.O., Palsdottir, V., Hagg, D.A., Schele, E., Dickson, S.L., Anesten, F., Bake, T., Montelius, M., Bellman, J., Johansson, M.E., et al. (2017). Body weight homeostat that regulates fat mass independently of leptin in rats and mice. *Proc Natl Acad Sci U S A*.
- Jikomes, N., Ramesh, R.N., Mandelblat-Cerf, Y., and Andermann, M.L. (2016). Preemptive Stimulation of AgRP Neurons in Fed Mice Enables Conditioned Food Seeking under Threat. *Curr Biol* 26, 2500-2507.
- Joly-Amado, A., Cansell, C., Denis, R.G., Delbes, A.S., Castel, J., Martinez, S., and Luquet, S. (2014). The hypothalamic arcuate nucleus and the control of peripheral substrates. *Best practice & research. Clinical endocrinology & metabolism* 28, 725-737.
- Joly-Amado, A., Denis, R.G., Castel, J., Lacombe, A., Cansell, C., Rouch, C., Kassis, N., Dairou, J., Cani, P.D., Ventura-Clapier, R., et al. (2012). Hypothalamic AgRP-neurons control peripheral substrate utilization and nutrient partitioning. *EMBO J* 31, 4276-4288.
- Kang, L., Dunn-Meynell, A.A., Routh, V.H., Gaspers, L.D., Nagata, Y., Nishimura, T., Eiki, J., Zhang, B.B., and Levin, B.E. (2006). Glucokinase is a critical regulator of ventromedial hypothalamic neuronal glucosensing. *Diabetes* 55, 412-420.
- Kasser, T.R., Deutch, A., and Martin, R.J. (1986). Uptake and utilization of metabolites in specific brain sites relative to feeding status. *Physiol Behav* 36, 1161-1165.
- Kasser, T.R., Harris, R.B., and Martin, R.J. (1985). Level of satiety: fatty acid and glucose metabolism in three brain sites associated with feeding. *Am J Physiol* 248, R447-452.
- Kaushik, S., Rodriguez-Navarro, J.A., Arias, E., Kiffin, R., Sahu, S., Schwartz, G.J., Cuervo, A.M., and Singh, R. (2011). Autophagy in hypothalamic AgRP neurons regulates food intake and energy balance. *Cell Metab* 14, 173-183.

- Kennedy, G.C. (1953). The role of depot fat in the hypothalamic control of food intake in the rat. *Proc R Soc Lond B Biol Sci* 140, 578-596.
- Kleinridders, A., Konner, A.C., and Bruning, J.C. (2009). CNS-targets in control of energy and glucose homeostasis. *Current opinion in pharmacology* 9, 794-804.
- Kong, D., Dagon, Y., Campbell, J.N., Guo, Y., Yang, Z., Yi, X., Aryal, P., Wellenstein, K., Kahn, B.B., Sabatini, B.L., et al. (2016). A Postsynaptic AMPK-->p21-Activated Kinase Pathway Drives Fasting-Induced Synaptic Plasticity in AgRP Neurons. *Neuron* 91, 25-33.
- Kong, D., Vong, L., Parton, L.E., Ye, C., Tong, Q., Hu, X., Choi, B., Bruning, J.C., and Lowell, B.B. (2010). Glucose stimulation of hypothalamic MCH neurons involves K(ATP) channels, is modulated by UCP2, and regulates peripheral glucose homeostasis. *Cell Metab* 12, 545-552.
- Konner, A.C., Janoscsek, R., Plum, L., Jordan, S.D., Rother, E., Ma, X., Xu, C., Enriori, P., Hampel, B., Barsh, G.S., et al. (2007). Insulin action in AgRP-expressing neurons is required for suppression of hepatic glucose production. *Cell Metab* 5, 438-449.
- Kosse, C., Gonzalez, A., and Burdakov, D. (2015). Predictive models of glucose control: roles for glucose-sensing neurones. *Acta Physiol (Oxf)* 213, 7-18.
- Koves, T.R., Ussher, J.R., Noland, R.C., Slentz, D., Mosedale, M., Ilkayeva, O., Bain, J., Stevens, R., Dyck, J.R., Newgard, C.B., et al. (2008). Mitochondrial overload and incomplete fatty acid oxidation contribute to skeletal muscle insulin resistance. *Cell Metab* 7, 45-56.
- Kowalski, G.M., Kloehn, J., Burch, M.L., Selathurai, A., Hamley, S., Bayol, S.A., Lamon, S., Watt, M.J., Lee-Young, R.S., McConville, M.J., et al. (2015). Overexpression of sphingosine kinase 1 in liver reduces triglyceride content in mice fed a low but not high-fat diet. *Biochim Biophys Acta* 1851, 210-219.
- Krashes, M.J., Koda, S., Ye, C., Rogan, S.C., Adams, A.C., Cusher, D.S., Maratos-Flier, E., Roth, B.L., and Lowell, B.B. (2011). Rapid, reversible activation of AgRP neurons drives feeding behavior in mice. *J Clin Invest* 121, 1424-1428.
- Krashes, M.J., Shah, B.P., Koda, S., and Lowell, B.B. (2013). Rapid versus delayed stimulation of feeding by the endogenously released AgRP neuron mediators GABA, NPY, and AgRP. *Cell Metab* 18, 588-595.
- Krashes, M.J., Shah, B.P., Madara, J.C., Olson, D.P., Strohlic, D.E., Garfield, A.S., Vong, L., Pei, H., Watabe-Uchida, M., Uchida, N., et al. (2014). An excitatory paraventricular nucleus to AgRP neuron circuit that drives hunger. *Nature* 507, 238-242.
- Krishnaiah, S.Y., Wu, G., Altman, B.J., Growe, J., Rhoades, S.D., Coldren, F., Venkataraman, A., Olarerin-George, A.O., Francey, L.J., Mukherjee, S., et al. (2017). Clock Regulation of Metabolites Reveals Coupling between Transcription and Metabolism. *Cell Metab* 25, 961-974 e964.
- Kuperman, Y., Weiss, M., Dine, J., Staikin, K., Golani, O., Ramot, A., Nahum, T., Kuhne, C., Shemesh, Y., Wurst, W., et al. (2016). CRFR1 in AgRP Neurons Modulates Sympathetic Nervous System Activity to Adapt to Cold Stress and Fasting. *Cell Metab* 23, 1185-1199.
- Kurata, K., Fujimoto, K., Sakata, T., Etou, H., and Fukagawa, K. (1986). D-glucose suppression of eating after intra-third ventricle infusion in rat. *Physiol Behav* 37, 615-620.
- Lam, C.K., Chari, M., Wang, P.Y., and Lam, T.K. (2008). Central lactate metabolism regulates food intake. *Am J Physiol Endocrinol Metab* 295, E491-496.
- Lam, T.K., Gutierrez-Juarez, R., Poci, A., and Rossetti, L. (2005a). Regulation of blood glucose by hypothalamic pyruvate metabolism. *Science* 309, 943-947.
- Lam, T.K., Poci, A., Gutierrez-Juarez, R., Obici, S., Bryan, J., Aguilar-Bryan, L., Schwartz, G.J., and Rossetti, L. (2005b). Hypothalamic sensing of circulating fatty acids is required for glucose homeostasis. *Nat Med* 11, 320-327.
- Le Foll, C., Irani, B.G., Magnan, C., Dunn-Meynell, A.A., and Levin, B.E. (2009). Characteristics and mechanisms of hypothalamic neuronal fatty acid sensing. *Am J Physiol Regul Integr Comp Physiol* 297, R655-664.

- Lee, J., and Wolfgang, M.J. (2012). Metabolomic profiling reveals a role for CPT1c in neuronal oxidative metabolism. *BMC Biochem* 13, 23.
- Leloup, C., Magnan, C., Benani, A., Bonnet, E., Alquier, T., Offer, G., Carriere, A., Periquet, A., Fernandez, Y., Ktorza, A., et al. (2006). Mitochondrial reactive oxygen species are required for hypothalamic glucose sensing. *Diabetes* 55, 2084-2090.
- Leloup, C., Turrel-Cuzin, C., Magnan, C., Karaca, M., Castel, J., Carneiro, L., Colombani, A.L., Ktorza, A., Casteilla, L., and Penicaud, L. (2009). Mitochondrial reactive oxygen species are obligatory signals for glucose-induced insulin secretion. *Diabetes* 58, 673-681.
- Lemus, M.B., Bayliss, J.A., Lockie, S.H., Santos, V.V., Reichenbach, A., Stark, R., and Andrews, Z.B. (2015). A stereological analysis of NPY, POMC, orexin, GFAP astrocyte and Iba1 microglial cell number and volume in diet-induced obese male mice. *Endocrinology*.
- Levin, B.E., Becker, T.C., Eiki, J., Zhang, B.B., and Dunn-Meynell, A.A. (2008). Ventromedial hypothalamic glucokinase is an important mediator of the counterregulatory response to insulin-induced hypoglycemia. *Diabetes* 57, 1371-1379.
- Li, A.J., Wiater, M.F., Ostrom, M.T., Smith, B.R., Wang, Q., Dinh, T.T., Roberts, B.L., Jansen, H.T., and Ritter, S. (2012). Leptin-sensitive neurons in the arcuate nuclei contribute to endogenous feeding rhythms. *Am J Physiol Regul Integr Comp Physiol* 302, R1313-1326.
- Li, Z., Okamoto, K., Hayashi, Y., and Sheng, M. (2004). The importance of dendritic mitochondria in the morphogenesis and plasticity of spines and synapses. *Cell* 119, 873-887.
- Liu, T., Kong, D., Shah, B.P., Ye, C., Koda, S., Saunders, A., Ding, J.B., Yang, Z., Sabatini, B.L., and Lowell, B.B. (2012). Fasting activation of AgRP neurons requires NMDA receptors and involves spinogenesis and increased excitatory tone. *Neuron* 73, 511-522.
- Lo, M.T., Chiang, W.Y., Hsieh, W.H., Escobar, C., Buijs, R.M., and Hu, K. (2016). Interactive Effects of Dorsomedial Hypothalamic Nucleus and Time-Restricted Feeding on Fractal Motor Activity Regulation. *Frontiers in physiology* 7, 174.
- Lockie, S.H., and Andrews, Z.B. (2013). The hormonal signature of energy deficit: Increasing the value of food reward. *Molecular metabolism* 2, 329-336.
- Lockie, S.H., McAuley, C.V., Rawlinson, S., Guiney, N., and Andrews, Z.B. (2017). Food Seeking in a Risky Environment: A Method for Evaluating Risk and Reward Value in Food Seeking and Consumption in Mice. *Frontiers in neuroscience* 11, 24.
- Longo, N., Amat di San Filippo, C., and Pasquali, M. (2006). Disorders of carnitine transport and the carnitine cycle. *Am J Med Genet C Semin Med Genet* 142C, 77-85.
- Lu, K., Xu, Y., Yin, P., Oxenham, A.J., Fritz, J.B., and Shamma, S.A. (2017). Temporal coherence structure rapidly shapes neuronal interactions. *Nature communications* 8, 13900.
- Lu, X.Y., Shieh, K.R., Kabbaj, M., Barsh, G.S., Akil, H., and Watson, S.J. (2002). Diurnal rhythm of agouti-related protein and its relation to corticosterone and food intake. *Endocrinology* 143, 3905-3915.
- Luquet, S., Perez, F.A., Hnasko, T.S., and Palmiter, R.D. (2005). NPY/AgRP neurons are essential for feeding in adult mice but can be ablated in neonates. *Science* 310, 683-685.
- Lynch, R.M., Tompkins, L.S., Brooks, H.L., Dunn-Meynell, A.A., and Levin, B.E. (2000). Localization of glucokinase gene expression in the rat brain. *Diabetes* 49, 693-700.
- Madiraju, P., Pande, S.V., Prentki, M., and Madiraju, S.R. (2009). Mitochondrial acetylcarnitine provides acetyl groups for nuclear histone acetylation. *Epigenetics : official journal of the DNA Methylation Society* 4, 399-403.
- Mandelblat-Cerf, Y., Ramesh, R.N., Burgess, C.R., Patella, P., Yang, Z., Lowell, B.B., and Andermann, M.L. (2015). Arcuate hypothalamic AgRP and putative POMC neurons show opposite changes in spiking across multiple timescales. *Elife* 4.

- Marcheva, B., Ramsey, K.M., Peek, C.B., Affinati, A., Maury, E., and Bass, J. (2013). Circadian clocks and metabolism. *Handbook of experimental pharmacology*, 127-155.
- Marty, N., Dallaporta, M., and Thorens, B. (2007). Brain glucose sensing, counterregulation, and energy homeostasis. *Physiology (Bethesda)* 22, 241-251.
- Mauvoisin, D., Atger, F., Dayon, L., Nunez Galindo, A., Wang, J., Martin, E., Da Silva, L., Montoliu, I., Collino, S., Martin, F.P., et al. (2017). Circadian and Feeding Rhythms Orchestrate the Diurnal Liver Acetylome. *Cell reports* 20, 1729-1743.
- Meex, R.C., Hoy, A.J., Morris, A., Brown, R.D., Lo, J.C.Y., Burke, M., Goode, R.J.A., Kingwell, B.A., Kraakman, M.J., Febbraio, M.A., et al. (2015). Fetuin B Is a Secreted Hepatocyte Factor Linking Steatosis to Impaired Glucose Metabolism. *Cell Metabolism* 22, 1078-1089.
- Melegh, B., Seress, L., Bedekovics, T., Kispal, G., Sumegi, B., Trombitas, K., and Mehes, K. (1999). Muscle carnitine acetyltransferase and carnitine deficiency in a case of mitochondrial encephalomyopathy. *J Inherit Metab Dis* 22, 827-838.
- Meng, Y., Guan, Y., Zhang, W., Wu, Y.E., Jia, H., Zhang, Y., Zhang, X., Du, H., and Wang, X. (2016). RNA-seq analysis of the hypothalamic transcriptome reveals the networks regulating physiopathological progress in the diabetic GK rat. *Scientific reports* 6, 34138.
- Merkestein, M., van Gestel, M.A., van der Zwaal, E.M., Brans, M.A., Luijendijk, M.C., van Rozen, A.J., Hendriks, J., Garner, K.M., Boender, A.J., Pandit, R., et al. (2014). GHS-R1a signaling in the DMH and VMH contributes to food anticipatory activity. *Int J Obes (Lond)* 38, 610-618.
- Miki, T., Liss, B., Minami, K., Shiuchi, T., Saraya, A., Kashima, Y., Horiuchi, M., Ashcroft, F., Minokoshi, Y., Roeper, J., et al. (2001). ATP-sensitive K⁺ channels in the hypothalamus are essential for the maintenance of glucose homeostasis. *Nat Neurosci* 4, 507-512.
- Miselis, R.R., and Epstein, A.N. (1975). Feeding induced by intracerebroventricular 2-deoxy-D-glucose in the rat. *Am J Physiol* 229, 1438-1447.
- Mitchell, S.E., Delville, C., Konstantopelos, P., Derous, D., Green, C.L., Wang, Y., Han, J.D., Promislow, D.E., Douglas, A., Chen, L., et al. (2016). The effects of graded levels of calorie restriction: V. Impact of short term calorie and protein restriction on physical activity in the C57BL/6 mouse. *Oncotarget* 7, 19147-19170.
- Miyamoto, J., Hasegawa, S., Kasubuchi, M., Ichimura, A., Nakajima, A., and Kimura, I. (2016). Nutritional Signaling via Free Fatty Acid Receptors. *International journal of molecular sciences* 17, 450.
- Moreno, C., Yang, L., Dacks, P., Isoda, F., Poplawski, M., and Mobbs, C.V. (2013). Regulation of peripheral metabolism by substrate partitioning in the brain. *Endocrinol Metab Clin North Am* 42, 67-80.
- Mouille, V.S., Le Foll, C., Philippe, E., Kassis, N., Rouch, C., Marsollier, N., Bui, L.C., Guissard, C., Dairou, J., Lorsignol, A., et al. (2013). Fatty acid transporter CD36 mediates hypothalamic effect of fatty acids on food intake in rats. *PLoS One* 8, e74021.
- Mucerino, S., Di Salle, A., Alessio, N., Margarucci, S., Nicolai, R., Melone, M.A., Galderisi, U., and Peluso, G. (2017). Alterations in the carnitine cycle in a mouse model of Rett syndrome. *Scientific reports* 7, 41824.
- Mugabo, Y., Zhao, S., Seifried, A., Gezzar, S., Al-Mass, A., Zhang, D., Lamontagne, J., Attane, C., Poursharifi, P., Iglesias, J., et al. (2016). Identification of a mammalian glycerol-3-phosphate phosphatase: Role in metabolism and signaling in pancreatic beta-cells and hepatocytes. *Proc Natl Acad Sci U S A* 113, E430-439.
- Muoio, D.M. (2014). Metabolic inflexibility: when mitochondrial indecision leads to metabolic gridlock. *Cell* 159, 1253-1262.
- Muoio, D.M., and Neuffer, P.D. (2012). Lipid-induced mitochondrial stress and insulin action in muscle. *Cell Metab* 15, 595-605.

- Muoio, D.M., Noland, R.C., Kovalik, J.P., Seiler, S.E., Davies, M.N., DeBalsi, K.L., Ilkayeva, O.R., Stevens, R.D., Kheterpal, I., Zhang, J., et al. (2012). Muscle-specific deletion of carnitine acetyltransferase compromises glucose tolerance and metabolic flexibility. *Cell Metab* 15, 764-777.
- Nakajima, K., Cui, Z., Li, C., Meister, J., Cui, Y., Fu, O., Smith, A.S., Jain, S., Lowell, B.B., Krashes, M.J., et al. (2016). Gs-coupled GPCR signalling in AgRP neurons triggers sustained increase in food intake. *Nature communications* 7, 10268.
- Namvar, S., Gyte, A., Denn, M., Leighton, B., and Piggins, H.D. (2016). Dietary fat and corticosterone levels are contributing factors to meal anticipation. *Am J Physiol Regul Integr Comp Physiol* 310, R711-723.
- Neufeld-Cohen, A., Robles, M.S., Aviram, R., Manella, G., Adamovich, Y., Ladeuix, B., Nir, D., Rousso-Noori, L., Kuperman, Y., Golik, M., et al. (2016). Circadian control of oscillations in mitochondrial rate-limiting enzymes and nutrient utilization by PERIOD proteins. *Proc Natl Acad Sci U S A* 113, E1673-1682.
- Niswender, K.D., Morrison, C.D., Clegg, D.J., Olson, R., Baskin, D.G., Myers, M.G., Seeley, R.J., and Schwartz, M.W. (2003). Insulin activation of phosphatidylinositol 3-kinase in the hypothalamic arcuate nucleus - A key mediator of insulin-induced anorexia. *Diabetes* 52, 227-231.
- Nogueiras, R., Lopez, M., and Dieguez, C. (2009). Regulation of lipid metabolism by energy availability: a role for the central nervous system. *Obesity reviews : an official journal of the International Association for the Study of Obesity*.
- Nogueiras, R., Wiedmer, P., Perez-Tilve, D., Veyrat-Durebex, C., Keogh, J.M., Sutton, G.M., Pfluger, P.T., Castaneda, T.R., Neschen, S., Hofmann, S.M., et al. (2007). The central melanocortin system directly controls peripheral lipid metabolism. *J Clin Invest* 117, 3475-3488.
- Noland, R.C., Koves, T.R., Seiler, S.E., Lum, H., Lust, R.M., Ilkayeva, O., Stevens, R.D., Hegardt, F.G., and Muoio, D.M. (2009). Carnitine insufficiency caused by aging and overnutrition compromises mitochondrial performance and metabolic control. *J Biol Chem* 284, 22840-22852.
- O'Rahilly, S., and Farooqi, I.S. (2008). Human obesity: a heritable neurobehavioral disorder that is highly sensitive to environmental conditions. *Diabetes* 57, 2905-2910.
- Obici, S., Feng, Z., Arduini, A., Conti, R., and Rossetti, L. (2003). Inhibition of hypothalamic carnitine palmitoyltransferase-1 decreases food intake and glucose production. *Nature medicine* 9, 756-761.
- Obici, S., Feng, Z., Morgan, K., Stein, D., Karkanas, G., and Rossetti, L. (2002). Central administration of oleic acid inhibits glucose production and food intake. *Diabetes* 51, 271-275.
- Oomura, Y., Nakamura, T., Sugimori, M., and Yamada, Y. (1975). Effect of free fatty acid on the rat lateral hypothalamic neurons. *Physiol Behav* 14, 483-486.
- Oosterman, J.E., Kalsbeek, A., la Fleur, S.E., and Belsham, D.D. (2015). Impact of nutrients on circadian rhythmicity. *Am J Physiol Regul Integr Comp Physiol* 308, R337-350.
- Osborne, B., Bentley, N.L., Montgomery, M.K., and Turner, N. (2016). The role of mitochondrial sirtuins in health and disease. *Free Radic Biol Med* 100, 164-174.
- Padilla, S.L., Qiu, J., Soden, M.E., Sanz, E., Nestor, C.C., Barker, F.D., Quintana, A., Zweifel, L.S., Ronnekleiv, O.K., Kelly, M.J., et al. (2016). Agouti-related peptide neural circuits mediate adaptive behaviors in the starved state. *Nat Neurosci* 19, 734-741.
- Padwal, R., Leslie, W.D., Lix, L.M., and Majumdar, S.R. (2016). Relationship Among Body Fat Percentage, Body Mass Index, and All-Cause Mortality: A Cohort Study. *Ann Intern Med* 164, 532-541.
- Park, S., Komatsu, T., Kim, S.E., Tanaka, K., Hayashi, H., Mori, R., and Shimokawa, I. (2017). Neuropeptide Y resists excess loss of fat by lipolysis in calorie-restricted mice: a trait potential for the life-extending effect of calorie restriction. *Aging Cell* 16, 339-348.
- Patton, D.F., Katsuyama, A.M., Pavlovski, I., Michalik, M., Patterson, Z., Parfyonov, M., Smit, A.N., Marchant, E.G., Chung, S.H., Abizaid, A., et al. (2014). Circadian mechanisms of food anticipatory

- rhythms in rats fed once or twice daily: clock gene and endocrine correlates. *PLoS One* 9, e112451.
- Patton, D.F., and Mistlberger, R.E. (2013). Circadian adaptations to meal timing: neuroendocrine mechanisms. *Frontiers in neuroscience* 7, 185.
- Peek, C.B., Affinati, A.H., Ramsey, K.M., Kuo, H.Y., Yu, W., Sena, L.A., Ilkayeva, O., Marcheva, B., Kobayashi, Y., Omura, C., et al. (2013). Circadian clock NAD⁺ cycle drives mitochondrial oxidative metabolism in mice. *Science* 342, 1243417.
- Pietrocola, F., Galluzzi, L., Bravo-San Pedro, J.M., Madeo, F., and Kroemer, G. (2015). Acetyl Coenzyme A: A Central Metabolite and Second Messenger. *Cell Metabolism* 21, 805-821.
- Pocai, A., Lam, T.K., Obici, S., Gutierrez-Juarez, R., Muse, E.D., Arduini, A., and Rossetti, L. (2006). Restoration of hypothalamic lipid sensing normalizes energy and glucose homeostasis in overfed rats. *J Clin Invest* 116, 1081-1091.
- Pocai, A., Obici, S., Schwartz, G.J., and Rossetti, L. (2005). A brain-liver circuit regulates glucose homeostasis. *Cell Metab* 1, 53-61.
- Poplawski, M.M., Mastaitis, J.W., Yang, X.J., and Mobbs, C.V. (2010). Hypothalamic responses to fasting indicate metabolic reprogramming away from glycolysis toward lipid oxidation. *Endocrinology* 151, 5206-5217.
- Power, R.A., Hulver, M.W., Zhang, J.Y., Dubois, J., Marchand, R.M., Ilkayeva, O., Muoio, D.M., and Mynatt, R.L. (2007). Carnitine revisited: potential use as adjunctive treatment in diabetes. *Diabetologia* 50, 824-832.
- Pozo, M., Rodriguez-Rodriguez, R., Ramirez, S., Seoane-Collazo, P., Lopez, M., Serra, D., Herrero, L., and Casals, N. (2017). Hypothalamic Regulation of Liver and Muscle Nutrient Partitioning by Brain-Specific Carnitine Palmitoyltransferase 1C in Male Mice. *Endocrinology* 158, 2226-2238.
- Przyrembel, H. (1987). Therapy of mitochondrial disorders. *J Inherit Metab Dis* 10 Suppl 1, 129-146.
- Qi, Y., and Yang, Y. (2015). Hunger States Control the Directions of Synaptic Plasticity via Switching Cell Type-Specific Subunits of NMDA Receptors. *J Neurosci* 35, 13171-13182.
- Ramsay, R.R., and Zammit, V.A. (2004). Carnitine acyltransferases and their influence on CoA pools in health and disease. *Mol Aspects Med* 25, 475-493.
- Randle, P.J., Garland, P.B., Hales, C.N., and Newsholme, E.A. (1963). The glucose fatty-acid cycle. Its role in insulin sensitivity and the metabolic disturbances of diabetes mellitus. *Lancet* 1, 785-789.
- Rappsilber, J., Mann, M., and Ishihama, Y. (2007). Protocol for micro-purification, enrichment, pre-fractionation and storage of peptides for proteomics using StageTips. *Nature protocols* 2, 1896-1906.
- Rastogi, A., and Mintz, E.M. (2017). Neural correlates of food anticipatory activity in mice subjected to once- or twice-daily feeding periods. *Eur J Neurosci* 46, 2265-2275.
- Rebouche, C.J. (2004). Kinetics, pharmacokinetics, and regulation of L-carnitine and acetyl-L-carnitine metabolism. *Ann N Y Acad Sci* 1033, 30-41.
- Redman, L.M., Martin, C.K., Williamson, D.A., and Ravussin, E. (2008). Effect of caloric restriction in non-obese humans on physiological, psychological and behavioral outcomes. *Physiol Behav* 94, 643-648.
- Reichenbach, A., Stark, R., Denis, R.R.G., Mequinion, M., Goularte, J.F., Clarke, R.E., Lockie, S.H., Kowalski, G.M., Bruce, C.R., Huang, C., et al. (2018). AgRP neurons require carnitine acetyltransferase (CRAT) to regulate metabolic flexibility and peripheral nutrient partitioning *Cell reports* 22, 1745-1759.
- Rosen, E.D., and Spiegelman, B.M. (2014). What we talk about when we talk about fat. *Cell* 156, 20-44.
- Ruan, H.B., Dietrich, M.O., Liu, Z.W., Zimmer, M.R., Li, M.D., Singh, J.P., Zhang, K., Yin, R., Wu, J., Horvath, T.L., et al. (2014). O-GlcNAc transferase enables AgRP neurons to suppress browning of white fat. *Cell* 159, 306-317.

- Samuel, V.T., and Shulman, G.I. (2016). The pathogenesis of insulin resistance: integrating signaling pathways and substrate flux. *Journal of Clinical Investigation* 126, 12-22.
- Scafidi, S., Fiskum, G., Lindauer, S.L., Bamford, P., Shi, D., Hopkins, I., and McKenna, M.C. (2010). Metabolism of acetyl-L-carnitine for energy and neurotransmitter synthesis in the immature rat brain. *J Neurochem* 114, 820-831.
- Schotz, M.C., Scanu, A., and Page, I.H. (1957). Effect of Triton on Lipoprotein Lipase of Rat Plasma. *American Journal of Physiology* 188, 399-402.
- Schrepfer, E., and Scorrano, L. (2016). Mitofusins, from Mitochondria to Metabolism. *Mol Cell* 61, 683-694.
- Schwartz, M.W., Erickson, J.C., Baskin, D.G., and Palmiter, R.D. (1998). Effect of fasting and leptin deficiency on hypothalamic neuropeptide Y gene transcription in vivo revealed by expression of a lacZ reporter gene. *Endocrinology* 139, 2629-2635.
- Seiler, S.E., Koves, T.R., Gooding, J.R., Wong, K.E., Stevens, R.D., Ilkayeva, O.R., Wittmann, A.H., DeBalsi, K.L., Davies, M.N., Lindeboom, L., et al. (2015). Carnitine Acetyltransferase Mitigates Metabolic Inertia and Muscle Fatigue during Exercise. *Cell Metab* 22, 65-76.
- Seiler, S.E., Martin, O.J., Noland, R.C., Slentz, D.H., DeBalsi, K.L., Ilkayeva, O.R., An, J., Newgard, C.B., Koves, T.R., and Muoio, D.M. (2014). Obesity and lipid stress inhibit carnitine acetyltransferase activity. *J Lipid Res* 55, 635-644.
- Shadel, G.S., and Horvath, T.L. (2015). Mitochondrial ROS signaling in organismal homeostasis. *Cell* 163, 560-569.
- Shamsi, N.A., Salkeld, M.D., Rattanaray, L., Voultios, A., Varcoe, T.J., Boden, M.J., and Kennaway, D.J. (2014). Metabolic consequences of timed feeding in mice. *Physiol Behav* 128, 188-201.
- Sharma, S., and Black, S.M. (2009). Carnitine Homeostasis, Mitochondrial Function, and Cardiovascular Disease. *Drug discovery today. Disease mechanisms* 6, e31-e39.
- Sharma, S., Sun, X., Agarwal, S., Rafikov, R., Dasarathy, S., Kumar, S., and Black, S.M. (2012). Role of carnitine acetyl transferase in regulation of nitric oxide signaling in pulmonary arterial endothelial cells. *International journal of molecular sciences* 14, 255-272.
- Sharma, V., Mustafa, S., Patel, N., Wambolt, R., Allard, M.F., and McNeill, J.H. (2009). Stimulation of cardiac fatty acid oxidation by leptin is mediated by a nitric oxide-p38 MAPK-dependent mechanism. *Eur J Pharmacol* 617, 113-117.
- Sharpe, M.J., Marchant, N.J., Whitaker, L.R., Richie, C.T., Zhang, Y.J., Campbell, E.J., Koivula, P.P., Necarsulmer, J.C., Mejias-Aponte, C., Morales, M., et al. (2017). Lateral Hypothalamic GABAergic Neurons Encode Reward Predictions that Are Relayed to the Ventral Tegmental Area to Regulate Learning. *Curr Biol* 27, 2089-2100 e2085.
- Shi, Y.C., Lau, J., Lin, Z., Zhang, H., Zhai, L., Sperk, G., Heilbronn, R., Mietzsch, M., Weger, S., Huang, X.F., et al. (2013). Arcuate NPY controls sympathetic output and BAT function via a relay of tyrosine hydroxylase neurons in the PVN. *Cell Metab* 17, 236-248.
- Shi, Z., Madden, C.J., and Brooks, V.L. (2017). Arcuate neuropeptide Y inhibits sympathetic nerve activity via multiple neuropathways. *J Clin Invest* 127, 2868-2880.
- Simon, J.J., Wetzel, A., Sinno, M.H., Skunde, M., Bendszus, M., Preissl, H., Enck, P., Herzog, W., and Friederich, H.C. (2017). Integration of homeostatic signaling and food reward processing in the human brain. *JCI Insight* 2.
- Skibicka, K.P., Hansson, C., Alvarez-Crespo, M., Friberg, P.A., and Dickson, S.L. (2011). Ghrelin directly targets the ventral tegmental area to increase food motivation. *Neuroscience* 180, 129-137.
- Skibicka, K.P., Shirazi, R.H., Hansson, C., and Dickson, S.L. (2012). Ghrelin interacts with neuropeptide Y Y1 and opioid receptors to increase food reward. *Endocrinology* 153, 1194-1205.

- Smeland, O.B., Meisingset, T.W., Borges, K., and Sonnewald, U. (2012). Chronic acetyl-L-carnitine alters brain energy metabolism and increases noradrenaline and serotonin content in healthy mice. *Neurochem Int* 61, 100-107.
- Smith, G.P., and Epstein, A.N. (1969). Increased feeding in response to decreased glucose utilization in the rat and monkey. *Am J Physiol* 217, 1083-1087.
- Soare, A., Cangemi, R., Omodei, D., Holloszy, J.O., and Fontana, L. (2011). Long-term calorie restriction, but not endurance exercise, lowers core body temperature in humans. *Aging (Albany NY)* 3, 374-379.
- Soriano, F.X., Liesa, M., Bach, D., Chan, D.C., Palacin, M., and Zorzano, A. (2006). Evidence for a mitochondrial regulatory pathway defined by peroxisome proliferator-activated receptor-gamma coactivator-1 alpha, estrogen-related receptor-alpha, and mitofusin 2. *Diabetes* 55, 1783-1791.
- St-Pierre, J., Drori, S., Uldry, M., Silvaggi, J.M., Rhee, J., Jager, S., Handschin, C., Zheng, K., Lin, J., Yang, W., et al. (2006). Suppression of reactive oxygen species and neurodegeneration by the PGC-1 transcriptional coactivators. *Cell* 127, 397-408.
- Stark, R., Reichenbach, A., and Andrews, Z.B. (2015a). Hypothalamic carnitine metabolism integrates nutrient and hormonal feedback to regulate energy homeostasis. *Mol Cell Endocrinol* 418 Pt 1, 9-16.
- Stark, R., Reichenbach, A., Lockie, S.H., Pracht, C., Wu, Q., Tups, A., and Andrews, Z.B. (2015b). Acyl ghrelin acts in the brain to control liver function and peripheral glucose homeostasis in male mice. *Endocrinology* 156, 858-868.
- Stauffer, W.R., Lak, A., Kobayashi, S., and Schultz, W. (2016). Components and characteristics of the dopamine reward utility signal. *J Comp Neurol* 524, 1699-1711.
- Steculorum, S.M., Ruud, J., Karakasilioti, I., Backes, H., Engstrom Ruud, L., Timper, K., Hess, M.E., Tsaousidou, E., Mauer, J., Vogt, M.C., et al. (2016). AgRP Neurons Control Systemic Insulin Sensitivity via Myostatin Expression in Brown Adipose Tissue. *Cell* 165, 125-138.
- Steiber, A., Kerner, J., and Hoppel, C.L. (2004). Carnitine: a nutritional, biosynthetic, and functional perspective. *Mol Aspects Med* 25, 455-473.
- Stephan, F.K., and Davidson, A.J. (1998). Glucose, but not fat, phase shifts the feeding-entrained circadian clock. *Physiol Behav* 65, 277-288.
- Stern, J.H., Rutkowski, J.M., and Scherer, P.E. (2016). Adiponectin, Leptin, and Fatty Acids in the Maintenance of Metabolic Homeostasis through Adipose Tissue Crosstalk. *Cell Metab* 23, 770-784.
- Stolarczyk, E., Guissard, C., Michau, A., Even, P.C., Grosfeld, A., Serradas, P., Lorsignol, A., Penicaud, L., Brot-Laroche, E., Leturque, A., et al. (2010). Detection of extracellular glucose by GLUT2 contributes to hypothalamic control of food intake. *Am J Physiol Endocrinol Metab* 298, E1078-1087.
- Storozhevskiy, T.P., Senilova, Y.E., Persiyantseva, N.A., Pinelis, V.G., and Pomytkin, I.A. (2007). Mitochondrial respiratory chain is involved in insulin-stimulated hydrogen peroxide production and plays an integral role in insulin receptor autophosphorylation in neurons. *BMC Neurosci* 8, 84.
- Su, Z., Alhadeff, A.L., and Betley, J.N. (2017). Nutritive, Post-ingestive Signals Are the Primary Regulators of AgRP Neuron Activity. *Cell reports* 21, 2724-2736.
- Sun, X., Veldhuizen, M.G., Wray, A.E., de Araujo, I.E., Sherwin, R.S., Sinha, R., and Small, D.M. (2014). The neural signature of satiation is associated with ghrelin response and triglyceride metabolism. *Physiol Behav* 136, 63-73.
- Szklarczyk, D., Franceschini, A., Wyder, S., Forslund, K., Heller, D., Huerta-Cepas, J., Simonovic, M., Roth, A., Santos, A., Tsafou, K.P., et al. (2015). STRING v10: protein-protein interaction networks, integrated over the tree of life. *Nucleic acids research* 43, D447-452.

- Taib, B., Bouyakdan, K., Hryhorczuk, C., Rodaros, D., Fulton, S., and Alquier, T. (2013). Glucose regulates hypothalamic long-chain fatty acid metabolism via AMP-activated kinase (AMPK) in neurons and astrocytes. *J Biol Chem* 288, 37216-37229.
- Tamai, I., Ohashi, R., Nezu, J., Yabuuchi, H., Oku, A., Shimane, M., Sai, Y., and Tsuji, A. (1998). Molecular and functional identification of sodium ion-dependent, high affinity human carnitine transporter OCTN2. *J Biol Chem* 273, 20378-20382.
- Tan, K., Knight, Z.A., and Friedman, J.M. (2014). Ablation of AgRP neurons impairs adaption to restricted feeding. *Molecular metabolism* 3, 694-704.
- Tang, S., Xu, S., Lu, X., Gullapalli, R.P., McKenna, M.C., and Waddell, J. (2016). Neuroprotective Effects of Acetyl-L-Carnitine on Neonatal Hypoxia Ischemia-Induced Brain Injury in Rats. *Dev Neurosci* 38, 384-396.
- Tellez, L.A., Han, W., Zhang, X., Ferreira, T.L., Perez, I.O., Shammah-Lagnado, S.J., van den Pol, A.N., and de Araujo, I.E. (2016). Separate circuitries encode the hedonic and nutritional values of sugar. *Nat Neurosci* 19, 465-470.
- Thirupathi, A., and de Souza, C.T. (2017). Multi-regulatory network of ROS: the interconnection of ROS, PGC-1 alpha, and AMPK-SIRT1 during exercise. *J Physiol Biochem* 73, 487-494.
- Thomas, J.M., Higgs, S., Dourish, C.T., Hansen, P.C., Harmer, C.J., and McCabe, C. (2015). Satiation attenuates BOLD activity in brain regions involved in reward and increases activity in dorsolateral prefrontal cortex: an fMRI study in healthy volunteers. *Am J Clin Nutr* 101, 697-704.
- Toda, C., Kim, J.D., Impellizzeri, D., Cuzzocrea, S., Liu, Z.W., and Diano, S. (2016). UCP2 Regulates Mitochondrial Fission and Ventromedial Nucleus Control of Glucose Responsiveness. *Cell* 164, 872-883.
- Tong, Q., Ye, C.P., Jones, J.E., Elmquist, J.K., and Lowell, B.B. (2008). Synaptic release of GABA by AgRP neurons is required for normal regulation of energy balance. *Nat Neurosci*.
- Tyanova, S., Temu, T., Sinitcyn, P., Carlson, A., Hein, M.Y., Geiger, T., Mann, M., and Cox, J. (2016). The Perseus computational platform for comprehensive analysis of (prote)omics data. *Nature methods* 13, 731-740.
- Uner, A., Goncalves, G.H., Li, W., Porceban, M., Caron, N., Schonke, M., Delpire, E., Sakimura, K., and Bjorbaek, C. (2015). The role of GluN2A and GluN2B NMDA receptor subunits in AgRP and POMC neurons on body weight and glucose homeostasis. *Molecular metabolism* 4, 678-691.
- Vaanholt, L.M., Mitchell, S.E., Sinclair, R.E., and Speakman, J.R. (2015). Mice that are resistant to diet-induced weight loss have greater food anticipatory activity and altered melanocortin-3 receptor (MC3R) and dopamine receptor 2 (D2) gene expression. *Horm Behav* 73, 83-93.
- van de Wall, E., Leshan, R., Xu, A.W., Balthasar, N., Coppari, R., Liu, S.M., Jo, Y.H., MacKenzie, R.G., Allison, D.B., Dun, N.J., et al. (2008). Collective and individual functions of leptin receptor modulated neurons controlling metabolism and ingestion. *Endocrinology* 149, 1773-1785.
- van den Top, M., Lyons, D.J., Lee, K., Coderre, E., Renaud, L.P., and Spanswick, D. (2007). Pharmacological and molecular characterization of ATP-sensitive K(+) conductances in CART and NPY/AgRP expressing neurons of the hypothalamic arcuate nucleus. *Neuroscience* 144, 815-824.
- Verhagen, L.A., Luijendijk, M.C., de Groot, J.W., van Dommelen, L.P., Klimstra, A.G., Adan, R.A., and Roeling, T.A. (2011). Anticipation of meals during restricted feeding increases activity in the hypothalamus in rats. *Eur J Neurosci* 34, 1485-1491.
- Verma, D., Wood, J., Lach, G., Herzog, H., Sperk, G., and Tasan, R. (2016). Hunger Promotes Fear Extinction by Activation of an Amygdala Microcircuit. *Neuropsychopharmacology* 41, 431-439.
- Wang, Q., Liu, C., Uchida, A., Chuang, J.C., Walker, A., Liu, T., Osborne-Lawrence, S., Mason, B.L., Mosher, C., Berglund, E.D., et al. (2014). Arcuate AgRP neurons mediate orexigenic and glucoregulatory actions of ghrelin. *Molecular metabolism* 3, 64-72.

- Wang, R., Cruciani-Guglielmacci, C., Migrenne, S., Magnan, C., Cotero, V.E., and Routh, V.H. (2006). Effects of oleic acid on distinct populations of neurons in the hypothalamic arcuate nucleus are dependent on extracellular glucose levels. *Journal of neurophysiology* 95, 1491-1498.
- Wang, S.S., Denk, W., and Hausser, M. (2000). Coincidence detection in single dendritic spines mediated by calcium release. *Nat Neurosci* 3, 1266-1273.
- Weise, C.M., Thiyyagura, P., Reiman, E.M., Chen, K., and Krakoff, J. (2015). A potential role for the midbrain in integrating fat-free mass determined energy needs: An H₂ (15) O PET study. *Hum Brain Mapp* 36, 2406-2415.
- West, K.S., and Roseberry, A.G. (2017). Neuropeptide-Y alters VTA dopamine neuron activity through both pre- and postsynaptic mechanisms. *Journal of neurophysiology* 118, 625-633.
- Whittemore, L.A., Song, K., Li, X., Aghajanian, J., Davies, M., Girgenrath, S., Hill, J.J., Jalenak, M., Kelley, P., Knight, A., et al. (2003). Inhibition of myostatin in adult mice increases skeletal muscle mass and strength. *Biochem Biophys Res Commun* 300, 965-971.
- Wiater, M.F., Li, A.J., Dinh, T.T., Jansen, H.T., and Ritter, S. (2013). Leptin-sensitive neurons in the arcuate nucleus integrate activity and temperature circadian rhythms and anticipatory responses to food restriction. *Am J Physiol Regul Integr Comp Physiol* 305, R949-960.
- Wiater, M.F., Mukherjee, S., Li, A.J., Dinh, T.T., Rooney, E.M., Simasko, S.M., and Ritter, S. (2011). Circadian integration of sleep-wake and feeding requires NPY receptor-expressing neurons in the mediobasal hypothalamus. *Am J Physiol Regul Integr Comp Physiol* 301, R1569-1583.
- Wortley, K.E., Anderson, K.D., Garcia, K., Murray, J.D., Malinova, L., Liu, R., Moncrieffe, M., Thabet, K., Cox, H.J., Yancopoulos, G.D., et al. (2004). Genetic deletion of ghrelin does not decrease food intake but influences metabolic fuel preference. *Proc Natl Acad Sci U S A* 101, 8227-8232.
- Wortman, M.D., Clegg, D.J., D'Alessio, D., Woods, S.C., and Seeley, R.J. (2003). C75 inhibits food intake by increasing CNS glucose metabolism. *Nat Med* 9, 483-485.
- Wu, C.S., Bongmba, O.Y.N., Yue, J., Lee, J.H., Lin, L., Saito, K., Pradhan, G., Li, D.P., Pan, H.L., Xu, A., et al. (2017). Suppression of GHS-R in AgRP Neurons Mitigates Diet-Induced Obesity by Activating Thermogenesis. *International journal of molecular sciences* 18.
- Wu, Q., Boyle, M.P., and Palmiter, R.D. (2009). Loss of GABAergic signaling by AgRP neurons to the parabrachial nucleus leads to starvation. *Cell* 137, 1225-1234.
- Wu, Q., Lemus, M.B., Stark, R., Bayliss, J.A., Reichenbach, A., Lockie, S.H., and Andrews, Z.B. (2014). The temporal pattern of cfos activation in hypothalamic, cortical, and brainstem nuclei in response to fasting and refeeding in male mice. *Endocrinology* 155, 840-853.
- Xie, Z., Zhang, J., Wu, J., Viollet, B., and Zou, M.H. (2008). Upregulation of mitochondrial uncoupling protein-2 by the AMP-activated protein kinase in endothelial cells attenuates oxidative stress in diabetes. *Diabetes* 57, 3222-3230.
- Yang, Y., Atasoy, D., Su, H.H., and Sternson, S.M. (2011). Hunger states switch a flip-flop memory circuit via a synaptic AMPK-dependent positive feedback loop. *Cell* 146, 992-1003.
- Yasumoto, Y., Hashimoto, C., Nakao, R., Yamazaki, H., Hiroyama, H., Nemoto, T., Yamamoto, S., Sakurai, M., Oike, H., Wada, N., et al. (2016). Short-term feeding at the wrong time is sufficient to desynchronize peripheral clocks and induce obesity with hyperphagia, physical inactivity and metabolic disorders in mice. *Metabolism* 65, 714-727.
- Yavari, A., Stocker, C.J., Ghaffari, S., Wargent, E.T., Steeples, V., Czibik, G., Pinter, K., Bellahcene, M., Woods, A., Martinez de Morentin, P.B., et al. (2016). Chronic Activation of gamma2 AMPK Induces Obesity and Reduces beta Cell Function. *Cell Metab* 23, 821-836.
- Yoshihara, T., Honma, S., and Honma, K. (1996). Effects of restricted daily feeding on neuropeptide Y release in the rat paraventricular nucleus. *Am J Physiol* 270, E589-595.
- Youle, R.J., and van der Bliek, A.M. (2012). Mitochondrial fission, fusion, and stress. *Science* 337, 1062-1065.

Zhou, L., Yueh, C.Y., Lam, D.D., Shaw, J., Osundiji, M., Garfield, A.S., Evans, M., and Heisler, L.K. (2011). Glucokinase inhibitor glucosamine stimulates feeding and activates hypothalamic neuropeptide Y and orexin neurons. *Behav Brain Res* 222, 274-278.

Zwighaft, Z., Aviram, R., Shalev, M., Rousso-Noori, L., Kraut-Cohen, J., Golik, M., Brandis, A., Reinke, H., Aharoni, A., Kahana, C., et al. (2015). Circadian Clock Control by Polyamine Levels through a Mechanism that Declines with Age. *Cell Metab* 22, 874-885.

Appendix

Table 2 Primer Sequences

gene	forward primer	reverse primer	Accession number
18S Ribosomal RNA (18S)	TTCCGATAACGAACGAGACTCT	TGGCTGAACGCCACTTGTC	NR_003278.3
Carnitine acetyltransferase (CRAT)	TCCCCAAGTCCGAGAAGCTA	GGCTGACACGGAGAAGTTGA	NM_007760.3
neuropeptide Y (NPY)	CCGCCACGATGCTAGGTAAC	CAGCCAGAATGCCCAAACAC	NM_023456.2
agouti related protein (AgRP)	AAGTCTGAATGGCCTCAAGAAGA	GACTCGTGCAGCCTTACACAG	NM_007427.2
pro-opiomelanocortin-alpha (POMC)	GCGACGGAAGAGAAAAGAGGT	ATTGGAGGGACCCCTGTCTG	NM_008895.3
glial fibrillary acidic protein, transcript variant 1 (GFAP)	CGTTAAGCTAGCCCTGGACA	GGTGAGCCTGTATTGGGACAA	NM_001131020.1
Phosphoenolpyruvate Carboxykinase 1 (cytosol) (Pck1)	TGCCCAAGGCAACTTAAGGG	CAGTAAACACCCCCATCGCT	NM_011044.2
Phosphoenolpyruvate Carboxykinase 2 (mitochondrial) (Pck2)	GTACCACTGGTGTACGAGGC	GTCTTTCCTTTGTGCTCCGC	NM_028994.2
glucose-6-phosphatase, catalytic (G6p)	AGTCTTGTGTCAGGCATTGCTGT	AAAGTCCACAGGAGGTCCAC	NM_008061.3
glyceraldehyde-3-phosphate dehydrogenase (Gapdh)	TCAAGCTCATTTCCTGGTATGACA	TCTTGCTCAGTGTCTTGCT	NM_008084.2
glycogen synthase kinase 3 beta (Gsk3b)	GCCAGACACTATAGTCGAGCC	GACCAGCTGCTTTGCACTTC	NM_019827.6
glycogen phosphorylase, liver (Pygl)	AAGAAGGGGTATGAGGCCAAA	GACACTTGACATAGGCTTCGT	NM_133198.2
interleukin 6 (IL6)	GTG GCT AAG GAC CAA GAC CA	TAA CGC ACT AGG TTT GCC GA	NM_031168.2
Fatty acid synthase (Fasn)	TGGGTGTGGAAGTTCGTCAG	CTGTCGTGTCAGTAGCCGAG	NM_007988.3
Stearoyl-Coenzyme A desaturase 1 (Scd1)	GAACACCCATCCCGAGAGTC	GAACTGGAGATCTCTTGAGCA	NM_009127.4
Lipoprotein Lipase (Lpl)	AGAAGTCTGGCTGACACTGGA	AACCCACTTTCAAACACCCAAA	NM_008509.2

gene	forward primer	reverse primer	Accession number
Adipose triglyceride lipase (Atgl)	AGAGCCCATGGTCCTCCGA	AGCAAAGGGTTGGGTTGGTT	NM_001163689.1
carnitine palmitoyltransferase 1a (Cpt1a)	ATCGCTTTGGGAGTCCACAT	CCATCGTTAAGGCACTGGGT	NM_013495.2
Glycerol kinase, transcript variant 1 (Gk)	GCAACCAGAGGGAAACCACA	TAGGTCAAGCCACACCACG	NM_008194.3
Protein kinase A (Pka) (Prkaca)	AGATCGTCCTGACCTTTGAGT	GGCAAACCGAAGTCTGTCAC	NM_008854.6
Phosphoglycolate Phosphatase (Pgp)	TCACTTTCCTGATTGCTCTTCA	CTGGACACAGACATCCTCCTG	NM_025954.3
CD36 antigen, transcript variant 1 (Cd36)	GATGAATGGTTGAGACCCCGT	ACATTTCAGAAGGCAGCAACTT	NM_001159558.1
Insulin receptor (Insr)	CGAGTGCCCGTCTGGCTATA	GGCAGGGTCCCAGACATG	
glycogen phosphorylase, muscle (Pym)	GCCGGAGTGGAAAATGTGTC	AGTAGATCCTCTTGGGGTCCTT	NM_011224.1
Carnitine palmitoyltransferase 1b (Cpt1b)	TGGCTACGGGGTCTCTTACA	GGGCGTTCGTCTCTGAACTT	NM_009948.2
citrate synthase (Cs)	TGTAGCTCTCTCCCTTCGGT	ACGAGGCAGGATGAGTTCTTG	NM_026444.3
Glucose Transporter 4 (Glut4)	CCTTTCTCATTGGCATCATTTTC	CACGGCCAAGACATTGTTG	NM_009204.2

Table 3 MSprotein_enrichment_KOvsWT_fed.

All proteins in the spreadsheet are significantly different between genotypes. Proteins highlighted in blue are listed as 2-fold higher, whereas those highlighted in yellow are listed as 2-fold lower expression, in KO mice relative to WT mice.

N: -Log Student's T-test p-value KO_FED_WT_FED	N: Student's T-test Difference KO_FED_WT_FED	N: Student's T-test Test statistic KO_FED_WT_FED	T: Protein IDs	T: Majority protein IDs	T: Protein names	T: Gene names
1.64971	4.89617	6.56841	Q8BJY1	Q8BJY1	26S proteasome non-ATPase regulatory subunit 5	Psm5
1.84731	3.63549	8.29826	Q9CQ75	Q9CQ75	NADH dehydrogenase [ubiquinone] 1 alpha subcomplex subunit 2	Ndufa2
2.86611	3.44551	27.0776	P84075	P84075	Neuron-specific calcium-binding protein hippocalcin	Hpca
2.2602	2.22331	13.4371	P60521	P60521	Gamma-aminobutyric acid receptor-associated protein-like 2	Gabarapl2
1.83596	2.03445	8.18813	Q91WK5	Q91WK5	Glycine cleavage system H protein, mitochondrial	Gcsh
1.48208	1.78893	5.37148	Q61036	Q61036	Serine/threonine-protein kinase PAK 3	Pak3
1.52009	1.40492	5.62383	Q922D8	Q922D8	C-1-tetrahydrofolate synthase, cytoplasmic;Methylenetetrahydrofolate dehydrogenase;Methenyltetrahydrofolate cyclohydrolase;Formyltetrahydrofolate synthetase;C-1-tetrahydrofolate synthase, cytoplasmic, N-terminally processed	Mthfd1
1.41776	0.8594	4.96763	P02088;P02089;P02104	P02088;P02089	Hemoglobin subunit beta-1;Hemoglobin subunit beta-2	Hbb-b1, Hbb-b2
1.56383	0.775357	5.92756	Q61016	Q61016	Guanine nucleotide-binding protein G(I)/G(S)/G(O) subunit gamma-7	Gng7
1.46085	0.348897	5.23502	Q9WU78	Q9WU78	Programmed cell death 6-interacting protein	Pdcd6ip
1.38209	0.29401	4.75551	P24472	P24472	Glutathione S-transferase A4	Gsta4
1.92625	0.255625	9.1041	P16125	P16125	L-lactate dehydrogenase B chain	Ldhb

N: -Log Student's T-test p-value KO_FED_WT_FED	N: Student's T-test Difference KO_FED_WT_FED	N: Student's T-test Test statistic KO_FED_WT_FED	T: Protein IDs	T: Majority protein IDs	T: Protein names	T: Gene names
2.14869	0.244333	11.8038	P14094	P14094	Sodium/potassium-transporting ATPase subunit beta-1	Atp1b1
2.20896	0.219357	12.6608	Q9CQJ8	Q9CQJ8	NADH dehydrogenase [ubiquinone] 1 beta subcomplex subunit 9	Ndufb9
1.34559	0.196001	4.54672	P24527	P24527	Leukotriene A-4 hydrolase	Lta4h
1.83099	0.148111	8.14038	P05063	P05063	Fructose-bisphosphate aldolase C	Aldoc
2.01122	0.128487	10.0558	Q922E4	Q922E4	Ethanolamine-phosphate cytidyltransferase	Pcyt2
1.45915	0.126523	5.22426	P62761	P62761	Visinin-like protein 1	Vsnl1
1.38415	0.11665	4.76753	O08749	O08749	Dihydrolipoyl dehydrogenase, mitochondrial	Dld
1.58341	0.084197	6.06836	Q91YT0	Q91YT0	NADH dehydrogenase [ubiquinone] flavoprotein 1, mitochondrial	Ndufv1
1.7049	0.0493698	7.01371	Q62465	Q62465	Synaptic vesicle membrane protein VAT-1 homolog	Vat1
1.96603	-0.147323	-9.53825	Q6P1B1	Q6P1B1	Xaa-Pro aminopeptidase 1	Xpnpep1
1.46471	-0.151314	-5.25961	Q9R0X4;Q32 MW3	Q9R0X4	Acyl-coenzyme A thioesterase 9, mitochondrial	Acot9
1.31189	-0.279612	-4.36109	Q8VBV7	Q8VBV7	COP9 signalosome complex subunit 8	Cops8
1.50091	-0.36514	-5.49519	P68369;P0521 4	P68369;P05214	Tubulin alpha-1A chain;Tubulin alpha-3 chain	Tuba1a, Tuba3a
1.45174	-0.372433	-5.17744	P11983	P11983	T-complex protein 1 subunit alpha	Tcp1
1.66491	-0.516349	-6.68834	Q9CQF9	Q9CQF9	Prenylcysteine oxidase	Pcyox1
2.06757	-0.871495	-10.7395	Q8VE62	Q8VE62	Polyadenylate-binding protein-interacting protein 1	Paip1
1.56746	-0.918902	-5.95349	Q6P8X1;Q80Z J7	Q6P8X1	Sorting nexin-6;Sorting nexin-6, N-terminally processed	Snx6

N: -Log Student's T-test p-value KO_FED_WT_FED	N: Student's T-test Difference KO_FED_WT_FED	N: Student's T-test Test statistic KO_FED_WT_FED	T: Protein IDs	T: Majority protein IDs	T: Protein names	T: Gene names
1.36163	-1.16919	-4.63743	Q8K212	Q8K212	Phosphofurin acidic cluster sorting protein 1	Pacs1
1.48776	-1.27025	-5.40856	P50171	P50171	Estradiol 17-beta-dehydrogenase 8	Hsd17b8
1.40369	-3.80369	-4.88296	O08547	O08547	Vesicle-trafficking protein SEC22b	Sec22b

Table 4 MSprotein_enrichment_KOvsWT_fast.

All proteins in the spreadsheet are significantly different between genotypes. Proteins highlighted in blue are listed as 2-fold higher, whereas those highlighted in yellow are listed as 2-fold lower expression, in KO mice relative to WT mice.

N: -Log Student's T-test p-value KO_FAST_WT_F AST	N: Student's T-test Difference KO_FAST_WT_F AST	N: Student's T-test Test statistic KO_FAST_WT_F FAST	T: Protein IDs	T: Majority protein IDs	T: Protein names	T: Gene names
3.30532	4.15586	10.3325	P50114	P50114	Protein S100-B	S100b
3.61296	3.97788	12.3915	P99028	P99028	Cytochrome b-c1 complex subunit 6, mitochondrial	Uqcrh
3.10259	3.61365	9.15679	P46096;Q9R0 N5	P46096	Synaptotagmin-1	Syt1
4.69247	3.5893	23.2445	Q61644	Q61644	Protein kinase C and casein kinase substrate in neurons protein 1	Pacsin1
3.02987	3.35616	8.76626	Q9D172	Q9D172	ES1 protein homolog, mitochondrial	D10Jhu81 e
2.75524	3.18188	7.42426	P62897;CON_ _P62894;P000 15	P62897	Cytochrome c, somatic	Cycs
4.39127	2.95861	19.5194	Q6ZQ38	Q6ZQ38	Cullin-associated NEDD8-dissociated protein 1	Cand1

N: -Log Student's T-test p-value KO_FAST_WT_F AST	N: Student's T-test Difference KO_FAST_WT_F AST	N: Student's T-test Test statistic KO_FAST_WT_F FAST	T: Protein IDs	T: Majority protein IDs	T: Protein names	T: Gene names
3.55699	2.92956	11.9899	Q80TB8	Q80TB8	Synaptic vesicle membrane protein VAT-1 homolog-like	Vat1l
2.48587	2.87423	6.28831	O08585	O08585	Clathrin light chain A	Clta
3.05857	2.78865	8.91853	Q62048	Q62048	Astrocytic phosphoprotein PEA-15	Pea15
2.35209	2.68482	5.78176	P56564	P56564	Excitatory amino acid transporter 1	Slc1a3
2.39065	2.66007	5.92414	P12367	P12367	cAMP-dependent protein kinase type II-alpha regulatory subunit	Prkar2a
5.07077	2.54981	28.9313	Q9CPU0	Q9CPU0	Lactoylglutathione lyase	Glo1
2.29381	2.46829	5.57193	Q9QXS1	Q9QXS1	Plectin	Plec
2.66089	2.45244	7.00756	P63141;P1638 8;P16390;Q61 923;Q61762;Q 61423	P63141;P1 6388;P163 90	Potassium voltage-gated channel subfamily A member 2;Potassium voltage-gated channel subfamily A member 1;Potassium voltage-gated channel subfamily A member 3	Kcna2, Kcna1, Kcna3
2.94925	2.44562	8.35118	Q9DCS9	Q9DCS9	NADH dehydrogenase [ubiquinone] 1 beta subcomplex subunit 10	Ndufb10
4.69933	2.43859	23.337	Q9WUA3	Q9WUA3	ATP-dependent 6-phosphofructokinase, platelet type	Pfkip
2.65815	2.36011	6.99575	Q9CQI6	Q9CQI6	Coactosin-like protein	Cotl1
2.9695	2.32571	8.45368	O88935	O88935	Synapsin-1	Syn1
2.86588	2.29326	7.94077	Q9R0K7	Q9R0K7	Plasma membrane calcium-transporting ATPase 2	Atp2b2
3.40207	2.20442	10.9422	P63011	P63011	Ras-related protein Rab-3A	Rab3a
2.9485	2.17159	8.34737	Q9Z1S5	Q9Z1S5	Neuronal-specific septin-3	Sep3
2.63799	2.15928	6.90957	P61164	P61164	Alpha-centractin	Actr1a
3.47452	2.13019	11.4209	Q99104;P212 71	Q99104	Unconventional myosin-Va	Myo5a
3.38556	2.00745	10.8358	Q91ZZ3	Q91ZZ3	Beta-synuclein	Sncb
2.26006	1.93742	5.45325	P68404	P68404	Protein kinase C beta type	Prkcb

N: -Log Student's T-test p-value KO_FAST_WT_F AST	N: Student's T-test Difference KO_FAST_WT_F AST	N: Student's T-test Test statistic KO_FAST_WT_F AST	T: Protein IDs	T: Majority protein IDs	T: Protein names	T: Gene names
2.1082	1.93071	4.94395	Q8BPN8	Q8BPN8	DmX-like protein 2	Dmxl2
2.06056	1.91764	4.79208	Q64521	Q64521	Glycerol-3-phosphate dehydrogenase, mitochondrial	Gpd2
2.92008	1.91634	8.20545	P48318	P48318	Glutamate decarboxylase 1	Gad1
2.1167	1.89213	4.97146	Q9D855	Q9D855	Cytochrome b-c1 complex subunit 7	Uqcrb
2.516	1.88258	6.40738	Q8K596	Q8K596		Slc8a2
2.87815	1.86706	8.00001	Q3THE2;Q9C Q19	Q3THE2	Myosin regulatory light chain 12B	Myl12b
2.56978	1.86457	6.62475	Q80TJ1;Q8BY R5	Q80TJ1	Calcium-dependent secretion activator 1	Cadps
2.08319	1.85341	4.86377	Q9Z1G4	Q9Z1G4	V-type proton ATPase 116 kDa subunit a isoform 1	Atp6v0a1
3.75376	1.84364	13.4593	O08599	O08599	Syntaxin-binding protein 1	Stxbp1
2.54023	1.81688	6.50456	Q8CHC4	Q8CHC4	Synaptojanin-1	Synj1
2.78984	1.77291	7.58244	Q64332	Q64332	Synapsin-2	Syn2
2.40723	1.72577	5.98623	Q6IRU5	Q6IRU5	Clathrin light chain B	Cltb
2.68461	1.72044	7.11033	Q9QZ06	Q9QZ06	Toll-interacting protein	Tollip
2.56169	1.69107	6.59167	Q8K1M6	Q8K1M6	Dynamin-1-like protein	Dnm1l
2.19947	1.68358	5.24532	O55143;Q8R4 29;Q64518	O55143	Sarcoplasmic/endoplasmic reticulum calcium ATPase 2	Atp2a2
2.05425	1.67121	4.77222	Q6PHZ2	Q6PHZ2	Calcium/calmodulin-dependent protein kinase type II subunit delta	Camk2d
2.50413	1.57611	6.36023	P35486	P35486	Pyruvate dehydrogenase E1 component subunit alpha, somatic form, mitochondrial	Pdha1
2.70319	1.55874	7.19173	Q9D164	Q9D164	FXYD domain-containing ion transport regulator 6	Fxyd6
2.47196	1.52181	6.23394	Q9Z0E0	Q9Z0E0	Neurochondrin	Ncdn

N: -Log Student's T-test p-value KO_FAST_WT_F AST	N: Student's T-test Difference KO_FAST_WT_F AST	N: Student's T-test Test statistic KO_FAST_WT_F FAST	T: Protein IDs	T: Majority protein IDs	T: Protein names	T: Gene names
2.29312	1.50749	5.56948	P70404	P70404	Isocitrate dehydrogenase [NAD] subunit gamma 1, mitochondrial	ldh3g
2.80185	1.48745	7.63806	P61922	P61922	4-aminobutyrate aminotransferase, mitochondrial	Abat
2.45304	1.47498	6.16068	P63085	P63085	Mitogen-activated protein kinase 1	Mapk1
2.95704	1.47222	8.39046	P62821	P62821	Ras-related protein Rab-1A	Rab1A
3.1806	1.46023	9.5936	Q9QYG0	Q9QYG0	Protein NDRG2	NdrG2
2.37575	1.45933	5.86876	P17183	P17183	Gamma-enolase	Eno2
2.28223	1.41397	5.53095	P97807	P97807	Fumarate hydratase, mitochondrial	Fh
2.88637	1.36443	8.03994	Q9Z1G3	Q9Z1G3	V-type proton ATPase subunit C 1	Atp6v1c1
2.88244	1.35617	8.02081	P30275;Q6P8 J7	P30275	Creatine kinase U-type, mitochondrial	Ckmt1
2.59296	1.354	6.72041	Q9EQH3	Q9EQH3	Vacuolar protein sorting-associated protein 35	Vps35
2.27867	1.33962	5.51844	P11798	P11798	Calcium/calmodulin-dependent protein kinase type II subunit alpha	Camk2a
2.45776	1.30811	6.17887	Q9DC69	Q9DC69	NADH dehydrogenase [ubiquinone] 1 alpha subcomplex subunit 9, mitochondrial	Ndufa9
2.2124	1.30574	5.28917	P06745	P06745	Glucose-6-phosphate isomerase	Gpi
2.84681	1.29123	7.84952	Q61768	Q61768	Kinesin-1 heavy chain	Kif5b
2.11003	1.27122	4.94988	P48722	P48722	Heat shock 70 kDa protein 4L	Hspa4l
3.0524	1.25589	8.88556	Q8BGQ7	Q8BGQ7	Alanine--tRNA ligase, cytoplasmic	Aars
2.15019	1.24975	5.08088	Q9EQF6	Q9EQF6	Dihydropyrimidinase-related protein 5	Dpysl5
2.72439	1.2424	7.28564	P50516	P50516	V-type proton ATPase catalytic subunit A	Atp6v1a
2.1035	1.20787	4.92883	Q99LC3	Q99LC3	NADH dehydrogenase [ubiquinone] 1 alpha subcomplex subunit 10, mitochondrial	Ndufa10
2.33716	1.19997	5.7274	P17182	P17182	Alpha-enolase	Eno1
2.69651	1.19874	7.16236	Q68FD5	Q68FD5	Clathrin heavy chain 1	Cltc

N: -Log Student's T-test p-value KO_FAST_WT_F AST	N: Student's T-test Difference KO_FAST_WT_F AST	N: Student's T-test Test statistic KO_FAST_WT_F FAST	T: Protein IDs	T: Majority protein IDs	T: Protein names	T: Gene names
2.71147	1.19773	7.22829	P63094;Q6R0 H7	P63094;Q6 R0H7	Guanine nucleotide-binding protein G(s) subunit alpha isoforms short;Guanine nucleotide-binding protein G(s) subunit alpha isoforms XLas	Gnas
2.14426	1.13881	5.06139	B2RSH2;P206 12;Q3V3I2;P5 0149;Q8CGK7	B2RSH2	Guanine nucleotide-binding protein G(i) subunit alpha-1	Gnai1
2.33351	1.13283	5.71415	P58389	P58389	Serine/threonine-protein phosphatase 2A activator	Ppp2r4
2.21363	1.11217	5.29335	O88342	O88342	WD repeat-containing protein 1	Wdr1
2.41043	1.08447	5.99828	Q91V41	Q91V41	Ras-related protein Rab-14	Rab14
2.66156	1.08049	7.01046	P84078;P6120 5;Q8BSL7;P61 750	P84078;P6 1205;Q8BS L7	ADP-ribosylation factor 1;ADP-ribosylation factor 3;ADP-ribosylation factor 2	Arf1, Arf3, Arf2
2.1669	1.07728	5.13618	P52480;P5365 7	P52480	Pyruvate kinase PKM	Pkm
2.38242	1.06984	5.89349	O35129	O35129	Prohibitin-2	Phb2
2.77297	1.06773	7.50492	Q02053;P312 54	Q02053	Ubiquitin-like modifier-activating enzyme 1	Uba1
2.35363	1.0669	5.78738	P39053	P39053	Dynamin-1	Dnm1
2.32636	1.06301	5.68834	P08249	P08249	Malate dehydrogenase, mitochondrial	Mdh2
2.18596	1.06237	5.19984	Q8BWF0	Q8BWF0	Succinate-semialdehyde dehydrogenase, mitochondrial	Aldh5a1
2.02408	1.05981	4.67815	P53810	P53810	Phosphatidylinositol transfer protein alpha isoform	Pitpna
2.56083	1.04571	6.58817	P17710;O085 28;Q91W97;Q 3TRM8	P17710	Hexokinase-1	Hk1
2.17443	1.0279	5.16127	Q03517	Q03517	Secretogranin-2;Secretoneurin;Manserin	Scg2
2.86371	1.00736	7.93034	Q60932	Q60932	Voltage-dependent anion-selective channel protein 1	Vdac1
2.93509	1.00337	8.28012	Q8VDD5	Q8VDD5	Myosin-9	Myh9

N: -Log Student's T-test p-value KO_FAST_WT_F AST	N: Student's T-test Difference KO_FAST_WT_F AST	N: Student's T-test Test statistic KO_FAST_WT_F FAST	T: Protein IDs	T: Majority protein IDs	T: Protein names	T: Gene names
3.08443	1.00045	9.0578	P63101	P63101	14-3-3 protein zeta/delta	Ywhaz
2.79045	0.987784	7.58526	P63038	P63038	60 kDa heat shock protein, mitochondrial	Hspd1
2.17773	0.987478	5.17229	Q60931	Q60931	Voltage-dependent anion-selective channel protein 3	Vdac3
2.47136	0.962045	6.23164	Q80XN0	Q80XN0	D-beta-hydroxybutyrate dehydrogenase, mitochondrial	Bdh1
2.44888	0.959249	6.14466	Q91VD9	Q91VD9	NADH-ubiquinone oxidoreductase 75 kDa subunit, mitochondrial	Ndufs1
2.29143	0.929169	5.56347	Q9CQ92	Q9CQ92	Mitochondrial fission 1 protein	Fis1
2.20107	0.913856	5.25073	Q9DB20	Q9DB20	ATP synthase subunit O, mitochondrial	Atp5o
2.07568	0.913443	4.83988	Q64433	Q64433	10 kDa heat shock protein, mitochondrial	Hspe1
2.03335	0.913153	4.7069	Q76MZ3;Q7TNP2	Q76MZ3	Serine/threonine-protein phosphatase 2A 65 kDa regulatory subunit A alpha isoform	Ppp2r1a
2.88493	0.907374	8.03292	Q9CZW5	Q9CZW5	Mitochondrial import receptor subunit TOM70	Tomm70a
2.23341	0.870998	5.361	Q9D1G1	Q9D1G1	Ras-related protein Rab-1B	Rab1b
3.06912	0.85779	8.97509	P56135	P56135	ATP synthase subunit f, mitochondrial	Atp5j2
2.49667	0.84421	6.33076	P16546	P16546	Spectrin alpha chain, non-erythrocytic 1	Sptan1
2.67767	0.821484	7.08011	G5E829;Q6Q477	G5E829;Q6Q477	Plasma membrane calcium-transporting ATPase 1;Calcium-transporting ATPase	Atp2b1, Atp2b4
2.01999	0.735073	4.66552	P09411;P09041	P09411	Phosphoglycerate kinase 1	Pgk1
3.07494	0.715569	9.00647	P16858	P16858	Glyceraldehyde-3-phosphate dehydrogenase	Gapdh
2.07092	0.709902	4.8248	O88685	O88685	26S protease regulatory subunit 6A	Psmc3
2.09069	0.705196	4.88771	P50396	P50396	Rab GDP dissociation inhibitor alpha	Gdi1
3.41237	0.67976	11.0091	P05202	P05202	Aspartate aminotransferase, mitochondrial	Got2
2.04113	0.647145	4.73113	Q61553	Q61553	Fascin	Fscn1
2.03374	0.644548	4.70812	rgliRTpep IRT	rgliRTpep IRT		
2.76286	0.57429	7.45885	P05201	P05201	Aspartate aminotransferase, cytoplasmic	Got1
2.03294	0.537773	4.70564	Q8CAQ8	Q8CAQ8	MICOS complex subunit Mic60	Immt
2.30566	0.504844	5.61407	Q91V61	Q91V61	Sideroflexin-3	Sfxn3
2.01605	0.433929	4.65338	P40142	P40142	Transketolase	Tkt

N: -Log Student's T-test p-value KO_FAST_WT_F AST	N: Student's T-test Difference KO_FAST_WT_F AST	N: Student's T-test Test statistic KO_FAST_WT_F FAST	T: Protein IDs	T: Majority protein IDs	T: Protein names	T: Gene names
2.20401	0.429171	5.26068	P14152	P14152	Malate dehydrogenase, cytoplasmic	Mdh1
2.59573	0.427283	6.73191	Q60930	Q60930	Voltage-dependent anion-selective channel protein 2	Vdac2
2.04281	-0.475418	-4.73638	P20029	P20029	78 kDa glucose-regulated protein	Hspa5
3.34441	-0.762355	-10.5749	Q91WC3	Q91WC3	Long-chain-fatty-acid--CoA ligase 6	Acsl6
2.70019	-0.771753	-7.17856	Q9QUI0;Q621 59	Q9QUI0;Q6 2159	Transforming protein RhoA;Rho-related GTP-binding protein RhoC	Rhoa, Rhoc
2.00615	-0.965442	-4.62294	Q9DC51	Q9DC51	Guanine nucleotide-binding protein G(k) subunit alpha	Gnai3
2.07209	-1.04021	-4.8285	P13020;CON_ _Q3SX14	P13020	Gelsolin	Gsn
2.32165	-1.34827	-5.67137	O08788	O08788	Dynactin subunit 1	Dctn1
2.63596	-1.36238	-6.90093	Q8CGP6;Q8R 1M2;Q8CGP7; Q8CGP5;Q8B FU2;P22752	Q8CGP6;Q 8R1M2;Q8 CGP7;Q8C GP5;Q8BF U2;P22752	Histone H2A type 1-H;Histone H2A.J;Histone H2A type 1- K;Histone H2A type 1-F;Histone H2A type 3;Histone H2A type 1	Hist1h2ah , H2afj, Hist1h2ak , Hist1h2af, Hist3h2a, Hist1h2ab
3.25198	-1.39326	-10.0102	P62806	P62806	Histone H4	Hist1h4a
2.37947	-1.48136	-5.88257	P99027	P99027	60S acidic ribosomal protein P2	Rplp2
2.99752	-1.58628	-8.59749	Q06185	Q06185	ATP synthase subunit e, mitochondrial	Atp5k
3.35846	-1.81266	-10.6633	P40124	P40124	Adenylyl cyclase-associated protein 1	Cap1
2.58714	-1.92385	-6.69627	P60202	P60202	Myelin proteolipid protein	Plp1
2.12572	-2.01314	-5.00074	Q9D8E6	Q9D8E6	60S ribosomal protein L4	Rpl4
2.21375	-2.64252	-5.29375	P63054	P63054	Purkinje cell protein 4	Pcp4
3.65106	-2.88864	-12.6721	P04370	P04370	Myelin basic protein	Mbp
2.37508	-2.95957	-5.86628	P52503	P52503	NADH dehydrogenase [ubiquinone] iron-sulfur protein 6, mitochondrial	Ndufs6
2.05954	-3.20493	-4.78887	P63168	P63168	Dynein light chain 1, cytoplasmic	Dynll1
4.24685	-3.31179	-17.948	P51880	P51880	Fatty acid-binding protein, brain	Fabp7
2.48368	-3.61256	-6.27972	P43274	P43274	Histone H1.4	Hist1h1e

N: -Log Student's T-test p-value KO_FAST_WT_F AST	N: Student's T-test Difference KO_FAST_WT_F AST	N: Student's T-test Test statistic KO_FAST_WT_F FAST	T: Protein IDs	T: Majority protein IDs	T: Protein names	T: Gene names
2.44969	-4.09524	-6.14777	P19536	P19536	Cytochrome c oxidase subunit 5B, mitochondrial	Cox5b
2.66288	-5.20101	-7.01612	Q91XV3	Q91XV3	Brain acid soluble protein 1	Basp1

Table 5 MSprotein_enrichment_KOvsWT_refed.

All proteins in the spreadsheet are significantly different between genotypes. Proteins highlighted in blue are listed as 2-fold higher, whereas those highlighted in yellow are listed as 2-fold lower expression, in KO mice relative to WT mice.

N: -Log Student's T-test p-value KO_Refed_WT_R efed	N: Student's T-test Difference KO_Refed_WT_ Refed	N: Student's T-test Test statistic KO_Refed_WT_ Refed	T: Protein IDs	T: Majority protein IDs	T: Protein names	T: Gene names
1.45293	3.55735	3.12832	P63028	P63028	Translationally-controlled tumor protein	Tpt1
3.2673	3.25913	10.1018	O35098	O35098	Dihydropyrimidinase-related protein 4	Dpysl4
2.40934	3.12195	5.99418	P97351	P97351	40S ribosomal protein S3a	Rps3a
3.14629	3.1174	9.39918	Q9R0P5	Q9R0P5	Dextrin	Dstn
2.33486	2.887	5.71907	Q9CQ54	Q9CQ54	NADH dehydrogenase [ubiquinone] 1 subunit C2	Ndufc2
1.53252	2.86452	3.32135	P49312	P49312	Heterogeneous nuclear ribonucleoprotein A1;Heterogeneous nuclear ribonucleoprotein A1, N-terminally processed	Hnrnpa1
1.46296	2.6403	3.15229	P84104	P84104	Serine/arginine-rich splicing factor 3	Srsf3
2.06045	2.52658	4.79172	P62897;CON_P62894;P00015	P62897	Cytochrome c, somatic	Cycc
1.4307	2.35598	3.07551	P80316	P80316	T-complex protein 1 subunit epsilon	Cct5
1.41428	2.29213	3.03679	P10107	P10107	Annexin A1	Anxa1
1.46312	2.28797	3.15266	Q9ESN6	Q9ESN6	Tripartite motif-containing protein 2	Trim2

N: -Log Student's T-test p-value KO_Refed_WT_Refed	N: Student's T-test Difference KO_Refed_WT_Refed	N: Student's T-test Test statistic KO_Refed_WT_Refed	T: Protein IDs	T: Majority protein IDs	T: Protein names	T: Gene names
3.20975	2.1591	9.76178	Q8BP92	Q8BP92	Reticulocalbin-2	Rcn2
2.5746	2.02595	6.64455	Q91YQ5	Q91YQ5	Dolichyl-diphosphooligosaccharide--protein glycosyltransferase subunit 1	Rpn1
1.59672	2.01173	3.48186	P17225	P17225	Polypyrimidine tract-binding protein 1	Ptbp1
1.60284	1.89464	3.49739	Q61411	Q61411	GTPase HRas;GTPase HRas, N-terminally processed	Hras
1.49441	1.88035	3.22811	Q920E5	Q920E5	Farnesyl pyrophosphate synthase	Fdps
1.7546	1.87419	3.89638	P63085	P63085	Mitogen-activated protein kinase 1	Mapk1
1.52409	1.85337	3.30061	Q791V5	Q791V5	Mitochondrial carrier homolog 2	Mtch2
1.51329	1.84263	3.27412	Q9CPQ3	Q9CPQ3	Mitochondrial import receptor subunit TOM22 homolog	Tomm22
1.43463	1.83305	3.08481	P61979	P61979	Heterogeneous nuclear ribonucleoprotein K	Hnrnpk
2.3556	1.80787	5.79458	Q61990;P57722	Q61990;P57722	Poly(rC)-binding protein 2;Poly(rC)-binding protein 3	Pcbp2, Pcbp3
1.40208	1.74666	3.0082	P14131	P14131	40S ribosomal protein S16	Rps16
1.82122	1.70706	4.08044	O88487	O88487	Cytoplasmic dynein 1 intermediate chain 2	Dync1i2
1.56912	1.68059	3.41232	P62849	P62849	40S ribosomal protein S24	Rps24
1.4106	1.66278	3.02816	Q8BGH2	Q8BGH2	Sorting and assembly machinery component 50 homolog	Samm50
1.95186	1.63931	4.4586	Q62186	Q62186	Translocon-associated protein subunit delta	Ssr4
1.47484	1.60681	3.18081	P51660	P51660	Peroxisomal multifunctional enzyme type 2;(3R)-hydroxyacyl-CoA dehydrogenase;Enoyl-CoA hydratase 2	Hsd17b4
1.31095	1.54207	2.79881	Q64727	Q64727	Vinculin	Vcl
1.75011	1.51515	3.88416	Q61205	Q61205	Platelet-activating factor acetylhydrolase IB subunit gamma	Pafah1b3

N: -Log Student's T-test p-value KO_Refed_WT_R efed	N: Student's T-test Difference KO_Refed_WT_ Refed	N: Student's T-test Test statistic KO_Refed_WT_ Refed	T: Protein IDs	T: Majority protein IDs	T: Protein names	T: Gene names
1.87438	1.46436	4.23149	O88844	O88844	Isocitrate dehydrogenase [NADP] cytoplasmic	Idh1
1.30205	1.39084	2.77874	P49722	P49722	Proteasome subunit alpha type-2	Psma2
2.18217	1.36412	5.18713	P60335	P60335	Poly(rC)-binding protein 1	Pcbp1
1.96558	1.33936	4.49973	Q9CQX2	Q9CQX2	Cytochrome b5 type B	Cyb5b
3.04527	1.33342	8.84766	Q9D0K2	Q9D0K2	Succinyl-CoA:3-ketoacid coenzyme A transferase 1, mitochondrial	Oxct1
1.40009	1.32528	3.00355	Q9CS42;Q9D7G0	Q9CS42;Q9D7G0	Ribose-phosphate pyrophosphokinase 2;Ribose-phosphate pyrophosphokinase 1	Prps2, Prps1
2.73413	1.21206	7.32914	P60766	P60766	Cell division control protein 42 homolog	Cdc42
2.62911	1.20564	6.87192	O35678	O35678	Monoglyceride lipase	Mgll
1.46737	1.17555	3.16286	Q9CQW1	Q9CQW1	Synaptobrevin homolog YKT6	Ykt6
1.35094	1.15479	2.88979	P02088;P02104	P02088	Hemoglobin subunit beta-1	Hbb-b1
1.38211	1.1468	2.96168	P20152;P31001;P15331	P20152	Vimentin	Vim
1.30594	1.14378	2.7875	Q6ZPE2	Q6ZPE2	Myotubularin-related protein 5	Sbf1
1.70804	1.09492	3.77105	P56564	P56564	Excitatory amino acid transporter 1	Slc1a3
2.53419	1.08819	6.48022	P68372	P68372	Tubulin beta-4B chain	Tubb4b
1.91158	1.07918	4.33948	Q99P72	Q99P72	Reticulon-4	Rtn4
2.05002	1.07051	4.75895	Q99LC3	Q99LC3	NADH dehydrogenase [ubiquinone] 1 alpha subcomplex subunit 10, mitochondrial	Ndufa10
1.61545	1.04544	3.52952	P54775	P54775	26S protease regulatory subunit 6B	Psmc4
1.49947	1.03	3.24042	Q99KK7	Q99KK7	Dipeptidyl peptidase 3	Dpp3
4.22124	0.985763	17.6827	Q61171	Q61171	Peroxisome oxidoreductin-2	Prdx2
2.48671	0.964971	6.2916	P68369	P68369	Tubulin alpha-1A chain	Tuba1a
2.8813	0.955545	8.0153	P63242;Q8BGY2	P63242;Q8BGY2	Eukaryotic translation initiation factor 5A-1;Eukaryotic translation initiation factor 5A-2	Eif5a, Eif5a2

N: -Log Student's T-test p-value KO_Refed_WT_R_efed	N: Student's T-test Difference KO_Refed_WT_Refed	N: Student's T-test Test statistic KO_Refed_WT_Refed	T: Protein IDs	T: Majority protein IDs	T: Protein names	T: Gene names
2.80521	0.954814	7.6537	Q01853	Q01853	Transitional endoplasmic reticulum ATPase	Vcp
2.00682	0.951695	4.62499	Q9DAK9	Q9DAK9	14 kDa phosphohistidine phosphatase	Phpt1
2.06227	0.949598	4.79747	P06801	P06801	NADP-dependent malic enzyme	Me1
2.3701	0.94684	5.84791	P99024	P99024	Tubulin beta-5 chain	Tubb5
2.46101	0.920426	6.19146	Q76MZ3;Q7TNP2	Q76MZ3	Serine/threonine-protein phosphatase 2A 65 kDa regulatory subunit A alpha isoform	Ppp2r1a
1.89748	0.903649	4.29831	Q80XN0	Q80XN0	D-beta-hydroxybutyrate dehydrogenase, mitochondrial	Bdh1
1.57576	0.902327	3.42896	P51855	P51855	Glutathione synthetase	Gss
1.91873	0.899623	4.36044	Q9CPV4	Q9CPV4	Glyoxalase domain-containing protein 4	Glod4
1.51759	0.894659	3.28465	P40142	P40142	Transketolase	Tkt
1.64703	0.893851	3.6108	Q9DC69	Q9DC69	NADH dehydrogenase [ubiquinone] 1 alpha subcomplex subunit 9, mitochondrial	Ndufa9
2.90341	0.87627	8.1232	P06745	P06745	Glucose-6-phosphate isomerase	Gpi
1.78354	0.866188	3.97562	Q62188	Q62188	Dihydropyrimidinase-related protein 3	Dpysl3
1.79119	0.85591	3.99674	Q9CZC8	Q9CZC8	Secernin-1	Scrn1
2.03829	0.855565	4.7223	Q9CQF9	Q9CQF9	Prenylcysteine oxidase	Pcyox1
1.59894	0.848499	3.48749	Q9CQI6	Q9CQI6	Coactosin-like protein	Cotl1
1.32339	0.847679	2.82697	Q9EQF6	Q9EQF6	Dihydropyrimidinase-related protein 5	Dpysl5
3.17571	0.841465	9.5657	Q02053;P31254	Q02053	Ubiquitin-like modifier-activating enzyme 1	Uba1
1.87099	0.819467	4.22174	P61164	P61164	Alpha-centractin	Actr1a
2.17264	0.816897	5.1553	Q9CQI3	Q9CQI3	Glia maturation factor beta	Gmfb
2.48901	0.814853	6.3006	P17183	P17183	Gamma-enolase	Eno2
2.00445	0.808555	4.61771	P26043	P26043	Radixin	Rdx
1.55625	0.807855	3.38018	P50516	P50516	V-type proton ATPase catalytic subunit A	Atp6v1a
1.3586	0.782492	2.90739	Q9DCS9	Q9DCS9	NADH dehydrogenase [ubiquinone] 1 beta subcomplex subunit 10	Ndufb10
1.32494	0.779148	2.8305	Q8BMS1	Q8BMS1	Trifunctional enzyme subunit alpha, mitochondrial;Long-chain enoyl-CoA hydratase;Long chain 3-hydroxyacyl-CoA dehydrogenase	Hadha

N: -Log Student's T-test p-value KO_Refed_WT_Refed	N: Student's T-test Difference KO_Refed_WT_Refed	N: Student's T-test Test statistic KO_Refed_WT_Refed	T: Protein IDs	T: Majority protein IDs	T: Protein names	T: Gene names
2.78113	0.771805	7.54234	O08709	O08709	Peroxiredoxin-6	Prdx6
2.82251	0.760338	7.7346	Q61553	Q61553	Fascin	Fscn1
1.51589	0.749049	3.28048	rgliRTpep iRT	rgliRTpep iRT		
1.41207	0.740664	3.03161	Q9WTT4	Q9WTT4	V-type proton ATPase subunit G 2	Atp6v1g2
1.42513	0.738023	3.06235	P58252	P58252	Elongation factor 2	Eef2
1.7799	0.723606	3.9656	P14824	P14824	Annexin A6	Anxa6
1.54408	0.721903	3.34992	P30275;Q6P8J7	P30275	Creatine kinase U-type, mitochondrial	Ckmt1
1.38522	0.717977	2.9689	P84078;P61205;Q8BSL7;P61750	P84078;P61205;Q8BSL7	ADP-ribosylation factor 1;ADP-ribosylation factor 3;ADP-ribosylation factor 2	Arf1, Arf3, Arf2
3.34352	0.692236	10.5693	P17182	P17182	Alpha-enolase	Eno1
1.48698	0.689775	3.21012	B2RSH2;P20612;Q3V3I2;P50149;Q8CGK7	B2RSH2	Guanine nucleotide-binding protein G(i) subunit alpha-1	Gnai1
2.06046	0.688866	4.79176	Q8K1M6	Q8K1M6	Dynamamin-1-like protein	Dnm1l
2.01565	0.688733	4.65213	Q9ERD7	Q9ERD7	Tubulin beta-3 chain	Tubb3
2.6723	0.687553	7.05683	Q9D819	Q9D819	Inorganic pyrophosphatase	Ppa1
1.93312	0.682222	4.40289	P20108	P20108	Thioredoxin-dependent peroxide reductase, mitochondrial	Prdx3
3.34708	0.68189	10.5916	P48036	P48036	Annexin A5	Anxa5
1.50004	0.678699	3.24181	P63101	P63101	14-3-3 protein zeta/delta	Ywhaz
1.41582	0.660905	3.04042	P18242	P18242	Cathepsin D	Ctsd
1.61486	0.660743	3.52802	P11983	P11983	T-complex protein 1 subunit alpha	Tcp1
2.61888	0.660233	6.82875	P70404	P70404	Isocitrate dehydrogenase [NAD] subunit gamma 1, mitochondrial	Idh3g
2.09574	0.659897	4.90389	O35350	O35350	Calpain-1 catalytic subunit	Capn1
2.37247	0.648428	5.85666	P97807	P97807	Fumarate hydratase, mitochondrial	Fh
1.75034	0.637201	3.88479	P19157;P46425	P19157	Glutathione S-transferase P 1	Gstp1
1.35349	0.629189	2.89564	O88685	O88685	26S protease regulatory subunit 6A	Psmc3

N: -Log Student's T-test p-value KO_Refed_WT_R efed	N: Student's T-test Difference KO_Refed_WT_ Refed	N: Student's T-test Test statistic KO_Refed_WT_ Refed	T: Protein IDs	T: Majority protein IDs	T: Protein names	T: Gene names
1.32983	0.620668	2.84159	P62814	P62814	V-type proton ATPase subunit B, brain isoform	Atp6v1b2
1.49976	0.613956	3.24112	Q8CHH9	Q8CHH9	Septin-8	1/09/2008
1.87691	0.611335	4.23877	Q9D1G1	Q9D1G1	Ras-related protein Rab-1B	Rab1b
2.27072	0.606526	5.4905	P52480;P53657	P52480	Pyruvate kinase PKM	Pkm
1.63008	0.606205	3.56704	P61922	P61922	4-aminobutyrate aminotransferase, mitochondrial	Abat
1.3867	0.60113	2.97234	Q9JHU4	Q9JHU4	Cytoplasmic dynein 1 heavy chain 1	Dync1h1
1.65273	0.601128	3.62557	P80314	P80314	T-complex protein 1 subunit beta	Cct2
1.38845	0.599186	2.97641	Q9JL62	Q9JL62	Glycolipid transfer protein	Gltp
2.37902	0.597848	5.88088	P08249	P08249	Malate dehydrogenase, mitochondrial	Mdh2
1.35283	0.595006	2.89413	Q9CR95	Q9CR95	Adaptin ear-binding coat-associated protein 1	Necap1
2.33002	0.594695	5.70155	P62821	P62821	Ras-related protein Rab-1A	Rab1A
1.69154	0.594633	3.72728	P63038	P63038	60 kDa heat shock protein, mitochondrial	Hspd1
1.3182	0.571925	2.81521	Q9CQ69	Q9CQ69	Cytochrome b-c1 complex subunit 8	Uqcrq
1.48927	0.566467	3.21567	Q91V41	Q91V41	Ras-related protein Rab-14	Rab14
1.30978	0.565685	2.79616	P53994;P59279	P53994;P59279	Ras-related protein Rab-2A;Ras-related protein Rab-2B	Rab2a, Rab2b
1.52554	0.558583	3.30418	P56399	P56399	Ubiquitin carboxyl-terminal hydrolase 5	Usp5
1.35009	0.55741	2.88785	P70349	P70349	Histidine triad nucleotide-binding protein 1	Hint1
1.59335	0.554598	3.47332	P62874;Q61011	P62874	Guanine nucleotide-binding protein G(I)/G(S)/G(T) subunit beta-1	Gnb1
1.50034	0.554125	3.24254	P62880	P62880	Guanine nucleotide-binding protein G(I)/G(S)/G(T) subunit beta-2	Gnb2
1.85338	0.553676	4.17135	Q04447;P07310	Q04447	Creatine kinase B-type	Ckb
2.37204	0.549178	5.85506	Q91V12	Q91V12	Cytosolic acyl coenzyme A thioester hydrolase	Acot7
1.43256	0.547898	3.07989	P05063;Q91Y97	P05063	Fructose-bisphosphate aldolase C	Aldoc
2.99118	0.544791	8.56476	P09411;P09041	P09411	Phosphoglycerate kinase 1	Pgk1
1.49279	0.539712	3.2242	Q80ZJ1	Q80ZJ1	Ras-related protein Rap-2a	Rap2a

N: -Log Student's T-test p-value KO_Refed_WT_R_efed	N: Student's T-test Difference KO_Refed_WT_Refed	N: Student's T-test Test statistic KO_Refed_WT_Refed	T: Protein IDs	T: Majority protein IDs	T: Protein names	T: Gene names
1.3722	0.537007	2.93875	O08749	O08749	Dihydrolipoyl dehydrogenase, mitochondrial	Dld
1.89438	0.527409	4.28929	P47738	P47738	Aldehyde dehydrogenase, mitochondrial	Aldh2
2.73163	0.495006	7.31795	O35129	O35129	Prohibitin-2	Phb2
1.46748	0.494048	3.16313	Q61598	Q61598	Rab GDP dissociation inhibitor beta	Gdi2
1.52343	0.488463	3.29898	P16546	P16546	Spectrin alpha chain, non-erythrocytic 1	Sptan1
2.37667	0.481167	5.87217	P51150	P51150	Ras-related protein Rab-7a	Rab7a
1.57825	0.473578	3.43522	P05213	P05213	Tubulin alpha-1B chain	Tuba1b
1.45335	0.467718	3.12931	P70296	P70296	Phosphatidylethanolamine-binding protein 1;Hippocampal cholinergic neurostimulating peptide	Pebp1
1.33851	0.458869	2.86137	Q6ZQ38	Q6ZQ38	Cullin-associated NEDD8-dissociated protein 1	Cand1
3.37256	0.453573	10.7527	P16858	P16858	Glyceraldehyde-3-phosphate dehydrogenase	Gapdh
1.82117	0.452302	4.08029	P80318	P80318	T-complex protein 1 subunit gamma	Cct3
1.60993	0.451635	3.51543	Q9DBJ1;O70250	Q9DBJ1	Phosphoglycerate mutase 1	Pgam1
1.30159	0.423903	2.7777	Q9D6J6	Q9D6J6	NADH dehydrogenase [ubiquinone] flavoprotein 2, mitochondrial	Ndufv2
1.86445	0.41421	4.20297	Q8BGN3	Q8BGN3	Ectonucleotide pyrophosphatase/phosphodiesterase family member 6	Enpp6
1.71196	0.398838	3.78149	Q91YT0	Q91YT0	NADH dehydrogenase [ubiquinone] flavoprotein 1, mitochondrial	Ndufv1
1.35085	0.396019	2.8896	Q8BMF4	Q8BMF4	Dihydrolipoyllysine-residue acetyltransferase component of pyruvate dehydrogenase complex, mitochondrial	Dlat
1.30941	0.367159	2.79534	Q8BWF0	Q8BWF0	Succinate-semialdehyde dehydrogenase, mitochondrial	Aldh5a1
2.05072	0.325994	4.76114	O09111	O09111	NADH dehydrogenase [ubiquinone] 1 beta subcomplex subunit 11, mitochondrial	Ndufb11
1.33103	0.228087	2.84433	Q60597	Q60597	2-oxoglutarate dehydrogenase, mitochondrial	Ogdh
4.10233	-0.274806	-16.4999	Q03265	Q03265	ATP synthase subunit alpha, mitochondrial	Atp5a1
2.0098	-0.340855	-4.63414	P08553	P08553	Neurofilament medium polypeptide	Nefm
1.58419	-0.405517	-3.45019	P14152	P14152	Malate dehydrogenase, cytoplasmic	Mdh1
1.81072	-0.412544	-4.05103	P52760	P52760	Ribonuclease UK114	Hrsp12

N: -Log Student's T-test p-value KO_Refed_WT_Refed	N: Student's T-test Difference KO_Refed_WT_Refed	N: Student's T-test Test statistic KO_Refed_WT_Refed	T: Protein IDs	T: Majority protein IDs	T: Protein names	T: Gene names
1.61274	-0.453104	-3.52259	P51881	P51881	ADP/ATP translocase 2;ADP/ATP translocase 2, N-terminally processed	Slc25a5
1.4298	-0.559378	-3.07338	P16125	P16125	L-lactate dehydrogenase B chain	Ldhb
1.44168	-0.595306	-3.10153	Q9QYC0;Q9QYB8	Q9QYC0	Alpha-adducin	Add1
1.36433	-0.611506	-2.92057	Q9DCW4	Q9DCW4	Electron transfer flavoprotein subunit beta	Etfb
1.91507	-0.629098	-4.34971	P19783	P19783	Cytochrome c oxidase subunit 4 isoform 1, mitochondrial	Cox4i1
2.16906	-0.98928	-5.14338	P62259	P62259	14-3-3 protein epsilon	Ywhae
1.80465	-0.99072	-4.03412	P61161	P61161	Actin-related protein 2	Actr2
2.47177	-1.01129	-6.23323	P14094	P14094	Sodium/potassium-transporting ATPase subunit beta-1	Atp1b1
1.86654	-1.02174	-4.20896	Q8K4L4	Q8K4L4	Protein POF1B	Pof1b
2.10566	-1.05062	-4.93577	P16330	P16330	2,3-cyclic-nucleotide 3-phosphodiesterase	Cnp
2.05987	-1.06677	-4.78988	P28661	P28661	Septin-4	Sep4
2.30559	-1.16278	-5.61382	Q99JR1	Q99JR1	Sideroflexin-1	Sfxn1
2.20535	-1.22971	-5.26522	Q9R0P9	Q9R0P9	Ubiquitin carboxyl-terminal hydrolase isozyme L1	Uchl1
1.58821	-1.25143	-3.46033	P62830	P62830	60S ribosomal protein L23	Rpl23
1.46605	-1.50792	-3.1597	P63044	P63044	Vesicle-associated membrane protein 2	Vamp2
2.35222	-1.54957	-5.78223	P55012;P55014	P55012	Solute carrier family 12 member 2	Slc12a2
1.69148	-1.71477	-3.72712	P63040	P63040	Complexin-1	Cplx1
2.99172	-1.77025	-8.56751	Q9WV98	Q9WV98	Mitochondrial import inner membrane translocase subunit Tim9	Timm9
1.84044	-1.90434	-4.13459	P61089;Q9CQ37	P61089	Ubiquitin-conjugating enzyme E2 N	Ube2n
2.42465	-1.91715	-6.05209	P62071	P62071	Ras-related protein R-Ras2	Rras2
2.85886	-1.9471	-7.90709	P40237	P40237	CD82 antigen	Cd82

N: -Log Student's T-test p-value KO_Refed_WT_R efed	N: Student's T-test Difference KO_Refed_WT_ Refed	N: Student's T-test Test statistic KO_Refed_WT_ Refed	T: Protein IDs	T: Majority protein IDs	T: Protein names	T: Gene names
1.33322	-1.97956	-2.84931	Q06185	Q06185	ATP synthase subunit e, mitochondrial	Atp5i
1.54036	-2.0678	-3.34071	P47757	P47757	F-actin-capping protein subunit beta	Capzb
3.06559	-2.08438	-8.95614	P24288	P24288	Branched-chain-amino-acid aminotransferase, cytosolic	Bcat1
2.27536	-2.1299	-5.50679	P63328	P63328	Serine/threonine-protein phosphatase 2B catalytic subunit alpha isoform	Ppp3ca
2.01805	-2.16064	-4.65954	Q9ES97	Q9ES97	Reticulon-3	Rtn3
3.18831	-2.16148	-9.63783	P63168	P63168	Dynein light chain 1, cytoplasmic	Dynll1
1.9027	-2.167	-4.31353	P52503	P52503	NADH dehydrogenase [ubiquinone] iron-sulfur protein 6, mitochondrial	Ndufs6
1.57119	-2.25153	-3.41751	Q9JLF6	Q9JLF6	Protein-glutamine gamma-glutamyltransferase K	Tgm1
2.0681	-2.33617	-4.81586	P63005	P63005	Platelet-activating factor acetylhydrolase IB subunit alpha	Pafah1b1
1.93772	-2.48238	-4.41653	P63054	P63054	Purkinje cell protein 4	Pcp4
1.71091	-2.80542	-3.77869	Q61176	Q61176	Arginase-1	Arg1
2.19922	-2.81293	-5.2445	P60202	P60202	Myelin proteolipid protein	Plp1
3.69227	-2.84486	-12.9825	P14231	P14231	Sodium/potassium-transporting ATPase subunit beta-2	Atp1b2
3.15462	-3.02762	-9.44605	Q99LX0	Q99LX0	Protein deglycase DJ-1	Park7
2.05357	-3.18751	-4.77007	Q80YN3	Q80YN3	Breast carcinoma-amplified sequence 1 homolog	Bcas1
2.04353	-3.5066	-4.73863	Q8BJY1	Q8BJY1	26S proteasome non-ATPase regulatory subunit 5	Psm5
1.76732	-3.50827	-3.93107	P48771	P48771	Cytochrome c oxidase subunit 7A2, mitochondrial	Cox7a2
3.33995	-3.54794	-10.547	P04370	P04370	Myelin basic protein	Mbp

N: -Log Student's T-test p-value KO_Refed_WT_R efed	N: Student's T-test Difference KO_Refed_WT_ Refed	N: Student's T-test Test statistic KO_Refed_WT_ Refed	T: Protein IDs	T: Majority protein IDs	T: Protein names	T: Gene names
3.9187	-3.55648	-14.8234	Q70IV5	Q70IV5	Synemin	Synm
3.06984	-3.61869	-8.97898	P43274	P43274	Histone H1.4	Hist1h1e
2.44142	-3.98353	-6.11603	P03930	P03930	ATP synthase protein 8	Mtatp8
4.93805	-3.99249	-26.7945	P06837	P06837	Neuromodulin	Gap43
4.47767	-4.20603	-20.5232	P61027	P61027	Ras-related protein Rab-10	Rab10
3.01425	-5.13979	-8.68436	P19536	P19536	Cytochrome c oxidase subunit 5B, mitochondrial	Cox5b
2.67525	-5.42994	-7.06963	Q91XV3	Q91XV3	Brain acid soluble protein 1	Basp1